Tsunami Hazard and Enhanced Vulnerability Assessment along the Makran Coast, Pakistan

From the Faculty of Georesources and Materials Engineering of the RWTH Aachen University

to obtain the academic degree of

Doctor of Natural Science

approved thesis

submitted by

Rashid Haider, MSc

from Gujrat (Pakistan)

Advisors: Herr Univ.-Prof. Dr. rer. nat. Klaus Reicherter
Herr PD Dr. rer. nat. Gösta Hoffmann

Date of the oral examination: March 12th, 2025

This thesis is available in electronic format on the university library's website

©2025

Rashid Haider

ORCID: 0000-0002-9802-8575

Printed and/or published with the support of the German Academic Exchange Service

Declarations on the doctoral thesis

(Dr. rer. nat.)

I herewith declare that I have not previously participated in any doctoral examination procedure in a mathematics or natural science discipline.

I hereby declare that the submitted thesis entitled ***Tsunami Hazard and Enhanced Vulnerability Assessment along the Makran Coast, Pakistan*** was written independently and that only the resources and aids specified in the thesis were used. In particular, all references borrowed from external sources are clearly acknowledged and identified.

_____

Aachen, 14.04.2025

This thesis is dedicated to the memory of those who tragically lost their lives in the tsunami disasters. May their memories keep us motivated for our collective efforts towards research, preparedness, and resilience in helping to prevent such tragedies in the future.

“Seek knowledge from cradle to grave”

– Prophet Muhammad (PBUH) (570 – 632 CE)

Ancient Greek Philosopher

”گود سے قبر تک علم کی تلاش کرو”

– Urdu translation by Rashid Haider

"Suche Wissen vom Wiege bis zum Grabe”

–Translated with
https://www.deepl.com/translator

Abstract

The active Makran Subduction Zone and transform tectonics in the Arabian Sea makes the region seismically active and prone to tsunamis. The region has witnessed several catastrophic earthquakes and tsunamis in the past. The thesis deals with the tsunami potential and enhanced vulnerability assessment along the Makran Coast of Pakistan. The first part of the thesis encompasses the tsunami potential assessment through a cross-analysis of multidisciplinary proxies. The second part deals with vulnerability and preliminary risk assessment through a detailed analysis of tsunami modelling and inundation for various hazard scenarios. In the third part an attempt is being made to comprehend and understand the four puzzling dynamics of the 1945 Tsunami event at Pasni.

For tsunami hazard and potential assessment an integrated assessment of various approaches and proxies is carried out. It involves a comprehensive compilation, review and cross-analysis of geophysical, probabilistic-deterministic modelling, sedimentological-geomorphical extreme wave evidence, and historical records around the Arabian coastline. Also, the tsunamites (tsunami deposits) exhibiting worst-case morphological modifications and impacts around the Arabia Sea are modelled to estimate the tsunami wave potential. These morphodynamic changes are modelled backwards in terms of wave height, wavelength, flow depth, flow velocity and inundation extents. The analysis also resulted in a recurrence interval between 500 and 1000 years for a mega-tsunami event (≥12 m).

The second part deals with vulnerability and preliminary risk assessment though a detailed tsunami generation and inundation analysis for various hazard scenarios. It utilizes both static and dynamic inundation models for comparative analysis and for better understanding. The vulnerability assessment of the Makran Coast particularly focuses on the towns of Pasni and Gwadar in detail. Based on the evaluation of hazard potential, three different tsunami wave scenarios (7m, 10m, 15m) are modelled for each town. In addition to simulations, spot observations of key areas in the study region are presented, detailing flow velocity and depth. The tsunami modelling also evaluates the effectiveness of the early warning system by comparing tsunami generation, arrival, and evacuation timings for near-field and far-field tsunamis.

In the third part an attempt is being made to comprehend four puzzling facts of the 1945 Tsunami event at the Pasni Coast. These are i) arrival time delay of 1-2 hours, ii) wave height ≥10 m which is exceptionally high as compared to earthquake size, iii) occurrence of three waves, and iv) temporary beach line regression or the initial draw-down. Moreover, the mystery deepened as deterministic numerical models from various studies failed to align with reports especially arrival timings and wave height. The models failed to achieve a wave height exceeding 5 meters, accompanied by a

delay of over an hour. This discrepancy prompted the consideration of a submarine landslide-generated triggered subsequent tsunami. We discuss that the earthquake was the sole tsunami source, capable of elucidating the reported tsunami characteristics. The factors contributing to the delay and exceptionally high wave height are explained. In brief, we argue that the reflection-amplification phenomenon between the coastal cliffs and continental shelf edge is responsible for all these anomalous values.

Chapter 4 presents the paleotsunami deposits (tsunamites) in the Pasni area, marking the first study conducted within this domain in Pakistan. We detected two tsunamites older than that of 1945 Tsunami horizon. The event dated 1539 CE is very close to an already reported 1524 CE Tsunami in the Arabian Sea. The second event could date back to 17th BCE maximum. These deposits need further investigations.

The synthesis of the thesis concludes the hazard vulnerability assessment including effects of tsunamis along the coastline of Pakistan. The study underscores the importance of comprehensive mitigation strategies to enhance coastal resilience and minimize the impacts of future tsunamis along the coastline. As one outlook, we encourage continued research efforts to deepen our understanding of these complex phenomena and improve disaster preparedness and response capabilities in the region.

Kurzfassung

Die aktive Makran-Subduktionszone und die Tektonik der Transform-Störungen im Arabischen Meer machen die Region seismisch aktiv und anfällig für große Tsunamis. Die Region hat in der Vergangenheit mehrere katastrophale Erdbeben und Tsunamis erlebt. Die Dissertation befasst sich mit dem Tsunami-Potenzial und der Bewertung der erhöhten Vulnerabilität entlang der Makran-Küste Pakistans. Der erste Teil der Arbeit umfasst die Bewertung des Tsunami-Potenzials durch eine Kreuz-analyse multidisziplinärer Proxies. Der zweite Teil befasst sich mit der Vulnerabilität und der vorläufigen Risikobewertung durch eine detaillierte Analyse von Tsunamimodellierungen und Überschwemmungsszenarios für verschiedene Gefahrenszenarien. Im dritten Teil wird der Versuch unternommen, die rätselhafte Dynamik des Tsunami-Ereignisses von 1945 am Pasni mit weiteren Modellierungen zu verstehen.

Für die Bewertung der Tsunami-Gefahr und des Tsunami-Potenzials wird eine integrierte Bewertung verschiedener Ansätze und Proxies durchgeführt. Sie umfasst eine umfassende Zusammenstellung, Überprüfung und Kreuzanalyse von geophysikalischen, probabilistisch-deterministischen Modellen, sedimentologisch-geomorphologischen Hinweisen für extreme Wellen und historischen Aufzeichnungen rund um die arabische Küste. Außerdem werden die Tsunamiite (Tsunamiablagerungen), die im schlimmsten Fall morphologische Veränderungen und Auswirkungen rund um das Arabische Meer aufweisen, modelliert, um das Tsunamipotenzial abzuschätzen. Diese morphodynamischen Veränderungen werden in Bezug auf Wellenhöhe, Wellenlänge, Fließtiefe, Fließgeschwindigkeit und Überschwemmungsausmaß rückwärts modelliert. Die Analyse ergab auch ein Wiederholungsintervall zwischen 500 und 1000 Jahren für ein Mega-Tsunami-Ereignis (≥12 m).

Der zweite Teil befasst sich mit der Vulnerabilität und der vorläufigen Risikobewertung durch eine detaillierte Tsunami-Erzeugungs- und Überschwemmungsanalyse für verschiedene Gefahrenszenarien. Dabei werden sowohl statische als auch dynamische Überschwemmungsmodelle für eine vergleichende Analyse und zum besseren Verständnis eingesetzt. Die Bewertung der Anfälligkeit der Makran-Küste, insbesondere der Städte Pasni und Gwadar im Detail. Auf der Grundlage der Bewertung des Gefährdungspotenzials werden für jede Stadt drei verschiedene Tsunamiwellenszenarien (7 m, 10 m, 15 m) modelliert. Zusätzlich zu den Simulationen werden stichprobenartige Beobachtungen der wichtigsten Gebiete in der Untersuchungsregion mit detaillierten Angaben zu Strömungsgeschwindigkeit und -tiefe vorgestellt. Die Tsunami-

Modellierung bewertet auch die Wirksamkeit des Frühwarnsystems, indem sie die Tsunami-Erzeugung, die Ankunft und die Evakuierungszeiten für Nahfeld- und Fernfeld-Tsunamis vergleicht.

Im dritten Teil wird versucht, vier rätselhafte Fakten des Tsunami-Ereignisses von 1945 an der Küste von Pasni zu verstehen. Dabei handelt es sich um i) eine Ankunftszeitverzögerung von 1-2 Stunden, ii) eine Wellenhöhe von ≥10 m, die im Vergleich zur Größe des Erdbebens außergewöhnlich hoch ist, iii) das Auftreten von drei Wellen und iv) die vorübergehende Rückbildung der Strandlinie oder die anfängliche Absenkung des Meeresspiegels. Darüber hinaus erklären die deterministischen numerischen Modelle verschiedener Studien nicht die in Berichten überlieferten Informationen, insbesondere nicht mit den Ankunftszeiten und der Wellenhöhe. Ihre Modelle erreichten keine Wellenhöhe von mehr als 5 Metern, begleitet von einer Verzögerung von über einer Stunde. Diese Diskrepanz führte zur Theorie, einen durch einen submarinen Erdrutsch ausgelösten Tsunami in Betracht zu ziehen. Wir diskutieren, dass das Erdbeben die einzige Tsunami-Quelle war, die in der Lage war, die berichteten Tsunami-Eigenschaften zu erklären. Die Faktoren, die zu der Verzögerung und der außergewöhnlich hohen Wellenhöhe beigetragen haben, werden erläutert. Kurz gesagt, wir argumentieren, dass das Phänomen der Reflexionsverstärkung zwischen den Küstenklippen und der Kontinentalschelfkante für all diese anomalen Werte verantwortlich ist.

In Kapitel 4 werden die Paläo-Tsunami-Ablagerungen (Tsunamiite) im Pasni-Gebiet vorgestellt, was die erste derartige Studie in diesem Bereich in Pakistan darstellt. Es wurden zwei Tsunamilagen gefunden, die älter sind als der Tsunamihorizont von 1945. Von diesen beiden ist das auf 1539 CE datierte Ereignis sehr nah an einem bereits 1524 CE gemeldeten Tsunami im Arabischen Meer. Das zweite Ereignis könnte maximal auf das 17. Jahrhundert BCE zurückgehen. Diese Ablagerungen müssen aber weiter untersucht werden.

Die Synthese der Arbeit schließt die Bewertung der Gefährdung einschließlich der Auswirkungen von Tsunamis entlang der pakistanischen Küste ab. Die Studie unterstreicht die Bedeutung umfassender Abwehr- und Sicherungsstrategien, um die Resilienz der Küsten zu verbessern und die Auswirkungen künftiger Tsunamis entlang der Küste zu minimieren. Als Ausblick ermutigen wir zu weiteren geowissenschaftlichen Forschungen zur Gefährdung der Küsten, um unser Verständnis dieser komplexen Phänomene zu vertiefen und die Katastrophenvorsorge und die Reaktionsfähigkeit in der Region zu verbessern.

Acknowledgments

My PhD journey is loaded with growth, joy and of course, challenges too. This journey would have never been possible without the contributions and support of several individuals and organizations from various walks of life. My sincere gratitude and acknowledgement to all those. I sincerely apologize for the unintentional omission of those who I forget to mention here.

My deepest appreciation and regards to Professor Dr. Klaus Reicherter for his continuous support, motivation, insights, advice, and kindness. Thank you for granting me flexibility and for trusting me to bring up my ideas into the project during my career at the Neotectonics and Natural Hazards Institute (NUG). You were scientifically and morally an inspiration to me.

I am greatly thankful to Dr. rer. nat. Gösta Hoffmann for his prompt and sincere support in shaping the project proposal and insights. Also, providing valuable assistance in facilitating my transition from Pakistan to Germany.

Special thanks to Madam Naghma Haider for her sincere contributions in handling institutional matters and enabling me for effortless navigation through bureaucratic hurdles to pass on. Her humbleness and sincerity are truly priceless, and I am indebted to her for her unwavering support and assistance throughout this journey. There are no proper words to convey my deep love and appreciation for you.

I extend my heartfelt gratitude to Dr. Sajid Ali and Family, a true friend of mine, who have always stood by my side and aided beyond their capacity. Their unwavering support and generosity have been invaluable throughout my journey. I thank you all for this.

I am deeply thankful to the DAAD (German Academic Exchange Service) for their generous financial support during my study and stay in Germany. Their support has been instrumental in enabling me to pursue my academic and research goals, and I am truly grateful for the other opportunities this scholarship has afforded me.

Sincere thanks to Mr. Jan Muhammad for rendering his best possible support to accommodate my field excursion in Pasni, Pakistan. His support is invaluable in facilitating the success of this important aspect of my research.

Sincere thanks to Ms. Sara Pena-Castellnou, for guiding and helping in processing the samples for radiometric dating. Ms. Vanessa Steinritz, Mr. Jochen Hürtgen, Xianghe Ji and Napoleon Njeng for their support in casual and official matters.

To my beloved wife (Farah Naz) and daughters (Rabia Rashid, Mahnoor Rashid, Aiza Rashid), who patiently stood by me all the way. You were engaged from the very first moment of this journey. The sacrifices you have made for me kept me stable, motivated, and confident to pursue my career. I feel incredibly blessed to have your presence in my life.

My parents (Ghulam Haider, Bashir Begum) and brothers (Zafar, Iqbal, Javed Iqbal, Pervaiz Iqbal, Azhar Iqbal, Yasir Iqbal) and their families, who made countless sacrifices and set aside their own needs to support my journey towards success in life. I am eternally grateful for your guidance and encouragement, which have been instrumental in shaping my personality today and fueling my ongoing growth. Despite lack of formal education, my parents, their tireless efforts, unwavering motivation, and endless love continue to inspire and propel me forward. Both of you passed away just before this phase of my research journey began. I deeply miss your presence and feel saddened by the realization that I must navigate this

accomplishment and celebration without you both. However, I believe that your souls will feel the gratitude and love that reside in my heart.

Table of Contents

Abstract vi
Kurzfassung viii
Acknowledgments x
Table of Contents xiii
1. Scope and Introduction 1
1.0 Motivation and societal relevance 1
1.1 State of the art and study gaps 1
1.2 Main Objectives 3
1.3 Thesis structure and brief 4
2. Tsunami Hazard assessment using a multi-proxy approach 6
2.0 Abstract 6
2.1 Introduction 6
2.2 Study area 8
2.2.1 Geodynamics 8
2.2.1 Seismicity 8
2.2.2 Submarine landslide potential 11
2.3 Methodology and Data 12
2.4 Results 14
2.5 Discussion 19
2.6 Conclusions 22
3. Tsunami hit the Makran Coast repeatedly; evidence for extreme wave events at the Pasni Coast, Pakistan 23
3.0 Abstract 23
3.1 Introduction 23
3.2 Historic Archive 26

3.3 Geological and Archeological Archive 1524 AD tsunami event 26
3.4 Methodology and Results 27
3.4.1 Field work and Laboratory analysis 27
3.4.2 Tsunamites Morpho-flow dynamics 27
3.4.3 Tsunami Modelling and Simulation 30
3.5 Origin: Shell middens or natural extreme wave action 32
3.6 Discussion 34
3.7 Conclusions 37
3.8 Outlook 38
4. Static Inundation Analysis of Karachi, Gwadar, Pasni and Ormara 39
4.0 Abstract 39
4.1 Introduction 39
4.2 Approach and Models 40
4.2.1 Bathtub Model 40
4.2.2 Standing wave model 41
4.2.3 Data and parameters 41
4.3 Modeling Limitation 42
4.4 Results and comparative analysis 43
4.4.1 Karachi: 45
4.4.2 Pasni 45
4.4.3 Ormara and Gwadar 47
4.5 Discussion 52
4.6 Conclusion 53
5. Dynamic inundation and vulnerability analysis of major cities along the Makran Coast 54
5.0 Abstract 54
5.1 Introduction 54
5.2 Tectonic settings and Associated Seismicity 55
5.3 Methods 56
5.3.1 Establishing the tsunami wave potential in the Arabian Sea 56
5.3.2 Source Type and Parameters 57
5.3.3 Tsunami Modeling and Data Sets 58
5.3.4 Vulnerability analysis 59
5.4 Results and interpretations 60

5.4.1 Pasni scenarios 60
5.0.1 Gwadar scenarios 60
5.0.2 Vulnerability Analysis 63
5.1 Discussion and Conclusions 64
6. The case of 1945 Tsunami; wave height, number of waves and arrival time 68
6.0 Abstract 68
6.1 Introduction 68
6.2 Seismic sources and tsunami potential 70
6.3 Methodology and Data 72
6.4 Results and Analysis 74
6.5 Discussion 77
6.6 Conclusions 79
7. Re-evaluation and Synthesis 80
7.0 Concluding discussion 80
7.1 Outlook 81
References 84
List of Figures 138
List of Tables 142
List of Pre-Publications 144

1. Scope and Introduction

1.0 Motivation and societal relevance

The motivation to conduct the titled research stems from the critical need to safeguard lives, property, and ecosystems against the significant threat posed by tsunami hazards. As of the current understanding, the coastline of Pakistan is considered one of the most hazardous coastlines around the Arabian Sea due to its proximity to the seismically active Makran Subduction Zone (MSZ), which has the potential to generate large-magnitude earthquakes and subsequent tsunamis. Historical events, such as the 1945 Makran tsunami, serve as stark reminders of the devastating impacts these natural disasters can have on coastal communities, infrastructure, and economies. Despite this high risk, the region severely lacks comprehensive investigations into extreme wave events, including their recurrence intervals, potential magnitudes, and coastal impacts. This glaring gap in scientific understanding has motivated us to contribute to the body of knowledge on tsunami hazards in the region.

By conducting a detailed tsunami hazard and vulnerability assessment, we aim to contribute some valuable insights that could bridge the existing technical gaps. The findings may provide a scientific foundation for developing effective disaster risk reduction strategies, enhancing emergency response planning, and informing policy development. Ultimately, this work seeks to enhance the overall resilience of Pakistan's coastal areas, ensuring that communities are better prepared to withstand and recover from future tsunami events.

1.1 State of the art and study gaps

1.1.1. Geodynamics of Hazard Source (spatial and parametric uncertainties)

Significant progress has been made in understanding marine geo-hazards in the North Arabian Sea (NAS) and the Makran Subduction Zone (MSZ), yet several critical knowledge gaps persist, hindering a comprehensive assessment of seismic and tsunami risks in the region. The tectonic complexity of the area, particularly the low-angle subduction of the MSZ, remains poorly understood. This is largely due to insufficient geodetic and seismic instrumentation, as well as a lack of high-resolution scans that could provide deeper insights into stress regimes, decollement geometry, and strain segmentation. These factors are crucial for accurately modelling the behavior of the subduction zone and predicting potential earthquake and tsunami events. One area of uncertainty is the geodynamics of the earthquake cluster located south of Pasini offshore. The mechanisms driving this clustering and their implications for regional seismic hazards are not well understood. Additionally, a review of existing literature reveals that key geological features, such as the nature of the decollement and the Sonne Fault, remain enigmatic. Coastal geodetic measurements,

which are essential for monitoring crustal deformation and strain accumulation, also present unresolved mysteries. These measurements are critical for understanding how stress is distributed and released along the subduction zone, yet the data available is either limited or inconclusive.

Further studies are urgently needed to explore the geodynamics of these features in more detail. Such research could significantly enhance our ability to estimate the earthquake and tsunami potential of the region. Advanced geophysical surveys, improved seismic networks, and high-resolution imaging techniques could provide the necessary data to better understand the tectonic processes at play.

1.1.2. Earthquake and Tsunami return period (Uncertainties in estimations)

The uncertainties in estimating the return periods of earthquakes and tsunamis across different scales and intensities highlight a significant challenge in seismic and tsunami hazard assessment. For instance, the wide range of conflicting and inconsistent estimates for the recurrence of major seismic events, such as those with a moment magnitude (Mw) of 8 or greater, spans from 70 to 2500 years. This variability underscores the complexity of predicting when and where such events might occur. Additionally, the potential for both single-segment and multi-segment ruptures, particularly for extremely high-magnitude events ($Mw \leq 9.2$), further complicates the picture. Multi-segment ruptures, which involve the simultaneous breaking of multiple fault segments, can lead to significantly larger and more destructive earthquakes and tsunamis than single-segment ruptures. These uncertainties emphasize the need for more refined probabilistic seismic models that can better account for the variability and complexity of seismic events. To achieve this, it is essential to integrate multiple approaches and proxies, such as paleo-seismic studies, which provide long-term records of past earthquakes through geological evidence; geodetic data, which measure crustal deformation and strain accumulation; field studies, which offer detailed observations of fault behavior and surface ruptures; and historical data, which document past seismic events and their impacts. By combining these diverse sources of information, scientists can develop more accurate and comprehensive models that improve our understanding of seismic hazards and enhance our ability to prepare for and mitigate the risks associated with earthquakes and tsunamis.

1.1.3. Deterministic Modelling (parametric association)

Deterministic tsunami hazard assessments face significant limitations due to the unresolved and highly variable nature of tsunami source parameters. For a given seismic event of a specific magnitude, there is considerable scatter in key source characteristics such as fault slip distribution, rupture depth, rupture thickness, and dip angle. These variations arise from the complex geodynamics and heterogeneous geological conditions that influence how earthquakes and other tsunami-generating mechanisms occur. For example, the same magnitude earthquake can produce vastly different tsunami impacts depending on whether the rupture occurs in a shallow or deep fault, the amount of slip, or the geometry of the fault plane. This variability makes it challenging to accurately predict tsunami behavior and impacts using deterministic models alone.

1.1.4. Probabilistic Tsunami Hazard Assessment (data gaps)

Probabilistic Tsunami Hazard Analyses (PTHA) in the region are currently limited by their heavy reliance on seismic sources, such as earthquakes, Also, this approach suffers a setback on aspects of data completeness and highest intensity event. Moreover, it largely overlooks non-seismic sources like submarine landslides and volcanic activity. This oversight leads to an underestimation of the return periods of tsunamis and the correlations between different hazard sources. For example, submarine landslides, which can be triggered by seismic activity or occur independently due to slope

instability, have the potential to generate tsunamis with significant local impacts. Similarly, underwater volcanic eruptions, particularly in regions with active volcanic arcs, can produce tsunamis through mechanisms such as caldera collapses, pyroclastic flows, or explosive eruptions. Ignoring these sources in PTHA results in an incomplete understanding of the tsunami hazard landscape, potentially leaving coastal communities underprepared for low-probability but high-impact events.

1.2 Main Objectives

i. **Tsunami hazard assessment**:

This component focuses on analyzing the tsunami hazard, including the recurrence intervals and intensity of potential tsunami events, using a multi-proxy approach. This involves integrating diverse datasets such as historical records, geological evidence (e.g., tsunami sediment deposits), geophysical findings, and probabilistic and deterministic modeling and findings. By compiling and cross-analysis of these proxies, the study aims to develop a comprehensive understanding of the tsunami hazard in the region, including the likelihood of future events and their potential impacts. This approach helped to identify high-risk zones and provide a scientific basis for developing mitigation strategies.

ii. **Tsunamites exploration**:

Fieldwork is conducted to identify and study tsunami sedimentary deposits (tsunamites) left behind by past tsunami events. These deposits, often found in coastal and near-shore environments, provide critical evidence of palaeo-tsunami events, including their frequency, magnitude, and dynamics. By analyzing the sedimentology, stratigraphy, and geochemistry of these deposits, the study aims to reconstruct the characteristics of past tsunamis, such as wave height, run-up, and inundation extent. This information will help refine estimates of recurrence intervals and improve our understanding of the long-term tsunami hazard in the region.

iii. **An attempt to resolve the debate on 1945 Tsunami wave height and time delay**: The 1945 Makran tsunami remains a subject of debate, particularly regarding its wave height and the time delay between the earthquake and the tsunami's arrival. This study aims to address these uncertainties by mapping the inundation extents of the 1945 tsunami using field evidence and historical accounts. Numerical modeling is employed to simulate various scenarios of wave height and time delay, which then were validated against the mapped inundation extents. By resolving these uncertainties, the study provided a better picture of the 1945 event, which can serve as a benchmark for assessing future tsunami risks.

iv. **Tsunami vulnerability assessment of the Pasni, Gwadar towns and surrounding areas**:

This component focuses on assessing the vulnerability of two important coastal towns, including Pasni and Gwadar, to tsunami inundations. Using numerical

modeling, the study simulated a range of tsunami scenarios with varying wave heights and wavelengths to estimate potential inundation extents and impacts. The vulnerability assessment considered factors such as population density, infrastructure, land use, and socio-economic conditions to identify areas and communities at greatest risk. The findings will inform disaster preparedness and response planning, helping to enhance the resilience of these coastal areas to future tsunami events.

v. Early warning assessment of prevailing system

The effectiveness of the installed tsunami early warning system is evaluated based on modeling, simulated results, and recent practices of issuing early warning alerts for three tsunami case studies (one near-field and two far-field). Both near-field and far-field scenarios are examined, with a focus on the detection process and the issuance of early warning alerts in relation to wave arrival times.

1.3 Thesis structure and brief

Chapter 1: Scope and Introduction

The chapter presents a brief overview of motivation and the main objectives of this study. It also presents an outline of the thesis structure.

Self-assessment: RH contributed 95%

Chapter 2: Tsunami Hazard assessment using a multi-proxy approach.

It addresses the tsunami potential in the Arabian Sea. Previously, tsunami hazard assessment is carried out either by probabilistic or deterministic approach or by both in an integrated form. Also, the studies carried out solely for seismic hazard are incorporated. Along with compiling the findings from these approaches, we compile tsunamites record around the Arabian Coastline to test any correlation in terms of tsunami potential and recurrence interval. The tsunamites demonstrating the most severe morphodynamics are modeled to estimate the potential of tsunami waves in the Arabian Sea. These morphodynamics are modeled in terms of flow depth, flow velocity, and inundation extents.

Self-assessment: RH contributed ~90%

Chapter 3: Evidence for extreme wave events at the Pasni Coast, Pakistan.

The chapter presents findings of fieldwork conducted during the research period. This is the first such study conducted within this domain in Pakistan. A reconnaissance fieldwork is conducted along most of the coastline, followed by detailed work in Pasni town and its surrounding area. We report potential paleotsunami deposits or tsunamites in the Pasni area. These deposits represent two different tsunamite layers older than that of the 1945 Tsunami layer. The cumulative dating results bracket one event between 1444–1635 CE and the second event between 1984-1653 BCE.

Self-assessment: RH contributed ~90%

Chapter 4: Static Inundation Analysis of Karachi, Gwadar, Pasni and Ormara.

The chapter presents a preliminary vulnerability analysis of four major cities along the Makran Coast of Pakistan: Karachi, Ormara, Pasni, and Gwadar. The analysis is carried out using a bathtub model and the standing wave model. Despite employing a relatively nascent approach, these models effectively outline the vulnerable areas within each city, shedding light on potential risks and aiding disaster preparedness and mitigation efforts along the coastal region.

Self-assessment: RH contributed >90%

Chapter 5: Dynamic inundation and vulnerability analysis of major cities along the Makran Coast

We comprehensively present the enhanced tsunami vulnerability assessment along the Makran Coast, particularly for Pasni, Gwadar, and surrounding areas. A variety of tsunamigenic earthquake scenarios are modeled and simulated. The mechanism of tsunami generation, propagation, wave interaction (reflection, refraction, amplification), and impact of the tsunami source are analyzed. Moreover, the impact of these dynamics on inundation in Pasni and Gwadar areas is analyzed. Furthermore, we assess the effectiveness of the early warning system in place by comparing the timings of tsunami generation, alert issuance, arrival, and evacuation.

Self-assessment: RH contributed >90%

Chapter 6: The case of 1945 Tsunami; wave height, arrival time and number of waves.

The 1945 tsunami reached the Pasni Coast approximately 90 minutes after the earthquake, suggesting a secondary post-earthquake tsunami generation, particularly involving a submarine landslide. The reported tsunami height is around 12 meters, with three major waves arriving about 90 minutes after the earthquake. Despite attempts by several researchers to model this scenario, their results cannot explain these aspects. Their models suggest the tsunami should reach Pasni within 20 minutes from the 1945 earthquake rupture, with a maximum wave height of 5 meters. In this chapter, arguments based on earthquake source parameters, supporting the earthquake as the sole tsunami source for the 1945 event, are presented. Additionally, we discuss factors influencing the delay and unusually high wave height.

Self-assessment: RH contributed ~90%

Chapter 7: Resume

The chapter presents a concise overview of the key findings of this research and comprehends conclusions from all the chapters.

Self-assessment: RH contributed 100%

Chapter 8: Outlook

This section provides an overview of the research and data gaps, and unresolved issues of this research within the study area. Further, there are suggestions to address these challenges in future research.

Self-assessment: RH contributed 100%

2. Tsunami Hazard assessment using a multi-proxy approach

This chapter is an amalgamation of the two following papers.

- ***Haider, R**., Ali, S., Hoffmann, G., Reicherter, K., 2023. A multi-proxy approach to assess tsunami hazard with a preliminary risk assessment: A case study of the Makran Coast, Pakistan. Mar. Geol. 107032. https://doi.org/https://doi.org/10.1016/j.margeo.2023.107032*
- *Gardezi, S.A.H., Luan, X., Sun, Z., **Haider, R**., Zhang, Y., Qiu, Q., Raveendrasinghe, T.D., 2024. Geo-hazards in the North Arabian Sea with special emphasis on Makran Subduction Zone. Earth-Science Rev. 255, 104846.* https://doi.org/https://doi.org/10.1016/j.earscirev.2024.104846

2.0 Abstract

Tsunamis and cyclones are sea-borne hazards capable of inundating vast coastal areas. In this chapter, these hazards on Pakistan's coast are being assessed and estimated, along with a preliminary inundation analysis. Tsunami hazard is evaluated by synergising five approaches or proxies: (i) probabilistic tsunami hazard assessment (PTHA); (ii) deterministic tsunami hazard assessment (DTHA); (iii) geophysical-seismic (2-D thermal modelling), (iv) sedimentary tsunami deposits (tsunamites) and (v) the historical record. The analysis shows the recurrence interval for a mega-tsunami event (≥12 m) is between 500 and 1000 years.

2.1 Introduction

Tsunamis, cyclones and rising sea levels are the natural hazards to coastal areas. In the Indian Ocean, the 1998 Papua New Guinea Tsuanmi and the 2004 Indian Ocean Tsunami are some of the major catastrophic events that resulted in around 0.27 million casualties and more than USD 14 billion in property loss (Frank and Husain, 1971; Kalsi and Gupta, 2003; Bell, 2011). In spite of such huge losses, the lessons learned from these events are not widely anticipated on the mitigation side (Løvholt, 2017). In this regard, the Makran Coast of Pakistan is also poorly prepared, as the life and property losses during the 1945 tsunami and the cyclones of 1998, 1999, 2007, 2010 and 2021 reflect a dejected level of preparedness and resilience. Along the coastline of Pakistan, more than 24 million

people are exposed to these hazards (Figure 2.1). Another point of concern is the Karachi Nuclear Power Plant (KANUPP) at the coast near Karachi, which may create a cascading catastrophe similar to the 2011 Fukushima Daiichi nuclear disaster by releasing radioactive material in the ocean and atmosphere.

The historic record of tsunamis along the coast is perplexing due to the scarcity of historical records and the palaeo-dynamics of extreme wave events, which impedes hazard assessment. Further, the study area lacks field investigations for the palaeo-extreme wave events to approximate their recurrence intervals and coastal impacts. Significant exploratory work has been carried out along Oman's neighboring coastlines (Donato et al., 2008, 2009; Pilarczyk et al., 2011; Hoffmann et al., 2011, 2013, 2014, 2015, 2020; Koster et al., 2014), Iran (Shah-Hosseini et al., 2011; Vaziri et al., 2016) and India (Sangode & Meshram, 2013; Bhatt et al., 2016; Gandhi et al., 2017; Prizomwala et al., 2015, 2018, 2021, 2022), where sedimentary deposits (tsunamites) from extreme wave events are reported. These pieces of evidence suggest that the northern Arabian coastline was repeatedly hit by extreme waves. These extreme events are mostly attributed to the tectonic and climatic settings of the region. From a tectonic perspective, the Makran Coast is highly susceptible to tsunamis and the Makran Subduction Zone (MSZ) is the main source of tsunamigenic earthquakes. Since 1945, the coast has witnessed two tsunamigenic earthquakes; a major one in 1945 (Mw 8.1) claiming some hundred human lives (Pendse, 1946; Hoffmann et al., 2013) and a minor tsunami in 2013 (Mw 7.7) with no losses (Heidarzadeh and Satake, 2014b).

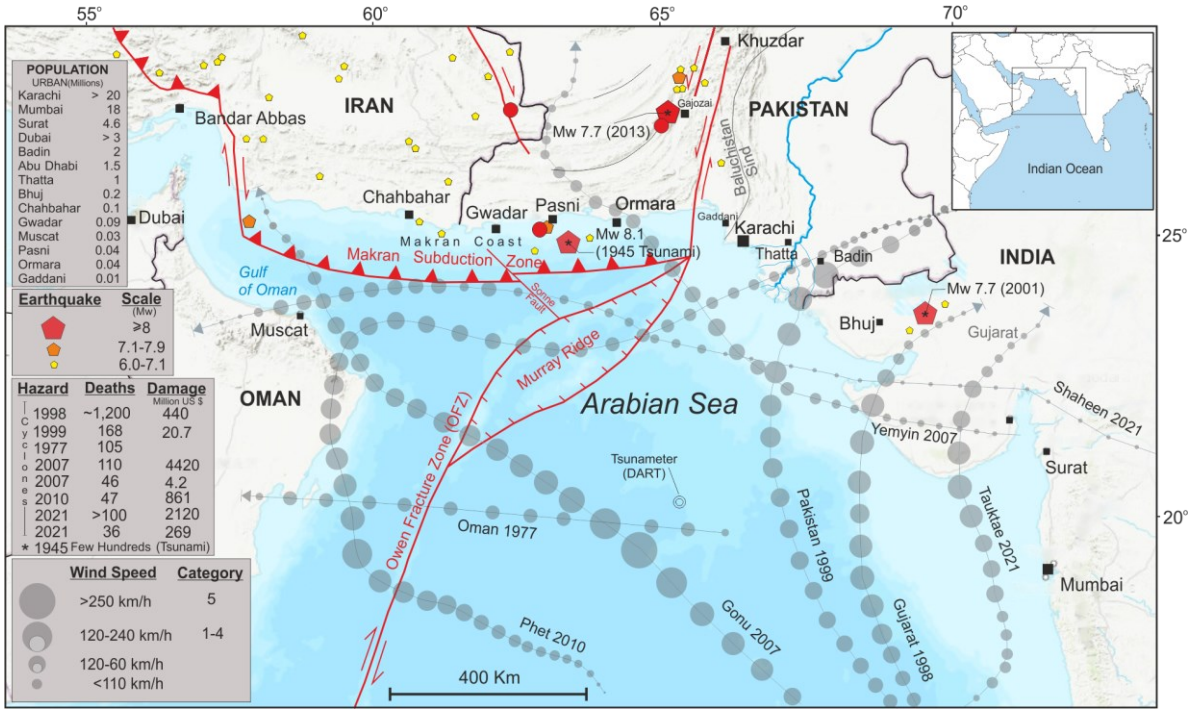

Figure 2.1: Location map showing the regional plate tectonic setting (red) and the major cyclones tracks (gray) which hit the coasts in the Arabian Sea. The size of the grey circle on the cyclone's tracks corresponds to the Saffir-Simpson Hurricane Scale. Data sources: International Best Track Archive for Climate Stewardship-IBTrACS (Knapp et al., 2010). Earthquake data: International Seismological Centre (ISC-2020). The figure also includes the cyclone tracks and associated losses which is also a major hazard in the region.

So far, at the Makran coast, either a deterministic or probabilistic approach is used to assess the tsunami hazard. The probabilistic approach is considered mature (Behrens et al., 2021) due to the advantage of equating the contribution of possible small and large events and of treating different sources of uncertainty (El-Hussain et al., 2018). On the other hand, the deterministic approach

considers a specific scenario that involves various components, including (i) source type and its parametrization; (ii) modelling tsunami generation and its propagation in shallow and deep ocean; and (iii) simulation of coastal inundation (Heidarzadeh et al., 2009b). For coastal engineering, a deterministic approach is considered more useful as it allows the derivation of the worst-case scenario (max. wave height, inundation extent and depth) to design an engineering structure and also avoids the complications associated with probabilistic analysis. For near field tsunamis, the problems with these approaches are associated with large data gaps, the maximum hazard potential and its spatial distribution. Furthermore, the former approach also entails knowledge gaps, assumptions and uncertainties. Also, there is no single accepted way of defining the worst-case scenario. Multidisciplinary and multiproxy approaches improve hazard and risk assessment (Koshimura et al., 2014; De Martini et al., 2021; Röbke et al., 2013, 2015, 2016, 2018). Regarding integrated analysis, the Makran Coast probabilistic and deterministic approaches are integrated for hazard and risk assessment by (Khan et al., 2003; Salmanidou et al., 2019; Rashidi et al., 2020; Yang et al., 2022). Here, we compiled and integrated five different approaches (geophysical, sedimentological-geomorphic, probabilistic modelling, numerical modelling and historical record), which we called a synergic approach for hazard assessment. As each approach has its own limitations, synergic analysis provides better outcomes and a higher level of confidence.

2.2 Study area

2.2.1 Geodynamics

The geodynamics of the study area is evolving from the interaction of three tectonic plates: the Eurasian, Indian, and Arabian plates (Figure 2.2 and Figure 2.3). The Eurasian plate is further segmented into micro plates, known as "blocks." Similarly, the Arabian Plate also has a submarine microplate known as the Ormara plate (Kukowski et al., 2000). The tectonic accommodation between these plates is complex and depends on the crust type at the converging fronts, the relative speed and the direction of plate motion. Plate interactions are variable, but along some boundaries certain patterns can be observed (Figure 2.2).

The rate of spreading at the mid-oceanic ridge (Red Sea) gradually increases from 7.1±5.0 mm at the north to 23.53±0.2 mm to the south at Sheba Ride (ArRajehi et al., 2010). This pattern of divergence is likewise accommodated at the Makran and Zagros subduction zones with average dipping of 3 degrees (Kopp et al., 2000), 2 degree (White and Louden, 1982). The convergence rate increases from 4±2 mm in the Persian Gulf to 19±2 mm in the Gulf of Oman (Vernant et al., 2004). The plate dynamics at the eastern part of the MSZ are anomalous, as the GPS velocity at the Pasni Coast is about half the speed of its eastern and western parts (Khan et al., 2008), which reflects a partial locking or the high-friction subduction zone. The Arabian Plate forms transform boundary with the Indian Plate with a relative motion of 3±1 mm/y (Reilinger et al., 2006; Fournier et al., 2008, Rodriguez et al., 2011).

2.2.1 Seismicity

Submarine earthquakes have triggered around 80% of the total tsunami events documented globally (Harbitz et al., 2014; Løvholt, 2017). The remaining 20% are caused by landslides, volcanos and meteoric impacts in water bodies (Behrens et al., 2021). Overall, the study area is moderately seismic, but events like the 1945 tsunamigenic earthquake (Mw: 8.1) have created uncertainty. The seismicity along the MSZ is not uniformly distributed; the western part of the MSZ (offshore Iran) is relatively silent as compared with its eastern part (offshore Pakistan). The silence in the western Makran

indicates either aseismic subduction or the interlocking of plate boundaries, which can generate great earthquakes with long recurrence intervals (Byrne et al., 1992). Moreover, Abbasi et al. (2024) identified a low-velocity, highly anisotropic layer in the western MSZ, characterized by low seismic velocities, high Vp/Vs ratios (2.0), and a low-strength shear zone at the plate interface. Mehrdar et al. (2025) indicated the presence of an intracrustal low-velocity layer beneath the Zagros Mountains. Geodetic measurements show 19.5 mm/y convergence (Vernant et al., 2004), therefore it is not locked. The Eastern MSZ is seismically active and most of this activity is attributed to the Sonne Fault (Kukowski et al., 2000). Smith et al. (2012) relates this seismicity to the nature of the decollement. Habib et al. (2025) analyzed gravity and seismic source parameters, uncovering contrasting stress regimes across subduction zones and their associated tectonic elements. The decollement in the south-west of Pasni is brittle as indicated by high seismic velocities (<4.4 km/s). The brittle behaviour is due to the absence of soft sediments (very thin or zero) in contrast to its western part. The velocities of these sediments are comparable to those observed at depth in the December 2004 Sumatra rupture area. The thermal modelling of MSZ shows that it has a potential to trigger an Mw 9.2 earthquake (Smith et al., 2012). Another thermal modelling study shows its potential as Mw 8.65 ± 0.26 and 8.75 ± 0.26 in western (Iran) and eastern (Pakistan) Makran respectively (Khaledzadeh and Ghods, 2022). Cheng et al. (2024) used GPS velocity and accretionary prism rheology through forward modelling to estimate a potential Mw 8.7 for a single-segment rupture and Mw 9.2 for a multisegmented rupture. Chen et al. (2024) quantitatively investigated how earthquake rupture speed and direction influence tsunami hazards in the Makran region using fault morphology, InSAR measurements, and high-resolution bathymetry.

Regarding the 1945 tsunamigenic earthquake (Mw: 8.1), Laane and Chen (1989) through P-wave first motion studies suggested that the event has a large component of normal faulting instead and proposed a lithospheric normal faulting event usually associated with down-going slabs of old age. In contrast, the detailed studies on the focal mechanism of the 1945 Makran earthquake by Byrne et al. (1992) show that it is related to a thrust event. Their dislocation models, body waveform inversion and moment estimates indicate that the earthquake ruptured 100 to 200 km of crust along the arc in a down-dip direction. The Murray Ridge has been the easternmost region of small earthquakes due to right-lateral strike-slip and normal faulting (Banghar and Syke, 1981). Quittmeyer et al. (1979) confine the seismicity only along its north-eastern half. The seismicity along the OFZ is also low to moderate, the maximum magnitude recorded is Mw 5.8 earthquake (Rodriguez et al., 2011).

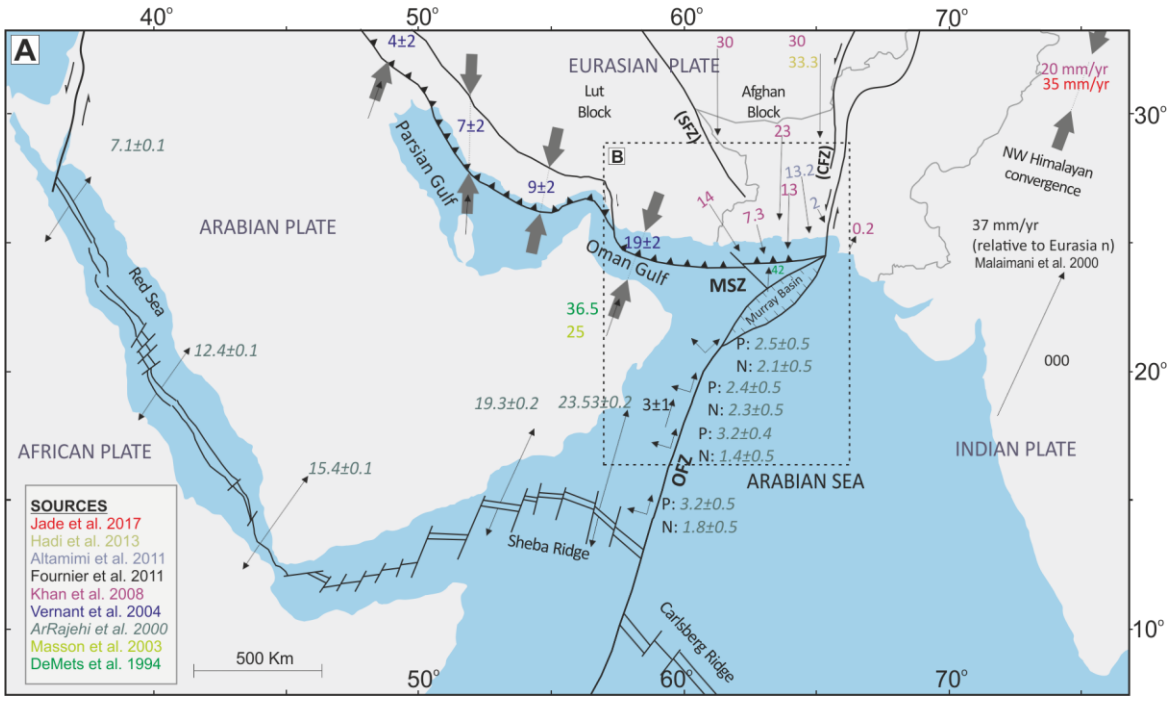

Figure 2.2: Figure showing the tectonic setting and the geodetic motions of the study area. All the velocity vectors are in millimeters (mm). Black Arrows (thin): Speed vector, P: perpendicular vector, N: normal vector, grey arrows (thick): convergence vectors. Different numbers against the vectors show reporting by different researchers, as indicated by different colours in the legend. Makran Subduction Zone (MSZ), Chaman-Ornach Nal Fault Zone (CFZ), Owen Fracture Zone (OFZ), Sistan Fault Zone (SFZ), Sonne Fault (SF).

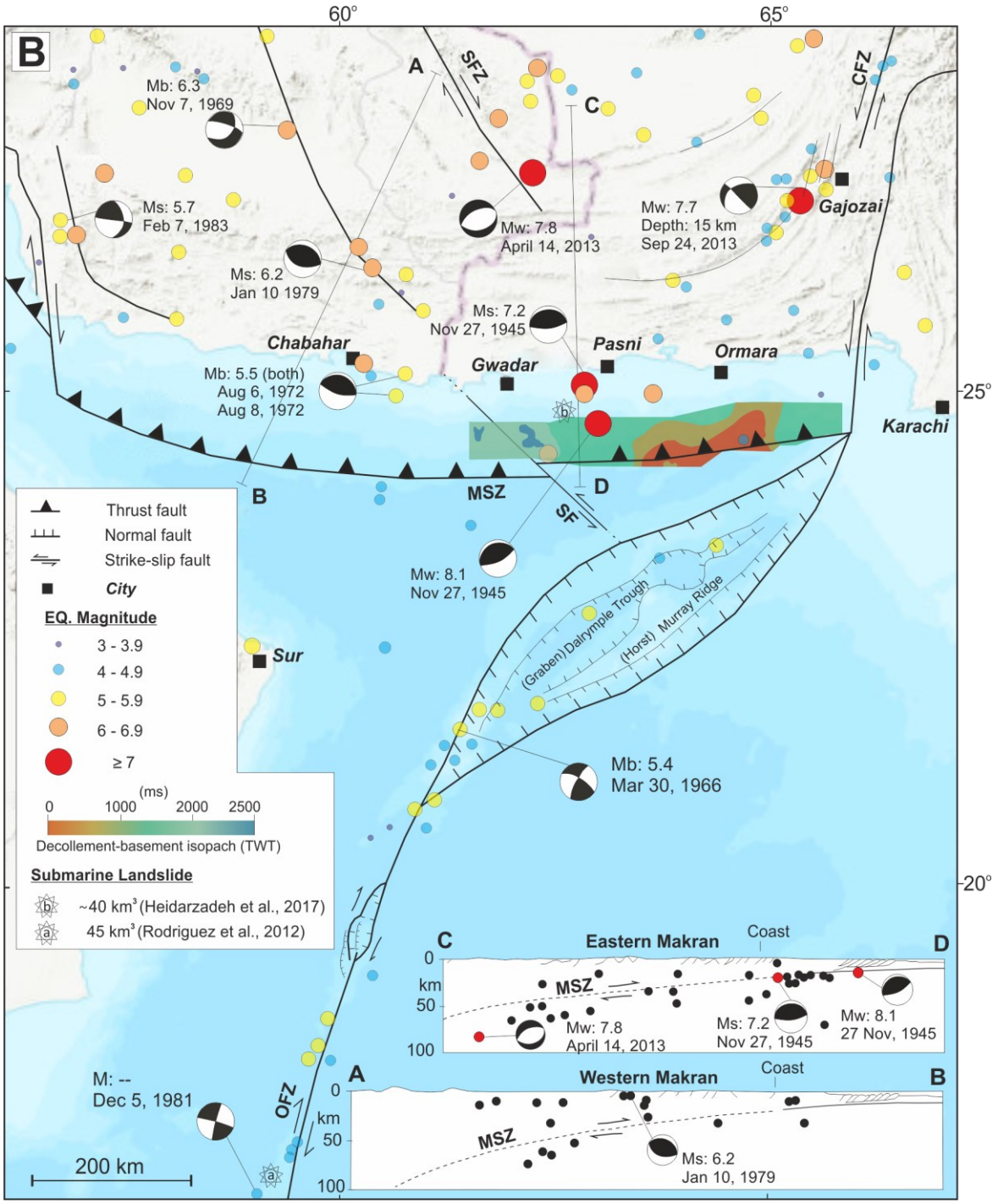

Figure 2.3: Seismo-tectonic map of the region Earthquake focal mechanisms are compiled from Quittmeyer and Kafka (1984); Gordon and Demets (1989); Byrne et al., (1992); Fournier et al., (2001). The simplified two-way travel time (TWT) map is from Smith et al., (2012) showing the nature of the horizon between the decollement and basement. The cross-sections are integrated from Byrne et al. (1992).

2.2.2 Submarine landslide potential

An underwater landslide has the potential to displace a large amount of water, which generates a set of waves formally known as a tsunami (Heidarzadeh and Satake, 2017; Röbke et al., 2018; Latcharote et al., 2018; Salmanidou et al., 2019). Mostly, under normal conditions, loose submarine sediments can withstand an angle of 12°-30° (Salaree and Okal, 2015) but other factors, especially seismic shaking can trigger a landslide with even lower steepness. The Arabian Sea has a considerable

potential for the huge offshore landslides due to a 7 km-thick sedimentary sequence in the Makran Accretionary Prism (MAP) (White and Louden, 1982) and a ~500 m thick pelagic drape on Owen Ridge (Shipboard Scientific Party, 1989). The high erosion rate is interpreted for these thick sequences (Kukowski et al., 2001; Ellouz et al., 2007).

The tsunamis of 1945 and 2013 are the most recent examples from the study area, which have been hypothesised to have been generated by offshore landslides (Heidarzadeh and Satake, 2014; Hoffmann et al., 2014). In the 1945 tsunami, there was a 3 hours delay between the earthquake and the first tsunami wave at Pasni, situated at about 40 km from the epicentre (Pendse, 1946). To explain this delay, Yanagisawa et al. (2009) through inverse numerical modelling argued for a 3 hour delay due to multi-wave reflection and amplification phenomena. Heidarzadeh and Satake (2017) simulated three possible secondary sources (splay faulting, delayed ruptures, and submarine landslides) and proposed that only a submarine landslide having a volume of ~40 km3 (Figure 2.3) can reproduce the near-field tsunami of 1945 at Pasni and Karachi.

On the bathymetric map of MAP, Kukowski et al. (2001) and Ellouz et al. (2007) identified many circular and linear slump scars. Grando and McClay (2007) interpreted slumping phenomena on the seismic lines. Slumping at MAP is generally noticed on the frontal, south-dipping folded limb, where the thrust faults propagated by folds have achieved significant height and relief. Mouchot et al. (2010) suggested that in this active setting, slope instabilities seem frequent but limited in size. Platt et al. (1985) attributes the slumping and the very rough morphology of the upper slope to the active uplift and actual tension. The mass movements ultimately settle in the deeper parts as turbidites. The age of the Late Quaternary turbidite sequence (sedimentary cores) and earthquake record show a good correlation (Prins et al., 2000; Bourget et al., 2010).

Along the Owen Ridge, Fournier et al. (2011) and Rodriguez et al. (2012, 2013) mapped the several types of giant mass failures along the western side of Owen Ridge by using the multibeam bathymetry and sediment echo-sounder. Southern Owen Ridge displays the largest failure area and the most voluminous landslides and the highest estimated volume of activated material during a landslide is up to 45 km3 (Figure 2.3). Their research shows that the mass-wasting frequency is low due to the chaotic nature and slow sedimentation rate, but earthquakes are more frequent, implying that mass failures are severely limited by sedimentation rates. In the eastern most part, the landslide potential of the Indus Delta is the least studied. The Indus River prior to modern damming used to supply at least 250 Mt/year to the Arabian Sea (Milliman and Syvitski, 1992), other estimates emphasise a larger range of 100 to 675 Mt/year (Ali and De-Boer, 2008). Since the last glaciation, the Indus River has shed about 4,050–5,675 km3 of sediment into the Arabian Sea and about half of the stored sediments lie offshore on the shelf and in the submarine Indus canyon (Clift and Giosan, 2014). The massive accumulation of sediments in the offshore and canyon areas makes the delta vulnerable to landslides and necessitates further investigation.

2.3 Methodology and Data

Multidisciplinary and multiproxy approaches improve hazard and risk assessment (Koshimura et al., 2014; De Martini et al., 2021; Röbke et al., 2013, 2015, 2016, 2018). At the Makran coast, PTHA and DTHA are used together by (Khan et al., 2003; El-Hussain et al., 2018, Salmanidou et al., 2019; Yang et al., 2022; Zafarani et al., 2022). We compiled and integrated five different approaches (geophysical, PTHA, DTHA, sedimentary tsunami deposits, and historical record), which we called a synergic approach for hazard and risk assessment. The data and workflow are summarised in Table 2.1 and Figure 2.4, respectively.

Table 2.1: Approaches, methodologies and data used.

	Approach	Methodology/ Model	Data/ Reference
Seismic hazard	Probabilistic	Poissonian model, (Cornell and Vanmarcke, 1969)	Khan et al. (2003)
		Cornell–McGuire (1968–1976)	Waseem et al. (2019, 2020)
		UBC 97 (International Conference of Building Officials, 1997)	Ahmed et al. (2019)
	Deterministic	Ambraseys and Boomer (1991) Model	Khan et al. (2003)
Tsunami hazard	Probabilistic	Synthetic tsunami-EQ catalogue spanning over 3 million years	Hoechner et al. (2016)
		logic tree technique	Zafarani et al. (2022)
	Deterministic	Tsunami triggered by faults and landslide-based parameters	Compiled: deterministic tsunami models (Table 2.2)
	Historical Tsunami	Makran historical and instrumental great earthquakes with Mw ≥ 6.5	Updated after Heidarzadeh et al. (2008)
	Tsunamites Record	Compilation of tsunamites discovered at different coasts along the Arabian Sea	Compiled: 14 studies/ 8 inferred tsunamites

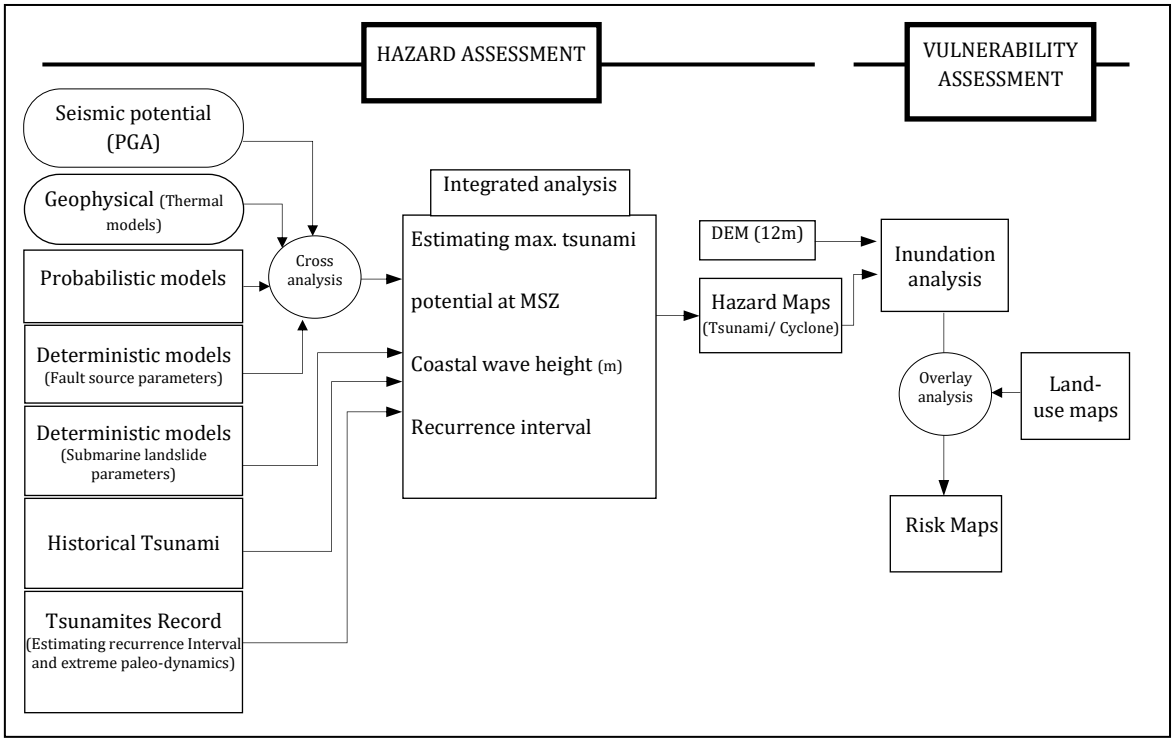

Figure 2.4: *Flowchart showing sequential order of various processes used for hazard and risk assessment.*

The problems with PTHA and DTHA are associated with large data gaps, maximum hazard potential determination, spatial distribution, assumed and uncertain variables and different computational types (Berryman, 2006; Behrens et al., 2021). To improve hazard assessment, the PTHA and DTHA results are compared with the more meticulously evaluated seismic hazard potential (PGA), which includes weightage from the area's tectonic elements and recurrence intervals. Further, analysis of the recurrence interval is improved by the compilation and correlation of historical records (Table

2.4) and tsunamites records discovered at different sites around the Arabian Sea (Table 2.5). For these tsunami deposits, MSZ is inferred as the tsunami source except for one mentioned in the table.

2.4 Results

The results from the multi-proxy approach imply that the MSZ has the potential to trigger ≥Mw 9.0 tsunamigenic earthquake with a recurrence interval between 500-1000 years, which may generate a tsunami up to ≥15 m (Figure 2.5, Table 2.2 and Table 2.5). The region south of Pasni is more susceptible to tsunamis due to high seismic activity. In this area, the rigid decollement (Smith et al., 2013), relative geodetic plate motions at Pasni (Figure 2.2) and differential motion(s) between the Sonne fault and MSZ (Kukowski et al., 2000) indicates stress accumulation and release in the area. In this regard, further investigations and evaluation are highly recommended. The seismic and tsunami hazards are very low for a 50-year recurrence interval. The historical record of tsunamis is insufficient, and data credibility may be another issue for result validation; however, a compilation of tsunamites bordering the Arabian Sea shows that these events occur every 500 years. For hazard assessment, the estimation of underwater landslides is yet another important milestone to cover, and it has serious implications on the recurrence interval.

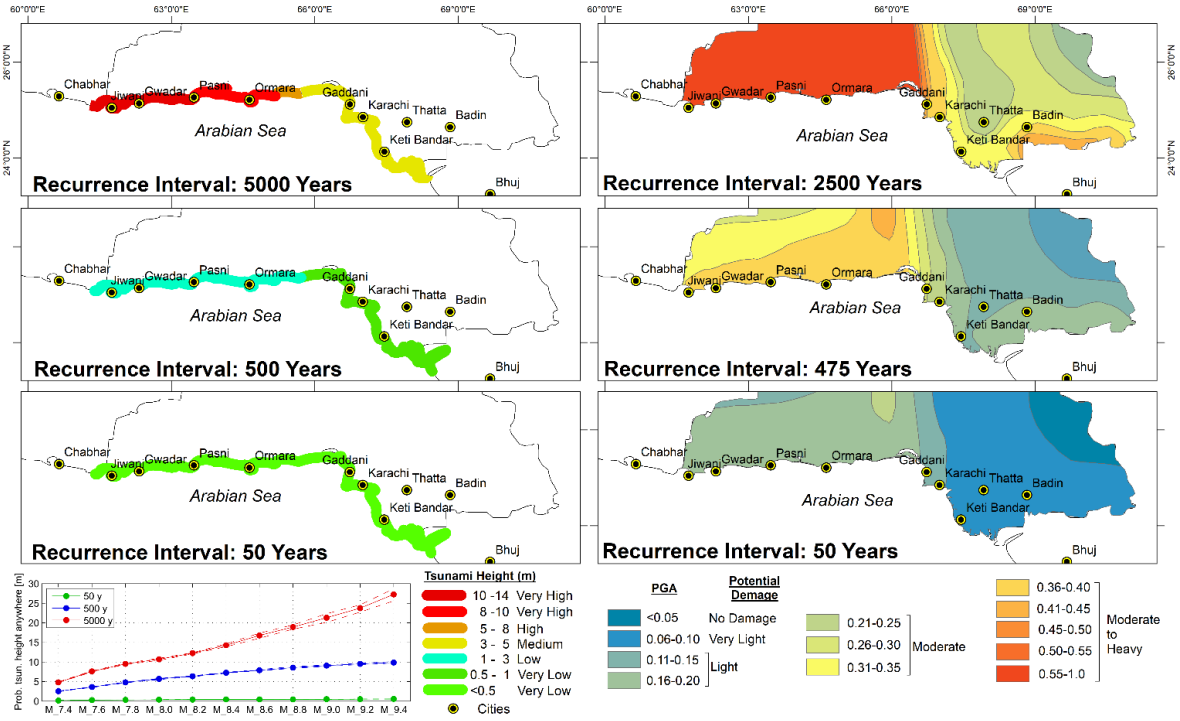

Figure 2.5: The left column shows probabilistic tsunami heights with different recurrence intervals by Hoechner et al. (2016). The right column shows the seismic hazard maps based on probabilistic peak ground acceleration (PGA) for different recurrence intervals by Ahmed et al. (2019). The probability of tsunami height is calculated from the instrumental and historical seismicity at the MSZ.

Table 2.2: A- The compilation of various tsunamis with fault source parameters in MSZ and adjoin tectonics. B- The compilation of various tsunamis for landslide source parameters in Arabian Sea.

A	Longitude	Latitude	Magnitude (Mw)	Azimuth	Length (km)	Width (km)	Water Depth (km)	Epicenter Depth (km)	Moment (N/m)	Min Slip (m)	Max Slip (m)	Avg. Slip (m)	Dip	Rake	Uplift	Wave Height (m)	Software/Code
Hosseini Mehr et al., 2018	24.77	58.8	7.2	270	57	22		10	0.708 × 10*18	0.8	1.8	1.25	7	90	Model not run		SMT
El-Hussain et al., 2017			8.2-8.8	263-281	201-461	82-110					6-11.1		7	90		2.34	COMCOT, MOST
El-Hussain et al., 2018	24.66	65.5	8.8	263	461	110						11	7	90		8	NSWING
	24.55	64.36	8.1	261	150	70						6.6	7	90		3	
M. A. Sarker, 2019	MSZ		8	246	55	70		27				10	7	89		1	MIKE21 Flow Model FM
	1945 EQ epicenter		8.4	246	55	70		27				10	7	89		3	
Saha & Srivastava, 2019	63.48	25.15	8.0	246	150	70		20				7	7	90		3	TSUNAMI-N2
	65.72	25.22	9	250	360	183		20				11	7	90		4	
Heidarzadeh et al., 2009	Jiwani-Pasni-Somiani		8.6	265	500	100		25	1.95 × 10*22			13	7	90		6-9	TSUNAMI-N2
	Jask-Jiwani-Pasni-Somiani		9	265	500	150		25	1.01 × 10*23			25	7	90		12-15	
Heidarzadeh, Pirooz, Zaker, et al., 2009	24.05	63.17	8.1	246	120-150	65-80	2000	27	1.8 × 10*21	5.3	6.6		7	89	1.7-2	Max 7	TSUNAMI-N2, TSUNAMI-N3
Heidarzadeh et al., 2008	25.06	64.01	8.4	240	200	100	50	20	1.8 × 10*21			7.3	6	90	2		TUNAMI-N2,
Heidarzadeh et al., 2007			8	246	Wells and Coppersmith (1994) [25]'s Equation Rupture × 0.55			20		Wells and Coppersmith (1994) [25]'s Equation Rupture × 1.187				90		3	
Heidarzadeh & Satake, 2014a				230-260	120-237	40-100		17-30	3 × 10*11 dyn/cm2			6-11	5-9	70-110		5-6	TUNAMI
Rajendran et al., 2008	1945 EQ epicenter		8.1	246	150	70		15				7	7	90		5	TUNAMI-N2,
Rajendran et al., 2020	66.20, 61.20 24.65, 24.30		9.3	265-280	400-500	150		25				25	7	90		4-5	COMCOT
Okal & Synolakis, 2008	Makran-Pak			265									7	90		2	MOST
	Makran-Pak & Iran			280-265	whole MSZ								7	90		<3	
Jaiswal et al., 2009	24.05	63.90	8.6	270	200	100	2000	30				15	15	90		7	Tunami-N2
Yanagisawa et al., 2009	25	64	8.1	246	40-130	65		15				8-30	7	90		5-10	
Rafi & Mahmood, 2010	1945 EQ epicenter		8.5									5.26				5	MOST
Mahmood et al., 2012	Complete MSZ		7.7-9.0	239-276		50		5-7.62					3	90		5.4	
Srivastava et al., 2011	1945 EQ epicenter		9	265	337	190		25				11	7	90		Max 5	TSUNAMI-N2
Arjun et al., 2011	EQ-1945		8.1	270	200	100		30				15	15	90		Max 5	TSUNAMI-N2
Akbarpour Jannat et al., 2011	326BC,1008,1897,1945		8.1	280	100-300	50		25					7	89-90		Max 10	ComMIT
Swapna & Srivastava, 2014	61.16N, 24.59E		9	278	366	183		25				11	7	90		3	TUNAMI N2
	66.3N, 25.20E		9	256	366	183		25				11	7	90		4	
	63.48N,25.15E		8.1	246	150	70		27				7	7	89		2.5	
Payande et al., 2014	1945 EQ epicenter		8.1					25									
	60.5N, 24.8E		7.5					10								4.5	MIKE 21 FM
			8.1					25								8	
			9.1					30								18	

Miranda et al., 2014	Chabhar-Ormara	8.6	268	394	100						8	25	90		Max 4	SW code
	Central Iran MSZ	7.7	286	108	40						3	30	90		Max 0.5	
	Murray Ridge	7.8	49	137	45						3.5	88	180		Max 0.15	
Rehman et al., 2015	63.01N, 24.72E	7-8.5	276	100-150	50		7.62				0.01-2.63	3	90		Max 1.9	ComMIT
Suppasri et al., 2016	MSZ	9.0		900	150						25				18	TUNAMI
		8.6		500	100						13				10	
		8.3		55	80						8.5				6	
		8.3		55	70						4.3-10				6	
Delavar et al., 2017	1945 EQ epicenter	8.1	246	130	70	2000	27	1.8 × 10*21			6.6	7	89	2	5	ComMIT
		8.1	270	130	70			1.8 × 10*21			15		90		10	
Rashidi et al., 2018a	Iranian Makran	9	280	400	150		25	1.01 × 10*23			25	7	90		10	COMCOT
		7.7	286	108	40	1000				3		30	90		2	
		7.8	49	137	45	1000				3.5			88		3	
Rashidi et al., 2018		9					25	4.5 × 10*22				5	88		23	
Rashidi et al., 2020	Western MSZ	8.9		400	210		25	2.5 × 10*22		28	10	7	90		8	COMCOT
Latcharote et al., 2018	MSZ	8.3-9	246-280	55-400	70-150		25-27		0	25		7	89-90		10	TUNAMI
Patel et al., 2011	MSZ	8.6	270	200	100	2000	30				15	15	90		7	TUNAMI N2
Patel et al., 2016	63.48E, 25.15N		246	200	100		15				7	7	90		5.8	NAMI-DANCE
Neetu et al., 2011	63.48°E, 25.15°N		246	100	100		15				7	7	98		2.5	
Ali et al., 2023	18°N to 27°N, 57°E to 69°E	8.2-8.6		195	40		20.45	2.57×10*28 1.01×10*29		11		7	89		7.71	New-TSM
Roshan et al., 2016	EW (±2)	8.0-9.5		151-1334	47-157				5.1	21.4		3-10			4 max	TSUNAMI
Aniel-Quiroga et al., 2018		7.75-9.25	240-270.9	104-860	21-234		6.1-20		7.5	15.6	5-35		90			COMCOT-C3
Yang et al., 2022	Eastern MSZ	6.3			13-29										0.5	COMCOT
Akbarpour Jannat, 2021	24.74 N, 59.72 E 24.75 N, 59.72 E	8.0-9.1	282-276	300-500	30-70		25	1.05×10*22 4.72×10*22	5.5	25		3	90		9-13	GEOWAVE
Heidarzadeh et al., 2020	Complete MSZ	8.1	265-280	120-150	65-80	2000	25				25	7	90	1.7-2	5	JAGURS
Matin and Praveen, 2021	Eastern MSZ	8.0-9.3	270	200-680	100-150		20-30				15	15	90			TUNAMI N2
Qiu et al., 2022	Eastern MSZ	7.8-9.0	253-262	360	17-277					0.14-1.1			90		~2	COMCOT
Al-Habsi et al., 2022	24.32E, 59.58N 24.66E, 65.50N	7.2-8.8	263-281	62-461	25-110				1.7	11		7	90		1.2	NSWING
Sultan, 2017	Eastern MSZ	7.0-8.3	276	50	7.62					7		3	90		3	ComMIT
Zuhair and Alam, 2017	63.48˚E, 25.15˚N	9.0	255	378	180		15			11		7	90		12	TUNAMI N2
Honarmand et al., 2020		8.1	Okada (1985)								7	10	90		4.25	OpenFOAM
Moradi, 2021	Eastern MSZ	8.1	1945 Tsunamigenic earthquake parameters (details not mentioned)												2.6	AVI-NAMI, SiTPros
(Oskamp et al., 2015)	MSZ			1000	Okada (1985)										6	Delft3D-FLOW
Giles et al., 2021	Eastern MSZ				Okada 1985 (100 scenarios)										8	Volna-OP2
Aguirre-Ayerbe et al., 2018	MSZ		6.5-9.25		Okada, 1985 (3181 focal mechanisms scenarios)										>8	COMCOT

B	Long	Lat	Bulk Density (kg/m^3)	Viscosity (m/s^2)	Initial Submergence (Travel Distance) (m)	Water Depth (m)	Seabed Slope (degree)	Volume (km^3)	Slide length (km)	Slide Thickness (m)	Slide width (km)	Wave Height (m)	Software/ Code
Rodriguez et al., 2013	60.27N,17.2E			25 to 500		2000		40		140		2.5	AVALANCHE
Rastgoftar & Soltanpour, 2016	64.1N,24.75E				1134		6		15	500	10	Max18-20	TOPICS and FUNWAVE
Suppasri et al., 2016	Persian Gulf					Coastal landslides		1	20	5	10	<1	TUNAMI
								0.5	10	5	10	<1	
Heidarzadeh & Satake, 2014; 2017	63N,24.8E		2150		1000-2000	1300-2000		45		600		29.9	TUNAMI-N2
			2150		1000-2000	1300-2000			20	600	20	15.2	
			2150		1000-2000	1300-2000			20	800	20	23.7	
Latcharote et al., 2018	Persian Gulf							0.75-2.0	15-40	5	10	1	TUNAMI
Salmanidou et al., 2019	67.06N,23.1E		2000		500–2000	250-450				100-300	6–10.5	Max 2	JAGURS
Baptista et al., 2020	61.6N,24.4E						5					0.2	
Nouri et al., 2020	58.75N,23.87E						25	4	4.5	600	4	24	COMCOT
Nouri et al., 2023	Iranian Offshore					792-1892	0.6-10	10-40	5-8	5-8	0.5-0.8	6	COMCOT
(Rajendran et al., 2020)	70.230N,18.352 E 70.526N,17.950 E 69.400N,19.480 E				3.2-8.6	1500		7.5-179	15-40	250-500	10-30	1–1.5 m	COMCOT

Table 2.3: Overview of Probabilistic Tsunami Hazard Assessment (PTHA) and Statistical Studies Undertaken in the MSZ, modified from (Zafarani et al., 2022).

Reference	Objectives	Modelling	Slip distribution	Bathymetry resolution	Mw	Output(s)	EQRM	Coupling	Study scale
(Burbidge et al., 2009)	Tsunami wave amplitudes in water depth of 100 m	Linear shallow water wave equations (URSGA model)	Uniform	2 arc min	7.0–8.2 and 9.1	Wells and Coppersmith (1994)	TGR	Average coupling for global subduction zones	Global
(Heidarzadeh and Kijko, 2011)	Tsunami wave amplitudes at coastline	Nonlinear shallow water wave equations (TUNAMI- N2 model)	Uniform	1 arc min	8.1	The 1945 Makran earthquake	TGR	Not included	Regional
(Løvholt et al., 2012)	Tsunami wave amplitudes at coast (water depth of 0.5 m) com- puted using amplification factors from water depth of 50 m	Linear shallow water wave equations (GloBouss model	Uniform	2 arc min	Up to 8.4	Wells and Coppersmith (1994)	TGR	Not included	Global

(El-Hussain et al., 2016)	Tsunami wave amplitudes at coastline	Nonlinear shallow water wave equations (NSWING model	Uniform	30 arc sec	7.9–9.1	--	TGR	Not included	Local
(Hoechner et al., 2016)	Tsunami wave amplitudes at coast (water depth of 1.0 m) computed based on Green's law from amplitudes in water depth of 50 m	Linear shallow water wave equations (easyWave model)	Non-uniform	30 arc sec	Up to 9.0	Blaser et al. (2010)	TGR	Not included	Regional
(Davies et al., 2018)	Tsunami wave amplitudes at coast (water depth of 0.5 m) computed using amplification factors and Green's law from amplitudes in water depths of 100 m	Linear shallow water wave equations (URSGA model	Uniform	30 arc sec	7.5–8.1	Strasser et al. (2010)	TGR	Different scenarios are considered	Global
(El-Hussain et al., 2018)	Tsunami wave amplitudes at coastline	Nonlinear shallow water wave equations (NSWING model)	Uniform	30 arc sec	7.5–8.8	--	TGR	Not included	Local
(Rashidi et al., 2020b)	Tsunami wave amplitudes at coastline	Nonlinear shallow water wave equations (COMCOT model)	Non-uniform	30 arc sec	9.06–9.12	Smith et al. (2012)	TGR	Not included	Regional
(Zafarani et al., 2022)	Tsunami wave amplitudes at coast	Linear and Nonlinear shallow water wave equations (COMCOT)	Heterogeneous	30, 15, 5 arc-sec	7.7 ~ 9.1			Different scenarios are considered	Local
(Gopinathan et al., 2021)	Generated tsunami hazard curves and maps	VOLNA-OP2	Uniform	15 arc sec	Up to 8.8		GR		Regional
(Salah et al., 2021)	Probability that a maximum wave will exceed 3 m somewhere along the coast reaches (13:5; 25; 52; 74; 91) for return periods (50; 100; 250; 500; 1000), respectively.	Funwave-TVD	Non-uniform	15 arc sec	Up to 9.3		TGR		Regional
(Momeni et al., 2020)	Develop stochastic earthquake slip models, tsunami simulation and effects of earthquake slip and fault geometry on tsunami simulation results	Inundation and run-up by solving non-linear shallow water equations using a leap-frog staggered-grid finite difference scheme (Goto et al., 1997)	stochastic slip distribution	15 arc sec	8.1-8.3				Regional
EQRM= Earthquake recurrence model, TGR= Truncated Gutenberg–Richter, GR= truncated Gutenberg									

Table 2.4: Catalogue of the Makran historical and instrumental great earthquakes with Mw ≥ 6.5. updated after Heidarzadeh et al., (2008)

No.	Date(yy-mm-dd)	Latitude (N)	Longitude (E)	Focal depth (km)	M_s	M_w	Intensity (MM)[c]
1	326 BC	24.00	67.30				Strong tsunami
2	1008-5	25.00	60.00 (52.3)[d]				8-9 Strong tsunami
3	1483-2-18	24.90	57.90				10
4	1668-5	25.00	68.00				8-9
5	1765	25.40	65.80				8-9
6	1851-4-19	25.10	62.30				8-9
7	1927-07-07	27.00	62.00		6.5		
8	1929-09-03	26.40	62.30		6.5		
9	1934-06-13	27.43	62.59	35.0	7.0		
10	1945-11-27	24.50	63.00	25.0		8.1	Strong tsunami
11	1947-08-05	25.10	63.40	35.0	7.6		
12	1969-11-07	27.90	60.10	35.0	6.5		
13	1983-04-18	27.79	62.05	64.0		7	
14	2013-09-24	27.01	65.55			7.7	Minor tsunami

M_s: Surface wave magnitude, M_w: Moment magnitude, [c]Modified Mercalli, [d]Reported by (Ambraseys and Melville, 1982)

2.5 Discussion

The establishment of the maximum tsunami potential of the region is essential for its hazard and risk assessment. In this regard, each approach has its own limitations, particularly gaps in data and knowledge and different computational types. As compared to a single proxy, the synergy of five proxies has improved the level of information and confidence in the hazard estimation and assessment. In comparative analysis for a scenario, the proxies either validate or negate and in some cases, narrow down the result range.

The probabilistic recurrence interval for a ≥ 12 m tsunamigenic earthquake using the logic tree technique is 2475 years (Zafarani et al., 2022). For the same dynamics, Hoechner et al. (2016) used Monte Carlo based technique similar to that commonly applied for seismic hazard assessment and estimated the recurrence interval as 5000 years. The former has a probability of 0.8, while the latter has a probability of 0.6. The probabilistic PGA values ≥ 0.7 based on the Cornell–McGuire technique have a recurrence interval of more than 2475 years (Waseem et al., 2020). With the same return period, it is up to 1.0 based on the regression analysis of strong motion global data (Ahmed et al., 2019). The probable PGA values imply that a mega earthquake (≥Mw 8.0) has a recurrence interval of 2500 years. Rehman and Zhang (2024a) analysed earthquake frequency-magnitude relations, revealing that magnitudes 8 and 8.5 have return periods ranging from 100 to 600 years and 200 to 1200 years, respectively. These different probability studies based on various techniques and methods estimate the recurrence interval of a mega tsunami event between 2500-5000 years.

These probable models only take earthquake sources into account and do not consider other non-seismic tsunami sources. In this regard, considering the well-studied tsunami events of 1945 AD and 1000 AD in the northern Arabian Sea, the recurrence interval narrows down to 1000 years. With these two arguments, a quick and crude analysis implies that non-seismic tsunami sources and/or cascading sources (coseismic landslides) generate about 40% to 80% of tsunamis in the Arabian Sea.

This ratio is high, so we keep the interpretation tentative. Globally, about 80% of tsunamis have an earthquake source (Harbitz et al., 2014; Løvholt, 2017; Behrens et al., 2021).

Non-seismic tsunami sources, particularly underwater landslides, complicate hazard assessment in terms of magnitude and recurrence interval. A landslide has a greater potential for larger wave heights due to its large vertical slip as compared to an earthquake (Table 2.2B). The 1945 (major) and 2013 (minor) tsunamis in the Arabian Sea are also attributed to a submarine landslide triggered by offshore and terrestrial earthquakes, respectively. These recent events reflect that the frequency of underwater slope failure is as high as postulated (Heidarzadeh and Satake, 2017; Hoffmann et al., 2014). Landslide stability is dependent on several geotechnical and lithological factors (slope angle, consolidation, specific gravity, density, particle type and size, consistency limits, and compaction). Many agents can lower the threshold of these factors, especially earthquakes, submarine volcanic activity, marine life, and submarine anthropogenic activities like communication cables, mining, and drilling. Considering moderate to high-scale offshore earthquakes (Mw ≥ 6.5) capable of destabilising a mega submarine landslide, the frequency of slope failures should be high because the Mw ≥ 6.5 occurs every 20 years (Table 2.4) and provides critical landslides that have completed or are near the completion of their angle of repose (Heidarzadeh et al., 2008). Rehman and Zhang (2024b) analyzed seismicity from 1934 to 2017 along the MSZ using the Weibull statistical distribution model, determining a return period of 4.45 years for earthquakes ≥ Mw 6.0. The landslide-related hazard is an important research gap, which greatly hampers the tsunami hazard assessment. The precise measurement and monitoring of these factors to estimate their slip rates and failure times is a mammoth task.

The compilation shows the sequence of events as 1945 CE, 1524 CE, 1000 CE, 4522±200 BP and 5840±200 BP. The interval between the first three clusters of events is about 500 years, while the fourth and fifth clusters have an interval of 1100 years, but there is a gap of more than 3000 years between these two clusters of events. This huge interval (3000 years) has three possible speculations: First, there was no such extreme wave event and if the event(s) occurred, either they could not be preserved in the sedimentary record or, if preserved, they have not been discovered yet. This approach has limitations: 1) Pakistan's coastline, which are highly susceptible to tsunamigenic earthquakes and have yet to be explored for palaeotsunami deposits that could enrich Table 2.5. The status of interpretation for most of these as tsunamites is tentative and not proven yet, as their deposition by other non-seismic tsunami sources and cyclones is not completely ruled out. 3) Date approximation, geological inferences and assumptions, and the correlation of an extreme wave event with a previously known event, such as the 1000 AD tsunami.

Table 2.5: The compilation of tsunamites discovered at different coasts along the Arabian Sea (sorted age-wise)

No	Event Year (radiometric)	Event Assigned	Location	Brief detail	Reference
1	1948 ± 9 to 1969 ± 10 (Back as of 2022)	1945	Pindara to Okha, India	The documented sand-sheet in the paleo mud flats shows physical, geochemical and biological characteristics such as basal erosional/sharp contact with the underlying unit and lack of sorting along with the presence of mud-clasts. The sedimentary layer also shows an abnormal inland extent of >570 m from the present high-water line.	(Prizomwala et al., 2022)

2	1945[a] Tsunamigenic earthquake event	1945	Sur Lagoon, Oman	In this study, particle size, stable isotopic and foraminiferal (taxa and taphonomy) analyses were conducted on surface sediment samples from Sur Lagoon to determine modern spatial trends in the lagoon for future comparison with over-wash sediments deeper in the geologic record	(Pilarczyk and Reinhardt, 2012)
3	Older than 1958 [b]	1945		5-25cm thick bed of bivalve shell taphonomy	(Donato et al., 2008)
4	C^{14} 722-905 cal BP	1000		They reinterpreted the age of 25-cm-thick tsunamigenic layer based on the new discovery of parallel-oriented woody axes in the sedimentological context of the tsunami shell layer in the Sur lagoon. The woody axes were analysed anatomically and identified as pertaining to the grey mangrove Avicennia.	(Decker et al., 2022)
6	1508–1681 CE	1524	Kelshi, India	This laterally extending 30–40-cm-thick tsunamites zone, coinciding with a habitation level, displays varied sedimentary structures including scour-fill features, and is inter-layered with shells, at a height of 3 m from the high-tide level.	(Rajendran et al., 2020)
7	C^{14} - ~ 872 BP OSL – (Ka) (1130 ± 170) (1110 ± 160)	1000	Fins to Tiwi, Oman	Sedimentological and archaeological evidence for past tsunamis and describe new data on the impact of the 1945 Makran tsunami in Oman.	(Hoffmann et al., 2020)
8	C^{14} - (BP) (1565 ± 35)(1930 ± 30)(950 ± 30) (1445 ± 30) OSL – (Ka) (1.11 ± 0.11) (1.18 ± 0.11)(1.29 ± 0.22)	1000	Panjor to Luni, India	Sedimentology and geochemistry reveal an offshore origin of this sand sheet, from where it was eroded by a high energy wave and deposited in a supratidal environment	(Prizomwala et al., 2018)
9	OSL – (1.3 ± 0.3) (6.6 ± 0.7) (35.4 ± 4.3)	1052	Mundra-Bhadreshwar, Madhavpur-Chorwad, Ratiya, India	GPR studies and trenching the subsurface sand layers shows features that identify and locate features that might have formed during a reported extreme event and its effects. a wave height of ~4–5 m along Saurashtra coast. Southern Owen Ridge is considered as tsunami source.	(Bhatt et al., 2016)
10	4522 ± 200 BP	4522	Ras ul Hadd, Oman	Archaeologically rich evidence of past extreme wave events is preserved in the onshore stratigraphic record. Comprehensive mapping and analysis of extreme wave deposits suggests an Early Bronze Age.	(Hoffmann et al., 2015)
11	5840 ± 30 BP	5840	Fins, Oman	Investigated coarse- to fine- grained, marine tsunami deposits using GPR. Wedging out of sediments and fining inland features, as well as several erosion features at the base of the deposit. Minimum calculated runup height of >17m.	(Koster et al., 2014)
12			Ramin, Iran	The boulders, weighing up to 18 t, are found up to 6 m above present mean sea level and up to 40 m from the present shoreline.	(Shah-Hosseini et al., 2011)
13			Dive Agar, India	Sediment signatures at the two nearby beach sites on the west Two sedimentary deposits are inferred as indicative of two palaeo tsunami events relating to the Sunda Arc in the south and the Makran tectonic zone in the north. The occurrence of sporadic boulders, wedge- shaped heavy mineral sand layers and capping of the deposit by a pedogenic surface at Guhagarh depicts an older tsunami of larger magnitude compared to Dive Agar.	(Sangode and Meshram, 2013)
14			Guhagar, India		

15			Fins to Sur, Oman	The blocks occur as individual rocks of up to 120 tons, as imbricated sets and as ‘‘boulder trains	(Hoffmann et al., 2013a)
[a] Age based on foraminiferal provenance and taphonomy [b] Age Based on Pb ^{210} (n=1). Sample immediately above the tsunamites					

2.6 Conclusions

1. The coastline along the high tsunami hazard zone (Gwadar to Ormara) should be investigated for field evidence (tsunamites) to foster the palaeo-tsunami record to estimate source potential and the recurrence interval.
2. The active seismic zone south of Pasni in relation to the Sonne Fault, nature of the decollement basement and the slow GPS velocity at Pasni should be investigated in detail.
3. Submarine landslide potential is poorly known, but detailed bathymetric studies may help in determining the potential. Further, the high hazard zones demarcated in the studies may be revisited at regular intervals to estimate the slip rate and time of slope failure. Though the forecast side of cyclones has much improved with time, the resilience and preparedness aspects are still far from satisfactory.
4. The estuaries of Ormara and Pasni are suitable sites for mangrove forestation. Karachi Beach (Clifton) may be turned into artificial estuaries that may serve the purpose of planting a mangrove forest. Along with many other benefits, it may act as a coastal defence structure against the extreme waves.
5. There is a considerable scientific understanding of the earthquake and tsunami dynamics, but still there are large data and knowledge gaps, assumptions and uncertainties. Due to these shortcomings and limitations, the timing and exact location of earthquakes and tsunamis are yet unpredictable (Behrens et al., 2021). Till there is a scientific breakthrough, the option in hand is to get well prepared by enhancing the awareness and resilience of the communities along the coast.

3. Tsunami hit the Makran Coast repeatedly; evidence for extreme wave events at the Pasni Coast, Pakistan

This chapter has been slightly modified from a drafted research paper, with the intention of submission for subsequent publication.

- ***Haider, R.,** Ali, S., Hoffmann, G., and Reicherter, K.: Tsunami hit the Pasni repeatedly; evidence for extreme wave events at the Pasni Coast, Pakistan.*

3.0 Abstract

The coastline along the Arabian Sea is prone to tsunamis especially due to the Makran Subduction Zone (MSZ). The coastline had yielded several palaeo-tsunami records (tsunamites). In the present study, two tsunamites horizons older than that of 1945 Tsunami horizon from the Pasni and its surrounding areas are presented. Off these two, the event dated 1539 AD is very close to an already reported 1524 AD Tsunami in the Arabian Sea. The second event could date back to 17th BC maximum. The depositional pattern and architecture of the tsunamites are substantiated by the tsunamites horizon of the 1945 Tsunami and minor cyclone-related recent inundation event in the coastal dunes. To evaluate the paleotsuanmi dynamics, source size, and position, various tsunami scenarios are modelled and simulated with earthquake parameters to find the most suitable scenario. The present findings indicate a high hazard level for the Makran Coast. We recommend more intensive and extensive work to enrich the tsunami and tsunamites catalogue.

3.1 Introduction

Predicting earthquakes and tsunamis is a major front that mostly relies on the approximation of recurrence intervals. These intervals are calculated from the different proxies using statistical and deterministic approaches. The level of confidence depends greatly on the quality and quantity of input data. In this regard, the field evidence, especially tsunamites enriches the tsunami archives and eventually improves the hazard assessment and predictability for a particular coast. The historic record of tsunamis along the Makran Coast in the Arabian Sea is scarce. Additionally, it lacks field investigations for past extreme-wave events to fill in data gaps to approximate their recurrence intervals and the coastal impacts. Significant field exploration is done at the neighboring coastlines,

yielding sedimentary deposits of repeated extreme wave events. The multiproxy analysis shows an approximate recurrence interval of 500 to 1000 years for a mega tsunami >10 m in the Arabian Sea (Haider et al., 2023). The proxies of sedimentology, geochemistry, geomorphology, geophysical (GPR) and paleontology are used for the identification and detailed analysis of the tsunamites. The findings suggest repeated extreme wave smashing for which the source mechanism is attributed to the Makran Subduction Zone (MSZ) and submarine landslides in the Arabian Sea, especially the former one. In this regard, for the remnants of minor events, high-category tropical cyclones may not be ruled out. Also, other possible tsunamigenic sources like submarine volcanic activity and meteoric impacts have been taken as exceptions so far. The MSZ, the main source of tsunamis, extends EW for ~1000km parallel to the Makran Coast. Here, the Arabian Plate with a thick pile of sediments (~7km) is subducting under the Eurasian Plate at a rate of ~4 cm/year, dipping ~2◦ north (Stoneley, 1974; White & Louden, 1982; Quittmeyer & Kafka, 1984; Ellouz et al., 2007).

The tectono-sedimentary and thermal dynamics of MSZ are comparable to those of the North Sumatra Subduction Zone, which triggered the deadly 2004 tsunamigenic earthquake. The comparison shows that MSZ has the capacity to trigger an earthquake as high as Mw. 9.1 (Klingelhoefer et al., 2010; Smith et al., 2013). Instrumental records show that the most active part of MSZ lies just south of Pasni-Ormara towns in the Arabian Sea, where the 1945 (Mw 8.1) tsunamigenic earthquake was also triggered (Figure 2.1). This high offshore seismicity is speculated to be due to the rigid nature of decollement in this part (Smith et al., 2013). The anomalous coastal geodetic plate motion and relative uplift rates support their finding. The Pasni-Ormara is moving southward at about half speed (7 mm/a) than its eastern and western counterparts (Khan et al., 2008). The present high coastal uplift rates at Pasni-Ormara are 0.1-0.2 mm/a as compared to 0.01-0.04 mm/a at Konrakh and 0.0 mm/a at Jask in Iran (Page et al., 1979). The integrated analysis reflects that the rigid nature of decollement has some locking effect which is compensated by the high uplift rate and high seismicity in this region (eastern MSZ; South Pasni).

The submarine landside mechanism also prevails in the Arabian Sea, and its potential is inadequately known, which greatly hampers the estimation of recurrence interval and tsunami size; hence, it makes the coastlines tsunamigenically more hazardous and the prediction more uncertain. Since 1945, the coast has experienced two tsunamigenic earthquakes, a major one in 1945 (Mw 8.1) claiming a few hundred human lives (Pendse, 1946; Hoffmann et al. 2013) and a minor tsunami in 2013 (Mw 7.7) with no loss (Heidarzadeh & Satake, 2014b). Both tsunamis are considered to have been generated by submarine landslides triggered by the respective earthquakes. However, for the former event, an antithesis for the source mechanism is also available (Yanagisawa et al., 2009; Neetu et al., 2011; Haider et al., 2024).

In this chapter, we are presenting two different horizons of tsunamites from the Pasni. One of them indicates a tsunami event of greater intensity than the 1945 Tsunami. The event with higher intensity is modeled and simulated to estimate the wave height, flow depths-velocities, source type, and position.

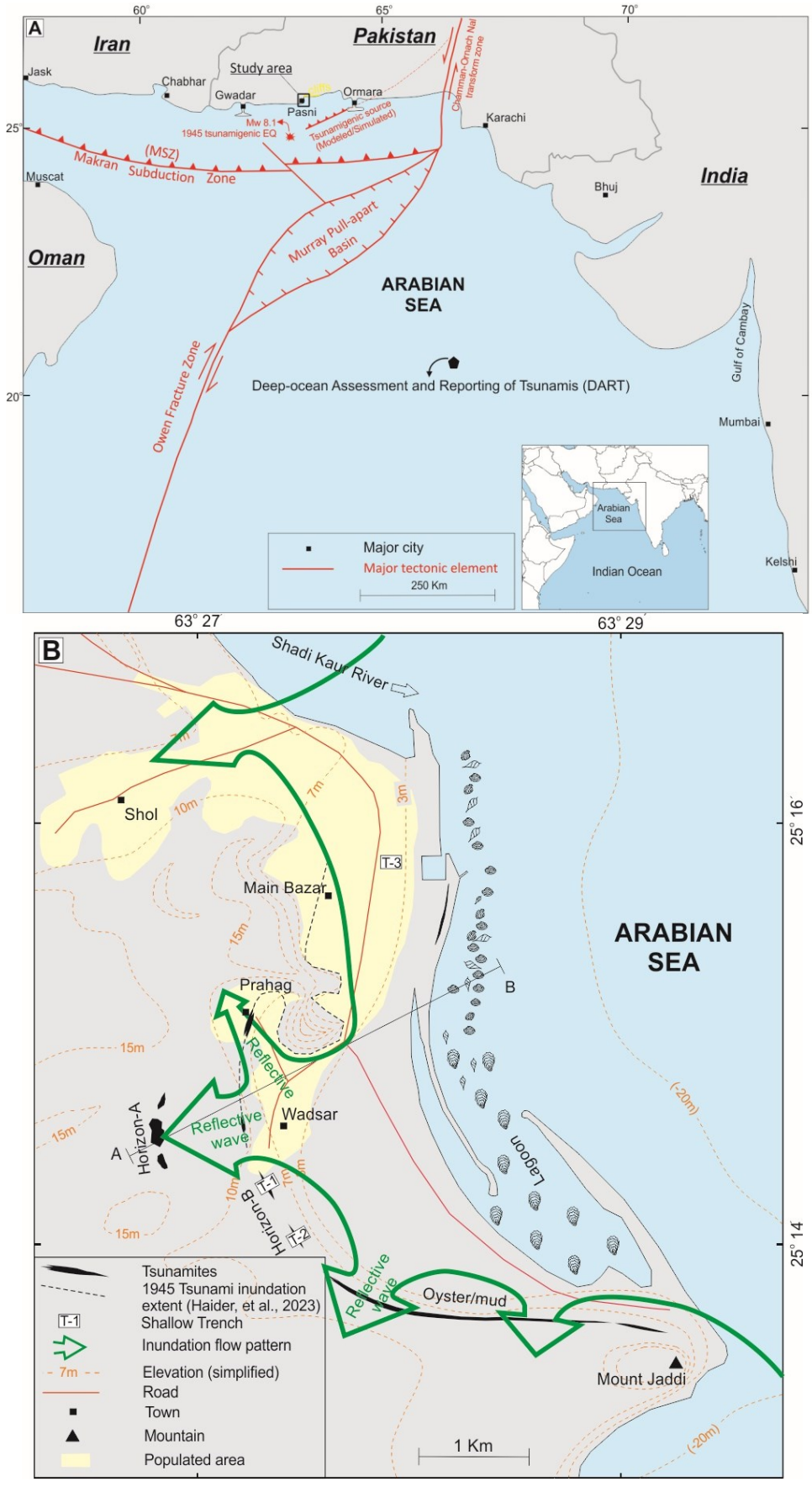

Figure 3.1: A) Location and regional tectonic setting of the study area. B) Map showing distribution of tsunamites along with inundation extents during the 1945 tsunami in the Pasni and surrounding area.

3.2 Historic Archive

From the historic contest, we tentatively bind our findings with the 1524 AD tsunami event. In this regard, two available historic reports are compiled as follows:

Kerr (1824) reported 1524 AD event from the Gulf of Cambay, west coast of India:

''…In 1524, Don Vasco De Gama was appointed viceroy of India by John III. king of Portugal, and sailed from Lisbon with fourteen ships, carrying 3000 fighting men. Three were lost during the voyage, with all the men belonging to two of them. While in the Gulf of Cambaya, in the dead calm, the ships were tossed about in so violent a manner that all on board believed themselves in imminent danger of perishing and began to consider how they might escape. One man leapt over-board, thinking to escape by swimming, but was drowned; and such as lay sick of fevers were cured by the freight. The viceroy, who perceived that the commotion was perceived by the effects of an earthquake called aloud to his people, ''courage my friends, for the sea trembles from the fear of you who are on it…''

Logan (1887) describes an account of the same event at Dabhol (Dabul), west coast of India as follows:

The historical records show major sea disturbance lasting for hours on September 11th or (perhaps) 21st 1524 off Dabhol (Dabul), west coast of India. Vasco da Gama along with 14 ships and 3,000 men arrived at Goa. On reaching the land at Dabul "*and with the wind becalmed, during the watch of daybreak, the sea trembled in such a manner giving such great buffets to the ships, that all thought they were on shoals, and struck the sails, and lowered the boats into the sea with great shouts and cries and discharge of cannon*." On sounding they found no bottom, "and they cried to God for mercy, because the ships pitched so violently that the men could not stand upright, and the chests were sent from one end of the ship to the other. "*The trembling came, died away, and was renewed each time during the space of a Credo*." The subterranean disturbance lasted about an hour, "in which the water made a great boiling up, one sea struggling with another" When daylight was fully come, they saw the land.

From these historical accounts, we ruled out sea disturbances due to meteorological sources, as no cyclone is reported along with the event but rather "*an earthquake perception... with the wind becalmed, during the watch...*". The cyclone in the Arabian Sea lasts for about 4 to 6 days, and during these days, sea voyages along east Indian Coast could hardly escape the effects of a cyclone, especially the average sized sailing vessels in 1524 AD. The event is reported in September, and the cyclones typically develop either during (May to June) or after (October to November). The sea disturbances lasted for about an hour, which is typically the run-up-down time for a tsunami.

3.3 Geological and Archeological Archive 1524 AD tsunami event

At Kelshi, ~ 500 km south of Cambay, Rajendran et al. (2020) reported a coastal dune complex preserving the tsunamites dated 1508–1681 calAD. The 30–40-cm-thick zone has considerable lateral extension and coincides with a human habitation horizon at an elevation of 3 m from the high-tide level. The horizon exhibits varied sedimentary structures, including scour fills and inter-layered shells with broken human artifacts. The archaeological studies on these artefacts reveal mediaeval habitation between 1312 and 1518 calAD (Deo et al., 2011; Marathe and Chandrashekhar, 2011). The modelling results rule out submarine landslide scenarios and indicate an earthquake source ~(Mw: 9.0) which may have originated in the MSZ (Rajendran et al., 2020).

3.4 Methodology and Results

3.4.1 Field work and Laboratory analysis

We mapped three tsunamites horizons (including 1945 tsunami) and their respective provenances in the study area using Google Earth satellite imagery as the base maps. The tsunamites are predominantly composed of bivalve/ gastropod shells, rolled pebbles with beach sand matrix. Four trenches are dug at different levels (Figure 3.1B) for sedimentary logging and ascertaining the geometry and depositional pattern(s). There are thin charcoal patches under and within the tsunamites horizon, except the farthest one. Three charcoal and one bivalve shell sample were collected for radiometric age determination. The assemblage represents the lagoonal and open-shore facies. However, there is a unique tsunamites segment composed of oyster shells supported by lagoonal mud matrix (discussed later). There exist both of these habitats hosting shelly fauna: the lagoonal-mud at the SE and the open-shore sand-gravel at the NE part of the study area (Figure 3.1B). Based on fauna and sedimentology, the provenance of the former is determined at the northern shoreline and later southern shoreline with lagoonal environments in the mapped area. In the SE and SW of the study area, there are anomalous thick deposits of shells, predominantly Meretrix genus of the Verindae Family. We traced and recorded the observations of these deposits to analyse any possible linkage (section 7) with the tsunamites.

These samples were processed at the Institute of Neotectonics and Natural Hazards, RWTH Aachen University, and radiocarbon dating was performed at the Keck Carbon Cycle AMS Laboratory, University of California, Irvine. The results are calibrated using the online Oxcal v4.4.4 facility with a 2-sigma (95.4%) probability (Https://C14.Arch.Ox.Ac.Uk/Calibration.Html). For the bivalve shell, a Marine20 radiocarbon age calibration curve is used with a reservoir effect of 163 ± 30 estimated for the Arabian Sea (Dutta et al., 2001). The charcoal sample under Horizon-B dates to 1444 calAD, while the charcoal sample within Horizon-B shows a little younger age with two age groups bracketing 1529-1635 calAD (Figure 3.2). The disarticulated bivalve shell (single valve) dates back to 1982–1651 calBC. The tsunamites elevation from the mean sea level (MSL) is calculated from the German Aerospace Centre's (DLR) 0.4 arcsec (~12 m) DEM, patented as TanDEM-X.

3.4.2 Tsunamites Morpho-flow dynamics

We mapped two levels of tsunamites laterally and vertically disconnected. We named these horizons Horizon-A and Horizon-B (Figure 3.1B) from west to east. Both horizons, especially Horizon-B pose a curvy-linear depositional trend. Horizon-A lies at an elevation of 12 m from MSL and portrays a maximum tsunami run-up. It is a mix of diverse species of bivalves, gastropod shells, and rolled pebbles. The shell size varies from a few millimeters to several 10 cm. In the assemblage, the bivalves outnumber the gastropods. The deposit is undergoing intense weathering and erosion, due to which its true thickness and depositional geometry cannot be ascertained. Also, wind erosion had blown away the sandy and/or muddy beach matrix of the exposed deposits. The beach processes followed by tsunami event, and finally the eolian sands abrasion resulted in the breakdown of shells, as no articulate bivalve shell was found. However, gastropods show a lower degree of weathering and breakdown in comparison to bivalves. It is probably due to singularity of the shell; however, it needs detailed testing and analysis to argue.

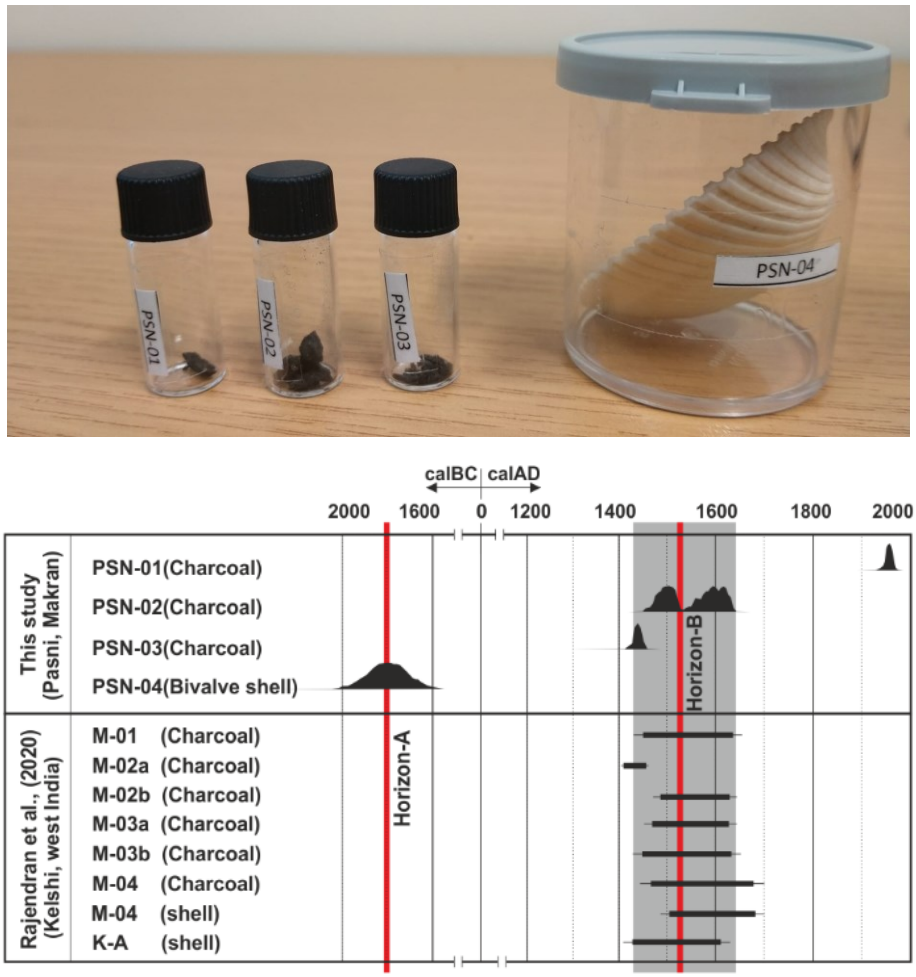

Figure 3.2: Results of radiocarbon dating at Pasni and Kelshi Tsunamites. The shaded area indicates the likely timing of the tsunami event (the shaded area is marked where at least three samples overlap within certainty). The red line in the shaded area marks the historical reporting of a 1524 AD tsunami event from the Gulf of Cambay, India (Kerr, 1824). All dates have been calibrated using the CALIB Radiocarbon Calibration (version 8.20) and the MARINE20 data set (Stuiver and Reimer, 1993). Two-sigma (r) ranges under 95.5% probability distribution curve. The Arabian Sea's marine correction factor DR = 163 ± 30 is after (Dutta et al., 2001).

The Horizon-B is 5–10 cm thick and is a mix of beach sand matrix with occasional charcoal patches within and underneath, showing a rapid burial of vegetation. The shell type in this horizon varies interestingly from SE to NW. In the SE, these are predominantly composed of oysters (order: Ostreida) supported by lagoonal mud as a matrix. Here, order venerida and gastropods are also observed but in minor concentration. In the NE major portion is composed of Bivalvia (order Venerida), and minor by Arcida. This is probably due to the difference in provenance for both sites, but we keep this interpretation tentative. As already mentioned, the oyster deposit embedded in mud represents a lagoonal provenance, while the bivalves demonstrate an open shore provenance (Figure 3.1B). The depositional pattern represents a typical extreme wave deposit, deposited when the inundating wave loses its energy near the run-up heights known as the quasi-stillstand (Shi et al., 1995). The quasi-stillstand deposition style is observed in 2011 Japan Tsunami at Misawa (Bellanova et al., 2021). Next, the backwash process initiates gaining magnitude downstream gradually. The runup heights of each deposit vary slightly from SE to NW, depending on the relative depositional flow dynamics. The SE part of the deposits seems to have been eroded considerably. However, in general, the inundation extent and runup heights increase NE-ward with a maximum of ~2.5 km as compared to 500 m in the SE.

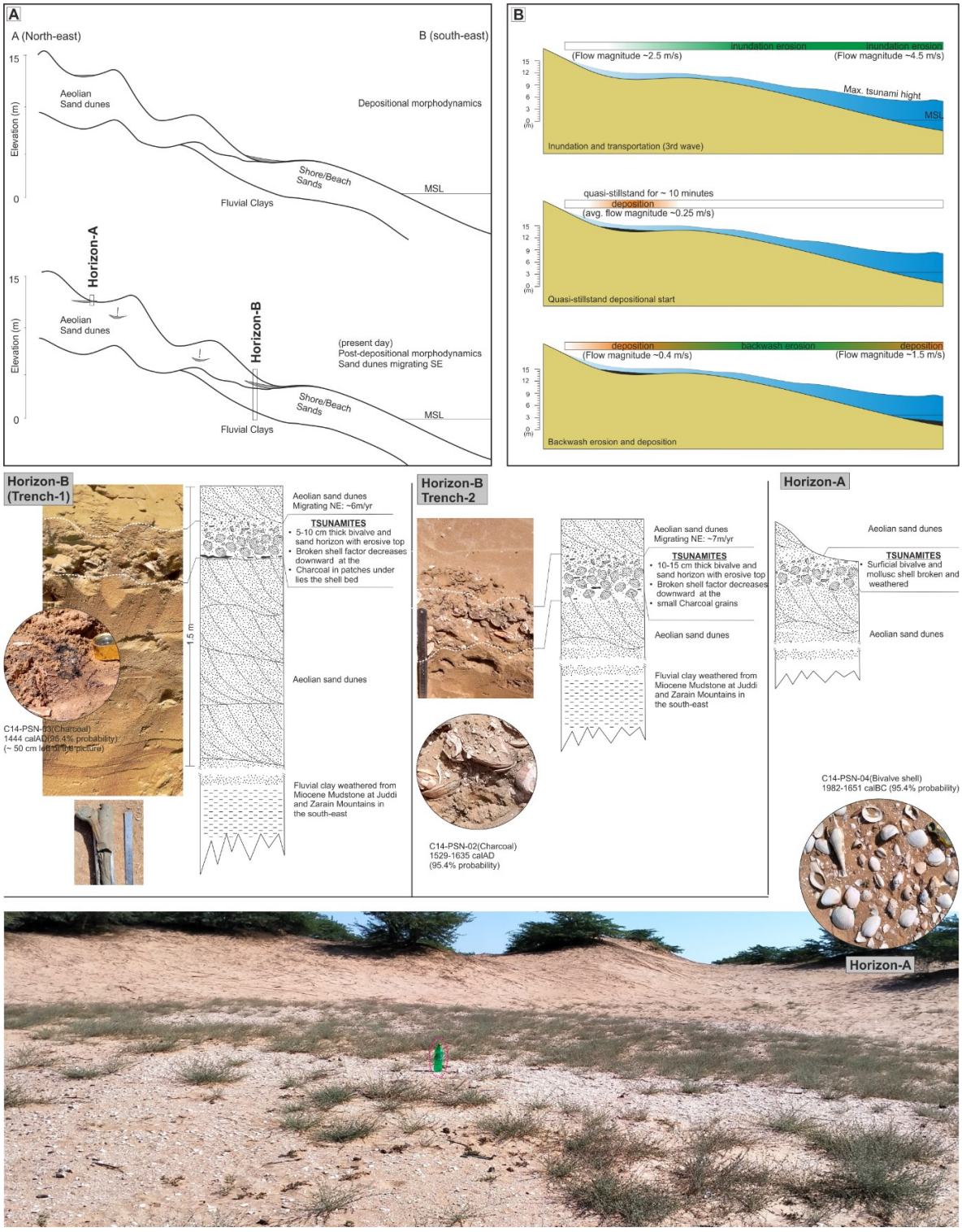

Figure 3.3: A) Schematic x-sections showing the vertical and lateral distribution of tsunamites along with the hosting style. B) Simplified schematic model showing the depositional mechanism for Horizon-B. The flow magnitudes are computed from numerical modelling. The measured litho-stratigraphic logs and respective field photos are appended with.

3.4.3 Tsunami Modelling and Simulation

Numerical modelling of past tsunami events is often used to improve the understanding and evaluation of a past tsunami (Heidarzadeh et al., 2008). Here, we took the farthest limits of mapped tsunamites as the inundation limits and maximum run-up heights to model the event. The modelling estimates three aspects: source size, source position, and inundation pattern consistent with the tsunamites. Various inundation wave scenarios are simulated to find the best fit satisfying the inundation extent and tsunami propagation pattern. The scenarios are generated with earthquake source parameters only; therefore, other possible tsunami sources, such as submarine land sliding, meteoric impacts, etc., could not be ruled out. However, the extreme morphodynamics of tsunamites rule-out cyclone-related inundation. For modelling, the General Bathymetric Chart of the Oceans (GEBCO) 15 arc seconds bathymetry is fused with the TanDEM-X topography. We employed a nested computational grid with a resolution of 0.0004×0.0004 (44 m × 44 m) for the nested model and 0.01 × 0.01 (1 km × 1 km) for the regional model. Reinmann boundary conditions are employed in the regional model to reduce the reflection impact and time-series boundaries for the nested models.

The Delft3D 4.04.01 programme by the Dutch Institute Deltares is used for numerical modelling with earthquake source parameters (Deltares, 2023). The hydrodynamic software module Delft3D-FLOW is employed, which solves non-linear shallow water equations in 2D and 3D for unsteady flow phenomena. The Navier-Stokes equations for water in three dimensions are used to create the shallow water equations (SWE), which are a suitable approximation for the Boussinesq approximation for incompressible fluids. The two-dimensional, depth-averaged calculation approach is used by the Delft3D-FLOW module to simulate tsunami wave calculations (for details, refer to (Deltares, 2017, pp. 175–181). By rupturing a hypothetical splay fault along MSZ trending the regional tectonics located in the SE of Pasni and the SW of Ormara. The fault location, parameters, and initial wave height are given in Figure 3.4.

Parameter	**value**
Location (km)	Figure 3.1
Length (km)	200
Width (km)	60
Depth (km)	10
Dip (Deg)	10
Rake (Deg)	90
Slip (m)	45

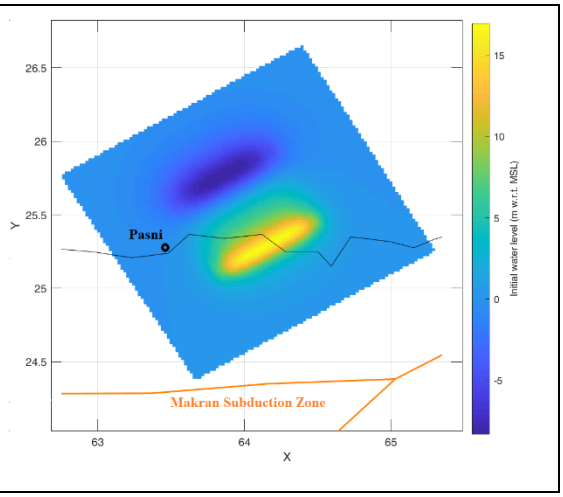

Table 3.1: Earthquake source parameters and initial wave height considered in the study.

In our previous study (Haider et al., 2024), we calibrated and validated our model with a 1945 Tsunami scenario at Pasni and Gwadar. The same calibration and validation are used to model and simulate the present scenario as well. Several tsunami scenarios based on different fault parameters and locations were put on trial to find a wave scenario satisfying the maximum run-up heights. It is

estimated that a tsunami with a wave height of approximately 8 m propagating from the southeast of Pasni can inundate Horizon-A. This scenario overestimates the tsunami dynamics (flow depth and flow velocity) at Horizon-B reflecting another tsunami event of relatively lower intensity. The coastal reflection factor from the coastal cliffs NW of the Pasni plays a major role in multi-wave and amplified wave impact at the Pasni coast. Moreover, the phenomenon generates two extreme reflective waves that completely destroy Pasni and surrounding towns (Figure 3.4).

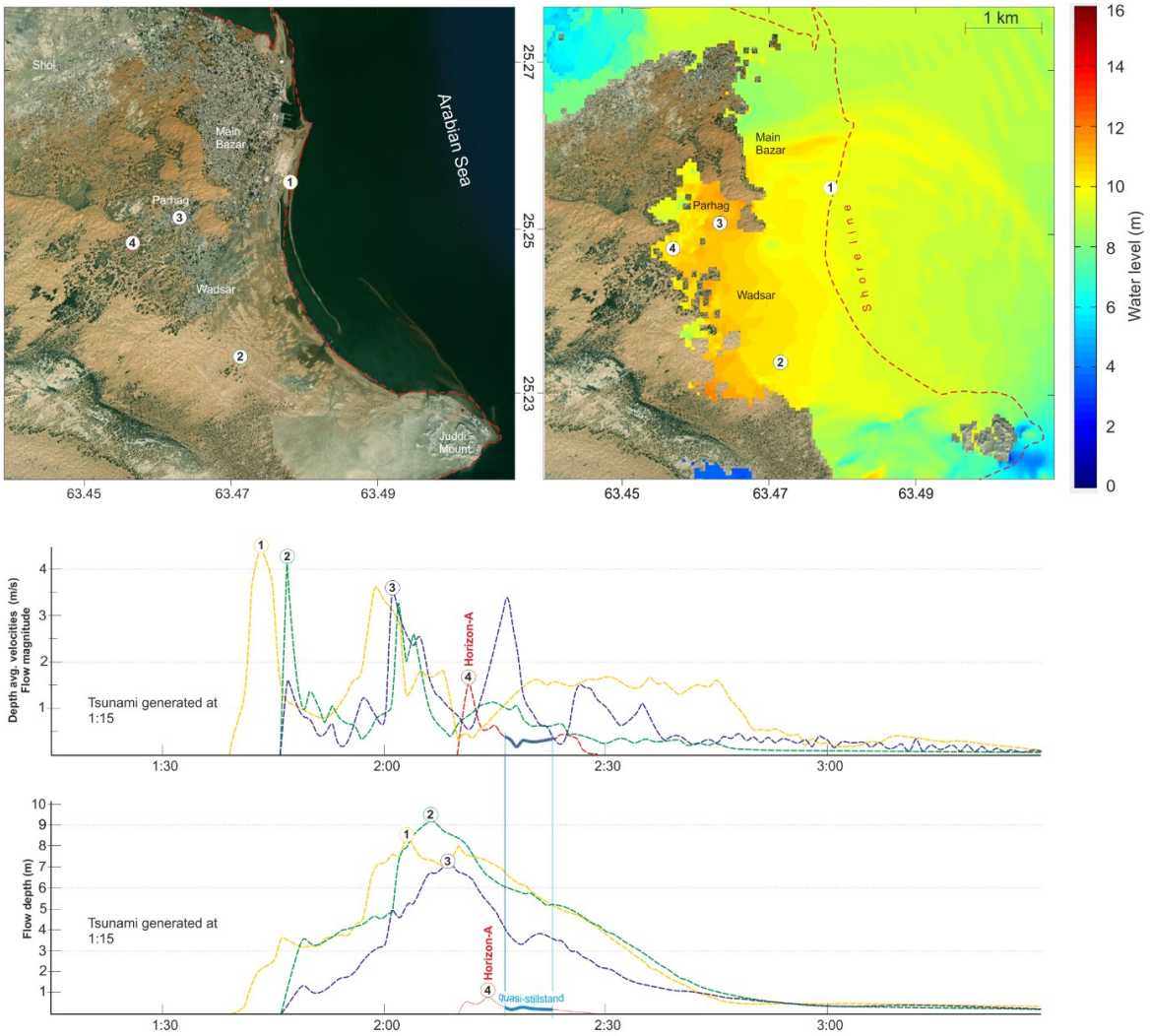

Figure 3.4: Simulation results; inundation extent and water elevations are shown at the Pasni and surrounding areas overlayed on the satellite image (Supplements: Simulations). The line graphs show the flow depth and flow magnitude at each monitoring point shown with a number in a circle (M1 to M4). In the flow magnitude graph, the three wave-package can clearly be marked (detail in discussion section). The second wave, being a little lesser in wave height than the first one, shows the maximum flow depth. The first wave provides conducive conditions to the second and third wave to propagate and penetrate far inland.

Flow depth and flow magnitude in terms of depth times average flow velocity are presented at four monitoring points (Figure 3.4). The mean flow velocity and depth for an average-sized bivalves (axis 28.5-23.2-9.0 mm) umbo facing downstream are approximately 0.71 m/s and 0.64 m, respectively (Silva et al., 2023). In this regard, for Horizon-A, the modelling results are 1.5 m/s and 1 m, which appear suitable for the size of sediments. However, in the same scenario, the two hydrodynamics at Horizon-B are extremely high (4 m/s, 9 m) which doesn't support the deposition but rather the

erosion of tsunamites found on site (if already deposited). It suggests Horizon-A represents a separate tsunami event.

3.5 Origin: Shell middens or natural extreme wave action

Archaeological and radiocarbon evidence from the Las Bela and the Indus delta shell middens indicates the first inhabitant's settlement along the NE Arabian Sea around the 8th millennium BP, and seafaring activity began during this time (Biagi, 2011; 2017). These middens show an assemblage of Telescopium telescopium and Anadara uropygmelana, Anadara rhombea and Terebralia palustris, Circenita callipyga, and Melanoides tuberculate (Biagi et al., 2013). Distinguishing the extreme wave coastal shell deposits from the shell middens is a problem often faced by geoscientists (Ceci, 1984; Dortch, 1991). In this regard, different proxies and standards are used by the researchers to ascertain the deposit's origin (Gill, 1954; Coutts, 1966; Hughes & Sullivan, 1974; Attenbrow, 1992). These proxies rely on the tools of palaeontology, sedimentology, and archaeology (human-related activities). We compiled and listed the set of proxies to compare our field observations with standards in Table 3.2.

At Pasni, the Holocene period demonstrates a complex geographical and geological evolution. Along with numerous traces of occupation, the beach progressed south, leaving behind a series of beaches or lagoonal floors (Sanlaville et al., 1991). The deposition of marine and lagoonal deposits, mostly composed of shells and lagoonal mud, poses a problem in distinguishing the agent of deposition. However, it brackets three possible origins: 1) deposits of the paleo beaches; 2) deposits by extreme natural phenomena (tsunamis, cyclones); and/or 3) deposits by anthropogenic agents (shell middens). We show the spatial distribution of each deposit in Figure 3.5 and Figure *3.6* and a brief explanation in the upcoming paragraphs.

The biggest and most eye-catching deposit lies in a linear valley bounded by high sand dunes on either side, stretching continuously for about 20 km from Chur to the east of Kholi (Figure 3.5). In this area, the work by Sanlaville et al. (1991) is a notable research contribution and sets the footing for further geo-archaeological research. The deposit is predominantly composed of the Meretrix genus (Veneridae family) with a minor sand matrix (Figure 3.5B). Beside the Meretrix bed, the Pirenella genus gastropods (Figure 3.5I) are found throughout the valley floor but not within the Meretrix bed itself, showing the presence of paleo mangroves at the site. Sanlaville et al. (1991) also reports Nassarius coronatus occasionally, but we didn't notice at this site particularly. The thickness of the shell deposits is maximum ~50 cm at the middle and ~ few cm at the eastern and western edges. Also, there are shell mounds in the middle part, which are around 1-2 m high (Figure 3.5G-H). The uniqueness of the middens is their uniform shell species with a narrow and continuous long extension. Sanlaville et al. (1991) and we did not notice any human artefacts along with this deposit; however, we observed some carbonised shells at some spots probably showing signs of burning. Along with burning activity, the mound structures in the middle part reflect some anthropogenic depositional origin, but on the other hand, the absence of any artefact and a minor but considerable number of articulate shells point to a natural depositional phenomenon. In the eastern part, the deposit shows signs of reworking; it is embedded in eolian sand dunes contrary to the parent deposit hosting over the paleo-beach sand (Figure 3.5E). Sanlaville et al. (1991) dated two Meretrix shells at two different sites near Kholi as 895–1266 calAD and 394–861 calAD. The deposit requires detailed geological and archeological investigations to understand its origin.

Table 3.2: Proxies and their comparative analysis distinguishing the depositional agent (shell middens, paleo-beach, and Tsunami-cyclones) at the Pasni and surrounding area. So far, no shell middens have been discovered at the Pasni Coast, therefore we compared our results with the shell midden found at the eastern part of the Makran Coast.

		Depositional agents		
	Proxy	***Shell middens (along Makran)**	**Paleo-Beaches (at Pasni)**	**Tsunamis/ Cyclones**
1	Radiocarbon age along the Makran Coast (calibrated)	• Typically, ~5000-6000 calBC • ~2000 calBC youngest shell middens dated so far at the Makran coast, Pakistan (Biagi et al., 2018)	394–1266 calAD (shell) (Sanlaville et al., 1991)	• 1444-1535 calAD (charcoal) • 1982-1651 calBC (shell) (This study)
2	Reworked/ transported	No	Yes	Highly affected
3	Articulated shells	No	May be Yes	May be yes
4	Small pebbles stones with pitted or corroded surfaces (commonly not used by middens as tools)	No	Yes	Yes
5	Type of soil hosting the deposit	Paleo-beach sand, the high marine terraces	Paleo-beach sand	Aeolian sand dunes (inhospitable life conditions)
6	Habitat of shell organism	Mostly subsidiary channels beside the main mangrove channels	Littoral zone (intertidal, tidal and subtidal)	Mixed species showing a variety of habitats. • Open shore (Littoral zone) • Lagoonal organism • Fresh water
7	Sand-clay matrix	No	Yes	Yes
8	burnt wood or signs of cooking	Usually found around the globe but not yet found along the Makran Coast	No	No
9	Charcoal			Occasional charcoal patches under/within the shell layer
10	Degree of selection: Specimen assemblage and their approximate proportions	• 99.9% Veneridae Family • 0.1% Glycymeridae Family and Genus Pirenella	Mostly Veneridae Family, but depend on the type of shell source at the beach	• 80% Veneridae Family • 15% Gastropods (several species littoral, lagoonal and fresh water) • 5% Anadara oceanica, Anadara rhomboidalis
11	Shell size: <15 mm is considered too small by the shell middens to be taken as a food and are speculated to be deposited by some natural processes	Doesn't host <15 mm		~3-5% <15 mm
12	The presence/absence of non-edible (non-economic) species	Typical species eaten by shell middens	Needs further work	Include unpreferred middens species, growth and sizes too small for food
13	Depositional style/ present day beach processes are analogue to past events	Not analogue to natural coastal processes, several shell mounds	Yes	A mix of different shell sizes and species with beach gravels is analogous to extreme wave beach processes (Figure 3.6). Analogous 1945 Tsunami deposits in the sand dunes of Prahag/ Wadsar area as identified by tsunami survivors
14	Deposit elevation	2 to 14 m	3 to 5 m	3m, 7m, 12m (three horizons)
15	Comparison with 1945 Tsunami Shells		comparable	

*the anomalous shell deposit between Chur-Kholi (Figure 3.5) is also tentatively taken as paleo beach deposit as it does not qualify the criteria to declare as a tsunamites.

Sanlaville et al. (1991) regards the curvilinear deposits of the shell horizon (Horizon-B) as a paleo-beach deposit, but we interpreted it as a deposit of an extreme wave event. Our interpretation is based on the analysis of depositional process and nature of deposit (Table 3.2). The radiocarbon dating on two Meretrix genus shells gave an age of 3699–3139 calBC and 3906–3447 calBC (Sanlaville et al., 1991). In the same horizon, we dated the two charcoal samples: one undelaying and the other embedded in the deposit, showing an age of 1444 calAD and 1529–1635 calAD respectively (Figure 3.2). The history of the Arabian Sea witnesses a tsunami event during this timeline (1524 AD Tsunami). The charcoal age determination gives precise and close age estimations as compared with

those of the shells. The shell may not represent the true age of the deposit, but rather the inception of the shell itself which could last for a much longer period.

Present-day coastal processes at the Pasni, including storm waves related to cyclones, provide a good example of such deposits in the coastal dunes (Figure 3.6 B1-B3). The coastal beach dunes preserve a mix of shells (predominantly Meretrix shells) and rolled pebbles like the ones found in the aeolian sand dunes as of the 1945 Tsunami deposit at Parhag and in tsunamites Horizon-A. The linear bed in the coastal dunes was deposited between 2006 and 2018, as interpreted by the sand accretion and progradation timing of beach formation. During this time, several cyclones affected the Pasni coast, especially Yemyin 2007 and Phet 2010. These shells are derived from the subtidal level, as the beachline and intertidal zone host only beach sand. This case study provides a good example of inundation-related deposits. If the magnitude of the waves increases, then the same type of deposits may be found further inland and at higher elevations. In this regard, the 1945 shell deposits at Parhag town are a validated example of tsunami-driven shells and pebbles which are also witnessed by the 1945 tsunami survivors. Mrs. Tanakko (11 y in 1945) states "The 1945 tsunami came up to here, where we are sitting right now (her house, Parhag). You can still see the scattered seashells here brought up the 1945 tsunami." Horizon-A and B west of Parhag, exhibit the same type of extreme wave deposit much larger in size and extent (Figure 3.6 B1-B3). The disarticulated (single valve) bivalve shell from this site dates to 1982–1651 calBC (Figure 3.2).

3.6 Discussion

The understanding of the tsunamites becomes blurred and hazy further it dates back because of their nature, preservation potential, dating uncertainties, and historical validation (Decker et al., 2022). In this regard, the arid regional climate, and active convergent tectonics, dim the chance to find a paleotsuanmi deposit along the tsunamigenic Makran. The durable nature of tsunami sediments (shells, beach gravels) poses some resistance to the aforementioned factors. It is supposed that the rapid burial of wet tsunamites partially hardens and might be preserved without a significant loss (Goff et al., 2009; Caron, 2011). Furthermore, the patches of charcoal under and within these horizons reflect the rapid burial of probably small shrubs on the dunes, providing a conducive reducing environment to turn into charcoal. In the context of the above discussion, the tsunamites at Pasni are durable to the weathering processes. As already mentioned, due to the arid climate precipitation rate is too low to generate surface runoff and erosion. On the other hand, the hard shells are resistant to the aeolian weathering. There may be more tsunamites horizons preserved in the sand dunes, which need more exploratory work. The correlation of newly reported tsunamites with those of 1945 tsunamites at Parhag area and the extreme wave deposit in the coastal dunes shows a good analogy to identify the extreme wave event(s). Similar types of extreme wave deposits are reported from Fins and Athaibah, Oman (Hoffmann et al., 2020).

There are some age constraints regarding the number of tsunami events. The present findings show a minimum of three and a maximum of four, including the 1945 Tsunami. The charcoals under and within Horizon-B show an age gap of 75 years, which raises questions as to whether it was two different events or was there some sampling, processing, analysis error or age difference in the alive vegetation then? However, the cumulative results bracketed as 1444–1635 calAD and the approximated average age (1539 AD) are very close to those of the 1524 Dabhol Tsunami event. Rajendran et al. (2020) sampling results from Kelshi, India brackets the dates as 1508–1681 calAD and averaging as 1594 AD. The disarticulated bivalve shell from Horizon-A dates to 1653-1984 calBC, representing the age of the shell and maximum possible age of the tsunami event. Various studies around the Arabian Sea coastlines (India-Oman) testify to a mega-tsunami event of greater

intensity than the 1945 tsunami around 1000 AD (Bhatt et al., 2016; Prizomwala et al., 2018; Hoffmann et al., 2020; Decker et al., 2022). All of them attribute the tsunami source to the MSZ due to the size of tsunami. However, further dating could precise the event age.



Figure 3.5: Field photographs with spatial distribution of possible source material in the study area. The locations of the photos are tagged in the topmost image (satellite image on the shaded relief). The field photos with closeups show the thick deposit between Chur and Kohli villages at different locations comprising predominantly Meretrix shells. The western and middle parts (Photos F, G, H, I) lie on the valley floor along with shell mounds over the paleo-beach sand while on the eastern side the thin bivalve bed (Photos E) is embedded in the aeolian sand dunes at higher elevation. This embedded portion is interpreted to be a reworked deposit.

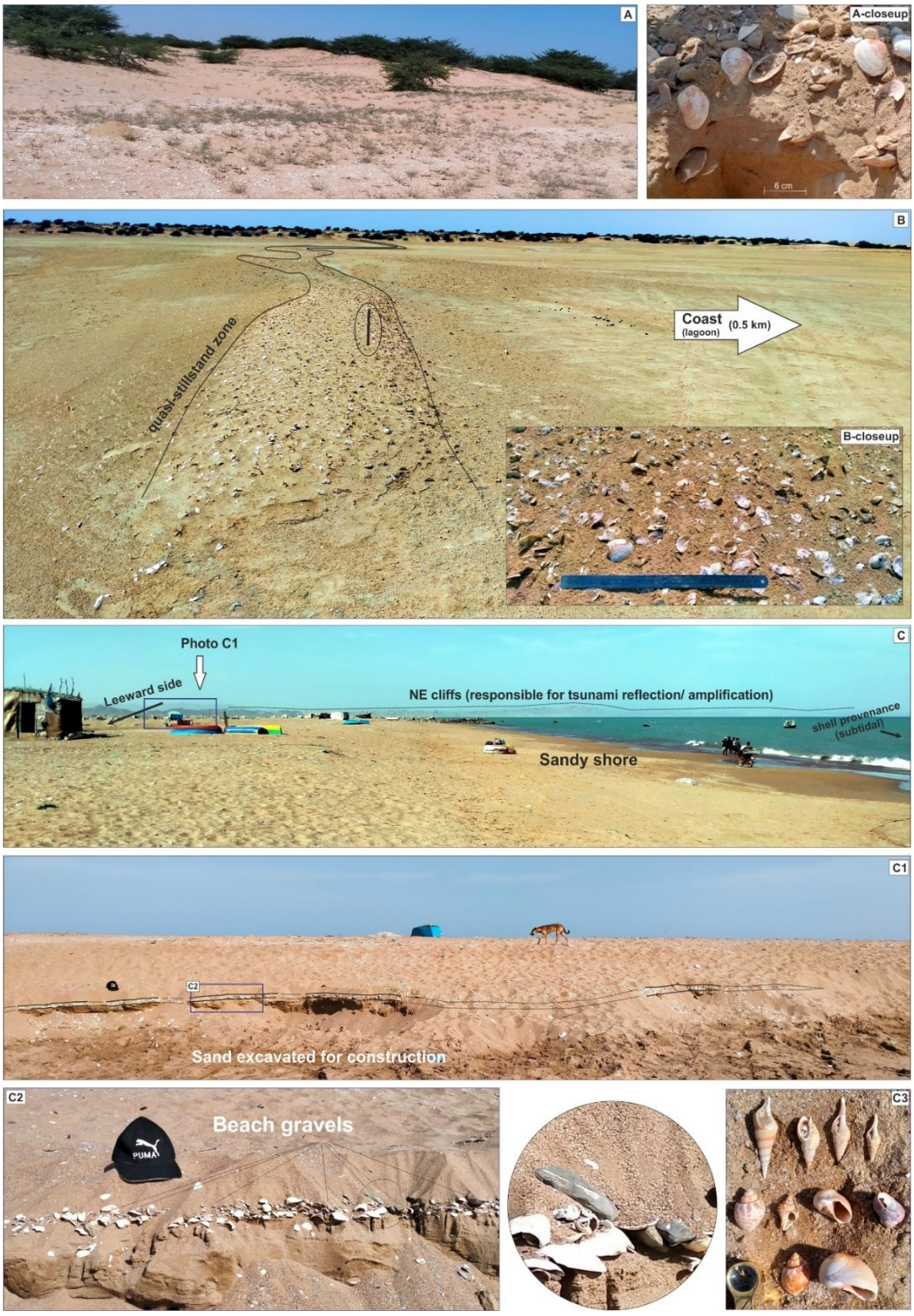

Figure 3.6: Examples of extreme wave deposits showing depositional style and architecture at Pasni and surrounding area. The location of the photos is tagged in *Figure 3.5* (satellite image overlayed shaded relief). A) The 1945 tsunami deposits at Parhag. B) a curvilinear deposit of predominantly oysters in the lagoonal mud and sand. Such a curvilinear linear depositional style is exhibited by the tsunami waves losing their flow magnitude (quasi-stillstand) at maximum inundation limits (Bellanova et al., 2021). C) A modern-day example of an extreme wave deposit from cyclone-related inundation It is composed of shells and beach gravel in a coastal dune setting. The NE field of view shows (faded) cliffs responsible for unusual high tsunami wave height and multiple wave reflection at the Pasni shore.

The simulation results clearly show an event of greater intensity than the 1945 Tsunami. Due to the position of the tsunami source, wave height satisfying the morphodynamics of Horizon-A varies. Based on the direction of transport and provenance of the tsunamites, we suggested and evaluated the source position SE of Pasni (Figure 3.1 A). The simulation shows that this is also the worst tsunami position for Pasni. For instance, with suggested source position, a wave height of ~8 m at the coast meets the tsunamites morpho-dynamics of the Horizon-A. Relocating the source position south of the Pasni (1945 EQ Position), it needs at least 15 m wave height to satisfy the same inundation hydrodynamics, however it affects the provenance and direction of transport. In this regard, the 1945 Tsunami inundation extents and runup heights (~ 10 m) may also be explained with a ~5 m wave scenario. This source position could explain the origin of three waves; the 1945 Tsunami survivors reported three waves, the second being the biggest one (Kakar et al., 2014). Along with wave height and number of waves, the time delay of one to two hours is perhaps also possible due to the time consumed in reflection and amplification phenomena.

The simulation corroborates that reflection phenomenon along the NW coastline of Pasni being responsible for generating three waves and the second one being the highest with maximum inundation extents (Figure 3.4). This finding is important in the aspect that it could rule out the landslide hypothesis for 1945 Tsunami. The landslide hypothesis was based on three aspects; 1) time delay between the earthquake and tsunami arrival, 2) The earthquake could generate maximum 5 m wave height at the coast, however reported 1945 wave heights are 7-12 m and 3) No. of waves. Three inundating waves aspect have not previously been studied. Furthermore, incorporating the 2 m reported coseismal subsidence at Pasni and 2 m coseismal uplift at Ormara further corroborates the modeling results. To address these concerns, our model shows that an earthquake source with the position and orientation mentioned in Figure 3.1 could possibly explain the geo-hydrodynamics of the 1945 Tsunami. The continuous beach cliff and curved nature of the beach (bay) could pile up a huge quantity of inundating water at the Pasni shore, resulting in far-inland inundation. Due to this geomorphological setting, the reflection phenomenon is maximum with the tsunami source directivity. Therefore, a fault striking ~N35E, positioned SE of Pasni will pose the maximum tsunami hazard.

We modeled the tsunami inundation with the current mean sea level (MSL) because of complexity and uncertainty to determine the local relative sea curve. The measured uplift rate of 0.1–0.2 cm/a at Pasni-Ormara shows an approximate uplift of 0.8 m and 5 m since 15th AD and 17th BC, respectively. On the other hand, the Pasni coast was subsided ~2m by the 1945 earthquake (Mw 8.1). The recurrence of such an earthquake along this particular part of the coast is 1000-2000 (Page et al., 1979). The recent sand accretion phenomenon since 1985 has accredited a 500-metre-wide beach with a height of 2 m from msl. Also, the lateral geodetic measurements show unusual tectonic behaviour: 7.3 cm/a SSE at Pasni as compared to 13 cm/a SE and 13 cm/a S at Gwadar and Ormara, respectively (Haider et al., 2023). The complex interplay of local tectonics and sedimentary beach process complexes the relative sea history curve estimation, especially within the current scope of research.

3.7 Conclusions

Pasni exhibits remnants of at least two extreme wave events: the 1945 AD tsunami, the 1524 AD tsunami. The third event of 17th BC tsunami deposits needs further investigation involving radiometric analysis to a certain age of the event. The tsunamites horizon dating from the 17th BC is based on the radiocarbon shell of a bivalve, hence representing a maximum age. The lower age bracket further needs high-frequency dating. The history of Pasni around 1524 AD needs further

studies to validate and to have more information about the disaster. The Cliff-Bay NE of Pasni generates high-amplitude tsunami reflections, which result in multiple wave arrivals at the Pasni shore. The reflection and amplification effect of bay is dependent on the direction of approaching waves and is maximum for tsunami sources laying SE of Pasni in the Arabian Sea.

3.8 Outlook

At location T3 shown in Figure 3.1, we encountered a 1.5 cm thick charcoal layer in a shallow trench at the Pasni rest house Figure 3.7). The rest-house was washed away during the 1945 tsunami (Lodhi et al., 2021). We suspected the deposition and burial of some organic material by a tsunami, probably the 1945 Tsunami (Figure 3.7). The radiocarbon dating results show a "modern age" sample, which means it contains excess 14C, probably from mid-20th century atmospheric thermonuclear weapons tests. Such samples need calibration other than the aforementioned. To convert the fraction Modern to calendar age, we used online calibration available at (http://calib.org/CALIBomb/). It gave an event around 1960, which may be some anthropogenic activity as the tsunami history post-1945 Tsunami is well documented.

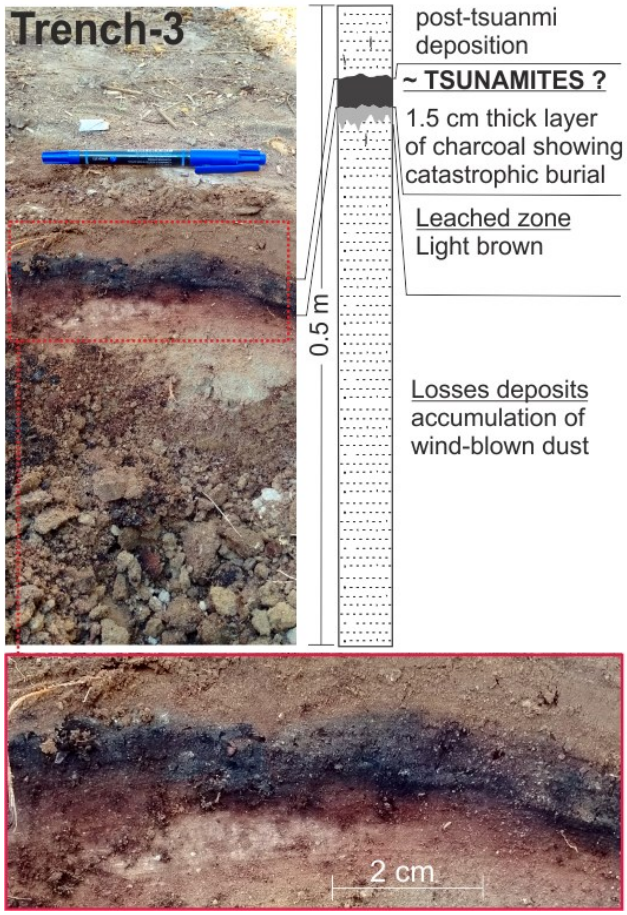

Figure 3.7: Sedimentary log of the shallow trench at Pasni. trench location in Figure 3.1.

4. Static Inundation Analysis of Karachi, Gwadar, Pasni and Ormara

This chapter includes contents from the following publication,

- ***Haider, R**., Ali, S., Hoffmann, G., Reicherter, K., 2023. A multi-proxy approach to assess tsunami hazard with a preliminary risk assessment: A case study of the Makran Coast, Pakistan. Mar. Geol. 107032. https://doi.org/https://doi.org/10.1016/j.margeo.2023.107032*

4.0 Abstract

To assess preliminary vulnerability of four major coastal cities (Karachi, Ormara, Pasni, Gwadar), a static inundation analysis is carried out for four different wave scenarios (3m, 7m, 10m, 15m). Each wave scenario is studied with two different models: Bathtub model and Standing wave model. The bathtub model considers the inundation as a relative sea transgression on the land while the later model conserves the inundating water mass and impart the Manning's Roughness. The results show minor coastal damage with a 3m high wave scenario but 7m and higher will result in moderate to heavy losses. Notably, a significant portion of the population in the Gwadar, Pasni and Ormara resides at an elevation of 5m (max. 12m) and within 1km of high tide limit. These factors substantially increase the vulnerability of these cities to inundation, with approximately 150,000 inhabitants at risk under a 15m wave scenario. In the case of Karachi, preliminary estimates suggest that a population of at least 2.0 million is susceptible to the 15m wave scenario. Furthermore, a comparative analysis of the models reveals that the Bathtub model tends to overestimate by a factor of 1.8 compared to the Standing wave model.

4.1 Introduction

The socio-economic significance of the coastal region amplifies its value for development and urbanization. Presently, Gwadar, Pasni, and Ormara stand as midsize cities with populations of approximately 100,000, 35,000, and 20,000, respectively (Figure 4.1). Over the past two decades, the pace of development has surged, particularly with the inception of mega projects under the Road and Belt Initiative. Additionally, the coast encompasses Karachi, the world's third-largest city with a population of around 22 million and recognized as the economic center of the country. The lack of

preparedness for extreme wave catastrophes, particularly tsunamis, in these cities underscores significant gaps in hazard and risk analysis, as well as in policy development and implementation. Currently, measures to mitigate tsunamis typically rely on worst-case scenario assessments of maximum wave height and inundation extent. However, the domain of risk analysis critically lacks in city-scale inundation analysis, crucial for estimating losses and formulating efficient evacuation strategies. Moreover, such inundation analysis is imperative for effective city and town planning. This chapter seeks to bridge this research gap by examining inundation dynamics using two distinct static models. These models and their methodologies are summarized in Table 4.1.

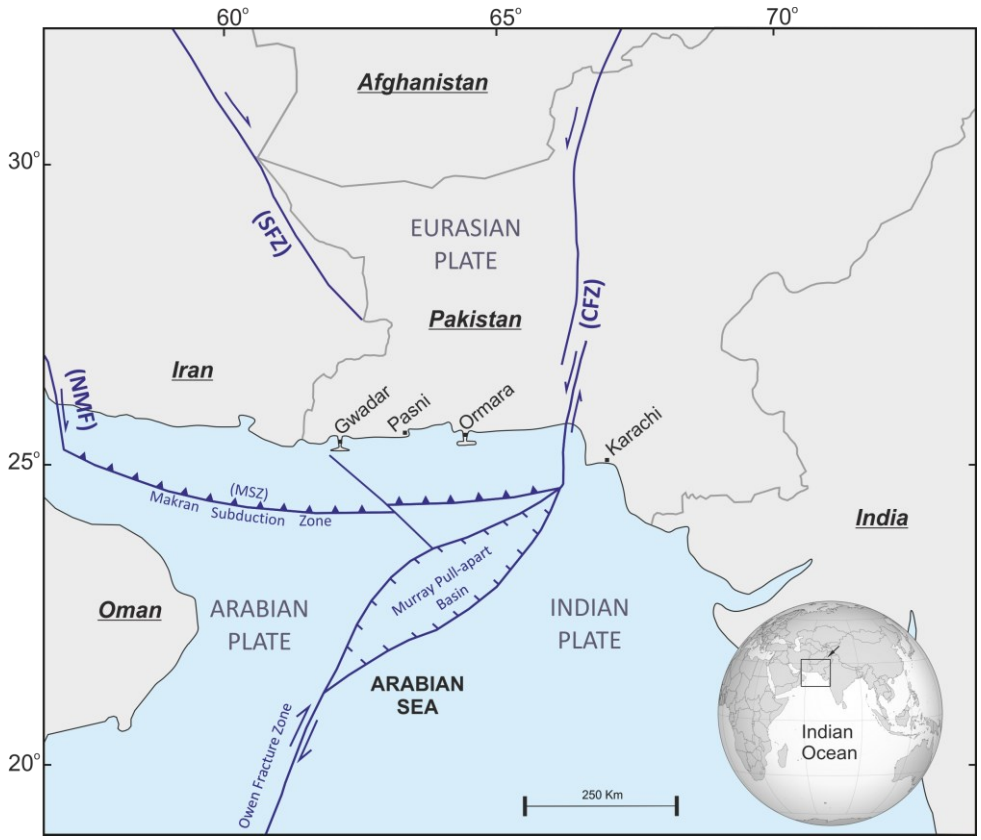

Figure 4.1 Location map of Makran region with major regional tectonic elements and cities along the Pakistan Coast.

4.2 Approach and Models

4.2.1 Bathtub Model

The bathtub or bucket-fill model is the simplest and most nascent model based on the static approach which considers the inundation as a relative sea transgression on the land. The run-up for each scenario is calculated by submerging the equal topographic contour height under the transgressing sea. For example, in the 7m scenario, areas with an elevation of 1.5m a.s.l. with base level connected to the coast would be inundated by 5.5 m. The approach, in sometimes modified versions, is used to study the tsunami risk assessment in Tohoku, Japan (Masuda et al., 2012); Akoli, Greece (Tarbotton et al., 2012); Samoa, Pacific (Smart et al., 2016); Muscat, Oman (Schneider et al., 2016); Augusta, Italy (Pagnoni et al. 2021; Williams et al., 2021). The static bathtub approach is modified in two ways for this study: 1) the tsunamites record for highest inundation height is reported from the Sur/Fins coast, Oman, which is at nearly equal distance to south of the Makran coast. The tsunami

mechanism for both of these coasts is inferred to be the same as the MSZ. Further, these runup heights are compared with the probabilistic and deterministic models and finally four different wave heights (3, 7, 10, 15 m) for four major cities (Karachi, Gwadar, Ormara and Pasni). Three wave-scenarios under 15 m are also analysed for a possible shorter return period. This approach only helps in demarcating the areas vulnerable to tsunami waves and does not consider the potential of inundating waves (mass) and surface friction. The models and approaches are surmised in Table 4.1.

4.2.2 Standing wave model

To conserve the inundating water mass and impart the Manning's Roughness Coefficients, a second hydrostatic model is used. We named it as the standing wave model which is based on the mathematical calculations developed by Berryman (2006). The equation-(i) in Table 4.1 calculates the tsunami height loss per cubic meter based on the value of distance to slope and the surface roughness. Next, the maximum inundation extent is calculated by equation (ii). Using the model builder scheme in ArcGIS 10.x, Anshori (2019) developed a toolbox to operate these equations which reduces the time and effort. The model is applied to the coastline of New Zealand by Berryman (2006), Temon, Indonesia by Prasojo et al., (2017) and Yogyakarta, Indonesia by Steinritz et al., (2021).

Table 4.1: Summary of models and approaches with respective governing equations

Model	Equation/s	Reference
Bathtub	Bucket-fill approach considering sea-level rise	(Masuda et al., 2012) (Tarbotton et al., 2012) (Smart et al., 2016) (Schneider et al., 2016) (Pagnoni et al., 2021)
Standing wave • mass conservation • Surface roughness	$Head_{\text{loss}} = \left(\frac{167n^2}{\frac{1}{Y_0^3}}\right) + 5\sin \sin s_0$ --------(i) $Inundation_{max} = \frac{Y_0}{Head_{\text{loss}}} 10$ --------(ii) n: roughness coefficient s_o : Topographic slope (radian) Y_o: Initial wave height on the shoreline	(Berryman, 2005) (Prasojo et al., 2017) (Juniansah et al., 2018) (Steinritz et al., 2021b)

4.2.3 Data and parameters

For inundation studies, the German Aerospace Center's (DLR) 0.4 arcsec digital elevation model (DEM) with spatial resolution of 12 meters is used. The trademark TanDEM-X in combination with TerraSAR-X generates DEM from bistatic X-Band interferometric SAR acquisitions and has a hypothetical ellipsoidal datum. The ellipsoidal heights are adjusted to the ground heights with reference to mean sea level from Survey of Pakistan's topographic maps (1:50,000). The post data acquisition developments are manually added in the DEM. For example, the coastal parts of Karachi (Sea view, DHA) and Gwadar (East Bay Express Way) are reclaimed from the Arabian Sea and were not part of original TanDEM-X data. These manually added features have a uniform slope angle with high tide water line in case of a beach at Karachi and vertical wall in case of Gwadar. Bathymetry is taken from the Survey of Pakistan toposheets (1:50,000).

To find the different inundation extents especially in the Bathtub model, bare ground elevations are required. As the DEM includes heights like top of plants, houses, poles and such other features. To exclude these elevations, the technique which gave the best results is the interpolation of bare/open

land elevations under the surrounding buildings and the planted/forested areas. The roads, streets, playgrounds, parks, graveyards, lakes and other open lands provided the best sites for the true ground elevations. For standing wave model land use maps are an important prerequisite for inundation analysis. The land use classification allows to assign these features a particular surface friction coefficient against the tsunami inundation. Land use dataset includes houses, roads, seaports, schools, mosques, hospitals, airport, nuclear facility, parks, and the bare land Figure 4.2. Also, the populated areas are classified as dense, moderate and scattered areas. The Manning Surface Coefficients listed in Figure 4.3 is assigned to each feature. The coefficients are adapted from Berryman, (2006) and Mourato et al., (2017). The maps are produced by interpreting the satellite images of Google Earth, ESRI and city maps by Survey of Pakistan. The dense network of roads is obtained from Open Street Maps (OSM). Through overlay analysis of land use with all four scenarios, a crude and preliminary estimation for population under risk is calculated. The population of municipalities is taken from the Pakistan Bureau of Statistics. The land use classification is also helpful in detailed risk analysis, but it is not taken up as it needs more data from the field such as Relative Vulnerability Index (RVI) and the households.

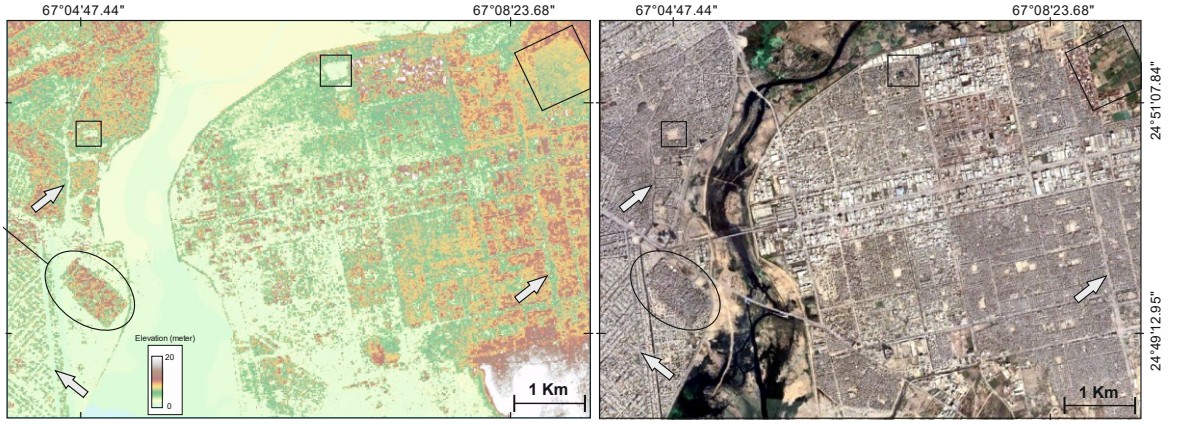

Figure 4.2: A comparison of the DEM (left) and a satellite image (right) of a section of Karachi. The buildings in the oval circle show roof-top elevations as compared with the ground elevations in the surroundings. The arrows and squares point to the few ground elevation sites (roads, open lands) in between the densely populated areas used for the DTM interpolation.

4.3 Modeling Limitation

1. The static bathtub approach does not account for the surface friction or a water wave rather it considers a relative sea level rise. Hence overestimating the inundation extents and depths.
2. In standing wave models, the buildings and the elevated hollow structures act as solid bodies in digital elevation model (Figure 4.2). These elevated solid structures could not account for water volume adjustment, hence pushing the inundating waters further ahead. Due to which the model may overestimate the risk. To minimize this water push, Manning's values on the higher side are opted, but for densely populated areas the issue needs to be worked out further.
3. Inundation analyses are made with high tide datum. In case of low tide, the corresponding effects will be relatively low.

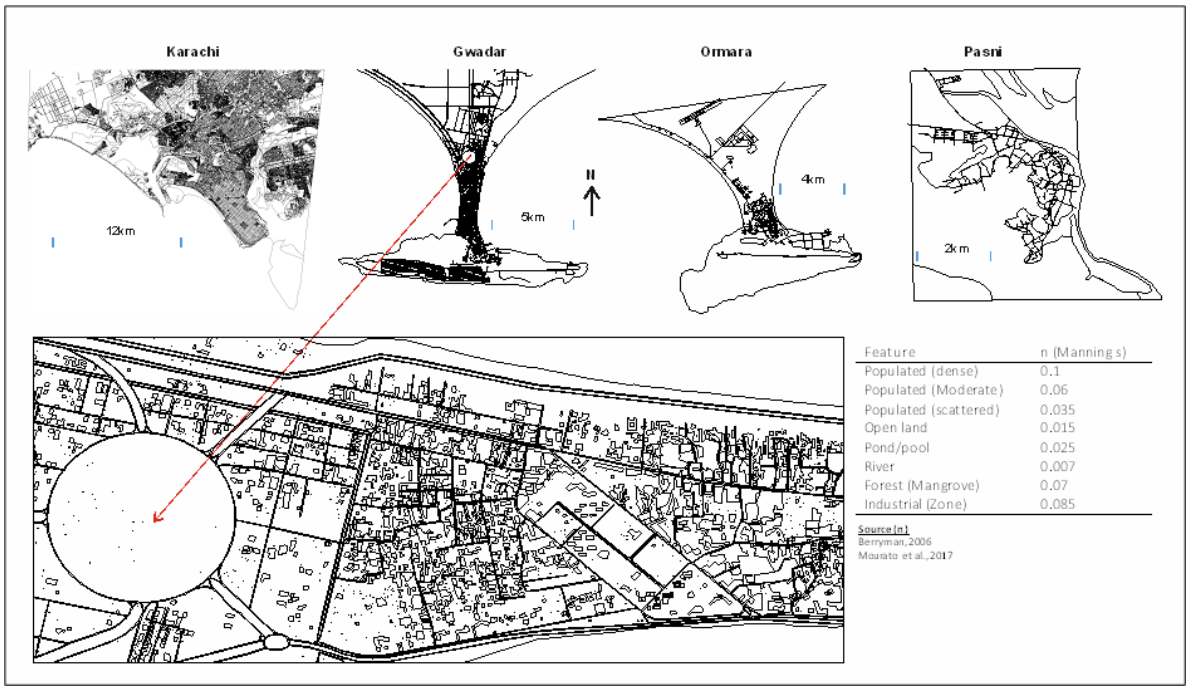

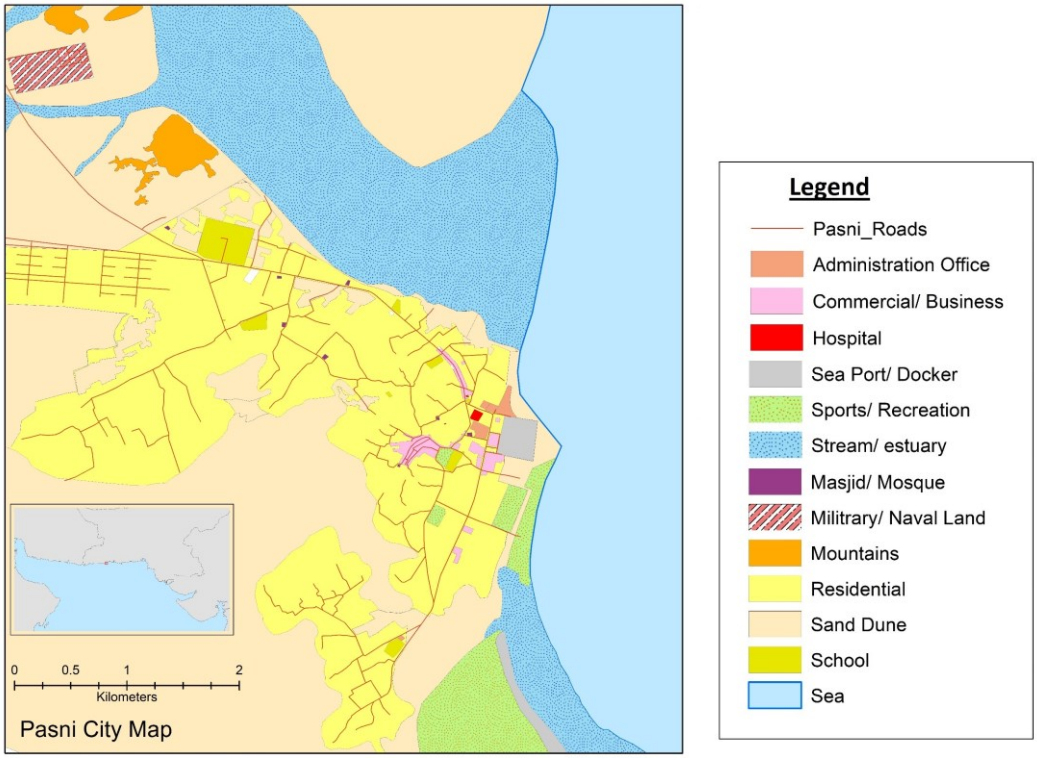

Figure 4.3: Land use maps of four cities. The inset table shows the Manning's Surface Roughness used for each feature in the map. The lower most map is (colored) land use map of Pasni.

4.4 Results and comparative analysis

The results are presented as maps and a comparative analysis of these models for each city is carried out. The results of 7m and 15m of each model are presented in this chapter while the detailed results as maps of each case and city are given as the supplement. As results of the dynamic model are dependent on proximity and source position, therefore the comparative analysis is limited with the given source location. The independent and comparative analysis is presented below city wise.

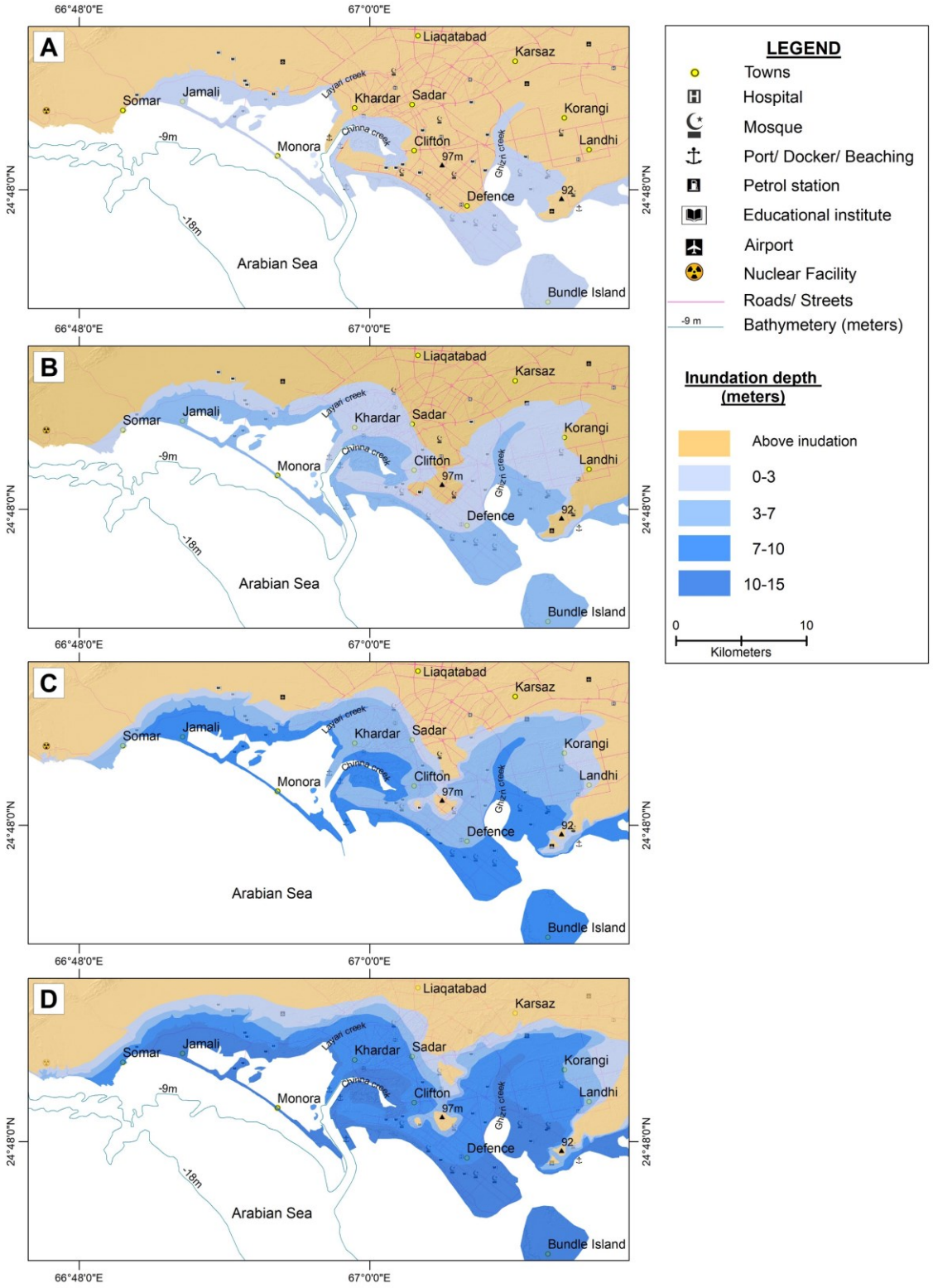

Figure 4.4: Inundation results for Karachi using bathtub model.

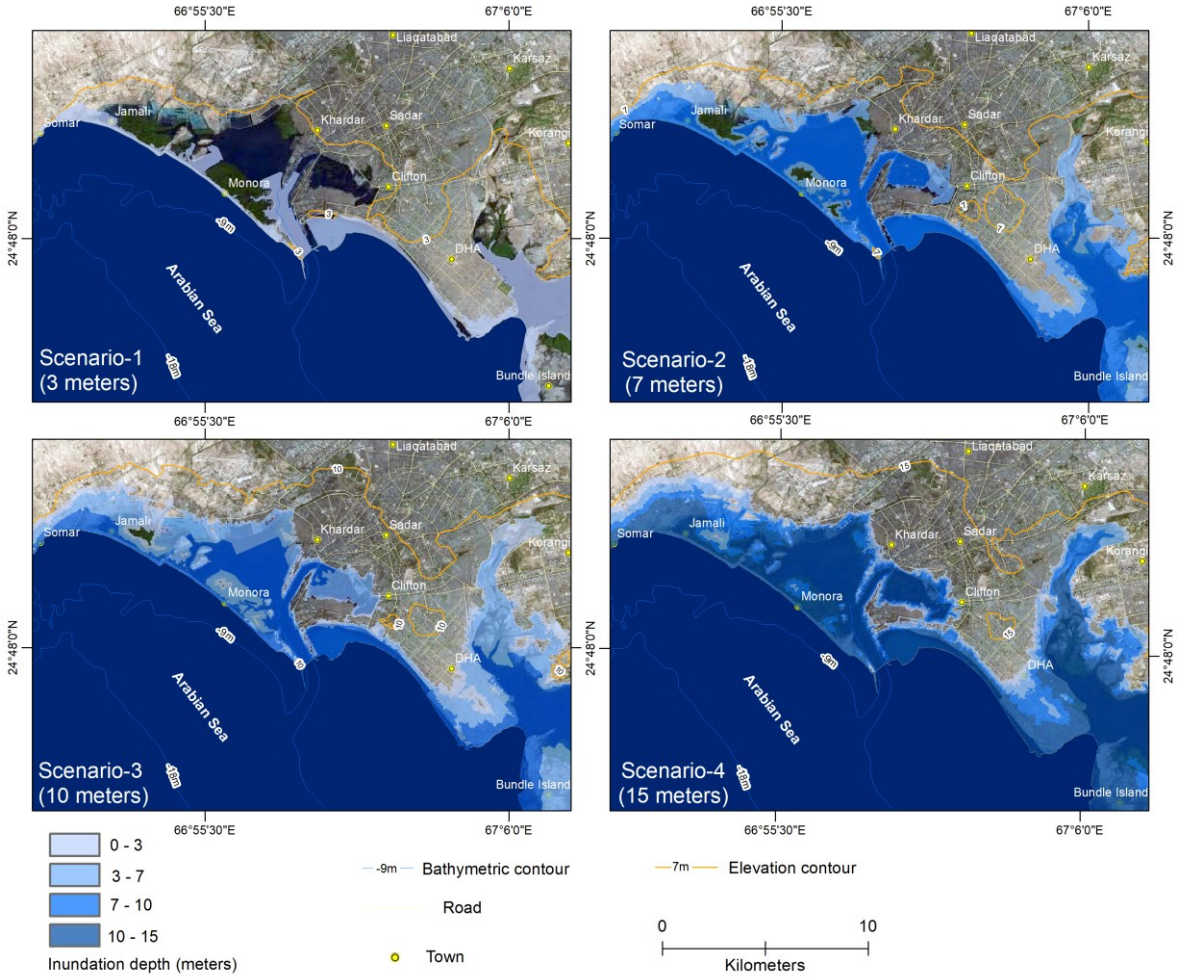

Figure 4.5: Inundation results for Karachi using standing wave model.

4.4.1 Karachi:

The bathtub inundated approximately 10% and 60% of Karachi city against the minimum and maximum wave scenario. Whereas the standing wave models inundation varies with location from 5%-35% respectively as shown in Figure 4.4 and Figure 4.5. The bathtub can maximum inundate 10km inland, while standing wave and dynamic models reach to about 6 and 3 km respectively. The comparative analysis shows that on average, the bathtub model overestimates the inundation extent by a factor of 1.5 in comparison to the standing wave models. Also, the analysis shows that a 3m wave scenario will have minor to negligible damage to the city while in the 15m scenario, approximately 1.5 million populations will be affected (Figure 4.12).

4.4.2 Pasni

The major portion of population resides at an elevation between 5-10m. The bathtub model inundates 22% to 90% of the Pasni study area in 7m and 15m scenarios respectively and the later one includes a major part of the city (Figure 4.6). The standing wave inundates 10%-65% as shown in Figure 4.7. Regarding maximum inundation extent, the bathtub can go up to 20km inland, while standing waves and the dynamic models can penetrate to 2 to 2.5km respectively. Few coastal settlements along the beach are inundated with 3m wave height. In the worst-case scenario (15m), both models completely drown the town (Figure 4.12).

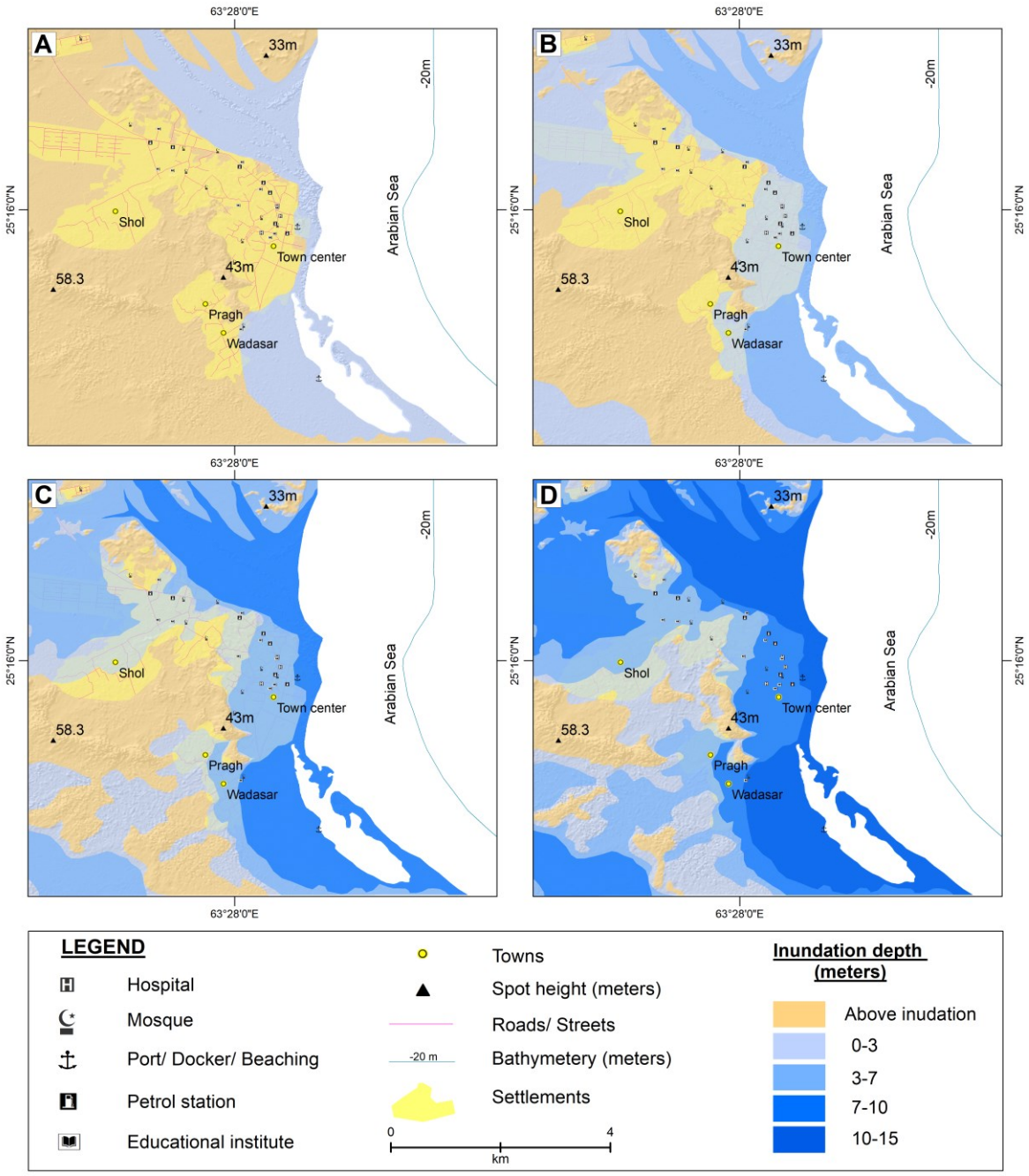

Figure 4.6: Inundation results for Pasni using bathtub model.

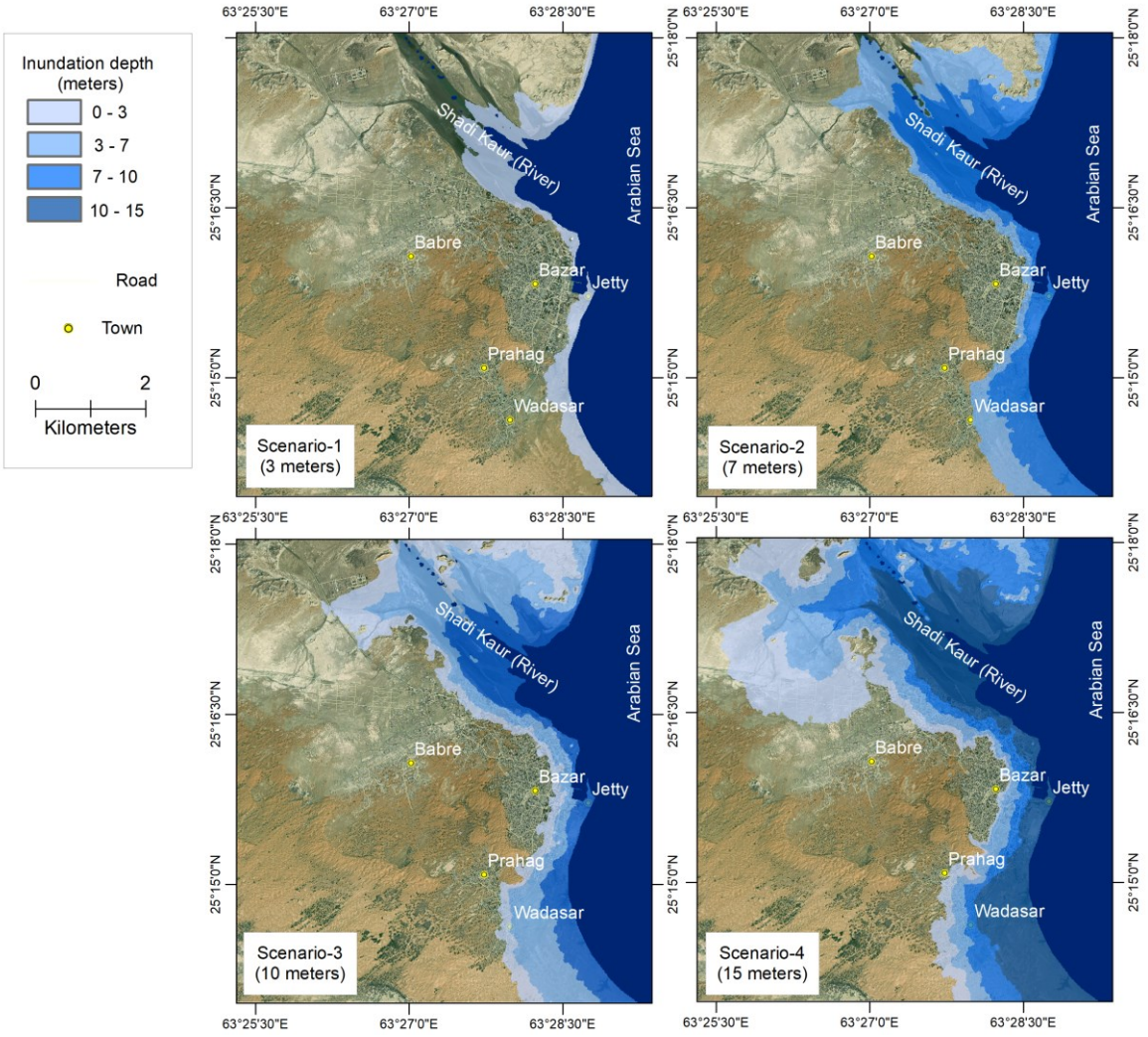

Figure 4.7: Inundation results for Pasni using standing wave model.

4.4.3 Ormara and Gwadar

Both cities are discussed under the same heading as both have almost the same results. The statically raised sea level up to 15m can submerge 100% of population dwelling areas in both the study areas (Figure 4.8 and Figure 4.10). The standing wave model inundated 4% (Ormara) and 2% (Gwadar), see Figure 4.11 and Figure 4.9 . Also, the maximum inundation extent of the models is not more than 2km.

The comparative analysis shows that on average, the bathtub overestimates result by a factor of 1.5 as compared to standing wave model. A 3m wave scenario will not affect any part of cities except minor losses to ships at ports and or docked at the beach, while in the 15m scenario both cities will bear heavy losses. The impact and effects vary depending upon topography and coastline proximity. The population of both cities resides almost at the same elevation (5m average) which may drown completely under 15m scenarios. The Gwadar has a safety edge over the Ormara that both sides (Bays) are raised and protected by a 4m high wall.

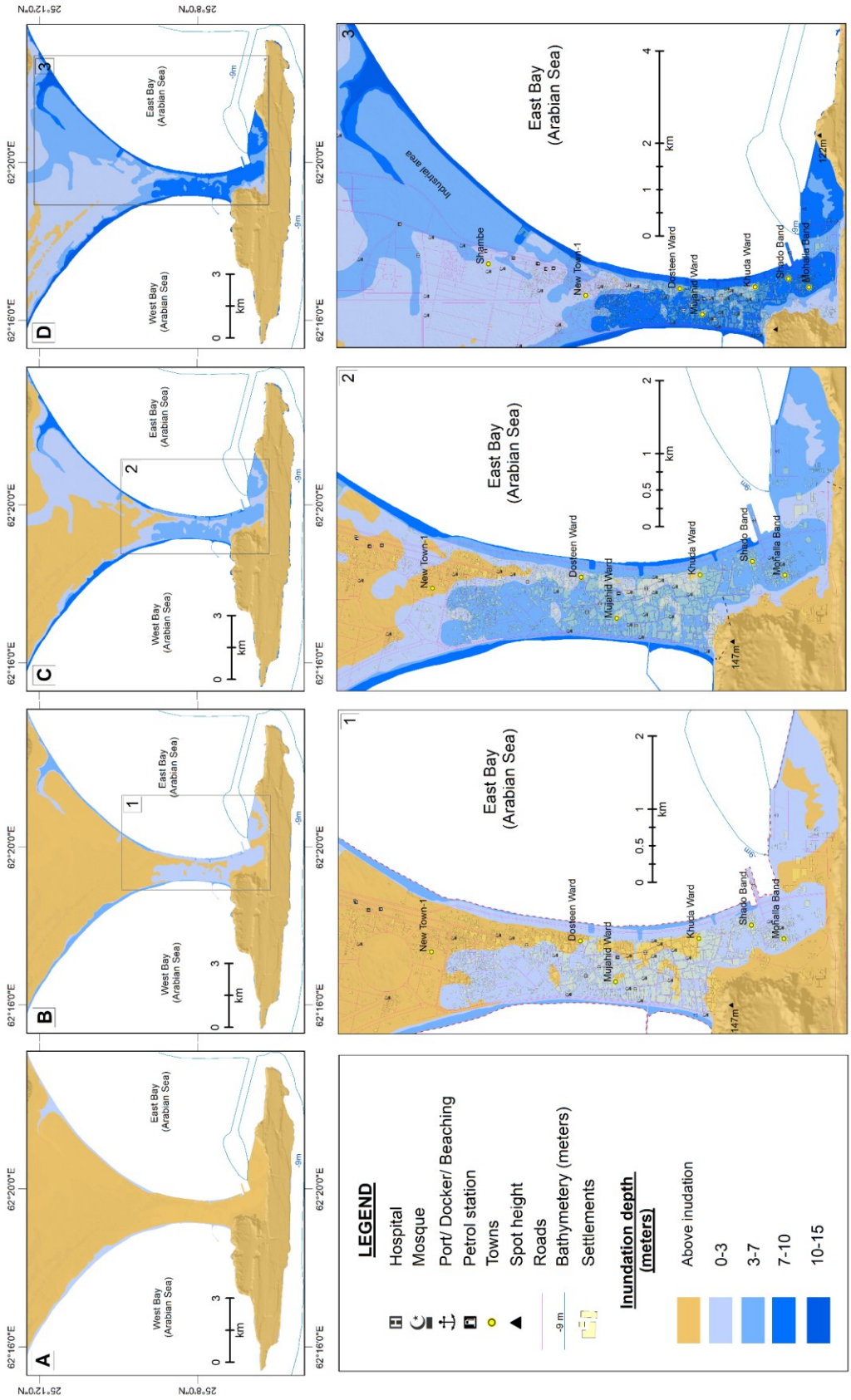

Figure 4.8: Inundation results for Gwadar using bathtub model.

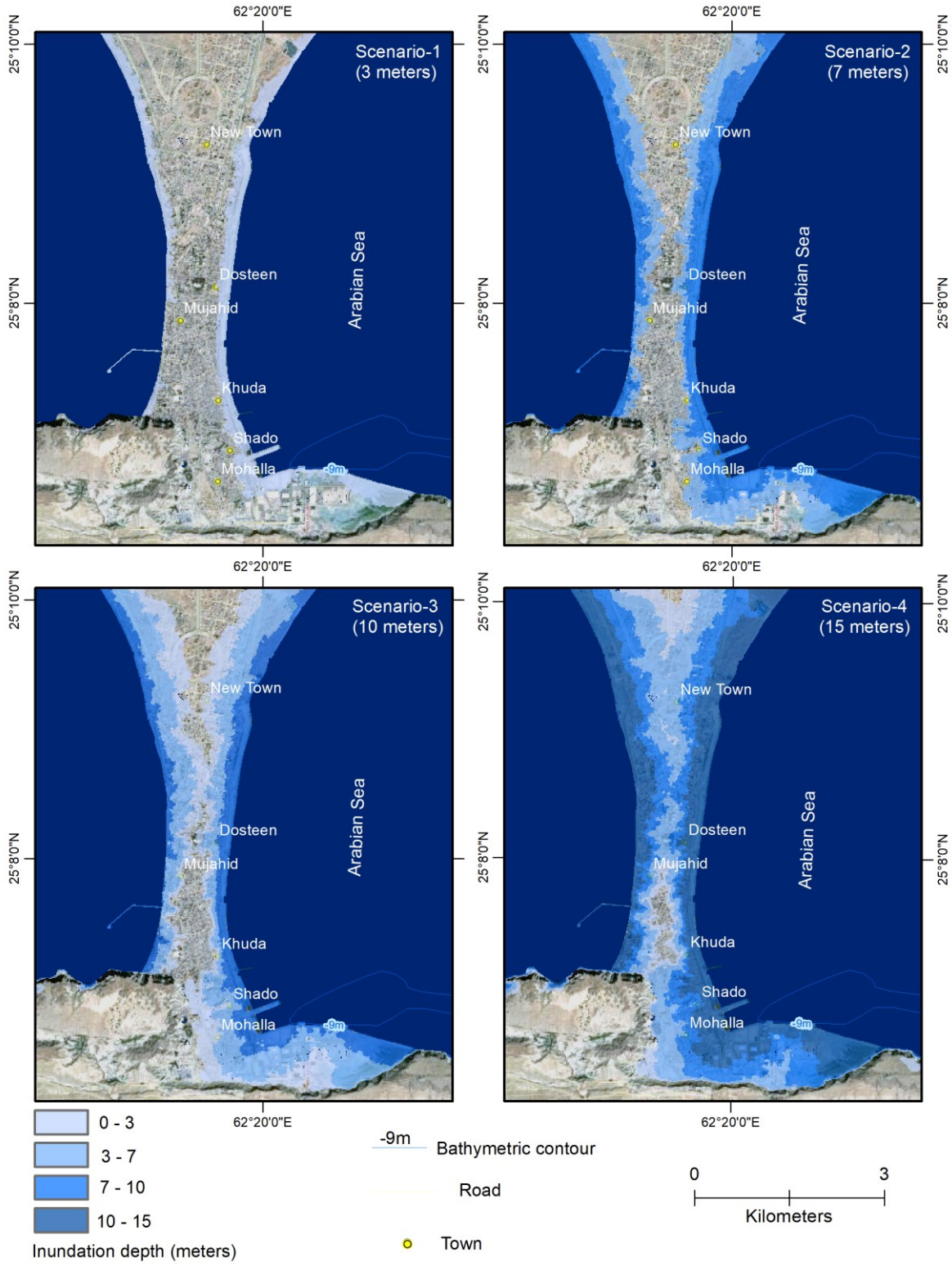

Figure 4.9: Inundation results for Gwadar using standing wave model.

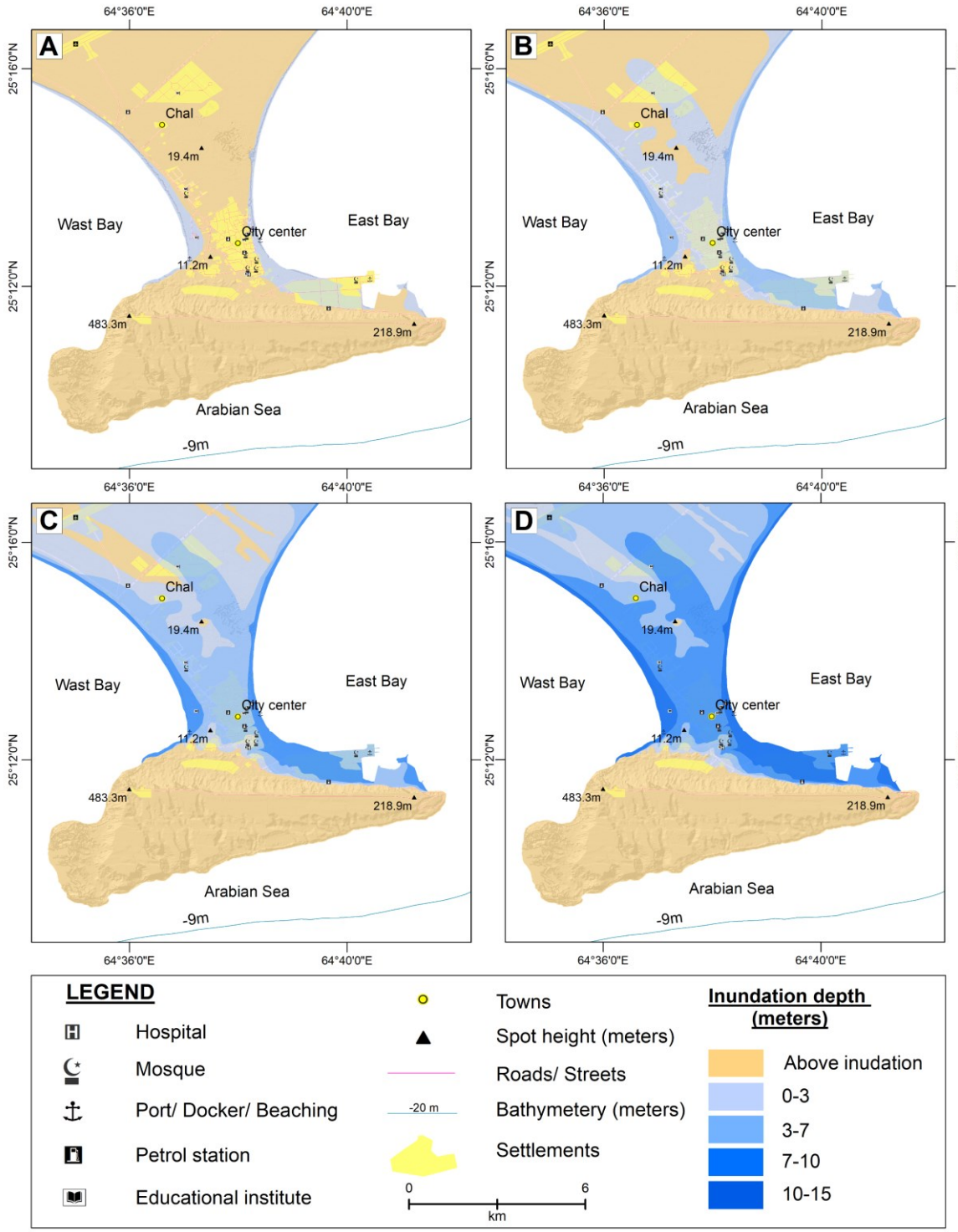

Figure 4.10: Inundation results for Ormara using bathtub model.

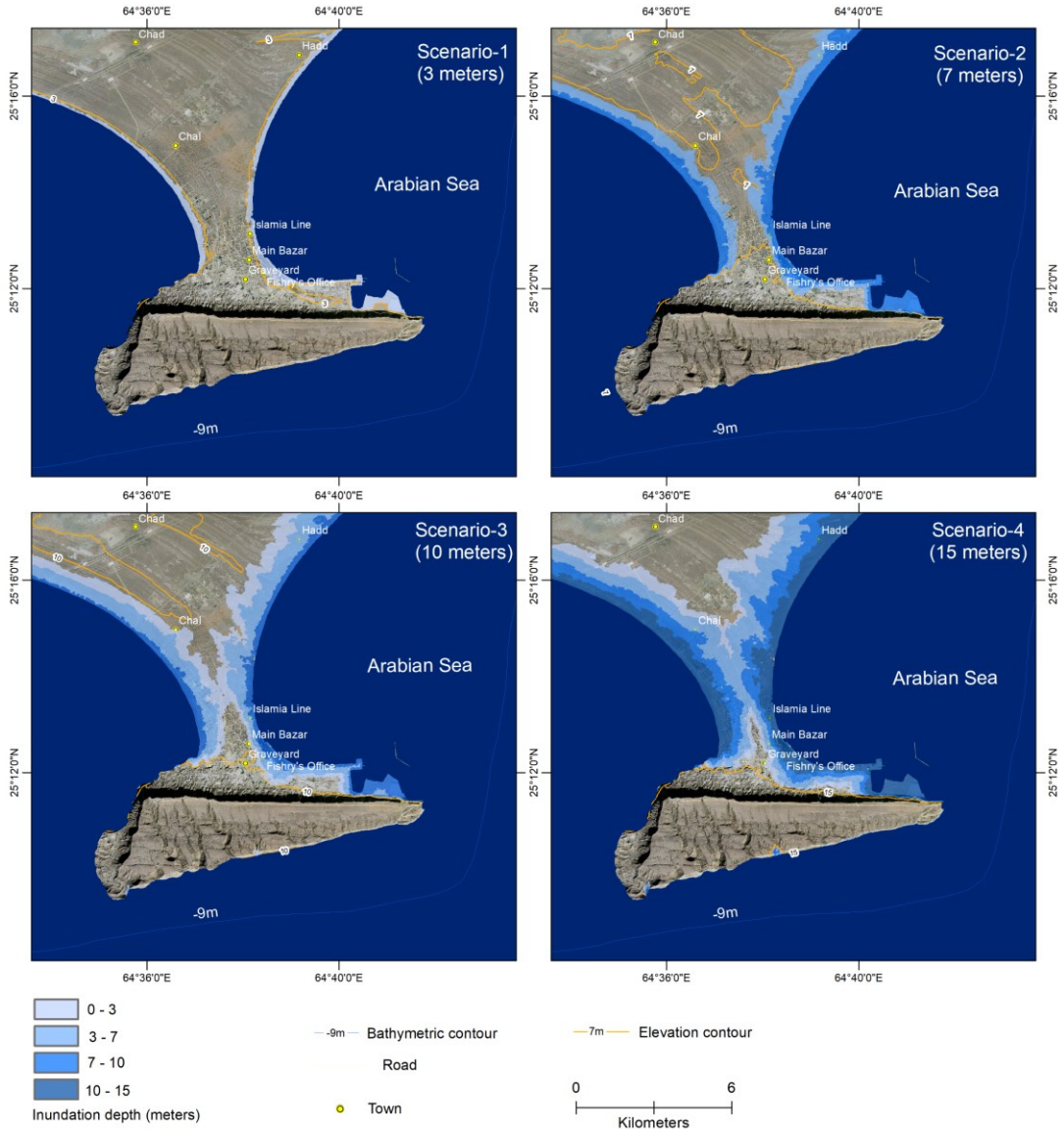

Figure 4.11: Inundation results for Ormara using standing wave model.

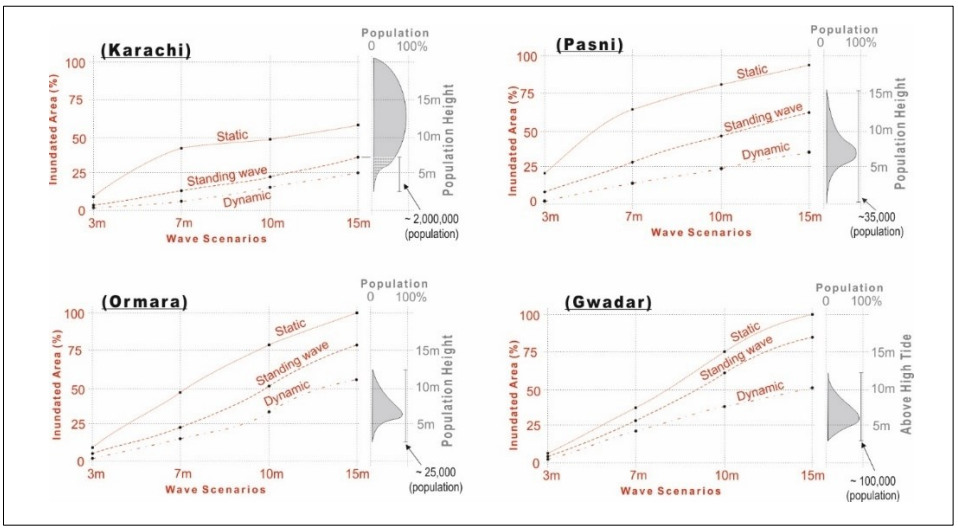

Figure 4.12: Comparative inundation curves for each model and scenario. The elevation-wise population spread (grey color) approximates the population under risk against each scenario.

4.5 Discussion

For robust inundation analysis, it is essential to utilize a high-resolution bare land digital terrain model (DTM) to calculate the actual head loss and flow depths. Also, to precisely assign Manning's Surface Friction coefficients to each feature. As DTM is not available in our case, the results of the Standing wave model are compromised to some extent in two ways; 1) in an area with densely pack buildings as in Karachi, the narrow streets are sometimes overlooked and whole area behaves as a solid barrier instead of a porous infrastructure. Digitally, such barriers obstruct the flow of water due to which models underestimate the inundation extent (Figure 4.13). On the other hand, these barriers resulted in an extra pile of inundating water on its downstream side where it overestimates the flow depth. Such compromises are evident in the DHA area in Karachi for 7-meter scenario. 2) In areas with moderate or scattered buildings, the water finds enough open land to invade but the volumetric loss of water against each building is not compensated and a volume equivalent to each building is pushed ahead. In such areas it overestimates the inundation. Such overestimation can be controlled by increasing the surface resistance, but the water mass lost against each structure yet needs more digital tools to be imparted in the software/s.

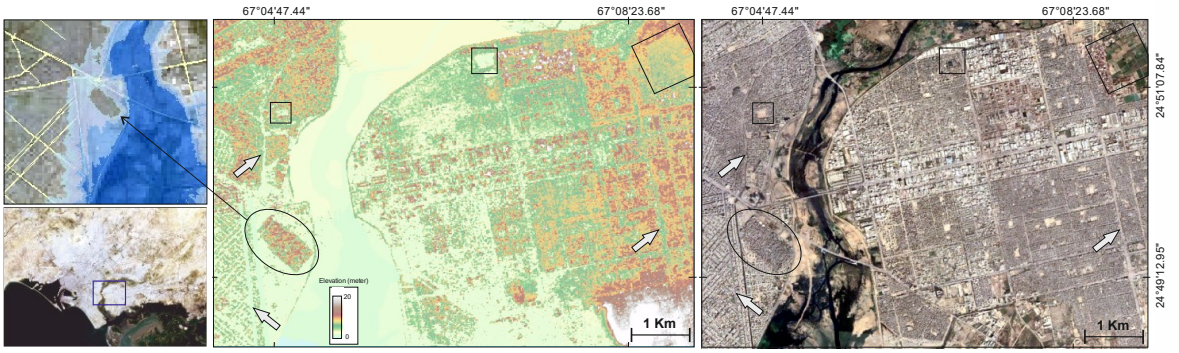

Figure 4.13: Satellite image (Google Earth) and DEM (TanDEM-X 0.4 arcsec) of Karachi. At this resolution (12m) the densely pack buildings in oval shaped polygon acted as a solid cuboid, through which inundating water could not penetrate. The squares and arrows point to some of the bare land values in the DEM.

Ormara and Gwadar have almost similar inundation results due to the similarity in topography and morphology (tombolo). In both cases, these tombolo headlands extend 12km east-west and most of the population resides at their necks at an elevation between 5-10 meters. The Gwadar has an advantage over the Ormara, that, the beach wall built on it's both bays, which reduces the risk factor against the low height tsunamis (<3m) as compared to gently sloping bays at the Ormara.

The comparative analysis shows that in quantifying the relative losses, Karachi poses the highest risk due to its huge vulnerable population, then comes the Gwadar, Pasni and Ormara (in descending order). The Karachi has two advantages over the other three cities; first that it is away from the high hazard zone (~350km). If a tsunami is triggered in an earthquake cluster south of Pasni, then it will reach Karachi in an hour as compared to Pasni (max 20 minutes), hence providing some time to Karachi for evacuation. Secondly, Karachi is full of multistory concrete buildings which may act as vertical evacuation structures. The Karachi Nuclear Power Plant (KANUPP), a coastal nuclear facility near Karachi is another matter of serious concern regarding the tsunami. These nuclear power plants are operating under the IAEA safeguards agreement. The plant is at least 15 meters above the mean sea level, the containment structures (hosting the fuel rods) are at least 17m high (as calculated from the DEM). Therefore, at preliminary analysis, the plant is on safer side with respect to the tsunami with a maximum 15m height provided its cooling and other important systems remain working during the catastrophe.

4.6 Conclusion

1. The Makran Coast may bear negligible to minor damage by 3-meter wave height, moderate by 7-meter and heavy by 10-15 meters.
2. The comparative inundation analysis shows that on the average bathtub models overestimate the inundation dynamics by a factor of 1.7 as compared to the standing wave.
3. Dynamic inundation modeling for the coast at high resolution is highly recommend delineating the vulnerable areas.
4. Still there prevail many uncertainties and data/knowledge gaps, the option in hand is to get well prepared.

5. Dynamic inundation and vulnerability analysis of major cities along the Makran Coast

This chapter is published as research article as

- *Haider, R., Ali, S., Hoffmann, G., Reicherter, K., 2024. Tsunami inundation and vulnerability analysis on the Makran coast, Pakistan. Nat. Hazards Earth Syst. Sci. 24, 3279–3290. https://doi.org/10.5194/nhess-24-3279-2024*

5.0 Abstract

The coastal cities of Gwadar and Pasni, situated along the Arabian Sea in the northwestern region of the Indian Ocean, are subjected to thorough investigation for inundation and vulnerability analysis. The estimation of maximum tsunami wave potential in the Arabian Sea involves evaluating paleo-morphodynamics records of tsunamites found along its coastlines, with a focus on the most severe case for modeling to determine the maximum wave potential. Subsequently, based on this assessment, three distinct wave scenarios (7 m, 10 m, and 15 m) are projected onto Pasni and Gwadar and their surrounding coastal areas. The results reveal high vulnerability of both cities to wave heights ≥7 m and wave lengths ≥ 15 km, with the 15 m scenario posing a near-complete disaster for both cities and adjoining towns. Furthermore, simulation results demonstrate that the coastal orientation and morphology contribute to the devastating impact of reflection, integration, and amplification phenomena in the region, with their intensity escalating with larger approaching waveforms. The reflection-amplification phenomenon notably and variably impacts inundation extents and depths. The installed tsunami early warning system's effectiveness is also evaluated based on the modeling and simulated results and the recent practices of early warning alerts issued.

5.1 Introduction

Tsunamis are rare events but have high damage potential for the coastal communities. Over the past 27 years, 64 tsunamis with a run-up higher than 3 m have been documented globally (Tarbotton et al., 2015). In the recent two decades, there has been a substantial advancement in understanding of tsunami generation, propagation, and inundation. This progress has enabled planners, administrators, and engineers to calibrate building design codes to mitigate disaster risk (Park et al., 2013; Macintosh, 2013). In this context, inundation analysis plays a crucial role in vulnerability and risk assessment. The assessment involves integrating infrastructure fragility curves (damage probability

curves) with various tsunami flow magnitudes (Rehman and Cho, 2016). These fragility curves are generated using various techniques based on deterministic and probabilistic approaches, while tsunami flow magnitude is determined by calculating flow depth and flow velocity through dynamic inundation modeling.

In this chapter, two aspects have been investigated: primarily the inundation analysis and secondarily a vulnerability estimation for the coastal cities of Pasni and Gwadar and surrounding areas (Figure 5.1). These cities were severely affected by the 1945 earthquake (Mw 8.1) entailing tsunami (~12m at Pasni) which resulted in hundreds of casualties (Pendse, 1946; Hoffmann et al., 2013b). In 2013, a small tsunami (<1m) associated with an earthquake (Mw 7.7) struck the same area once more but caused no damage (Heidarzadeh and Satake, 2014b). Both cities had grown many times as compared to those in 1945, and in the event of a similar disaster, substantial loss of life and property is anticipated.

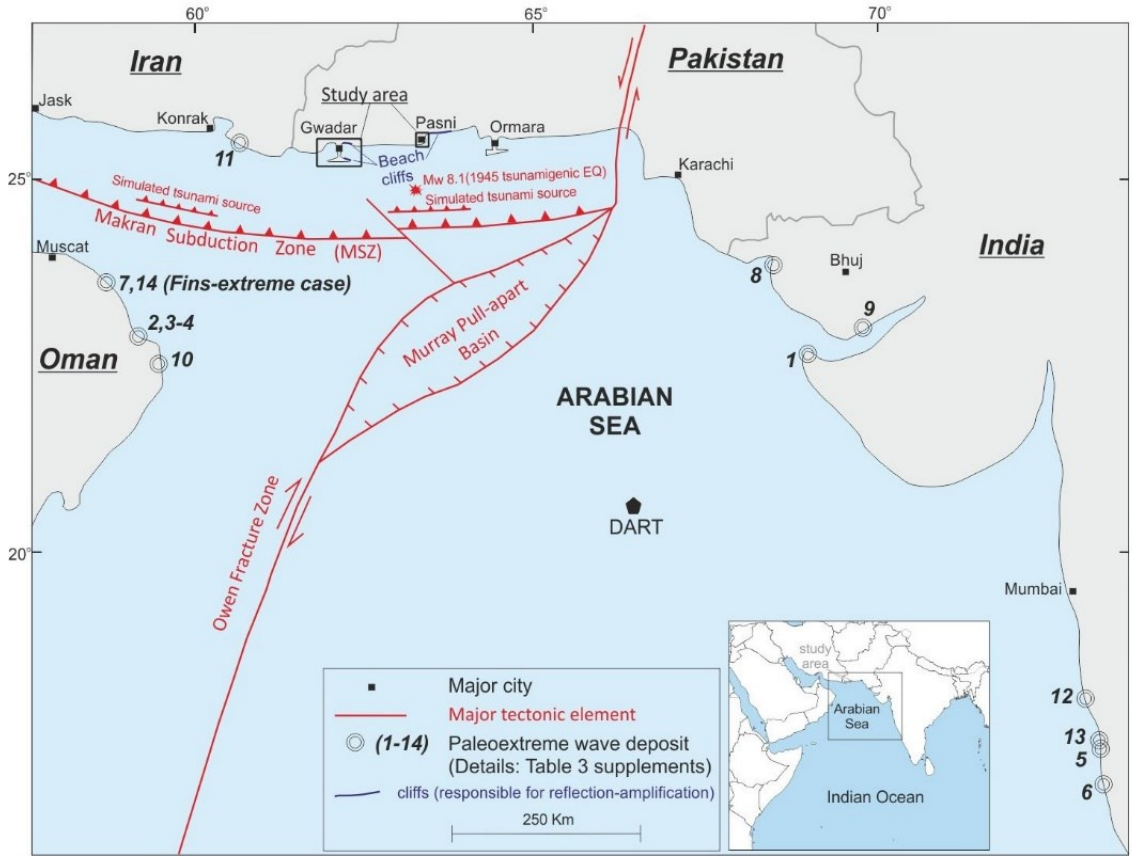

Figure 5.1: A Location and tectonic map of the study areas (Gwadar, Pasni). The circles with numbers show the reported palaeoextreme wave deposits; details are in Table 2.5: The compilation of tsunamites discovered at different coasts along the Arabian Sea (sorted age-wise). DART: Deep-ocean Assessment and Reporting of Tsunamis.

5.2 Tectonic settings and Associated Seismicity

The majority (80%) of tsunamis globally are triggered by underwater earthquakes (Harbitz et al., 2014; Løvholt, 2017) , while the remaining 20% are caused by other sources such as landslides, volcanoes, and meteoric impacts in the ocean water (Behrens et al., 2021). In the Arabian Sea, seismic activity is primarily attributed to the Makran Subduction Zone (MSZ) (Figure 5.1). The MSZ accommodates the crustal shortening between the Arabian Plate in the south and the Eurasian Plate in the north, converging at a rate of 0.5–20 mm/year (Vernant et al., 2004; Khan et al., 2008; Jade et

al., 2017). Most of the seismicity along the eastern MSZ, south of Pasni, is associated with the Sonne Fault (Kukowski et al., 2000). Additionally, the high seismic velocities (4.4 km/s) indicate a brittle decollement at the eastern MSZ, contributing to high seismicity (Smith et al., 2012). This brittle nature is attributed to the lack of soft sediments along the decollement in comparison to the western portion of the MSZ. Thermal modeling of the MSZ suggests a potential earthquake magnitude comparable to the December 2004 Sumatra rupture, possibly reaching up to Mw 9.2 (Smith et al., 2012). Estimates from another thermal modeling research estimates a potential magnitude of Mw 8.65 ± 0.26 in western Makran (Iran) and 8.75 ± 0.26 in eastern Makran, Pakistan (Khaledzadeh and Ghods, 2022). El-Hussain et al. (2016) inversely calculated the maximum moment of earthquake potential as Mw 8.8 using the geodetic slip rate based on a simplified relation by Brune (1968), Hanks and Kanamori (1979).

The focal mechanism of the 1945 tsunamigenic earthquake indicates a thrust event (Byrne et al., 1992). Dislocation models, body waveform inversion, and moment estimations suggest ruptured lengths ranging from 100 to 200 km, with an average crustal slip of 7 m along the MSZ. The Arabian Plate, while subducting its northern edge, also slides past the Indian Plate in the east at a rate of about 3±1 mm/yr (Reilinger et al., 2006; Rodriguez et al., 2011) making an active transform plate boundary. Murray Ridge (MR) and Owen Fracture Zone (OFZ) are two major tectonic features along this transform plate boundary. The former is a pull apart basin while the latter is a transform boundary (Figure 5.1). Minor earthquakes, resulting from right-lateral strike-slip and normal faulting occur in the Murray Ridge (Banghar and Syke, 1981). Seismic activity along the remaining OFZ is mild to moderate, with the largest observed magnitude being Mw 5.8 (Rodriguez et al., 2011), posing no significant tsunami threat.

5.3 Methods

5.3.1 Establishing the tsunami wave potential in the Arabian Sea

The potential for tsunami waves in the Arabian Sea is also assessed by utilizing the tsunamites proxy. We compiled the reported tsunamites cases around the Arabian Sea and specifically examined the case at Fins, Oman exhibiting extreme morpho-dynamics (Table 2.5). At Fins, the tsunamites are represented by block and boulder deposits up to 40 tonnes lying at a maximum height of 10 m from the mean sea level (msl) showing a landward transportation up to 50 m from their intact sites. Further, laboratory tests on a scaled model (t-LiDAR) of the largest block estimated wave velocities for dislodging, elevating, and transporting these boulders to be between 4.5 to 6.6 meters per second (Hoffmann et al., 2013a). The marine shells (C^{14}, n=4), attached to these blocks and boulders gave a wide range of age between 250±160 and 4595±185 cal. BP (Hoffmann et al., 2020). At the same site, loose tsunami sediments fining and wedging landward with a minimum elevation of 17 m is dated 5840 cal. BP (C^{14}, n=6) (Koster et al., 2014). These studies also applied corrections for tectonic uplift/subsidence, absolute sea level change and estimated a 14 m wave run-up. The long-axis rose plot of blocks and boulders indicates that the wave source azimuth (N30E) originates from the MSZ (Hoffmann et al., 2013a). We modeled this case study (Fins Scenario) to estimate the wave size capable of demonstrating the above dynamics. The tsunamis are generated using Okada's (1985) earthquake parameters at MSZ given in Table 5.1. Momeni and and Goda (2024) used stochastic tsunami simulations to estimate that tsunami heights from Mw 8.5–8.7 earthquakes in the western MSZ range from 1 m to 10 m, with a mean of ~4.5 m, influenced by factors such as large slip areas, nearshore bathymetry, and location. Rahimi et al. (2025) used a probabilistic approach to estimate ground motion and tsunami intensity for the western Makran region, revealing a 2475-year return period for events reaching 0.6 g PGA and 8.5 m tsunami waves in Chabahar.

The 1945 tsunami at Pasni is also a severe event in the known history of tsunamis in the Arabian Sea with reported wave height of 12 m - 15 m (Pendse, 1946). The 1945 tsunami event at Pasni and case of tsunamites at Fins serves as a reference, providing empirical evidence of tsunami potential and its impacts within the region. The recurrence interval for a tsunami event of such magnitude (≥ 10 m) estimated through multiproxy analysis is between 500 to 1000 years (Haider et al., 2023). Based on the above assessment, we establish a range of scenarios (7 m, 10 m, and 15 m) to thoroughly assess the vulnerability landscape of Gwadar and Pasni cities and their surrounding areas. The other tsunami sources such as landslides, volcanoes, and meteoric impacts in the ocean water have not yet been considered and therefore cannot be negated at this stage.

5.3.2 Source Type and Parameters

Tsunami propagation and inundation scenarios are modeled using the earthquake parameters on a hypothetical splay fault close to the MSZ. We applied Okada's (1985) mathematical model to estimate the seabed deformation induced by earthquakes, employing uniform parameters for a four-segmented fault rupture. The most severe source parameters were replicated based on those investigated in the Fins scenario. To enhance vulnerability assessment, we conducted two additional case studies with scenarios featuring relatively low intensity parameters (). These scenarios are likely to encompass varying degrees of seismic hazard and tsunami risk, thereby facilitating a more comprehensive evaluation of potential impacts and the formulation of effective mitigation strategies. The relationship between earthquake magnitude and its associated parameters is inherently intricate, primarily owing to the complex geological processes such as fault geometry, heterogeneous stress distribution, and uncertainties in earthquake rupture mechanisms (Zaccagnino et al., 2022). As already mentioned, the analysis suggests a return period between 500-1000 years for a tsunami ≥ 10 m in the Arabian Sea (Haider et al., 2023). This minimum recurrence interval of 500 years (475 in actuality) correspond to the life safety and infrastructural collapse performance levels (Ahmed et al., 2019). In total three different scenarios have been modeled for enhanced vulnerability assessment of the study area.

Table 5.1: Table showing the earthquake source parameters used to model each scenario with respective initial wave height.

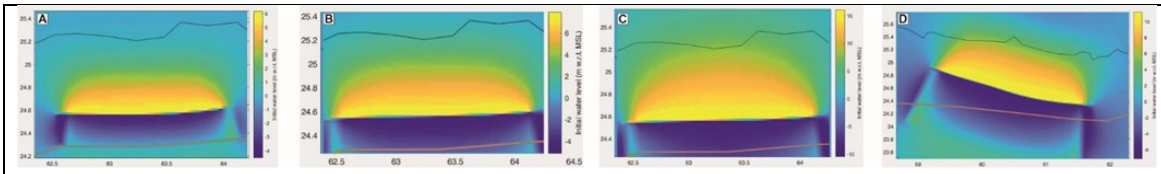

Initial Wave height		Length (km)	Strike (deg)	Width (km)	Depth (km)	Dip (deg)	Rake (deg)	Slip (m)
A)7m Scenario	East MSZ	200	266 to 269	110	10	35	90	8
B)10m Scenario		200	266 to 269	160	10	35	90	10
C)15m Scenario		200	266 to 269	211	10	35	90	22
D)Fins Scenario (15m)		200	-84 to -70	211	10	35	90	22
D represents the initial wave height generated for modeling the Fins Tsunamites case. A, B, and C represent the initial wave heights for the Pasni and Gwadar areas.								

5.3.3 Tsunami Modeling and Data Sets

Numerical modeling is performed using the Delft3D 4.04.01 software, developed by the Dutch Institute Deltares (Deltares, 2023). The hydrodynamic programme module Delft3D-FLOW is used for simulation, which solves non-linear 2D and 3D shallow water equations (SWE) for unsteady flow phenomena. The equations of the Boussinesq approximation for incompressible fluids are derived from the three-dimensional hydrodynamic Navier-Stokes equations. For further details about the software and governing equations, please see (Deltares, 2023; 168–186).

Table 5.2: Summarized methodology with flowchart showing sequential order of various processes used for hazard and vulnerability assessment.

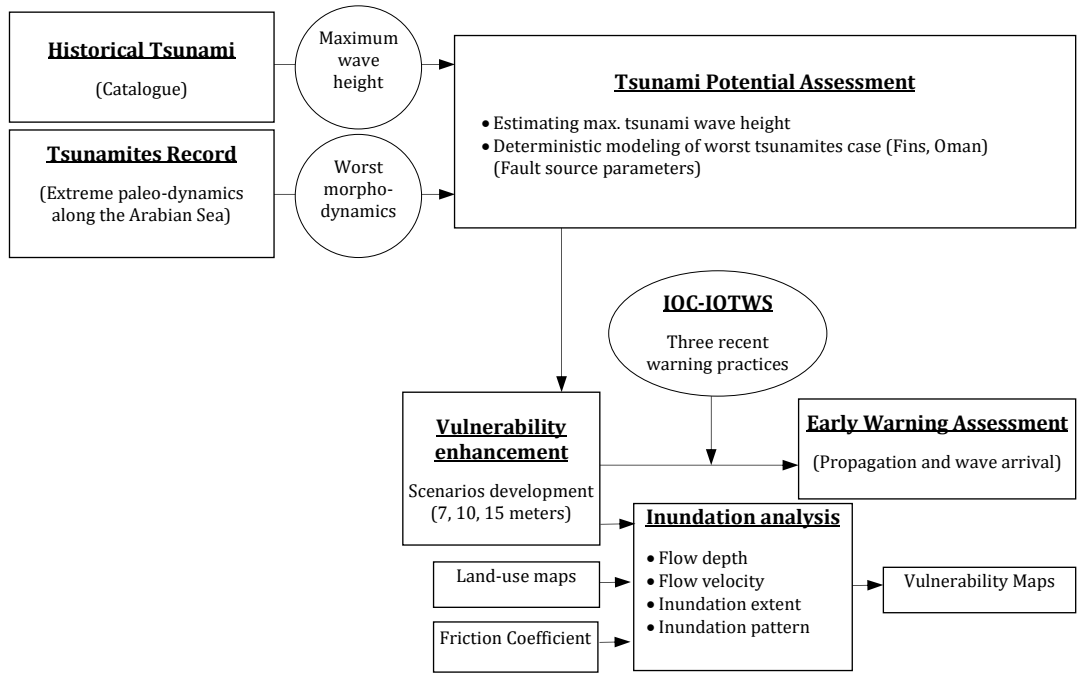

Approach	Model	Equation/s	Reference
Hydrodynamic	**Delft3D** **(Flow module, Dashboard)** • mass conservation • momentum eq. • surface roughness • simulations	• *Hydrodynamic equations* • *Continuity equation* • *Momentum equations in horizontal direction* • *Vertical velocities* • *Hydrostatic pressure assumption* • *Coriolis force and Reynolds stresses equations* * For details, referred to (Deltares, 2023), pp. 168–186)	(Deltares, 2023) (Gelfenbaum et al., 2007) (Chacón-Barrantes et al., 2013) (Röbke et al., 2016) (Röbke et al., 2018) (Van Ormondt et al., 2020) (Sujatmiko et al., 2023)

We employed a nested computational grid for both cities, with a grid resolution of 0.0004×0.0004 (44 m × 44 m) for the nested models and 0.01 × 0.01 (~1 km × 1 km) for the regional model. A schematic nesting model is provided in Supplements (Simulations-10). In the regional model, Reinmann Boundary Conditions are utilized to minimize the reflection effect, and time-series boundaries are applied for the nested models. For tsunami propagation and inundation analysis, we integrated bathymetric data from the General Bathymetric Chart of the Oceans (GEBCO) at 15 arc

seconds resolution and topographic data from the German Aerospace Centre's (DLR) at 0.4 arcsec (~12 m) resolution in a GIS environment. The DLR's topography Digital Elevation Model (DEM) is derived from bistatic X-Band interferometric Synthetic Aperture Radar (SAR) data, utilizing the patented TanDEM-X and TerraSAR-X systems. The post-data acquisition developments, including the addition of the East Bay Express Way and jetty (each 4 meters high), are manually incorporated in the fused DEM, which is particularly crucial for Gwadar. Furthermore, the terrain roughness is assigned using Manning's Coefficient with values ranging as 0.015 for sea floor and open land, 0.03 for thinly populated areas, 0.05 moderately populated areas to 0.08 for densely populated areas. The coefficient value assignment is based on fieldwork, photographs, and Google Earth Satellite Images. The GIS data is analyzed and processed using Quantum Geographical Information System (QGIS 3.28.1) software, providing a robust environment for spatial analysis and visualization. QGIS is an official project of the Open-Source Geospatial Foundation (OSGeo).

5.3.4 Vulnerability analysis

Damage probability refers to the likelihood or probability of damage that a particular type of property will sustain because of tsunami impact. The vulnerability analysis is carried with the fragility curves expressed as damage probabilities verse drag force of individual houses/structures for structural damage developed by Koshimura et al. (2009) and Rehman and Cho (2016). They computed fragility curves for tsunami damage through statistical approach synergised by GIS/ numerical modeling results of pre/post-tsunami (2004 Indian Ocean Tsunami) data from Banda Aceh, Indonesia. These curves are developed for low-rise, lightly reinforced, non-engineered reinforced concrete (RC). The major structural types in our study area and the Banda Aceh, Indonesia are comparable; mostly single-double story structures with conventional masonry and lightly engineered RC. The assessment of structural and building material types in the Gwadar and Pasni are based on visual estimates carried out during the field work and need to be worked on in detail for improved results.

In the Koshimura et al. (2009) fragility curves calculated for Banda Aceh, Indonesia, the drag force (hydrodynamic) per unit width of a structure is mathematically expressed as follows:

$$F = \frac{1}{2} C_D \rho u^2 D$$

where C_D is the drag coefficient equal to 0.99 (1.0 for simplicity) and it mainly depends on the shape of the structure as buildings in our case and the angle of incidence of the floodwater flow, ρ is water density (1,000 kg-m^{-3}), u is the wave velocity (ms^{-1}), and D the inundation/ flow depth (m). The drag force for each scenario is calculated using this hydrodynamics at each monitoring point in Gwadar and Pasni. For example, in Pasni, the drag force (F) for 15 m Scenario at Monitoring Point (M2) is calculated using the modeled flow depth/velocity as:

$$F = \frac{1}{2}(1)(1000)(2)^2(8)$$

$$F = 16{,}000\ Nm$$

$$F = 16\ kNm$$

5.4 Results and interpretations

5.4.1 Pasni scenarios

In the 7 m scenario, the first wave reaches the Pasni coast 20 minutes after the earthquake. From the coastline (shoreline) it further takes 20 minutes to reach its maximum inundation limit, partly affecting localities of Wadsar and Main Bazar. In this inundation course, only one monitoring point (M5) situated in inhabited locality experiences inundation. The M5 records a maximum flow depth of 1 meter and flow velocity of 0.5 m/s. However, areas like Shol, Parhag, and a significant part of the main Pasni town remain relatively unaffected (Figure 5.2; 7 m scenario).

In the 10 m scenario, along with first wave a secondary wave with a height of 8 m is generated due to reflection from the cliffs northeast of Pasni (Supplements: Simulations-3 Pasni 10 m scenario). These two waveforms reach the Pasni coast at intervals of 20 minutes and 45 minutes, respectively, following the earthquake (Figure 5.2 M6: 10 m scenario). In both cases, the direction of inundation pattern shifts based on wave propagation direction: initially, northward propagation inundates the southeast of area, while southward propagation due to reflection causes inundation from the northeast. Initially, the approaching wave inundates the study area from south and inundation extent decreases significantly northward, primarily due to the adjacent river (Shadi Kaur) consuming a significant portion of the inundating wave, resulting in lower water levels in the populated area. Nonetheless, the inundation dynamics pose a significant threat to loss of life and property. Spatially, the inundation gradually decreases from south to north, with maximum flow depth and flow velocity at M1 being 6 m and 2.5 ms^{-1}, to 2 m and 1 ms^{-1} at M6.

In the 15 m scenario, the inundation impact is approximately double in terms of flow depth as compared to that in the 10 m scenario due to the heightened wave characteristics and enhanced reflection phenomenon. The approaching and reflecting waves interact for a duration of 30 minutes, generating a series of wavelets that gradually increase in intensity and contributing to the formation of a larger and more complex waveform. Consequently, a significant accumulation of water along the shoreline in the study area results in far and deeper inundation (Supplements: Simulations-4 Pasni 15 m scenario). The spectral characteristics of the flow velocity exhibit a higher degree of complexity and variability in comparison to the corresponding flow depth. In populated areas, such as Pasni, Main Bazar, Parhag, and Wadsar, peak flow depths range between 6 to 8 meters, alongside maximum flow velocities reaching 1.5 ms^{-1}. The intense backwash process in this scenario poses a significant hazard too, as evidenced by the consistent recording of flow depths exceeding 1 meter at all monitoring points until the 5-hour simulation duration (Figure 5.2 M6: 15m scenario).

In general, for all three scenarios, the maximum flow velocity is recorded through the first wave and maximum flow depth is recorded at quasi-still stand. Quasi-still stand refers to a temporary pause or a halt at maximum inundation limit after which the backwash process initiates. The backwash tsunami phenomenon persists for more than 4 hours.

5.0.1 Gwadar scenarios

The East Gwadar Bay or simply the east bay is characterized by two prominent coastal wave reflectors; one to the north as coastal mountains namely Mehdi-Koh and other to the south as Gwadar-Hammer-Head (Figure 5.3). The Gwadar-Hammer-Head is a geological formation characterized by a protruding landmass extending into the sea. The subsequent reflection phenomena and the ingress of regular tsunami waves ($\leq$ 4m) contribute to wave integration and amplification along with delayed wave arrivals. For instance, in the 7 m scenario at M1 (Mohalla Band locality),

the first wave arrives 30 minutes after the earthquake, with a flow depth of 1 m. Further, with a lapse of 15 minutes, the second wave inundates the area increasing the flow depth to 2.6 m. This is succeeded by a third wave after a lapse of an additional 30 minutes further increasing the flow depth to 3 m. After the third and final wave the quasi still stand or a temporary water stabilization prevails for 15 minutes. Hence, with the reflection mechanism in place, the water level exhibits a continuous increase over a span of 60 minutes. However, if we eliminate the influence of reflection from the first tsunami wave, this duration would be reduced to merely 15 minutes with only 1 m flow depth at M1. The wave spectral analysis shows an inverse relation of flow depth and flow velocity because of the loss of kinetic energy during reflection-amplification phenomenon.

The Surbandar locality (M4) remains unaffected in the 7 m scenario, however in 10 m and 15 m scenarios the locality is severely affected. It is positioned at a lower elevation compared to the beach banks in the south from where the tsunami propagates and experiences wave overflow. Being situated on low-lying topography as compared to the beach banks and by the direct facing to the tsunami propagation, the torrential force achieves a flow velocity of 4 ms^{-1} and 6 ms^{-1} in 10 m scenario and 15 m scenario, respectively. Similar phenomenon is observed for Pishukan locality (M5) also. The cliffs, averaging a height of 12 meters, situated to the south of Pishkun provide protection against inundation in scenarios of 7 m and 10 m. However, in the 15 m scenario, waves spill over these natural defenses, resulting in flow depths and velocities of 3 m and 2.1 ms^{-1} respectively at M5. The New Town locality (M2) exhibits the highest flow depth in each scenario, reflecting its heightened vulnerability to tsunami inundation. Analysis reveals that this high vulnerability arises from inundation originating from both the east and west bays, where wave interactions lead to amplification of the inundating waves.

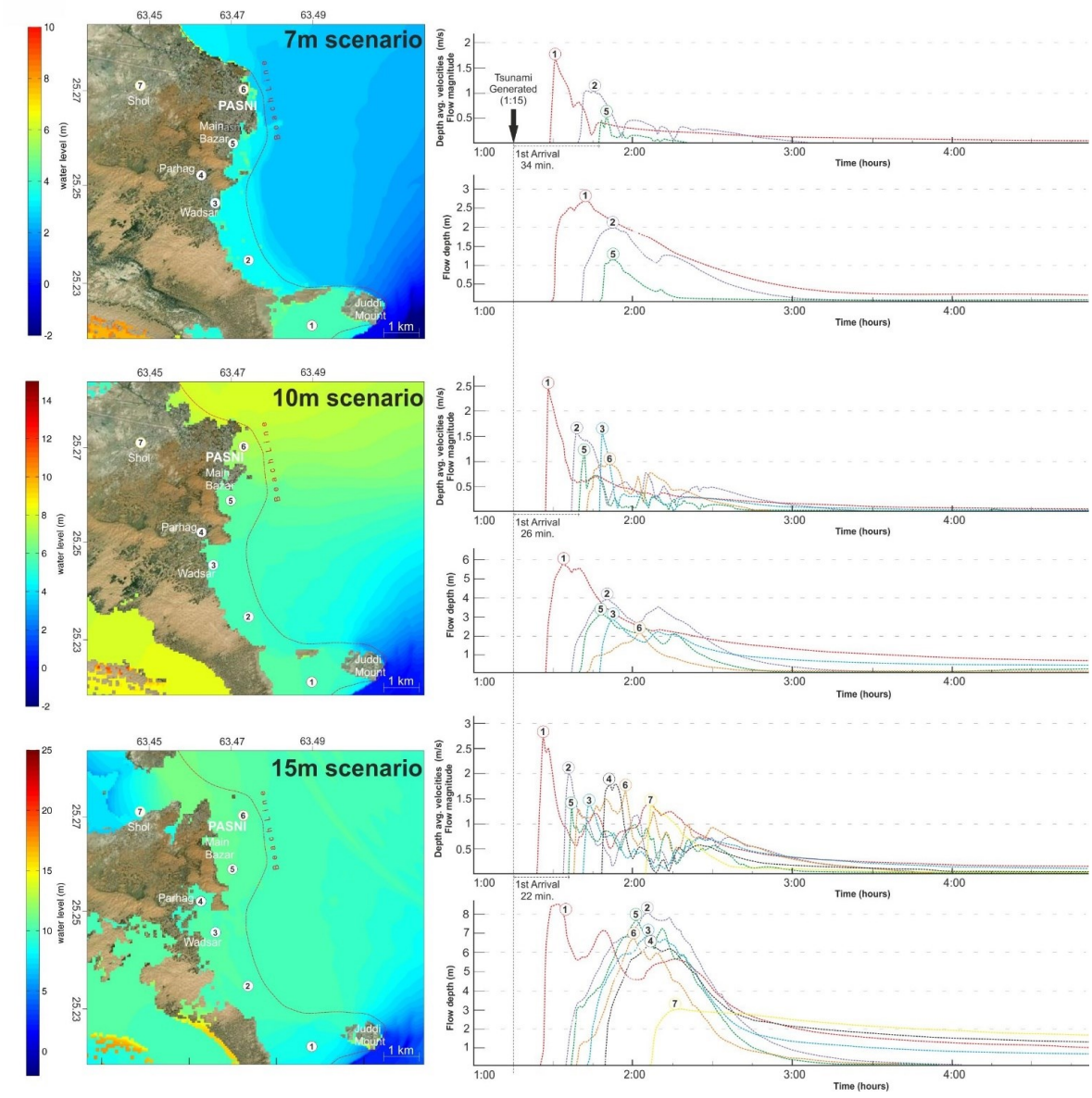

Figure 5.2: Hydrodynamic modeling results of each scenario with maximum inundation limits and depths at Pasni and surrounding areas. The graphs illustrate the flow depth and magnitude at monitoring points (M1 to M7). Simulation for each scenario are provided in the supplementary materials.

In the Gwadar town (M1 to M2), both sides of the bay are elevated to a height of 5 meters above mean sea level (MSL) to accommodate road construction. This elevated terrain, coupled with an inadequate and low-capacity drainage infrastructure, significantly impedes the backwash process of tsunamis (Figure 5.3 flow depths: all scenarios). Modeling results indicate a flow depth exceeding 2 m in the Gwadar town even after three hours.

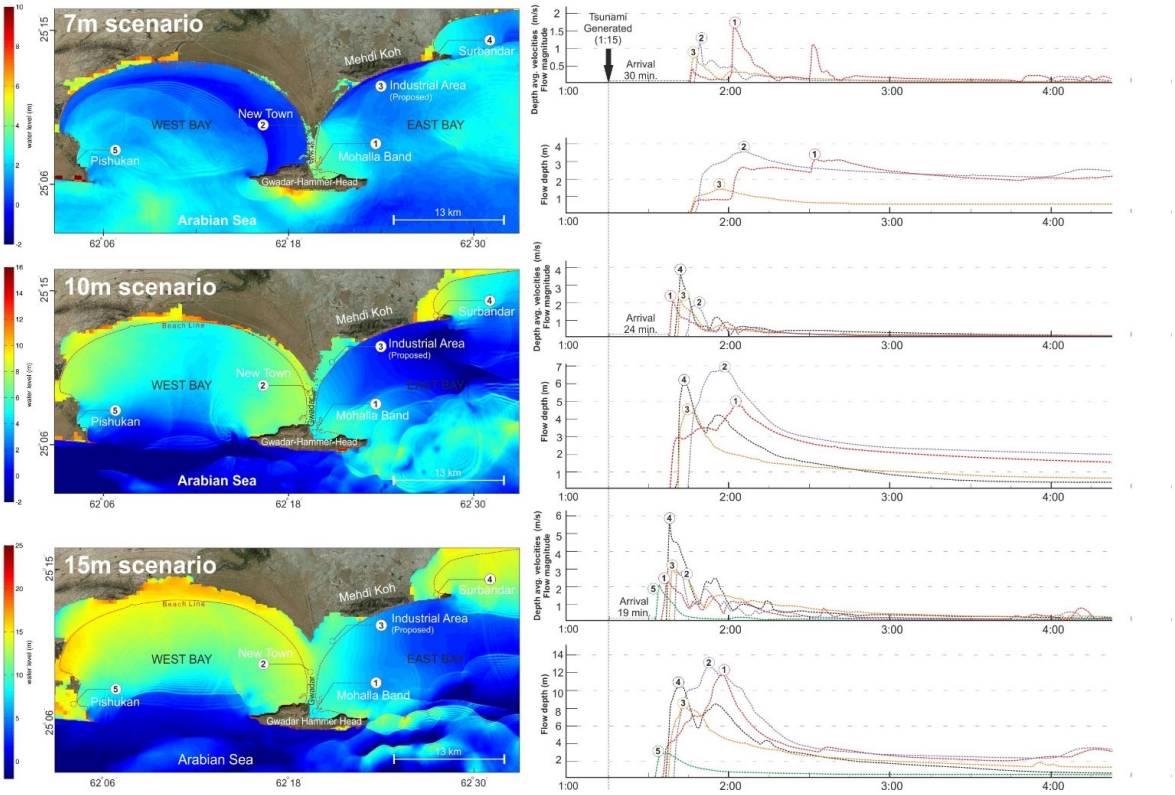

Figure 5.3: Hydrodynamic modeling results of each scenario with maximum inundation limits and depths at Gwadar and surrounding areas. The graphs illustrate the flow depth and magnitude at monitoring points (M1 to M5). Simulation for each scenario is provided in the supplementary materials.

5.0.2 Vulnerability Analysis

The damage probability for each scenario is assessed through hydrodynamic analysis conducted at each monitoring point in both cities. Consequently, damage intensity is expected to escalate towards the shoreline from these monitoring locations. However, exceptions are noted in the cases of the Surbandar and Pishukan in Gwadar area, which are elaborated later.

At Pasni, monitoring points M1 and M2 exhibit the most severe flow dynamics, indicating the highest vulnerability to tsunami inundation in each scenario (Figure 5.4; Pasni scenarios). For M1, the damage probabilities are 0.50, 0.95, and 1.0 for the 7 m, 10 m, and 15 m scenarios, respectively. Similarly, for M2, the corresponding probabilities are 0.05, 0.6, and 0.95. Despite being uninhabited, any development should undergo feasibility studies concerning extreme wave events, particularly tsunamis. Regarding the inhabited part, the 7 m scenario minorly affects the Main Bazar locality (M5) and surrounding areas with an estimated damage probability close to zero. However, it should be noted that infrastructure or communities residing in close proximity to the shoreline may still possess some degree of damage potential. In the 10 m scenario, the Wadsar locality (M3) poses the maximum damage potential with probability of 0.57, followed by Main Bazar (M5) with 0.37, and then Pasni locality (M6) with 0.05. In the 15 m scenario, no locality remains unaffected; all localities exhibit a probability of damage exceeding 0.6, except for Shol (M7), which registers a value of 0.4.

The results indicate that the level of vulnerability and probability of damage are higher in the Gwadar area as compared to the Pasni area. In the 7 m scenario, three localities, two of which are inhabited, are inundated (Figure 5.4; Gwadar scenarios). The Mohalla Band locality (M1) exhibits a damage probability of 0.4, followed by the New Town locality (M2) with 0.1. Additionally, the proposed site for industrial development (M3) is also inundated, with a damage probability of less than 0.1. The

10 m and 15 m scenarios pose significant challenges for the area. In the 10 m scenario, only Pishukan remains unimpacted, while all other localities are anticipated to experience a damage probability exceeding 0.8. The findings indicate that the Surbandar locality (M4) encounters a hydrodynamic force exceeding 40 kNm. This heightened level is attributed to tsunami overtopping the beach banks followed by a torrential downslope runoff effect, as discussed earlier in the section (section 4.2.). All localities, except Pishukan, have a damage probability of 1.0, with hydrodynamic force exceeding 35 kNm. The Pishukan locality (M5) indicates a probability of 0.6 in case of a 15 m tsunami only.

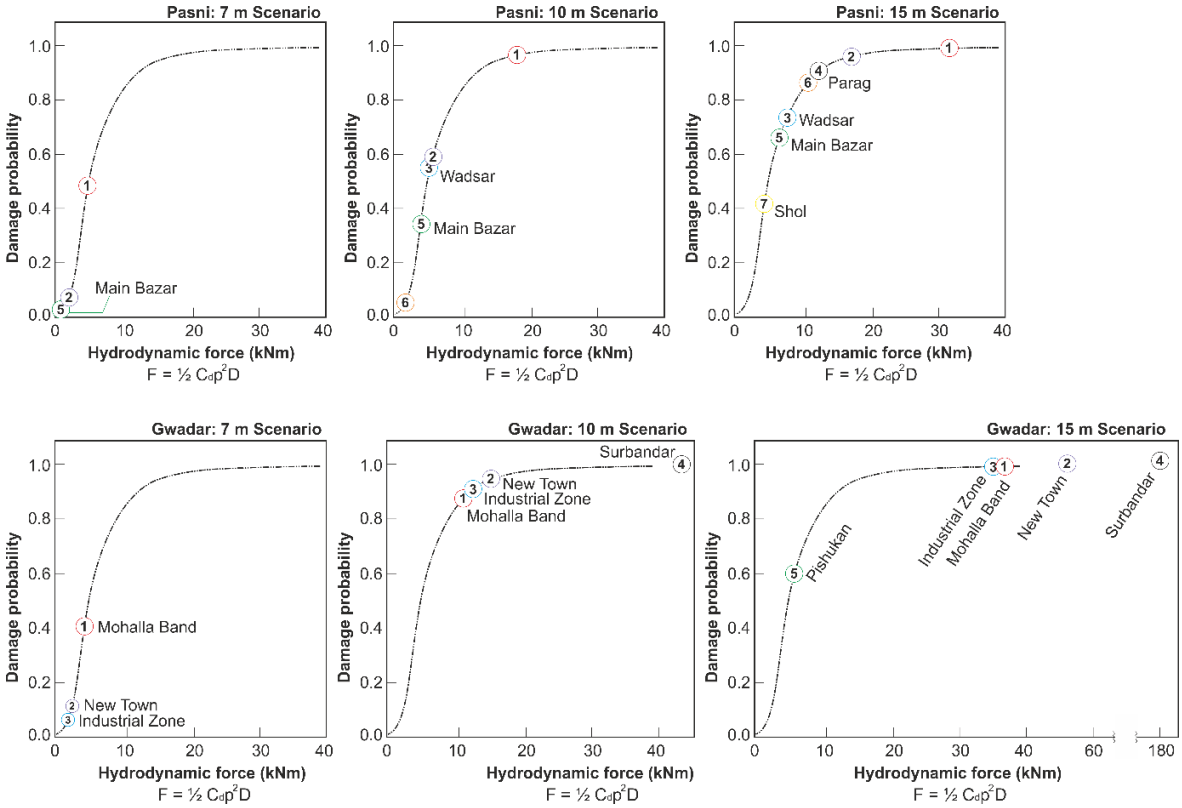

Figure 5.4: A Probability structural damage plotted against the hydrodynamic force at each monitoring point. Top row: Pasni, Bottom row: Gwadar. The results plotted on fragility curves are developed by (Koshimura et al., 2009).

5.1 Discussion and Conclusions

The process of tsunami modeling comprises three distinct phases: generation, propagation, and inundation. The generation phase involves calculation of sea floor deformation during an earthquake causing initial disturbance in the oceanic water. Subsequently, a hydrodynamic model utilizes this initial wave to model and simulate the propagation and inundation of the tsunami waves. For tsunami generation and potential estimation, utilizing Okada's (1985) model for the initial sea floor deformation is a valuable asset in seismic and tsunami hazard assessment. However, it is imperative to refer to the model's inherent limitations and their potential impact on our findings. Primarily, the model's static nature and its reliance on a single linear fault plane geometry, coupled with its exclusion of material properties considerations, pose notable constraints. These constraints may result in an underestimation or overestimation of tsunami hazard levels, emphasizing the need for caution and further investigation when interpreting our results. To have better results for generation and potential estimation, we compiled and analyzed the tsunamites discovered along the Arabian Sea shorelines and took the case exhibiting worse morphodynamics for modeling purposes.

Subsequently, utilizing Okada's (1985) fault parameters, various tsunami wave scenarios are generated along the MSZ to find the capable one aligning with both field and laboratory readings of tsunamites case taken up. As a result, our study provides a better waves tsunami potential estimation and an indirect approximation of potential fault parameters and earthquake potential, offering valuable insights into tsunami hazard assessment.

In tsunami hazard assessment, wave height is considered a yardstick, while wavelength tends to be overlooked. We assessed that for vulnerability and risk assessment, along with wave height, the wavelength must be taken into consideration. To illustrate this point, we conducted simulations involving two scenarios with identical wave heights of 5 m but differing wavelengths (λ/2) of 15 km and 3 km, impacting the Pasni coast (see Supplements: Simulations-9). The wave with the shorter wavelength dissipated faster without causing any inundation, whereas the longer wavelength resulted in considerable inundation, with a runup height of 2 m and an inundation extent of 0.7 km. This disparity can be attributed to a smaller quantity of displaced water and wave dispersion phenomenon that disperses rapidly and diminishes in magnitude during propagation, confining the hazards to local areas only. Vertical seafloor deformation or coseismic displacement tends to result in tsunamis characterized by longer wavelengths and longer periods when compared to those generated by landslide failures, mainly because of the broader source area associated with coseismic displacement events (Hammack, 1973; Watts, 1998; Heidarzadeh et al., 2014).

The bare ground elevation model represents a digital topography with no building infrastructure, plants, poles, etc. It is formally known as the digital terrain model (DTM). For inundation analysis, the deflection of DEM from DTM hampers the results in two aspects: i) the porous infrastructure, such as houses, mangroves etc., does not account for water balance adjustments. These features in DEM act as solid bodies, occupying the volume and deflecting the inundating water further ahead, resulting in higher inundation extents. ii) In the case of a low-resolution DEM which could not resolve the streets or passages results in water damming. It consequently, results in higher flow depths downstream than actual, and it also affects the backwash computations. Along with improving the spatial resolution, a water absorption and permeability value may be incorporated to each feature in the land use map. It could accounts for volumetric crossflow though structures adjustment of inundating water.

The effectiveness of the tsunami early warning system is assessed in terms of far-field and near-field sources particularly for the study area. An integrated Indian Ocean Tsunami Early Warning System is developed under the framework of Intergovernmental Oceanographic Commission (IOC-IOTWS) under the UNESCO umbrella in response to the tragic tsunami on 26th December 2004. The near-field tsunami warning is issued based on the location, size and initial evaluation of earthquake fault parameters through seismic spectral signatures. The Pakistan Meteorological Department (PMD) in collaboration with IOC-IOTWS is responsible for keeping track of coastal hazards and issuance of tsunami notifications and warning alerts. For earthquakes Mw ≥ 6.5 in the Arabian Sea, a near-shore early warning system puts the coastal community immediately under alert and watch status until confirmation of tsunami generation. The tsunami confirmation warning is issued once the tsunami wave is detected on any sensor or tide gauge which is either installed at the coast or DART station (Deep-ocean Assessment and Reporting of Tsunamis). In the study areas the tide gauges are installed at Gwadar and Pasni ports and the nearest DART station 450 km from the MSZ. The numerical models show, the first tsunami wave generated at eastern MSZ arrives at the Pasni coast (Pasni tide gauge) and the nearest DART station in 15 and 45 minutes, respectively. Heidarzadeh et al. (2007) calculated these timings as 15 and 60 minutes, respectively. If the tsunami had generated at eastern MSZ, it would reach the Makran Coast before its instrumental detection and confirmation warning. So, the coastal community will surpass the confirmation warning and therefore had to rely on the

advisory (alert and watch) warning only. On the other hand, the confirmation warning system works very well for the far-source tsunamis as a number of gauges installed at eastern Indian Coast, Maldives and DART stations detects the propagating tsunami several hours before reaching the Makran Coast (Srinivasa Kumar and Manneela, 2021). Further, three case studies from the Indian Ocean are presented for assessment of general practices and timelines in terms of detection, warning, and confirmation. The timeline for these chain of events during each tsunami case is given in Table 5.3.

Table 5.3: Timeline for chain of events and issuance of warning alerts during three (03) tsunami cases in the Indian Ocean.

17 September 2013 Makran tsunami (near-field case)		
Sequence of events	Timeline	Time lapsed (Minutes)
EQ occurrence	16:59 IST	0
Gwadar+		~10
1st warning (alert/watch advisory)	17:10 IST	11
2nd warning (no tsunami confirmation) *	17:15	16
Tsunami generated just around or after issuance of 2nd warning alert		
No further tsunami warning or bulletin issued		
1st tsunami detection (Qurayat tide station)	17:38	39
2nd tsunami detection (Oman tide station)	17:42	43
3rd tsunami detection (Sur tide station)	17:46	47
4th tsunami detection (Chahbahar tide station)	18:02	65
BPR detected tsunami	18:09	72
5th tsunami detection (Khawr Wudam tide station)	18:42	102
6th tsunami detection (Jask tide station)	18:47	107
7th tsunami detection (Dibba tide station)	18:52	112

17 July 2006 Java tsunami (far-field case)		
Sequence of events	Timeline	Time lapsed (Minutes)
EQ occurrence	15:19	0
Tsunami arrival at java coast, Indonesia (nearest one)	15:34	15
1st warning (alert/watch advisory) by United States Pacific Tsunami Warning Centre *	15:38	19
The tsunami reached at Makran coast after approx. 9 hours		~550

25 October 2010, Mw 7.7, Mentawai, Indonesia (far-field case)		
Sequence of events	Timeline	Time lapsed (Minutes)
EQ occurrence	21:42	0
1st warning (alert/watch advisory) by Indonesia Meteorological, Climatological and Geophysical Agency*	21:47	5
Tsunami arrival at Pagai coast, Indonesia (nearest one)	21:47	5
Japan Meteorological Agencies issued local tsunami watches 7 and 19 minutes after the earthquake. The tsunami warning announced at international early warning system.		
The tsunami reached at Makran coast after 9 hours		540

*Confirmation on bases of the epicentre being on the land part. Based on historical earthquake and tsunami data, Tsunami Threat does not exist for India.
+ Due to closeness of source, it should had arrived at the Gwadar earlier and had gone unnoticed due to its low hight and low tide level. The tide gauge record of event is not available at UNESCO's Sea level Monitoring Facility

---

Since the installation of IOTWS, 2013 Tsunami is the only near-field tsunami generated in the Arabian Sea. It was triggered remotely by a terrestrial earthquake located near the Khuzdar city, Pakistan. The tsunami waves remained almost unnoticed by the community due to the low wave heights and its occurrence at low tide. As it is thought to be triggered by an underwater landslide, the exact trigger time and location are not known. However, through reverse modeling the source

position at offshore of the Pakistan is estimated in between Gwadar and MSZ (Hoffmann et al., 2014). Form this tsunami source, the waves would have reached the Gwadar Coast within 5-20 minutes. After the earthquake, the first advisory warning followed by second confirming "no tsunami" warning was issued 11 minutes and 16 minutes, respectively after the earthquake. The advisory warning confirmation was particularly issued on the bases of epicentre being on the terrestrial (inland) part. The tsunami was first detected instrumentally 39 minutes after the earthquake at the Qurayat tide gauge in Oman. Various other tide gauges also recorded the tsunami afterward. The DART detected the tsunami wave 72 minutes after the earthquake. No further warning was issued may be due to small scale of the tsunami. Regarding the far-field tsunami, we analysed two cases: July 17, 2006, Java and October 25, 2010, Mentawai, Indonesia Tsunamis. In both cases, the system worked very well to warn the far-field communities. However, in both cases the waves arrived at nearest coast of Indonesia before issuance of (first) advisory warning (details in Table 5.3). The tsunami confirmation warnings in both cases were issued 19 minutes after the earthquake at the international early warning system where all local and regional warning systems are connected. These tsunamis took around 8 hours to reach the Makran Coast providing enough time to inform and evacuate the community. Here, we emphasize the importance of alert-watch awareness and preparedness for the communities residing close to tsunami source. In some tsunami cases, natural signs as the receding water after an earthquake and a strong and unusual roar sound may help an early warning for coastal communities. Technically, the initial recording of coastline or the draw down is due to development of initial wave trough along the coast. However, this may not always be the case because the trough development is subjected to source characteristic and position of the tsunami source. The awareness coupled with trainings, route evacuation and to react during such disasters is also very important. The PMD also has a well-established cyclone early warning system operating since 1960s. Despite multiple early warnings issued to coastal communities (couple of days earlier) the high number of fatalities and property losses from the cyclones in 1998, 1999, 2007, 2010, and 2021 demonstrate dismal levels in terms of resilience and preparedness. Likewise, in case of a tsunami the impact appears to be far harsher.

6. The case of 1945 Tsunami; wave height, number of waves and arrival time

This chapter represents a slightly modified amalgamation of two preliminary draft papers aimed at future publication.

- ***Haider, R.,** Ali, S., Javed, H., Gardezi, S.A.H., Hoffmann, G., and Reicherter, K..: The case of 1945 Tsunami; wave height, number of waves and arrival time.*

6.0 Abstract

An attempt has been made to comprehend four puzzling dynamics of the 1945 Tsunami event at the Pasni Coast: these are i) arrival time delay of 1-2 hours, ii) wave height ≥10 m which is exceptionally high as compared to earthquake size, iii) occurrence of three waves, and iv) temporary beach line regression or the initial draw-down. Three near-field tsunamigenic earthquake scenarios are tested to align with these four aspects and examined for generation, propagation, inundation and wave interaction (reflection and amplification). The analysis reveals that the exceptionally high wave height and delayed arrivals resulted from the reflection-amplification phenomenon. This phenomenon is influenced by two geomorphic reflectors: i) the coastal beach cliffs and ii) a bathymetric high (structural shelf rim). The former feature extends intermittently while the lateral continuously extends along the whole Makran Coast of Pakistan. A primary tsunami wave of approximately 5 m height can be amplified up to 10 m height due to the reflection-amplification which takes more than 80 minutes (1.5 hours) to develop and impact the coast. Overall, the wave package could be categorized into three major wave sets as reported by the tsunami survivors. Based on our integrated and comparative analysis, we propose an earthquake as an alone source for the 1945 Tsunami. We recommend further investigations, particularly assessing the 1945 earthquake in terms of fault parameters, fault location, and local tsunami reflection-amplification phenomenon.

6.1 Introduction

The Makran Subduction Zone (MSZ), located in the north Arabian Sea (Figure 6.1), with the presence of multiple splay faults has the potential to affect > 45 million people living in the coastal area, including Karachi, Mumbai, Oman, Chabahar and many other rural and urban communities (Haider et al., 2023). The Makran coast is economically important also due to its major sea-ports (Abbasi 2020; Kupriyanov and Makarevich 2024; Rashid and Shirazi 2023). Historically, Makran experienced great earthquakes and tsunamis (326, 1008, 1483, 1668, 1765, 1851 events) with their

seismic sources in the MSZ (Heidarzadeh et al., 2008), leading to devastating consequences such as life losses and infrastructural damages (Heidarzadeh et al., 2008; Qiu et al., 2022; Gardezi et al., 2024).

The Pasni, Gwadar and Ormara cities were worst affected by the 1945 earthquake (Mw 8.1) entailing tsunami which resulted in hundreds of casualties (Pendse, 1946; Hoffmann et al., 2013). These events, if replicated in present-day can cause even worse scenario due to the presence of ≈25 million population along the coastal areas of Makran (Haider et al., 2023). This 1945 mega-event which was the first instrumently recorded earthquake in this region, is a focal point of research, to exactly understand the dynamics of earthquake and sub-sequent tsunami in order to predict potential scenarios as well as to recommend mitigation strategies for future earthquakes, including those of similar or greater magnitude. Different proxies based on deterministic and statistical approaches are used by several researchers to assess the seismic and tsunami potential of Makran. However, the lack of instrumentally recorded local data poses challenges, causing curiosity among researchers, which further intensified over the past two decades, plausibly after the 2004 Indian Ocean tsunami and the 2011 Tohoku tsunami.

It is important to understand the tsunami-coast interaction especially in terms of vulnerability and risk assessment. The 1945 event gave many insights in this regard, however, poor record keeping raise constraints on information regarding the dynamics of the 1945 tsunami, particularly concerning arrival time, wave height and the number of waves. The interviews of 1945 Tsunami survivors (UNESCO/IOC, 2015) repeatedly report three waves impacting the study area (Table 6.2). The precise wave height, post-earthquake arrival delay and intra-wave duration is yet difficult to conclude from the interviews. Various hypotheses as splay faulting, delayed ruptures, and underwater landslides and combinations are proposed. For instance, Heidarzadeh and Satake (2014a) modeled a submarine landslide with a volume of around 40 km3 south of the Gwadar capable of replicating the tsunami wave heights at Pasni and Karachi in 1945. While Yanagisawa et al. (2009) and (Neetu et al. (2011) proposed, using inverse and forward numerical modeling approaches respectively, that the 3-hour delay in the 1945 Tsunami event was caused by the trapping of tsunami-wave energy on the continental shelf off the Makran coast. These trapped waves remained confined within a 300 km stretch of the continental shelf, moving along the shore. They further argue that along-shore trapping of tsunami energy is attributable to variations in the shelf width. This chapter aims to investigate wave reflection, amplification, and associated tsunami arrival delays at the Pasni Coast.

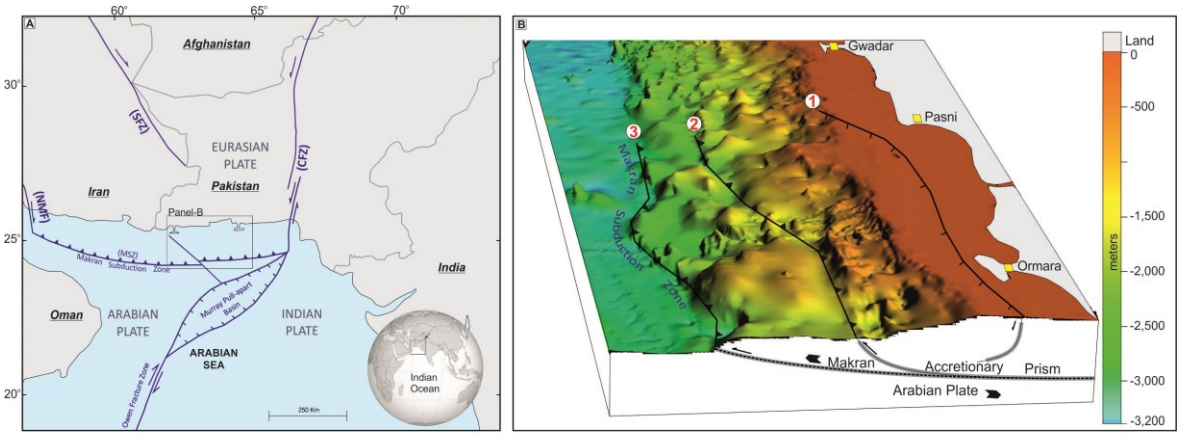

Figure 6.1 A) Location map of Makran with major regional tectonic elements. B) Schematic map showing location and type of faults on the bathymetric surface (GEBCO, 2023) used for modelling (numbered red along black circle). The thick shaded grey line under each fault shows an estimated ruptured part of the fault with parameters are given in Table 6.1.

We aim to understand the delay mechanism and tsunami wave height by examining three different tsunamigenic earthquake scenarios in the eastern MSZ and adjoining splay faults. The methodology involves the detailed analysis of reflection-amplification phenomenon along with its agents and its comparative analysis to other hypothesis in terms of tsunami intensity and arrival delay. Along with tsunami generation and propagation, an important component of the study is the inundation analysis at Pasni and Gwadar during 1945 Tsunami to test and confirm the affective wave height.

6.2 Seismic sources and tsunami potential

Makran's vulnerability to tsunamis and earthquakes is widely recognized. However, understanding of the local fault kinematics and tsunami-wave behavior remains challenging due to incomplete historical data and a lack of modern seismic and geodetic monitoring. The MSZ is characterized by a low dip angle subduction (2°-8°) extending to a depth of 250 km (Byrne et al., 1992; Kopp et al., 2000; Regard et al., 2010; Mousavi et al., 2022) with the slab steepening to an angle of ≈ 27° as it reaches a depth of 400 km (Manaman et al., 2011; Frohling and Szeliga, 2016; Penney et al., 2017). Mostly, subduction earthquakes occur at shallow depths (<20 km) (Jackson and McKenzie, 1984), the MSZ exhibits similar shallow seismicity offshore (Heidarzadeh et al., 2008; Pajang et al., 2022; Parvaiz et al., 2022 ; Qiu et al., 2022), with recent moderate quakes at 50-100 km depths revealing intra-slab seismicity onshore (Penney et al., 2017; Khan et al., 2020; Shah et al., 2021; Yang et al., 2022).

The accretionary prism or wedge (> 7 km thick) along the MSZ is the largest of its kind globally (Smith et al., 2012), which severely deformed over time and characterized by a series of splay faults connected to a decollement level at the Miocene base (Platt et al., 1988; Ellouz-Zimmermann et al., 2007; Grando and McClay, 2007; Parvaiz et al., 2022). Splay faults, which diverge steeply from the primary subduction zone interface during major earthquakes or may occur independently of these plate-boundary events (Plafker, 1972 ; Park et al., 2002; Heidarzadeh and Satake, 2014b; Mokhtari, 2015; Heidarzadeh et al., 2021). For instance, during earthquakes of 1960 Chili and 1964 Alaska (Plafker, 1972), 1944 Tonankai (Baba et al., 2006), 1946 Nankai (Cummins and Kaneda, 2000), 2004 Sumatra-Andaman (Sibuet et al., 2007) and 2019 Molucca Sea (Heidarzadeh et al., 2021), the splay faults played an important role in earthquake rupture propagation. Earthquakes typically initiate on the main subduction interface before the slip transfers to splay faults, especially in areas of the accretionary wedge where horizontal compressional stress dominates, such as near the trench line and topographic highs (Kame and Yamashita, 1999). Steep dip angles of splay fault, can cause significant vertical seafloor deformation, leading to the generation of large tsunamis with a localized affect due to their smaller size compared to the main subduction zone faults (Heidarzadeh et al., 2009a). Given the widespread distribution of splay faults in the MSZ (Grando and McClay, 2007; Mokhtari, 2015; Nemati, 2019; Pajang et al., 2021; Shah et al., 2021; (Cromie et al., 2022; Parvaiz et al., 2022; Qiu et al., 2022) and their historical impact on tsunami hazards globally, makes them an unavoidable seismic source in the assessment of tsunami potential in the Makran region. Particularly in offshore Makran Accretionary Prism, which is composed of recently accreted, loosely consolidated sediments with low seismic velocities and high pore-fluid pressures, can significantly increase tsunami risks by potentially amplifying wave heights locally.

The 1945 earthquake ruptured about 20% of the MSZ without breaching the trench (Byrne et al., 1992), resulting in the uplift of Ormara by roughly 2 m (Jacob and Quittmayer, 1979; Snead, 2002). This seismic event also generated tsunami run-up heights, reported to be between 10-15 m in Pasni (Pendse, 1946; Heidarzadeh et al., 2008; Hoffmann et al., 2013b, 2013a; Heidarzadeh and Satake, 2017), while Gates et al. (1977) and Page et al. (1979) indicate wave height ranges of 7 to 10 m. The

tsunami followed by this earthquake, may have been intensified due to slip on a splay fault off the coast of Pasni and Ormara, which could explain the 12–15 m wave height observed in the Pasni area. Many splay faults have been identified in both the eastern and western Makran regions using seismic reflection data, particularly highlighted in Smith et al. (2012). These thrust faults are primarily located near the deformation front, and the associated risk varies based on their proximity to coastal areas. In the context of the eastern Makran, we considered three asperity areas for splay fault, segmenting the eastern Makran from Pasni coast in north to the MSZ in the south (Figure 6.1B).

Table 6.1: Earthquake source parameters used to model tsunami scenarios.

Sr. No. (Figure 6.1)	Strike (°) Location in Figure 6.1	Width (km)	Depth (km)	Dip (°)	Rake (°)	Slip (m)
1	260 (east)	15	2	25 (Normal)	89	8
	260	20	2	25 (Normal)	89	9
	-82	25	2	25 (Normal)	89	10
	-84	30	2	45 (Normal)	89	12
	259	75	2	55 (Normal)	89	13
	246	80	2	55 (Normal)	89	14
	246	75	2	45 (Normal)	89	15
	243	40	2	35 (Normal)	89	14
	245	35	2	35 (Normal)	89	13
	250 (west)	30	2	30 (Normal)	89	12
2	257 (east)	90	10	17 (Reverse)	89	25
	257 (west)	45	10	15 (Reverse)	89	25
3	248 (east)	140	5	10 (Reverse)	89	10
	248	140	5	10 (Reverse)	89	20
	259	140	5	10 (Reverse)	89	25
	259	140	5	10 (Reverse)	89	25
	266	140	5	10 (Reverse)	89	25
	266	140	5	10 (Reverse)	89	25
	264	140	5	10 (Reverse)	89	25
	266	140	5	10 (Reverse)	89	10
	269 (west)	140	5	10 (Reverse)	89	5
The “east” and “west” mentions the respective end of the fault line.						

The interesting phenomena is the common occurrence of normal faults in the coastal area of Iranian Makran and their possible eastward extension in Pakistani Makran. Recent studies by Grando and McClay, (2007), Pajang et al. (2021; 2022) in western Makran, while, Khan et al. (2024) in eastern Makran, have reported the presence of south-dipping normal faults in the offshore, while the onshore focal mechanisms of several seismic events also indicate normal faulting (Mokhtari et al., 2019); Nemati, 2019). This transition of thrust to normal faulting creates ambiguity about the mechanical characteristics of the subduction. The plausible reason for the development of normal faults in an active MSZ is the negative buoyancy effect caused by the density contrast of the descending slab (which is ≈ 60 kg/m³ compared to the asthenosphere), as well as, the thermal erosion by the asthenosphere, which reduce the slab thickness to about 50 km (Mousavi et al., 2022). Another possible reason of normal faulting in Makran can be explained by its geological evolution over time. Initially, from the Middle Miocene to the Middle Pleistocene, renewed subduction activity created a fold and thrust belt (Khan et al. (2024). Subsequently, from the Middle Pleistocene to the present, a progradation deposition system over pre-existing fold and thrust belt, contributed to the development

of normal faults through gravitational collapse, as the deformation front migrated southwards (Grando and McClay, 2007; Khan et al. 2024). Therefore, their presence can also be a potential seismic source for tsunami hazard, particularly in the coastal areas of Makran. Further, Choy and Kirby (2004) suggested that normal faulting mechanisms radiate significantly higher energy compared to events with thrust faulting mechanisms in intra-slab earthquakes in the subduction zones. Globally, many earthquake events occurred in the subduction zones, where normal faults on the subducting plate propagate the rupture of mega thrust earthquake such as Chilean Subduction Zone (Malgrange and Madariaga 1983; Loveless et al., 2010), Antilles Subduction Zone (McCann et al., 1982), Mexican Subduction Zone (Mikumo et al., 1999), Nankai Subduction Zone (Heffernan et al., 2004). Similarly, the possibility of two separate ruptures identified on different faults (normal and thrust) on overriding plate as a result of an earthquake on the subducting plate interface e.g., (Hicks and Rietbrock, 2015). This underscores the critical role of normal fault over thrust faults in assessing tsunami potential within subducted slab.

We tested these three types of faults to understand the tsunami hazard potential of the region. The parameterization of the faults is the least understood mechanism of the region. However, we used the multi segmented faults with heterogeneous parameters given in Table 6.1.

6.3 Methodology and Data

The tsunami arrival timings and inundation extents of the 1945 Tsunami event at Pasni are determined through a fieldwork by mapping the maximum limits (Figure 6.3A) as indicated by survivors of the 1945 tsunami (Table 6.2) and technical reports (Table 6.3). The fault location and parameters are explained in section 2. We simulated several hypothetical wave scenarios based on earthquake source parameters to identify the best-fit models for these extents and runups. Among these modelling results, we are presenting three distinct cases. We also compared the arrival times and wave heights with tide gauge records from Karachi and Mumbai to test any ambiguity in co-seismic or post-seismic wave generation.

Numerical modeling is conducted using earthquake source parameters within the MSZ and Makran Accretionary Prim employing the Delft3D 4.04.01 software, developed by the Dutch Institute Deltares (Deltares, 2023). The hydrodynamic program module Delft3D-FLOW is utilized for simulation, which solves the non-linear 2D and 3D shallow water equations for unsteady flow phenomena. These shallow water equations (SWE), derived from the three-dimensional hydrodynamic Navier-Stokes equations for incompressible fluids, are well approximated by the Boussinesq approximation. The Delft3D-FLOW module facilitates simulation calculations of tsunami waves using a two-dimensional, depth-averaged calculation method (for further details, please refer to (Deltares, 2017, pp. 175–181).

The grid resolution for the nested models is set at 0.0004×0.0004 (44 m × 44 m) and 0.01 × 0.01 (~1 km × 1 km) for the regional model. Reinmann Boundary Conditions are applied in the regional model to minimize the reflection effect, while time-series boundaries are utilized for the nested models. For tsunami propagation and inundation, data from the General Bathymetric Chart of the Oceans (GEBCO) 15 arc seconds and the German Aerospace Centre's (DLR) 0.4 arcsec (~12 m) Digital Elevation Model (DEM) are fused (mosaicked) together. The DLR generated the DEM from bistatic X-Band interferometric Synthetic Aperture Radar (SAR) data using the DLR's patented TanDEM-X and TerraSAR-X. There has been no significant change in Pasni's topography since 1945, although a few survivors of the 1945 tsunami claim co-seismic subsidence (~2 m) at the northeastern part of

the city. As of 2023, this subsided topography has been largely replenished by beach sand accretion processes. Hence, no necessary modification in the DEM is required.

Table 6.2: showing the compilation of inundation observations at Pasni with the interviews of 1945 survivors and the field observations (UNESCO/IOC, 2015).

Interviewee	Age (years as of 1945)	Brief description	Run-up height	Inund. extent	Locality No. in Figure 6.3A
Tanakko Bibi	11	a) "The 1945 tsunami came up until here, where we are sitting right now (her house). You can still see the seashells (of the 1945 tsunami) scattered around here."" b) "Much of the casualties happened in the Main Bazar locality"	9 m 7 m	1.6 km 1.3 km	1a 1b
Rabia Bibi*	4-5	"Water came to Tanakko Bibi's house".	9 m	1.6 km	2
Khudai Dost	10-15	"Part of Wadsar was drowned"			4
Qadir Baksh	15	"Tsunami water came to Daragah (Shrine) and then receded back. There were already scattered bivalve shells on the inundated land, but the concentration had increased after the 1945 tsunami"	10 m	1.6 km	5
Ganj Baksh	14-15	"Tsunami destroyed houses, boats, and debris nearly as far inland as Parhag. Many houses and boats were stranded beside Jaddi Hill.	8 m	360 m to 1.52 km	3
Hajiani Guli	22	It didn't take much time to arrive tsunami after the earthquake.			
Abdul Rasheed	12	It took almost an hour to sea to create havoc and go back			
Sakhi Daad	11	Three tsunami waves came at about 3 o'clock to 4 o'clock in the morning. The water went back and then came back violently.			
Amna	12	It was dawn when the first wave arrived at the Gwadar coast (~06:45 am). Sea got dried up and water receded beyond eyesight.			
Field work (This study)		The above reported localities were identified in the field. We traced a curvilinear deposit of broken bivalve (shell bed) connecting these above-mentioned localities and interpreted it to be reworked deposits from the 1945 tsunami (tsunamites).	8 m	0.3 – 1.8 km	6,7,8
* Witness aged 4-5 years to remember the tsunami is doubtful. Most likely she repeats what she is told by others					

Table 6.3: Table showing compilation of technical reporting wave heights and times at Pasni, Karachi and Mumbai.

Reference	Observed Max. Wave height (location)	Observed arrival time (1st, 2nd, 3rd)	Explanation/ comments
(Pendse, 1946)	12-15 m (Pasni)	04:00, 07:15, --	"At about 4:00 IST a wave was noticed but it did not come inland. At about 7:15 IST another wave swept over the town and caused widespread havoc. The height of this wave has been estimated variously from 40 ft to 60 ft (~12 m to 18 m)"
	1.4 m (Karachi)	05:30, 07:00, 07:50	last wave was highest with wave height of 1.4 m
	1.9 m (Mumbai)	08:15, --, --	
(Gates et al., 1977)	7-10 m (Pasni)	04:00, 04:30, 5:00	(refers to their independent interviews conducted to tsunami survivors)
(Page et al., 1979)	7-10 m (Pasni)	04:30, 05:00, --	"Local inhabitants report that three tsunamis hit the Makran Coast 1.5 to 2 hours (4:30, 5:00 IST). Field investigation showed that there was no uplift of Pasni resulting from the earthquake, but the Ormara area rose about 2 m"
(Neetu et al., 2011)	0.28 m (Karachi)	05:00, --, --	Karachi Tide Gauge (1945), First wave arrival 5:00 IST
	0.35 m (Mumbai)	08:09, --, --	Mumbai Tide Gauge (1945), First wave arrival 08:09 IST
(UNESCO/IOC, 2015)	≥7 m (Pasni)	04:00, --, --	Three waves with interval of few minutes arrived ~30 minutes after the earthquake, Interviewees: i)-Khuadi Dost, ii)-Sakhi iii)-Daad, Madni

6.4 Results and Analysis

The results and analysis are explained in terms of four key aspects: inundation extents, arrival time delay, number of waves and the initial drawdown of shoreline (Table 6.4).

Table 6.4: Table showing comparative analysis of tsunami scenarios based on the criteria.

Scenario	Inundation extent	Arrival time delay	No. of waves	Initial drawdown	Reported wave height
Scenario-1	✓	✗	✗	✗	✓
Scenario-2	✓	✓	✓	✓	✓
Scenario-3	✗	✓	✓	✓	✗

Table 6.4 shows that Scenario-2 could demonstrate all four aspects as reported. This scenario can also convince the arrival of a low wave shortly after the earthquake as reported by the several eyewitnesses (Figure 6.3). Overall, two major wave packages can be distinguished from the model. This first waveform arrival in 28 minutes is maximum 5 m high while the second waveform arrival in 80 minutes is intense being 10 m high. This second waveform can be resolved further into two packages especially at the MS-1 monitoring point. On land, the second waveform again integrates into a big single waveform resulting in two waves at MS-3 (Figure 6.3). These are the worst hit locations and possibly the survivors recall the impact of three waves at these locations. The wave segregation or the trajectory resolution can be improved by decreasing the time-step duration of the model demanding more time and computational resources. Scenario-2 can also explain the initial drawdown of the beach line as reported by several tsunami survivors. The initial drawdown causing the beach line to recede is the result of the entailing trough of initial tsunami wave generated in the coastal parts. The source parametric sensitivity analysis shows that the width and depth of the earthquake rupture influences the position of the initial tsunami crest and trough. It is also possible that the 2 m subsidence observed during the 1945 earthquake at the Pasni coast could also be

attributed to this same phenomenon, although further detailed investigations are required to check this hypothesis.

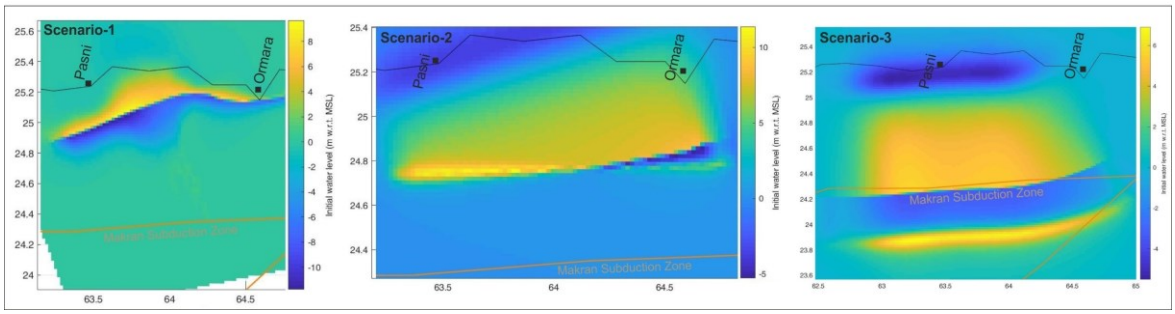

Figure 6.2: Initial tsunami wave heights of four distinct scenarios.

Scenario-1 examines a normal fault on the continental shelf as a potential source for the 1945 Tsunami event. This scenario is capable of explaining the observed wave heights and the extent of inundation recorded during the event. However, in this scenario several critical aspects remain unresolved. Notably, the post-earthquake time delay, the number of waves, and the phenomenon of shoreline drawdown are inadequately explained by this scenario. The primary limitation lies in the inability of the scenario to generate a significant wave reflection at the shelf rim. The reflection and subsequent amplification phenomena crucial to this process are insufficiently developed in the given geological setting, as illustrated in Figure 6.3. Therefore, while Scenario-1 provides a plausible explanation for certain aspects of the 1945 Tsunami, it fails to comprehensively account for the complex wave dynamics observed during the event.

Scenario-3 is the least fitting scenario in terms of explaining the dynamics of the 1945 Tsunami. While it can account for the observed time delay, number of waves generated, and the phenomenon of shoreline drawdown, it falls short in other critical areas. Specifically, the scenario fails to match the observed wave heights and inundation extents recorded during the event. The maximum height of the approaching wave cloud reaches 4 m which disperses upon impacting southern coast of the Pasni. This is significantly lower than the wave heights documented in historical records of the 1945 Tsunami. Additionally, the scenario generates extremely weak reflections from both reflectors. These weak reflections result in a minimal amplification effect, with the wave height only increasing to 2 m. Therefore, Pasni Coast remains un-inundated with this wave height and hence poses no tsunami hazard.

There are two prominent reflectors responsible for wave amplification, delayed arrivals and the number of waves. The first one is the beach-cliffs NE of Pasni, and the second one is the bathymetric high at the shelf break (Figure 6.5). The rimmed-high extends EW direction making a linear geomorphic valley which is a quite common geomorphic feature in the Makran Accretionary Prism. Reflective waves from both reflectors integrate to generate anomalous wave amplification and time delay. In Scenario-2 amplification factor is twice along with arrival delay for major tsunami waveform (Figure 6.4). The Makran, especially Pasni, is situated such that the interaction timing and location of both reflecting waves plays a major role in terms of tsunami hazard. Further refinement of the location and modelling parameters may enhance results and minimize source parametric values, thereby more effectively illustrating the dynamics of the 1945 tsunami.

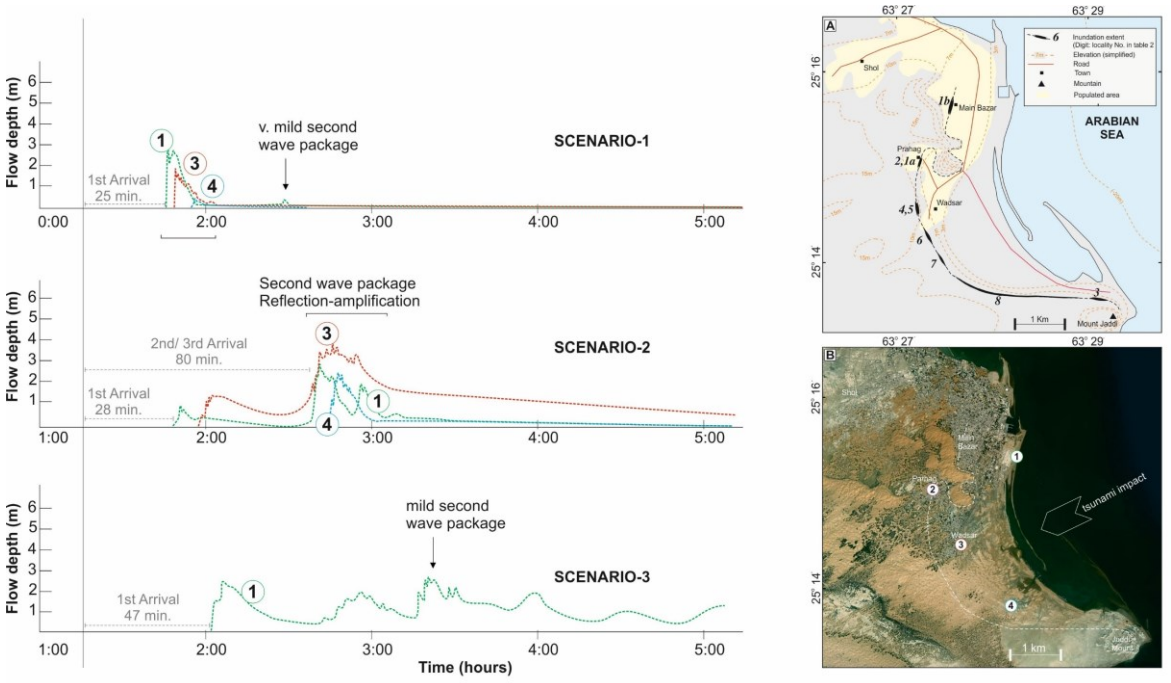

Figure 6.3: Illustrates the inundation results of the three scenarios; spectral characteristics of flow depth at four Monitoring Points (MP). Notably, Scenario-2 exhibits the generation of a substantial wave package with delayed timing, attributed to the reflection-amplification phenomenon. This secondary wave package is absent in the other two scenarios. A) The map delineates the inundation limits of the 1945 Tsunami. The details of the numbers along the limit-line are given in Table 6.2 and Table 6.3. The satellite image overlays the inundation limit and Monitoring Points for enhanced visualization.

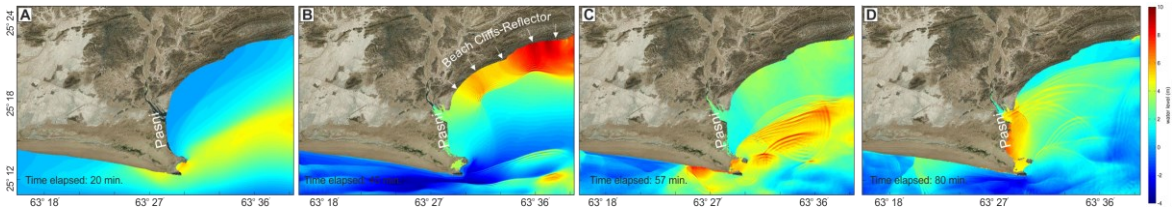

Figure 6.4: Temporal Evolution of Scenraio-4 Tsunami along the Pasni coast. A) Initial wave approaching the coast. It causes minimum inundation as can been seen in panel B. B) Generation of reflected waves. First reflection from the beach cliffs (norther one) and second reflected wave generated at the rim of the shelf (bathymetry in Figure 6.5). C) Interaction and amplification of both reflected waves forming a complex waveform. D) Inundation of integrated waveform at the Pasni beach.

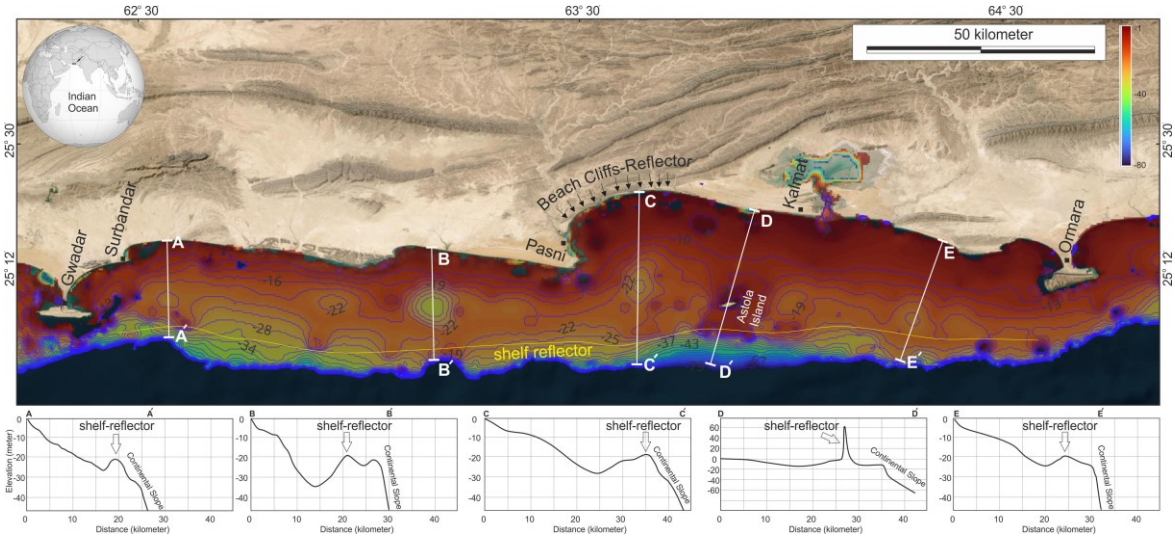

Figure 6.5: Illustration of the two wave reflectors responsible for amplification and delayed wave arrivals. The first reflector is the beach-cliffs northeast of Pasni (indicated by black arrows). The second reflector, marked by a yellow line, is a bathymetric high forming a linear rim at the shelf break. The wave crossing over the shelf rim generates secondary waves, which subsequently interact with the reflected waves from the cliffs, resulting in wave amplification, east of the Pasni offshore area.

6.5 Discussion

When discussing tsunami potential along the coastal areas of Pakistan, we refer specifically to the MSZ as a primary source which also has considerable potential to further trigger the secondary tsunami sources such as submarine landslide and mud-volcanoes. Several researchers (Rajendran et al., 2008; Heidarzadeh et al., 2008; Arjun et al., 2011; Akbarpour Jannat et al., 2011; Swapna & Srivastava, 2014; Payande et al., 2014; Delavar et al., 2017; El-Hussain et al., 2018) modelled the 1945 tsunami based on earthquake parameters, which could only produce a maximum wave height of 5 m at the Pasni coast, failing to explain the observed tsunami height of 10-15 meters (Pendse, 1946; Heidarzadeh et al., 2008; Hoffmann et al., 2013b, 2013a; Heidarzadeh and Satake, 2017), while Gates et al. (1977) and Page et al. (1979) indicate wave height ranges of 7 to 10 m. Moreover, aspects as the number of waves, arrival delays and initial draw-down, coast-waves interaction are further debatable. Mostly, the researchers dealt with either one or two aspects in modelling while the other aspects are either overlooked or compromised. For instance, wave height has been the focused by (Heidarzadeh et al., 2008; Akbarpour Jannat et al., 2011; Heidarzadeh and Satake, 2017; El-Hussain et al., 2018), arrival delay by (Rajendran et al., 2008), wave height in combination with time delay by (Yanagisawa et al., 2009; Neetu et al., 2011; Momeni et al., 2022; Haider et al., 2024). We attempted to investigate four key aspects as discussed in section-4. Along with these aspects, the integration of inundation analysis for the 1945 Tsunami event offers valuable understandings by aligning observed information with modeling results.

Analysis shows that the wave reflection and amplification are highly influenced by the resolution of both bathymetric and computational grids. The coastal wave reflection in regional model results in a nearly 50% reduction when compared to the high-resolution nested model. This finding underscores the critical importance of utilizing high-resolution models for precise calculation of wave amplification. Low-resolution models tend to significantly underestimate the potential coastal impacts of tsunamis, which can lead to inadequate hazard assessments and mitigation strategies. Alongside wave height, wavelength is one of the most important aspect to consider, particularly in

coastal regions where coastal and bathymetric reflectors prevail. Waves with large wavelengths play a critical role in reflection and amplification compared to shorter wavelengths.

There is a reasonable match between the simulation time and the actual tsunami arrival time at the Karachi and Mumbai tide gauge records of 1945 (Figure 6.6). These two instrumental records did not account for the time delays and a bigger wave later, providing additional evidence for a single co-seismic tsunami source. Regarding landslides as a potential tsunami source, if this was the case, then it might have triggered exclusively during the earthquake event and was not subsequently triggered. Based on wavelength analysis, arrival time delays possibility at Pasni, wave amplification and finally the consistency of time record at Karachi and Mumbai tide gauges, earthquake as a tsunami source in 1945 can be explained.

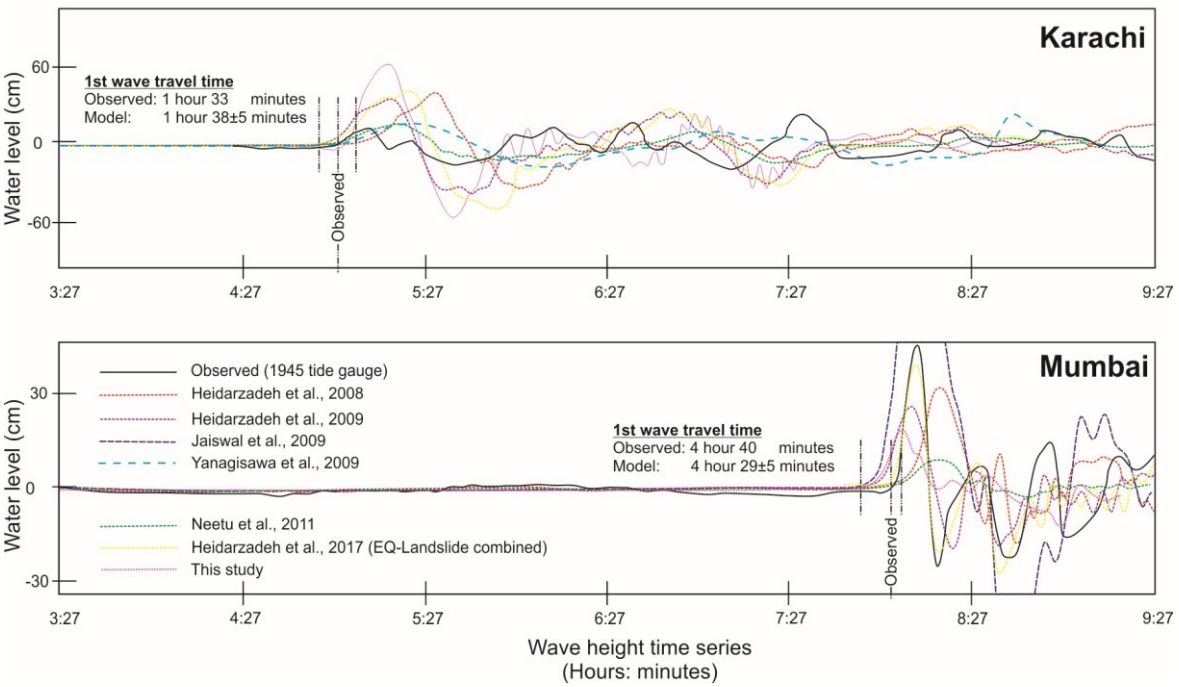

Figure 6.6: The line graphs above illustrate a comparison between the observed arrival times and the modeled ones at Karachi and Mumbai (Haider et al., 2024). The references to (Heidarzadeh et al. (2008, 2009), Jaiswal et al. (2009) are not explicitly mentioned in the text. The observed and modelled results align with the earthquake source and trigger timings and do not correspond to any time delay, as reported in the case of Pasni. This absence of delay reflects no secondary or delayed tsunami generation phenomenon.

The understanding of the fault location and source parameters of the 1945 earthquake remains inadequate. There are various estimates regarding the location and size of the earthquake rupture; Heck (1947) identified it at 25.001N and 61.501E, Pendse (1946) placed it at 24.201N and 62.601E, approximately 120km away from Pasni, Ambraseys and Melville (1982) reported it at 25.021N and 63.471E. Byrne et al. (1992), through a recalculation of seismic parameters, proposed the epicenter to be at 25.151N and 63.481E. The magnitude of reflection-amplification is sensitive to the location of the tsunami source, more accurately referred to as the fault trace. Furthermore, we recommend further investigation into the calculation of fault parameters related to the 1945 earthquake. The fault kinematics in the accretionary prism are also poorly understood, handicapping to estimate the fault rupture mechanism and entailing tsunami potential.

6.6 Conclusions

1. A primary tsunami wave measuring 5-6 m in height could elucidate the dynamics of the 1945 Tsunami including its inundation aspect. The reflection-amplification phenomenon is responsible for exceptionally high wave height (10 m) with delayed arrivals.
2. There exist two strong wave reflectors in the study area: the beach cliffs and the shelf rim. The interaction of tsunami waves between these two reflectors has the potential to cause amplification up to twofold. Furthermore, the resulting wave experience a delay of more than 80 minutes (>1.5 hours) before reaching the Pasni coast.
3. Based on wavelength analysis, examination of the arrival time delay mechanism, wave amplification, and the consistent record of tsunami arrival times at Karachi and Mumbai tide gauges, we propose an earthquake as the source of the 1945 tsunami.
4. We recommend a reassessment of the fault line ruptured during the 1945 earthquake, including its source parameters.

7. Re-evaluation and Synthesis

7.0 Concluding discussion

1. This study offers a comprehensive assessment of tsunami hazards and their potential impacts along Pakistan's coastline. By employing a multi-proxy approach, we evaluate the recurrence intervals of high-magnitude tsunami events (≥10 m wave height), particularly focusing on the seismically active Makran Subduction Zone. Our findings indicate that the recurrence interval for such high-magnitude tsunami events ranges between 500 to 1000 years. The multi-proxy approach integrates probabilistic and deterministic methodologies, complemented by historical records and paleo-sedimentary evidence. This holistic framework enables a robust understanding of tsunami dynamics, recurrence patterns, and their implications for coastal vulnerability and risk mitigation strategies in the region.

2. Field investigations have uncovered evidence of two significant paleo-tsunami events (tsunamites) along the Pasni Coast, predating the well-documented 1945 tsunami. These findings suggest a recurring pattern of tsunamigenic activity in the region, underscoring the persistent threat posed by such natural hazards. By calibrating dynamic tsunami models with observed inundation limits from historical events, we have gained critical insights into the vulnerability of key coastal cities, such as Gwadar and Pasni. The results highlight the urgent need for robust mitigation measures and the implementation of advanced early warning systems, particularly in Gwadar, given its strategic importance and rapidly growing infrastructure. This study emphasizes the necessity of integrating geological, historical, and modeling approaches to enhance awareness and preparedness to reduce the potential impacts of future tsunamis in the region.

3. A comparative analysis of inundation models highlights the critical role of coastal and shelf-bathymetric morphology in amplifying tsunami impacts. Wave reflection and amplification phenomena significantly influence inundation dynamics, shaping the severity and behavior of tsunami waves as they approach the shore. Our investigation into the dynamics of the 1945 tsunami provides new insights into previously puzzling aspects, such as wave height variability, arrival time delays, and the occurrence of multiple waves. These complexities arise from the intricate interactions between coastal geomorphology and wave propagation dynamics. For instance, wave amplification can double the height of tsunami waves, while arrival times can be delayed by more than 1.5 hours due to these interactions. In our case study, the occurrence of multiple waves is attributed to the reflection phenomenon, which further complicates the inundation pattern and underscores the need for detailed modeling to accurately predict tsunami behavior.

4. Through numerical modeling and simulation, we have investigated the plausibility of linking the 1945 tsunami to its respective earthquake. Our findings support the hypothesis that the earthquake was the primary source of the 1945 tsunami, based on wavelength analysis, consistent timing records, inundation limits, initial draw down of beach line and the observed reflection-amplification phenomenon. These factors collectively provide strong evidence for the earthquake's role in triggering the tsunami. However, further research is recommended to refine our understanding of the fault parameters and the underlying mechanisms driving tsunami generation, propagation, and wave interactions, including reflection and amplification processes in the region. Such studies are essential for improving predictive models and enhancing tsunami risk assessment and mitigation strategies.
5. In conclusion, this study highlights the critical need for comprehensive mitigation strategies to enhance coastal resilience and reduce the potential impacts of future tsunamis along Pakistan's coastline. By integrating advanced modeling techniques, historical data, and field observations, we have identified key vulnerabilities and recurring patterns of tsunamigenic activity in the region. These findings underscore the urgency of implementing robust early warning systems, community awareness programs, and infrastructure improvements to safeguard coastal populations and assets. Furthermore, we advocate sustained research efforts to deepen our understanding of the complex interplay between seismic activity, coastal geomorphology, and tsunami dynamics. Such efforts are essential to refine predictive models, enhance disaster preparedness, and strengthen response capabilities, ultimately contributing to the long-term safety and resilience of coastal communities in Pakistan.

7.1 Outlook

We recommend further investigations in following domains.

1. A reassessment of the fault line that ruptured during the 1945 earthquake, including its source parameters, is strongly recommended. This is particularly important as nearly all other aspects of the tsunami such as wave generation, propagation, and inundation patterns can be explained and attributed to an earthquake source. Additionally, the active seismic zone south of Pasni, in relation to the Sonne Fault, warrants detailed investigation. Key factors such as the nature of the décollement basement and the slow GPS velocity observed at Pasni should be examined in greater depth. Understanding these elements is crucial for refining seismic and tsunami hazard assessments, as well as for improving predictive models and mitigation strategies in the region. Such efforts will contribute to a more comprehensive understanding of the tectonic and geophysical processes driving seismic and tsunami risks along Pakistan's coastline.
2. Pasni has experienced at least two significant tsunami events in recorded history: the 1945 AD tsunami and the 1524 AD tsunami. However, further investigation is required to examine sedimentary deposits that may correspond to a potential third event, tentatively dated to the 17th century BC. Radiometric analysis, particularly radiocarbon dating of a bivalve shell found within the tsunamite horizon, has provided a maximum age estimate for this event. To achieve a more precise age range, high-resolution dating techniques, such as high-frequency radiocarbon dating or other geochronological methods, are necessary. Additionally, there is

a pressing need for further research into Pasni's history around 1524 AD to validate existing historical records and sedimentary data. Such studies would provide deeper insights into the frequency, magnitude, and impacts of past tsunamis, ultimately enhancing our understanding of the region's tsunami hazard profile and informing future risk mitigation strategies.

3. The phenomenon of tsunami reflection, amplification, and arrival delay warrants further detailed investigation. The unique coastal and bathymetric features northeast of Pasni, particularly the Cliff-Bay and shelf-bathymetry, play a critical role in generating substantial tsunami reflections. These reflections contribute to the arrival of multiple waves at the Pasni shoreline, significantly influencing inundation patterns and coastal impacts. The extent of wave reflection and amplification within the bay is highly dependent on the direction of the incoming tsunami waves. Maximum effects are observed for tsunamis originating from the southeast in the Arabian Sea, where the interaction between wave dynamics and coastal morphology is most pronounced. Additionally, the complex interplay of these factors can result in a delay of more than 90 minutes (>1.5 hours) before the tsunami waves reach the Pasni coast. Understanding these processes in greater detail is essential for improving tsunami hazard assessments, refining predictive models, and developing effective early warning systems to mitigate the risks posed to coastal communities.
4. The coastline should be thoroughly investigated for field evidence, such as tsunamites (tsunami deposits), to enhance the paleo-tsunami record and improve our understanding of past tsunami events. Identifying and analyzing these deposits can provide critical insights into the source potential, magnitude, and recurrence intervals of tsunamis in the region. This field-based approach, combined with advanced dating techniques and sedimentological analysis, will contribute to more accurate hazard assessments and inform the development of effective risk mitigation strategies. Strengthening the paleo-tsunami record is essential for building resilience against future tsunami threats and ensuring the safety of vulnerable populations along the coastline.
5. In tsunami hazard assessment, wave height is traditionally used as a primary benchmark for evaluating potential impacts. However, the wavelength of tsunami waves is often overlooked, despite its significant influence on inundation dynamics and coastal damage. Volume of water being a function of wavelength plays a critical role in determining the extent of coastal flooding, the duration of wave action, and the overall destructive potential of a tsunami. Furthermore, we recommend a comparative analysis of tsunami spectra generated by different sources, such as landslides and earthquakes, to better understand their distinct characteristics and associated hazards. By integrating these factors into hazard assessments, we can develop more accurate and comprehensive models to predict tsunami behavior, improve early warning systems, and enhance risk mitigation strategies for vulnerable coastal regions.
6. Further technical studies should be conducted to assess the feasibility of mangrove forestation along the coasts of Pasni, Ormara, and Karachi. Along with several other ecological advantages, mangrove forests can also serve as a natural coastal defense system, mitigating the impacts of extreme waves, storm surges, and tsunamis by dissipating wave energy and reducing erosion. A detailed feasibility study would evaluate factors such as soil conditions, tidal patterns, water salinity, and local biodiversity to determine the most suitable areas for mangrove restoration or plantation. Implementing such initiatives could significantly enhance coastal resilience, protect vulnerable communities, and contribute to sustainable development in the region. This approach aligns nature-based solutions for

disaster risk reduction and climate change adaptation, offering a cost-effective and environmentally friendly strategy to safeguard coastal areas

References

Abbasi, M.A., 2020. Regional Connectivity and Pakistan-Iran Trade Corridors. J. Glob. Peace Secur. Stud. 1, 44–59.

Aguirre-Ayerbe, I., Martínez Sánchez, J., Aniel-Quiroga, I., González-Riancho, P., Al-Yahyai, S., González, M., Medina, R., 2018. From tsunami risk assessment to disaster risk reduction - The case of Oman. Nat. Hazards Earth Syst. Sci. 18, 2241–2260. https://doi.org/10.5194/nhess-18-2241-2018

Ahmed, M., Lodi, S.H., Rafi, M.M., 2019. Probabilistic seismic hazard analysis based zoning map of Pakistan. J. Earthq. Eng. 1–36. https://doi.org/10.1080/13632469.2019.1684401

Akbarpour Jannat, M.R., 2021. Tsunami modeling in the Chabahar Bay-Iran from worst-case Makran seismic scenarios: new insights into spectral characterization, separation of the continental shelf, and topography effects. Arab. J. Geosci. 14. https://doi.org/10.1007/s12517-021-06449-0

Akbarpour Jannat, M.R., Noranian Esfahani, M., Chegini, V., Rezanejad, K., 2011. Hazards associated with tsunami waves in the gulf of Oman. J. Coast. Res. 865–869.

Al-Habsi, Z., Hereher, M., El-Hussain, I., Omira, R., Ana Baptista, M., Deif, A., Al-Awadhi, T., Al-Nasiri, N., 2022. Tsunami hazard and risk zoning for Qurayyat in northeast Oman coast: Worst-case credible scenarios along the Makran Subduction Zone, Western Asia. J. Asian Earth Sci. X 8, 100103. https://doi.org/10.1016/j.jaesx.2022.100103

Ali, B., Matsumaru, R., Janjuhah, H.T., 2023. A Source Model for Tsunami Hazards. A Case study from the Eastern Segment of the Makran Subduction Zone, Balochistan, Pakistan. J. Himal. Earth Sci. 56, 48–64.

Ali, K.F., De-Boer, D.H., 2008. Factors controlling specific sediment yield in the upper Indus River basin, northern Pakistan. Hydrol. Process. 2274, 2267–2274. https://doi.org/10.1002/hyp

Ambraseys, N.N., Melville, C., 1982. A history of Persian earthquakes. Cambridge University Press, Britain.

Aniel-Quiroga, Í., Álvarez-Gómez, J.A., González, M., Martínez Sánchez, J., Parro, L.M., Aguirre-Ayerbe, I., Fernández, F., Medina, R., Al-Yahyai, S., 2018. Tsunami Hazard assessment and Scenarios Database for the Tsunami Warning System for the coast of Oman. Nat. Hazards Earth Syst. Sci. 1–30. https://doi.org/10.5194/nhess-2018-221

Anshori, 2019. Tsunami-Inundation-Toolbox-ArcGIS-Desktop-10.x. https://github.com/anshori/Tsunami-Inundation-Toolbox-ArcGIS-Desktop-10.x (Last accessed: 01.02.2022).

Arjun, S., Kalarani, K., Dhanya, P., Praveen, S.S., Reshmi, A.K., Kurian, N.P., Murthy, M.V.R., Hameed, T.S.S., Prakash, T.N., 2011. Numerical simulation of the 1945 Makran tsunami on the southwest coast and Lakshadweep islands of India. Mar. Geod. 34, 68–76. https://doi.org/10.1080/01490419.2011.547801

ArRajehi, A., McClusky, S., Reilinger, R., Daoud, M., Alchalbi, A., Ergintav, S., Gomez, F., Sholan, J., Bou-Rabee, F., Ogubazghi, G., Haileab, B., Fisseha, S., Asfaw, L., Mahmoud, S., Rayan, A., Bendik, R., Kogan, L., 2010. Geodetic constraints on present-day motion of the Arabian Plate: Implications for Red Sea and Gulf of Aden rifting. Tectonics 29, 1–10. https://doi.org/10.1029/2009TC002482

Attenbrow, V., 1992. Shell Bed Or Shell Midden. Aust. Archaeol. 34, 3–21. https://doi.org/10.1080/03122417.1992.11681447

Baba, T., Cummins, P.R., Hori, T., Kaneda, Y., 2006. High precision slip distribution of the 1944 Tonankai earthquake inferred from tsunami waveforms: Possible slip on a splay fault. Tectonophysics 426, 119–134. https://doi.org/10.1016/j.tecto.2006.02.015

Banghar, A., Syke, L.R., 1981. Focal mechanism of an earthquake from the Southern Ocean. Tectonophysics 79, 37–41.

Baptista, M.A., Miranda, J.M., Omira, R., El-Hussain, I., 2020. Study of the 24 September 2013 Oman Sea tsunami using linear shallow water inversion. Arab. J. Geosci. 13. https://doi.org/10.1007/s12517-020-05632-z

Behrens, J., Løvholt, F., Jalayer, F., Lorito, S., Salgado-Gálvez, M.A., Sørensen, M., Abadie, S., Aguirre-Ayerbe, I., Aniel-Quiroga, I., Babeyko, A., Baiguera, M., Basili, R., Belliazzi, S., Grezio, A., Johnson, K., Murphy, S., Paris, R., Rafliana, I., De Risi, R., Rossetto, T., Selva, J., Taroni, M., Del Zoppo, M., Armigliato, A., Bureš, V., Cech, P., Cecioni, C., Christodoulides, P., Davies, G., Dias, F., Bayraktar, H.B., González, M., Gritsevich, M., Guillas, S., Harbitz, C.B., Kânoğlu, U., Macías, J., Papadopoulos, G.A., Polet, J., Romano, F., Salamon, A., Scala, A., Stepinac, M., Tappin, D.R., Thio, H.K., Tonini, R., Triantafyllou, I., Ulrich, T., Varini, E., Volpe, M., Vyhmeister, E., 2021. Probabilistic Tsunami Hazard and Risk Analysis: A Review of Research Gaps. Front. Earth Sci. 9, 1–28. https://doi.org/10.3389/feart.2021.628772

Bell, K.C., 2011. Lessons from the reconstruction of post-tsunami Aceh: Build back better through ensuring women are at the center of reconstruction of land and property. Washington, DC. © World Bank.

Bellanova, P., Frenken, M., Nishimura, Y., Schwarzbauer, J., Reicherter, K., 2021. Tracing woody-organic tsunami deposits of the 2011 Tohoku-oki event in Misawa (Japan). Sci. Rep. 11, 8947. https://doi.org/10.1038/s41598-021-88199-3

Berryman, K., 2005. Review of Tsunami Hazard and Risk in New Zealand. Inst. Geol. Nucl. Sci. 139.

Bhatt, N., Murari, M.K., Ukey, V., Prizomwala, S.P., Singhvi, A.K., 2016. Geological evidences of extreme waves along the Gujarat coast of western India. Nat. Hazards 84, 1685–1704. https://doi.org/10.1007/s11069-016-2507-6

Biagi, P., 2013. The shell middens of Las Bela coast and the Indus delta (Arabian Sea , Pakistan). https://doi.org/10.1111/aae.12013

Biagi, P., 2011. Changing the prehistory of Sindh and Las Bela coast: Twenty-five years of Italian contribution. World Archaeol. 43, 523–537. https://doi.org/10.1080/00438243.2011.624695

Biagi, P., Girod, A., Nisbet, R., 2013. Prehistoric shell middens, seascapes and landscapes at Lake Siranda (Las Bela, Balochistan) Preliminary results of the 2011 fieldwork season. J. Asian Civilizations 36, 1–25.

Biagi, P., Nisbet, R., Fantuzzi, T., 2018. Exploiting mangroves: Enviromental changes and human interference along the norhtern coast of the Arabian Sea (Pakistan) during the Holocene. Archaol. Mitteilungen aus Iran und Turan 1–34.

Bourget, J., Zaragosi, S., Ellouz-Zimmermann, S., Ducassou, E., Prins, M.A., Garlan, T., Lanfumey, V., Schneider, J.L., Rouillard, P., Giraudeau, J., 2010. Highstand vs. lowstand turbidite system growth in the Makran active margin: Imprints of high-frequency external controls on sediment

delivery mechanisms to deep water systems. Mar. Geol. 274, 187–208. https://doi.org/10.1016/j.margeo.2010.04.005

Brune, J.N., 1968. Seismic moment, seismicity, and rate of slip along Major fault zones. J. Geophys. Res. 73, 777–784.

Burbidge, D.R., Cummins, P.R., Mleczko, R., Latief, H., Mokhtari, M., Natawidjaja, D., Rajendran, C.P., Thomas, C., 2009. A probabilistic tsunami hazard assessment of the Indian Ocean Nations. Aust. Gov. Geosci. Aust. Prof. Opin.

Byrne, D.E., Sykes, L.R., Davis, D.M., 1992. Great thrust earthquakes and aseismic slip along the plate boundary of the Makran Subduction Zone. J. Geophys. Res. 97, 449–478.

Caron, V., 2011. Contrasted textural and taphonomic properties of high-energy wave deposits cemented in beachrocks (St. Bartholomew Island, French West Indies). Sediment. Geol. 237, 189–208. https://doi.org/10.1016/j.sedgeo.2011.03.002

Ceci, L., 1984. Shell midden deposits as coastal resources. World Archaeol. 16, 62–74. https://doi.org/10.1080/00438243.1984.9979916

Chacón-Barrantes, S., Narayanan, R., Mayerle, R., 2013. Several tsunami scenarios at the North Sea and their consequences at the German Bight.

Chen, Z., Lin, J., Qiu, Q., Zhou, Z., Zhang, F., 2024. Tsunami potential in the Makran subduction zone: Amplification effects from earthquake rupture directivity and speed. Terra Nov. 36, 201–209. https://doi.org/10.1111/ter.12698

Cheng, G., Bar, W.D., Small, D., 2024. Makran subduction zone and tsunami scenarios in the western Indian Ocean. Geophys. J. Int. 237, 288–301.

Choy, G.L., Kirby, S.H., 2004. Apparent stress, fault maturity and seismic hazard for normal-fault earthquakes at subduction zones. Geophys. J. Int. 159, 991–1012.

Clift, P.D., Giosan, L., 2014. Sediment fluxes and buffering in the post-glacial Indus Basin. Basin Res. 26, 369–386. https://doi.org/10.1111/bre.12038

Cornell, C.A., Vanmarcke, E.H., 1969. The major influences on seismic risk, in: Proceedings of the Fourth World Conference on Earthquake Engineering. pp. 69–83.

Coutts, P.J.F., 1966. Features of Prehistoric Campsites in Australia. Mankind 6, 338.

Cromie, C., Scarselli, N., Craig, J., Khan, M.R., Hussain, A., 2022. Tectonostratigraphic Evolution and Hydrocarbon Prospectivity South of Gwadar Bay, Makran Accretionary Wedge, Offshore Sw Pakistan. J. Pet. Geol. 45, 179–199. https://doi.org/10.1111/jpg.12812

Cummins, P.R., Kaneda, Y., 2000. Possible splay fault slip during the 1946 Nankai earthquake. Geophys. Res. Lett. 27, 2725–2728. https://doi.org/10.1029/1999GL011139

Davies, G., Griffin, J., Løvholt, F., Glimsdal, S., Harbitz, C., Thio, H.K., Lorito, S., Basili, R., Selva, J., Geist, E., Baptista, M.A., 2018. A global probabilistic tsunami hazard assessment from earthquake sources. Geol. Soc. Spec. Publ. 456, 219–244. https://doi.org/10.1144/SP456.5

De Martini, P.M., Bruins, H.J., Feist, L., Goodman-Tchernov, B.N., Hadler, H., Lario, J., Mastronuzzi, G., Obrocki, L., Pantosti, D., Paris, R., Reicherter, K., Smedile, A., Vött, A., 2021. The Mediterranean Sea and the Gulf of Cadiz as a natural laboratory for paleotsunami research: Recent advancements. Earth-Science Rev. 216, 103578. https://doi.org/10.1016/j.earscirev.2021.103578

Decker, V., Gee, C.T., Schucht, P.J., Lindauer, S., Hoffmann, G., 2022. Life on the Edge : A Powerful Tsunami Overwhelmed Indian Ocean Mangroves Life on the Edge : A Powerful Tsunami Overwhelmed Indian Ocean Mangroves One Millennium Ago. https://doi.org/10.3390/f13060922

Delavar, M.R., Mohammadi, H., Sharifi, M.A., Pirooz, M.D., 2017. Tsunami risk assessment

modelling in Chabahar port, Iran. Int. Arch. Photogramm. Remote Sens. Spat. Inf. Sci. - ISPRS Arch. 42, 461–467. https://doi.org/10.5194/isprs-archives-XLII-2-W7-461-2017

Deltares, 2023. Delft3d-Flow; simulation of multi-dimensional hydrodynamic flows and transport phenomena, including sediments. https://content.oss.deltares.nl/delft3d4/Delft3D-FLOW_User_Manual.pdf 1–725.

Deo, S.G., Ghate, S., Rajaguru, S.N., 2011. Holocene environmental changes and cultural patterns in coastal western India: A geoarchaeological perspective. Quat. Int. 229, 132–139. https://doi.org/10.1016/j.quaint.2010.05.001

Donato, S. V., Reinhardt, E.G., Boyce, J.I., Pilarczyk, J.E., Jupp, B.P., 2009. Particle-size distribution of inferred tsunami deposits in Sur Lagoon, Sultanate of Oman. Mar. Geol. 257, 54–64. https://doi.org/10.1016/j.margeo.2008.10.012

Donato, S. V., Reinhardt, E.G., Boyce, J.I., Rothaus, R., Vosmer, T., 2008. Identifying tsunami deposits using bivalve shell taphonomy. Geology 36, 199–202. https://doi.org/10.1130/G24554A.1

Dortch, C.E., 1991. Rottnest and Garden Island Prehistory and The Archaeological Potential of The Adjacent Continental Shelf, Western Australia. Aust. Archaeol. 33, 38–43. https://doi.org/10.1080/03122417.1991.11681430

Dutta, K., Bhushan, R., Somayajulu, B., 2001. ΔR Correction Values for the Northern Indian Ocean. Radiocarbon 43(2A). https://doi.org/10.1017/S0033822200038376

El-Hussain, I., Omira, R., Al-Bulushi, K., Deif, A., Al-Habsi, Z., Al-Rawas, G., Mohamad, A., Al-Jabri, K., Baptista, M.A., 2017. Tsunami hazard assessment along Diba-Oman and Diba-Al-Emirates coasts. MATEC Web Conf. 120, 1–11. https://doi.org/10.1051/matecconf/201712006007

El-Hussain, I., Omira, R., Al-Habsi, Z., Baptista, M.A., Deif, A., Mohamed, A.M.E., 2018. Probabilistic and deterministic estimates of near-field tsunami hazards in northeast Oman. Geosci. Lett. 5. https://doi.org/10.1186/s40562-018-0129-4

El-Hussain, I., Omira, R., Deif, A., Al-Habsi, Z., Al-Rawas, G., Mohamad, A., Al-Jabri, K., Baptista, M.A., 2016. Probabilistic tsunami hazard assessment along Oman coast from submarine earthquakes in the Makran subduction zone. Arab. J. Geosci. 9. https://doi.org/10.1007/s12517-016-2687-0

Ellouz-Zimmermann, N., Lallemant, S.J., Castilla, R., Mouchot, N., Leturmy, P., Battani, A., Buret, C., Cherel, L., Desaubliaux, G., Deville, E., Ferrand, J., Lügcke, A., Mahieux, G., Mascle, G., Mühr, P., Pierson-Wickmann, A.-C., Robion, P., Schmitz, J., Danish, M., Hasany, S., Shahzad, A., Tabreez, A., 2007. Offshore Frontal Part of the Makran Accretionary Prism: The Chamak Survey (Pakistan), Thrust Belts and Foreland Basins, Frontiers in Earth Sciences. https://doi.org/10.1007/978-3-540-69426-7_18

Fournier, M., Chamot-Rooke, N., Petit, C., Fabbri, O., Huchon, P., Maillot, B., Lepvrier, C., 2008. In situ evidence for dextral active motion at the Arabia-India plate boundary. Nat. Geosci. 1, 94–98. https://doi.org/10.1038/ngeo.2007.24

Fournier, M., Chamot-Rooke, N., Rodriguez, M., Huchon, P., Petit, C., Beslier, M.O., Zaragosi, S., 2011. Owen Fracture Zone: The Arabia-India plate boundary unveiled. Earth Planet. Sci. Lett. 302, 247–252. https://doi.org/10.1016/j.epsl.2010.12.027

Fournier, M., Patriat, P., Leroy, S., 2001. Reappraisal of the Arabia-India-Somalia triple junction kinematics. Earth Planet. Sci. Lett. 189, 103–114. https://doi.org/10.1016/S0012-821X(01)00371-5

Frank, N.L., Husain, S.A., 1971. The Deadliest Tropical Cyclone in History. Bull. Am. Meteorol. Soc. 52, 438–445. https://doi.org/10.1175/1520-0477(1971)052<0438:tdtcih>2.0.co;2

Frohling, E., Szeliga, W., 2016. GPS constraints on interplate locking within the Makran subduction

zone. Geophys. J. Int. 205, 67–76. https://doi.org/10.1093/gji/ggw001

Gandhi, D., Chavare, K.A., Prizomwala, S.P., Bhatt, N., Bhatt, N.Y., Mohan, K., Rastogi, B.K., 2017. Testing the numerical models for boulder transport through high energy marine wave event: An example from southern Saurashtra, western India. Quat. Int. 444, 209–216. https://doi.org/10.1016/j.quaint.2016.05.021

Gardezi, S.A.H., Luan, X., Sun, Z., Haider, R., Zhang, Y., Qiu, Q., Raveendrasinghe, T.D., 2024. Geo-hazards in the North Arabian Sea with special emphasis on Makran Subduction Zone. Earth-Science Rev. 255, 104846. https://doi.org/https://doi.org/10.1016/j.earscirev.2024.104846

Gates, G.O., Page, W.D., Savage, W.U., Zuberi, S., 1977. The Makran Earthquake November 28, (Mag. 8.3)1975 Field appraisal of geology and cultural effects, in: The Sixth World Conference on Earthquake Engineering New Delhi, India.

Gelfenbaum, G., Vatvani, D., Jaffe, B., Dekker, F., 2007. Tsunami inundation and sediment transport in vicinity of coastal mangrove forest. Coast. Sediments '07 - Proc. 6th Int. Symp. Coast. Eng. Sci. Coast. Sediment Process. 1–12. https://doi.org/10.1061/40926(239)86

Giles, D., Gopinathan, D., Guillas, S., Dias, F., 2021. Faster Than Real Time Tsunami Warning with Associated Hazard Uncertainties. Front. Earth Sci. 8, 1–16. https://doi.org/10.3389/feart.2020.597865

Gill, E.D., 1954. Aboriginal Kitchen Middens and Marine Shell Beds. Mankind 4, 249.

Goff, J.R., Lane, E., Arnold, J., 2009. The tsunami geomorphology of coastal dunes. Nat. Hazards Earth Syst. Sci. 9, 847–854. https://doi.org/10.5194/nhess-9-847-2009

Gopinathan, D., Heidarzadeh, M., Guillas, S., 2021. Probabilistic quantification of tsunami current hazard using statistical emulation. Proc. R. Soc. A Math. Phys. Eng. Sci. 477. https://doi.org/10.1098/rspa.2021.0180

Gordon, R.G., Demets, C., 1989. Present-day motion along the Owen fracture zone and Dalrymple trough in the Arabian Sea. J. Geophys. Res. 94, 5560–5570. https://doi.org/10.1029/JB094iB05p05560

Grando, G., McClay, K., 2007. Morphotectonics domains and structural styles in the Makran accretionary prism, offshore Iran. Sediment. Geol. 196, 157–179. https://doi.org/10.1016/j.sedgeo.2006.05.030

Habib, R.A., Iqbal, M.T., Salam, M., Tahir, M., Iqbal, J., Iqbal, T., 2025. Probing the Complex Interaction of Makran Subduction Zone with Regional Tectonic Features: Insights from Gravity and Seismic Source Parameters. Pure Appl. Geophys. 182, 55–77. https://doi.org/10.1007/s00024-024-03631-9

Haider, R., Ali, S., Hoffmann, G., Reicherter, K., 2024. Tsunami inundation and vulnerability analysis on the Makran coast, Pakistan. Nat. Hazards Earth Syst. Sci. 24, 3279–3290. https://doi.org/10.5194/nhess-24-3279-2024

Haider, R., Ali, S., Hoffmann, G., Reicherter, K., 2023. A multi-proxy approach to assess tsunami hazard with a preliminary risk assessment: A case study of the Makran Coast, Pakistan. Mar. Geol. 107032. https://doi.org/https://doi.org/10.1016/j.margeo.2023.107032

Hammack, J.L., 1973. A note on tsunamis: Their generation and propagation in an ocean of uniform depth. J. Fluid Mech. 60, 769–799. https://doi.org/10.1017/S0022112073000479

Hanks, T.C., Kanamori, H., 1979. A moment magnitude scale. J. Geophys. Res. B Solid Earth 84, 2348–2350. https://doi.org/10.1029/JB084iB05p02348

Harbitz, C.B., Løvholt, F., Bungum, H., 2014. Submarine landslide tsunamis: How extreme and how likely? Nat. Hazards 72, 1341–1374. https://doi.org/10.1007/s11069-013-0681-3

Heck, N.H., 1947. List of seismic sea waves. Bull. Seismol. Soc. Am. 37, 269–286.

Heffernan, A.S., Moore, J.C., Bangs, N.L., Moore, G.F., Shipley, T.H., 2004. Initial deformation in a subduction thrust system: polygonal normal faulting in the incoming sedimentary sequence of the Nankai subduction zone, southwestern Japan. Geol. Soc. London, Mem. 29, 143–148.

Heidarzadeh, M., Ishibe, T., Harada, T., Natawidjaja, D.H., Pranantyo, I.R., Widyantoro, B.T., 2021. High potential for splay faulting in the molucca sea, indonesia: november 2019 mw 7.2 earthquake and tsunami. Seismol. Res. Lett. 92, 2915–2926. https://doi.org/10.1785/0220200442

Heidarzadeh, M., Kijko, A., 2011. A probabilistic tsunami hazard assessment for the Makran subduction zone at the northwestern Indian Ocean. Nat. Hazards 56, 577–593. https://doi.org/10.1007/s11069-010-9574-x

Heidarzadeh, M., Krastel, S., Yalciner, A.C., 2014. The state-of-the-art numerical tools for modeling landslide tsunamis: a short review, in: Submarine Mass Movements and Their Consequences: 6th International Symposium. Springer, pp. 483–495.

Heidarzadeh, M., Pirooz, M.D., Zaker, N.H., 2009a. Modeling the near-field effects of the worst-case tsunami in the Makran subduction zone. Ocean Eng. 36, 368–376. https://doi.org/10.1016/j.oceaneng.2009.01.004

Heidarzadeh, M., Pirooz, M.D., Zaker, N.H., Mokhtari, M., 2007. Modeling of tsunami propagation in the vicinity of the southern coasts of Iran. Int. J. Civ. Eng. 5, 223–234. https://doi.org/10.1115/OMAE2007-29082

Heidarzadeh, M., Pirooz, M.D., Zaker, N.H., Yalciner, A.C., 2009b. Preliminary estimation of the tsunami hazards associated with the Makran subduction zone at the northwestern Indian Ocean. Nat. Hazards 48, 229–243. https://doi.org/10.1007/s11069-008-9259-x

Heidarzadeh, M., Pirooz, M.D., Zaker, N.H., Yalciner, A.C., Mokhtari, M., Esmaeily, A., 2008. Historical tsunami in the Makran Subduction Zone off the southern coasts of Iran and Pakistan and results of numerical modeling. Ocean Eng. 35, 774–786. https://doi.org/10.1016/j.oceaneng.2008.01.017

Heidarzadeh, M., Rabinovich, A., Kusumoto, S., Rajendran, C.P., 2020. Field surveys and numerical modelling of the 2004 December 26 Indian Ocean tsunami in the area of Mumbai, west coast of India. Geophys. J. Int. 222, 1952–1964. https://doi.org/10.1093/gji/ggaa277

Heidarzadeh, M., Satake, K., 2017. A combined earthquake-landslide source model for the tsunami from the 27 november 1945 Mw 8.1 makran earthquake. Bull. Seismol. Soc. Am. 107, 1033–1040. https://doi.org/10.1785/0120160196

Heidarzadeh, M., Satake, K., 2014a. Possible sources of the tsunami observed in the northwestern Indian ocean following the 2013 September 24 Mw 7.7 Pakistan inland earthquake. Geophys. J. Int. 199, 752–766. https://doi.org/10.1093/gji/ggu297

Heidarzadeh, M., Satake, K., 2014b. New Insights into the Source of the Makran Tsunami of 27 November 1945 from Tsunami Waveforms and Coastal Deformation Data. Pure Appl. Geophys. 172, 621–640. https://doi.org/10.1007/s00024-014-0948-y

Hicks, S.P., Rietbrock, A., 2015. Seismic slip on an upper-plate normal fault during a large subduction megathrust rupture. Nat. Geosci. 8, 955–960.

Hoechner, A., Babeyko, A.Y., Zamora, N., 2016. Probabilistic tsunami hazard assessment for the Makran region with focus on maximum magnitude assumption. Nat. Hazards Earth Syst. Sci. 16, 1339–1350. https://doi.org/10.5194/nhess-16-1339-2016

Hoffmann, G., Al-Yahyai, S., Naeem, G., Kociok, M., Grützner, C., 2014. An Indian Ocean tsunami triggered remotely by an onshore earthquake in Balochistan, Pakistan. Geology 42, 883–886. https://doi.org/10.1130/G35756.1

Hoffmann, G., Grützner, C., Reicherter, K., Preusser, F., 2015. Geo-archaeological evidence for a Holocene extreme flooding event within the Arabian Sea (Ras al Hadd, Oman). Quat. Sci. Rev.

113, 123–133. https://doi.org/10.1016/j.quascirev.2014.09.033

Hoffmann, G., Grützner, C., Schneider, B., Preusser, F., Reicherter, K., 2020. Large Holocene tsunamis in the northern Arabian Sea. Mar. Geol. 419. https://doi.org/10.1016/j.margeo.2019.106068

Hoffmann, G., Reicherter, K., 2014. Reconstructing Anthropocene extreme flood events by using litter deposits. Glob. Planet. Change 122, 23–28. https://doi.org/10.1016/j.gloplacha.2014.07.012

Hoffmann, G., Reicherter, K., Wiatr, T., Grützner, C., 2011. Evidence For Holocene Tsunami-Impact Along the Shoreline of Oman. 2nd INQUA-IGCP-567 Int. Work. Act. Tectonics, Earthq. Geol. Archaeol. Eng. 88–91.

Hoffmann, G., Reicherter, K., Wiatr, T., Grützner, C., Rausch, T., 2013a. Block and boulder accumulations along the coastline between Fins and Sur (Sultanate of Oman): Tsunamigenic remains? Nat. Hazards 65, 851–873. https://doi.org/10.1007/s11069-012-0399-7

Hoffmann, G., Rupprechter, M., Balushi, N. Al, Grützner, C., Reicherter, K., 2013b. The impact of the 1945 Makran tsunami along the coastlines of the Arabian Sea (Northern Indian Ocean) – a review. Zeitschrift für Geomorphol. Suppl. Issues 57, 257–277. https://doi.org/10.1127/0372-8854/2013/s-00134

Honarmand, M., Shanehsazzadeh, A., Zandi, S.M., 2020. 3D numerical simulation of tsunami generation and propagation, case study: Makran tsunami generation and penetrating in Chabahar Bay. Ocean Eng. 218, 108109. https://doi.org/10.1016/j.oceaneng.2020.108109

Hosseini Mehr, A., Maleki Asayesh, B., Mokhtari, M., 2018. Splay Faults in the Makran Subduction Zone and Changes of their Transferred Coulomb Stress. J. Earth Sp. Phys. 43, 1–10. https://doi.org/10.22059/jesphys.2017.61703

https://c14.arch.ox.ac.uk/calibration.html [WWW Document], n.d. URL https://c14.arch.ox.ac.uk/calibration.html

Hughes, P.J., Sullivan, M.E., 1974. The re-deposition of midden material by storm waves, in: Journal and Proceedings of the Royal Society of New South Wales. Australasian Medical Publishing Co., pp. 6–10.

Jackson, J., McKenzie, D., 1984. Active tectonics of the Alpine–Himalayan Belt between western Turkey and Pakistan. Geophys. J. R. Astron. Soc. 77, 185–264. https://doi.org/10.1111/j.1365-246X.1984.tb01931.x

Jacob, K.H., Quittmayer, R.C., 1979. The Makran Region of Pakistan and Iran: Trench–arc system with active plate subduction, in: Geodynamics of Pakistan. Geological Survey of Pakistan, Quetta, pp. 305–317.

Jade, S., Shrungeshwara, T.S., Kumar, K., Choudhury, P., Dumka, R.K., Bhu, H., 2017. India plate angular velocity and contemporary deformation rates from continuous GPS measurements from 1996 to 2015. Sci. Rep. 7, 1–16. https://doi.org/10.1038/s41598-017-11697-w

Jaiswal, R.K., Singh, A.P., Rastogi, B.K., 2009. Simulation of the Arabian Sea Tsunami propagation generated due to 1945 Makran Earthquake and its effect on western parts of Gujarat (India). Nat. Hazards 48, 245–258. https://doi.org/10.1007/s11069-008-9261-3

Juniansah, A., Tyas, B.I., Tama, G.C., Febriani, K.R., Farda, N.M., 2018. Spatial modelling for tsunami evacuation route in Parangtritis Village. IOP Conf. Ser. Earth Environ. Sci. 148. https://doi.org/10.1088/1755-1315/148/1/012003

Kakar, D.M., Naeem, G., Usman, A., Hasan, H., Lohdi, H.A., Srinivasalu, S., Andrade, V., Rajendran, C.P., Beni, A.N., Hamzeh, M.A., Hoffmann, G., 2014. Elders recall an earlier tsunami on Indian Ocean shores, Eos, Transactions American Geophysical Union. UNESCO.

Kalsi, S.R., Gupta, M., 2003. Success and failure of early warning systems: A case study of the

Gujarat Cyclone of June, 1998, in: Zschau, J., Küppers, A. (Eds.), Early Warning Systems for Natural Disaster Reduction. Springer Berlin Heidelberg, Berlin, Heidelberg, pp. 199–202. https://doi.org/10.1007/978-3-642-55903-7_26

Kame, N., Yamashita, T., 1999. Simulation of the spontaneous growth of a dynamic crack without constraints on the crack tip path. Geophys. J. Int. 139, 345–358.

Kerr, R., 1824. A general history and collection of voyages and travels, arranged in systematic order: forming a complete history of the origin and progress of navigation, discovery, and commerce, by sea and land, from the earliest ages to the present time. W. Blackwood.

Khaledzadeh, M., Ghods, A., 2022. Estimation of size of megathrust zone in the Makran subduction system by thermal modelling. Geophys. J. Int. 228, 1530–1540. https://doi.org/10.1093/gji/ggab417

Khan, M.A., Bendick, R., Bhat, M.I., Bilham, R., Kakar, D.M., Khan, S.F., Lodi, S.H., Qazi, M.S., Singh, B., Szeliga, W., Wahab, A., 2008. Preliminary geodetic constraints on plate boundary deformation on the western edge of the Indian plate from TriGGnet (Tri-University GPS Geodesy Network). J. Himal. Earth Sci. 41, 71–87.

Khan, M.J., Ali, M., Xu, M., Khan, M., 2020. Seismicity analysis of selected faults in Makran Southern Pakistan. Acta Geophys. 68, 965–978. https://doi.org/10.1007/s11600-020-00447-8

Khan, S.A., Shah, M.A., Qaisar, M., 2003a. Seismic risk analysis of coastal area of Pakistan. Acta Seismol. Sin. English Ed. 16, 382–394. https://doi.org/10.1007/s11589-003-0071-0

Khan, S.A., Shah, M.A., Qaisar, M., 2003b. Seismic risk analysis of coastal area of Pakistan. Acta Seismol. Sin. English Ed. 16, 382. https://doi.org/10.1007/s11589-003-0071-0

Khan, U., Khan, M., Wu, S., Jinwei, G., 2024. Middle Miocene renewed subduction of arabian-eurasian plates: Implications for convergent tectonic mechanisms, tectonically-induced fluid overpressures, and sediment recycling dynamics. Mar. Pet. Geol. 162, 106704. https://doi.org/https://doi.org/10.1016/j.marpetgeo.2024.106704

Klingelhoefer, F., Gutscher, M.A., Ladage, S., Dessa, J.X., Graindorge, D., Franke, D., André, C., Permana, H., Yudistira, T., Chauhan, A., 2010. Limits of the seismogenic zone in the epicentral region of the 26 December 2004 great Sumatra-Andaman earthquake: Results from seismic refraction and wide-angle reflection surveys and thermal modeling. J. Geophys. Res. Solid Earth 115, 1–23. https://doi.org/10.1029/2009JB006569

Knapp, K.R., Kruk, M.C., Levinson, D.H., Diamond, H.J., Neumann, C.J., 2010. The international best track archive for climate stewardship (IBTrACS). Bull. Am. Meteorol. Soc. 91, 363–376. https://doi.org/10.1175/2009BAMS2755.1

Kopp, C., Fruehn, J., Flueh, E.R., Reichert, C., Kukowski, N., Bialas, J., Klaeschen, D., 2000. Structure of the makran subduction zone from wide-angle and reflection seismic data. Tectonophysics 329, 171–191. https://doi.org/10.1016/S0040-1951(00)00195-5

Koshimura, S., Oie, T., Yanagisawa, H., Imamura, F., 2009. Developing fragility functions for tsunami damage estimation using numerical model and post-tsunami data from banda aceh, Indonesia. Coast. Eng. J. 51, 243–273. https://doi.org/10.1142/S0578563409002004

Koster, B., Hoffmann, G., Grützner, C., Reicherter, K., 2014. Ground penetrating radar facies of inferred tsunami deposits on the shores of the Arabian Sea (Northern Indian Ocean). Mar. Geol. 351, 13–24. https://doi.org/10.1016/j.margeo.2014.03.002

Kukowski, N., Schillhorn, T., Flueh, E.R., Huhn, K., 2000. Newly identified strike-slip plate boundary in the northeastern Arabian Sea. Geology 28, 355–358. https://doi.org/10.1130/0091-7613(2000)28<355:NISPBI>2.0.CO;2

Kukowski, N., Schillhorn, T., Huhn, K., Von Rad, U., Husen, S., Flueh, E.R., 2001. Morphotectonics and mechanics of the central Makran accretionary wedge off Pakistan. Mar. Geol. 173, 1–19. https://doi.org/10.1016/S0025-3227(00)00167-5

Kupriyanov, A. V, Makarevich, G.G., 2024. Chabahar Port: Between Geopolitics and Business, in: India's Economic Corridor Initiatives. Routledge, pp. 53–65.

Laane, J.L., Chen, W.-P., 1989. The Makran earthquake of 1983 April 18: A possible analogue to the Puget Sound earthquake of 1965. Geophys. J. Int. 98, 1–9.

Latcharote, P., Al-Salem, K., Suppasri, A., Pokavanich, T., Toda, S., Jayaramu, Y., Al-Enezi, A., Al-Ragum, A., Imamura, F., Anawat, K.A., 2018. Tsunami hazard evaluation for Kuwait and Arabian Gulf due to Makran Subduction Zone and Subaerial landslides. Nat. Hazards 93, 127–152. https://doi.org/10.1007/s11069-017-3097-7

Logan, W., 1887. Malabar Manual (2 volumes). Asia Educ. Serv. (1995 Repr. New Delhi.

Loveless, J.P., Allmendinger, R.W., Pritchard, M.E., González, G., 2010. Normal and reverse faulting driven by the subduction zone earthquake cycle in the northern Chilean fore arc. Tectonics 29.

Løvholt, F., 2017. Tsunami Hazard and Risk Assessment. United Nations Off. Disaster Risk Reduct. 1–9.

Løvholt, F., Glimsdal, S., Harbitz, C.B., Zamora, N., Nadim, F., Peduzzi, P., Dao, H., Smebye, H., 2012. Tsunami hazard and exposure on the global scale. Earth-Science Rev. 110, 58–73. https://doi.org/10.1016/j.earscirev.2011.10.002

Macintosh, A., 2013. Coastal climate hazards and urban planning : how planning responses can lead to maladaptation 1035–1055. https://doi.org/10.1007/s11027-012-9406-2

Mahmood, N., Khan, K., Rafi, Z., Lovholt, D.F., 2012. Mapping of Tsunami Hazard along Makran Coast of Pakistan 1–39.

Malgrange, M., Madariaga, R., 1983. Complex distribution of large thrust and normal fault earthquakes in the Chilean subduction zone. Geophys. J. Int. 73, 489–505.

Manaman, N.S., Shomali, H., Koyi, H., 2011. New constraints on upper-mantle S-velocity structure and crustal thickness of the Iranian plateau using partitioned waveform inversion. Geophys. J. Int. 184, 247–267. https://doi.org/10.1111/j.1365-246X.2010.04822.x

Marathe, A., Chandrashekhar, B.S., 2011. Application of Remote Sensing in Studying Holocene Sediments and Tectonic Episodes at Kelshi, Ratnagiri District, Maharashtra, India. J. Indian Soc. Remote Sens. 39, 241–247. https://doi.org/10.1007/s12524-011-0087-1

Masuda, M., Williams, C., Shahkarami, A., Rafique, F., Bryngelson, J., 2012. Tsunami Vulnerability Function Development Based on the 2011 Tohoku Earthquake in Japan. 15 World Conf. Earthq. Eng.

Matin, S., Praveen, S.S., 2021. Numerical simulation and comparison of tsunami inundation for different satellite-derived datasets for the Gujarat coast of India. Adv. Remote Sens. Nat. Resour. Monit. 431–443. https://doi.org/10.1002/9781119616016.ch21

McCann, W.R., Dewey, J.W., Murphy, A.J., Harding, S.T., 1982. A large normal-fault earthquake in the overriding wedge of the Lesser Antilles subduction zone: The earthquake of 8 October 1974. Bull. Seismol. Soc. Am. 72, 2267–2283.

Mehrdar, A., Motaghi, K., Ghods, A., Sobouti, F., Priestley, K., Pachhai, S., Shabanian, E., Zarunizadeh, Z., Zeynaddini-Meymand, R., El-Hussain, I., 2025. Crustal and uppermost mantle structure of the Iranian Makran subduction zone from ambient noise and earthquake surface wave tomography. Geophys. J. Int. 241, 70–85. https://doi.org/10.1093/gji/ggae419

Mikumo, T., Singh, S.K., Santoyo, M.A., 1999. A possible stress interaction between large thrust and normal faulting earthquakes in the Mexican subduction zone. Bull. Seismol. Soc. Am. 89, 1418–1427.

Milliman, J.D., Syvitski, J.P.M., 1992. Geomorphic/tectonic control of sediment discharge to the ocean: the importance of small mountainous rivers. J. Geol. 100, 525–544.

https://doi.org/10.1086/629606

Miranda, J.M., Baptista, M.A., Omira, R., 2014. On the use of Green's summation for tsunami waveform estimation: A case study. Geophys. J. Int. 199, 459–464. https://doi.org/10.1093/gji/ggu266

Mokhtari, M., 2015. The role of splay faulting in increasing the devastation effect of tsunami hazard in Makran, Oman Sea. Arab. J. Geosci. 8, 4291–4298. https://doi.org/10.1007/s12517-014-1375-1

Mokhtari, M., Ala Amjadi, A., Mahshadnia, L., Rafizadeh, M., 2019. A review of the seismotectonics of the Makran Subduction Zone as a baseline for Tsunami Hazard Assessments. Geosci. Lett. 6, 13.

Momeni, P., and Goda, K., 2024. Probabilistic tsunami hazard assessment for the makran subduction zone using logic tree and stochastic rupture sources. Coast. Eng. J. 66, 332–360. https://doi.org/10.1080/21664250.2024.2324520

Momeni, P., Goda, K., Heidarzadeh, M., Qin, J., 2020. Stochastic analysis of tsunami hazard of the 1945 Makran subduction zone MW 8.1–8.3 earthquakes. Geosci. 10, 1–20. https://doi.org/10.3390/geosciences10110452

Momeni, P., Goda, K., Mokhtari, M., Heidarzadeh, M., 2022. A new tsunami hazard assessment for eastern Makran subduction zone by considering splay faults and applying stochastic modeling. Coast. Eng. J. https://doi.org/10.1080/21664250.2022.2117585

Moradi, M., 2021. Integration of Geographical Information System and Tsunami generation/propagation models in the Makran region (North of the Arabian Sea). Int. J. Coast. Offshore Eng. 5, 40–48. https://doi.org/10.52547/ijcoe.5.3.40

Mouchot, N., Loncke, L., Mahieux, G., Bourget, J., Lallemant, S., Ellouz-Zimmermann, N., Leturmy, P., 2010. Recent sedimentary processes along the Makran trench (Makran active margin, off Pakistan). Mar. Geol. 271, 17–31. https://doi.org/10.1016/j.margeo.2010.01.006

Mourato, S., Fernandez, P., Pereira, L., Moreira, M., 2017. Improving a DSM Obtained by Unmanned Aerial Vehicles for Flood Modelling. IOP Conf. Ser. Earth Environ. Sci. 95. https://doi.org/10.1088/1755-1315/95/2/022014

Mousavi, N., Ardestani, V.E., Moosavi, N., 2022. Slab extension and normal faulting in a low-angle subduction-related environment: An example of the Makran subduction zone (Iran-Pakistan). J. Asian Earth Sci. 233, 105244. https://doi.org/https://doi.org/10.1016/j.jseaes.2022.105244

Neetu, S., Suresh, I., Shankar, R., Nagarajan, B., Sharma, R., Shenoi, S.S.C., Unnikrishnan, A.S., Sundar, D., 2011. Trapped waves of the 27 November 1945 Makran tsunami: Observations and numerical modeling. Nat. Hazards 59, 1609–1618. https://doi.org/10.1007/s11069-011-9854-0

Nemati, M., 2019. Seismotectonic and seismicity of Makran, a bimodal subduction zone, SE Iran. J. Asian Earth Sci. 169, 139–161. https://doi.org/10.1016/j.jseaes.2018.08.009

Nouri, M., Namin, M.M., Rashidi, A., 2020. A first-order Landslide Tsunami Hazard Assessment in the Western Makran, in: 18th Iranian Hydraulic Conference. University of Tehran, Tehran, Iran.

Nouri, M., Rashidi, A., Montazeri Namin, M., Shugar, D.H., 2023. Submarine landslide tsunami hazard assessment for the western Makran based on a deterministic approach. Nat. Hazards 118, 1117–1136. https://doi.org/10.1007/s11069-023-06040-8

Okada, Y., 1985. Surface deformation due to shear and tensile faults in a half space. Bull. - Seismol. Soc. Am. 75, 1135–1154. https://doi.org/10.1785/bssa0820021018

Okal, E.A., Synolakis, C.E., 2008. Far-field tsunami hazard from mega-thrust earthquakes in the Indian Ocean. Geophys. J. Int. 172, 995–1015. https://doi.org/10.1111/j.1365-246X.2007.03674.x

Oskamp, J.A., Dababneh, A.J.A., Barton, D.J., 2015. Tsunami Hazard in the Arabian Gulf Due to Earthquakes in the Makran Subduction Zone.

Page, W.D., Alt, J.N., Cluff, L.S., Plafker, G., 1979. Evidence for the recurrence of large-magnitude earthquakes along the makran coast of Iran and Pakistan. Tectonophysics 52, 533–547. https://doi.org/10.1016/B978-0-444-41783-1.50081-7

Pagnoni, G.I., Armigliato, A., Tinti, S., 2021. Estimation of human damage and economic loss of buildings related to tsunami inundation in the city of augusta, italy. Geol. Soc. Spec. Publ. 501, 327–342. https://doi.org/10.1144/SP501-2019-134

Pajang, S., Cubas, N., Letouzey, J., Le Pourhiet, L., Seyedali, S., Fournier, M., Agard, P., Khatib, M.M., Heyhat, M., Mokhtari, M., 2021. Seismic hazard of the western Makran subduction zone: Insight from mechanical modelling and inferred frictional properties. Earth Planet. Sci. Lett. 562, 116789. https://doi.org/10.1016/j.epsl.2021.116789

Pajang, S., Khatib, M.M., Heyhat, M., Cubas, N., Bessiere, E., Letouzey, J., Mokhtari, M., Le Pourhiet, L., 2022. The distinct morphologic signature of underplating and seamounts in accretionary prisms, insights from thermomechanical modeling applied to Coastal Iranian Makran. Tectonophysics 845, 229617. https://doi.org/10.1016/j.tecto.2022.229617

Park, J.-O., Tsuru, T., Kodaira, S., Cummins, P.R., Kaneda, Y., 2002. Splay fault branching along the Nankai subduction zone. Science (80-.). 297, 1157–1160.

Park, S., van de Lindt, J.W., Cox, D., Gupta, R., 2013. Concept of Community Fragilities for Tsunami Coastal Inundation Studies. Nat. Hazards Rev. 14, 220–228. https://doi.org/10.1061/(asce)nh.1527-6996.0000092

Parvaiz, S., Ali, A., Javed, F., Shah, M.A., 2022. Deformational pattern and seismogenic potential of the eastern Makran subduction zone. J. Asian Earth Sci. 235, 105298. https://doi.org/10.1016/j.jseaes.2022.105298

Patel, V.M., Dholakia, M.B., Singh, A.P., 2016. Emergency preparedness in the case of Makran tsunami: a case study on tsunami risk visualization for the western parts of Gujarat, India. Geomatics, Nat. Hazards Risk 7, 826–842. https://doi.org/10.1080/19475705.2014.983188

Patel, V.M., Patel, H.S., Singh, A.P., 2011. Comparative study of earthquake and tsunami loading on Vertical Evacuation Structure at Dwarka. Int. J. Earth Sci. Eng. 4, 659–663.

Payande, A.R., Niksokhan, M.H., Naserian, H., 2014. Tsunami hazard assessment of Chabahar bay related to megathrust seismogenic potential of the Makran subduction zone. Nat. Hazards 76, 161–176. https://doi.org/10.1007/s11069-014-1476-x

Pendse, C.G., 1946. The Mekran Earthquake of the 28th November 1945. Sci. Notes X, 141–146.

Penney, C., Tavakoli, F., Saadat, A., Nankali, H.R., Sedighi, M., Khorrami, F., Sobouti, F., Rafi, Z., Copley, A., Jackson, J., Priestley, K., 2017. Megathrust and accretionary wedge properties and behaviour in the Makran subduction zone. Geophys. J. Int. 209, 1800–1830. https://doi.org/10.1093/gji/ggx126

Pilarczyk, J.E., Reinhardt, E.G., 2012. Testing foraminiferal taphonomy as a tsunami indicator in a shallow arid system lagoon: Sur, Sultanate of Oman. Mar. Geol. 295–298, 128–136. https://doi.org/10.1016/j.margeo.2011.12.002

Pilarczyk, J.E., Reinhardt, E.G., Boyce, J.I., Schwarcz, H.P., Donato, S. V., 2011. Assessing surficial foraminiferal distributions as an overwash indicator in Sur Lagoon, Sultanate of Oman. Mar. Micropaleontol. 80, 62–73. https://doi.org/10.1016/j.marmicro.2011.06.001

Plafker, G., 1972. Alaskan earthquake of 1964 and Chilean earthquake of 1960: Implications for arc tectonics. J. Geophys. Res. 77, 901–925.

Platt, J.P., Leggett, J.K., Alam, S., 1988. Slip vectors and fault mechanics in the Makran accretionary wedge, southwest Pakistan. J. Geophys. Res. 93, 7955–7973.

https://doi.org/10.1029/jb093ib07p07955

Platt, J.P., Leggett, J.K., Young, J., Raza, H., Alam, S., 1985. Large-scale sediment underplating in the Makran accretionary prism, southwest Pakistan. Geology 13, 507–511. https://doi.org/10.1130/0091-7613(1985)13<507:LSUITM>2.0.CO;2

Prasojo, K., Afwani, M.Z., Lestari, I., Bramono, A.M.C.W., Bustomi, A.F., 2017. Berryman Tsunami Inundation Modelling on Temon: The Location of NYIA. Int. Conf. Environ. Resour. Manag. Glob. Reg. 1–8.

Prins, M.A., Postma, G., Cleveringa, J., Cramp, A., Kenyon, N.H., 2000. Controls on terrigenous sediment supply to the Arabian Sea during the late quaternary: The Indus fan. Mar. Geol. 169, 327–349. https://doi.org/10.1016/S0025-3227(00)00086-4

Prizomwala, S.P., Gandhi, D., Bhatt, N.N., Winkler, W., Kumar, M.R., Makwana, N., Bhatt, N.N., 2018. Geological evidence for AD 1008 tsunami along the Kachchh coast, Western India: Implications for hazard along the Makran Subduction Zone. Sci. Rep. 8, 1–8. https://doi.org/10.1038/s41598-018-35193-x

Prizomwala, S.P., Gandhi, D., Ukey, V.M., Bhatt, N., Rastogi, B.K., 2015. Coastal boulders as evidences of high-energy marine events from Diu Island, west coast of India: storm or palaeotsunami? Nat. Hazards 75, 1187–1203. https://doi.org/10.1007/s11069-014-1371-5

Prizomwala, S.P., Tandon, A., Joshi, N., Makwana, N., 2021. Reconstructing the catalogue for extreme wave events from the Gujarat coastline (Western India) and their implications to coastal settlers during the last 6000 years. Quat. Int. 599–600, 24–31. https://doi.org/10.1016/j.quaint.2021.03.004

Prizomwala, S.P., Vedpathak, C., Tandon, A., Das, A., Makwana, N., Joshi, N., 2022. Geological footprints of the 1945 Makran tsunami from the west coast of India. Mar. Geol. 446, 106773. https://doi.org/10.1016/j.margeo.2022.106773

Qiu, Q., Zhou, Z., Lin, J., Zhang, F., Chen, Z., Yang, X., 2022. Great earthquake and tsunami potential in the eastern Makran subduction zone: New insights from geodetic and structural constraints. Tectonophysics 837. https://doi.org/10.1016/j.tecto.2022.229462

Quittmeyer, R.C., Farah, A., Jacob H., K., 1979. The seismicity of Pakistan and its relation to surface faults, in: Farah, A., Dejong, K.A. (Eds.), Geodynamics of Pakistan. Geological Survey of Pakistan, Quetta, pp. 271–284.

Quittmeyer, R.C., Kafka, A.L., 1984. Constraints on plate motions in southern Pakistan and the northern Arabian Sea from the focal mechanisms of small earthquakes. J. Geophys. Res. 89, 2444–2458.

Rafi, Z., Mahmood, N., 2010. Numerical Modeling of Tsunami Inundation for Potential Earthquake at Makran Subduction Zone. Tech. Rep. No. PMD-45/2010.

Rahimi, M., Zafarani, H., Eskandari-Ghadi, M., Etemadsaeed, L., 2025. Dual risk-targeted seismic and tsunami hazard assessment for western Makran coasts, southeast Iran. Nat. Hazards. https://doi.org/10.1007/s11069-025-07184-5

Rajendran, C.P., Heidarzadeh, M., Sanwal, J., Karthikeyan, A., Rajendran, K., 2020. The Orphan Tsunami of 1524 on the Konkan Coast, Western India, and Its Implications. Pure Appl. Geophys. https://doi.org/10.1007/s00024-020-02575-0

Rajendran, C.P., Ramanamurthy, M. V., Reddy, N.T., Rajendran, K., 2008. Hazard implications of the late arrival of the 1945 Makran tsunami. Curr. Sci. 95, 1739–1743.

Rashid, A., Shirazi, S.A., 2023. Gwadar Port-Pakistan as an Axis for Regional Connectivity under CPEC: A Geographer's Perspective. J. Polit. Int. Stud. 9, 105–120.

Rashidi, A., Dutykh, D., Shomali, Z.H., 2020a. Horizontal displacement effect in tsunami wave generation in the western Makran region. J. Ocean Eng. Mar. Energy.

https://doi.org/10.1007/s40722-020-00182-8

Rashidi, A., Shomali, Z.H., Dutykh, D., Keshavarz Faraj Khah, N., 2018a. Evaluation of tsunami wave energy generated by earthquakes in the Makran subduction zone. Ocean Eng. 165, 131–139. https://doi.org/10.1016/j.oceaneng.2018.07.027

Rashidi, A., Shomali, Z.H., Dutykh, D., Keshavarz Farajkhah, N., 2020b. Tsunami hazard assessment in the Makran subduction zone. Nat. Hazards 100, 861–875. https://doi.org/10.1007/s11069-019-03848-1

Rashidi, A., Shomali, Z.H., Keshavarz Farajkhah, N., 2018b. Tsunami Simulations in the Western Makran Using Hypothetical Heterogeneous Source Models from World's Great Earthquakes. Pure Appl. Geophys. 175, 1325–1340. https://doi.org/10.1007/s00024-018-1842-9

Rastgoftar, E., Soltanpour, M., 2016. Study and numerical modeling of 1945 Makran tsunami due to a probable submarine landslide. Nat. Hazards 83, 929–945. https://doi.org/10.1007/s11069-016-2356-3

Regard, V., Hatzfeld, D., Molinaro, M., Aubourg, C., Bayer, R., Bellier, O., Yamini-Fard, F., Peyret, M., Abbassi, M., 2010. The transition between Makran subduction and the Zagros collision: recent advances in its structure and active deformation. Geol. Soc. London, Spec. Publ. 330, 43–64. https://doi.org/10.1144/SP330.4

Rehman, A., Zhang, H., 2024a. Seismicity and return period investigation of destructive earthquake in Makran subduction zone. Discov. Geosci. 2. https://doi.org/10.1007/s44288-024-00047-9

Rehman, A., Zhang, H., 2024b. Probabilistic forecast of next earthquake event in Makran subduction zone using Weibull distribution. Contrib. to Geophys. Geod. 54, 85–93. https://doi.org/10.31577/congeo.2024.54.1.5

Rehman, K., Cho, Y.S., 2016. Building damage assessment using scenario based tsunami numerical analysis and fragility curves. Water (Switzerland) 8. https://doi.org/10.3390/w8030109

Rehman, K., Jadoon, T., Hussain, M., Ahmad, Z., Ali, Aamir, Ali, Asghar, Ahmed, S., 2015. Tsunamigenic analysis in and around makran. J. Earthq. Eng. 19, 332–355. https://doi.org/10.1080/13632469.2014.982835

Reilinger, R., McClusky, S., Vernant, P., Lawrence, S., Ergintav, S., Cakmak, R., Ozener, H., Kadirov, F., Guliev, I., Stepanyan, R., Nadariya, M., Hahubia, G., Mahmoud, S., Sakr, K., ArRajehi, A., Paradissis, D., Al-Aydrus, A., Prilepin, M., Guseva, T., Evren, E., Dmitrotsa, A., Filikov, S. V., Gomez, F., Al-Ghazzi, R., Karam, G., 2006. GPS constraints on continental deformation in the Africa-Arabia-Eurasia continental collision zone and implications for the dynamics of plate interactions. J. Geophys. Res. Solid Earth 111, 1–26. https://doi.org/10.1029/2005JB004051

Röbke, B.R., Schüttrumpf, H., Vött, A., 2018. Hydro- and morphodynamic tsunami simulations for the ambrakian gulf (Greece) and comparison with geoscientific field traces. Geophys. J. Int. 213, 317–339. https://doi.org/10.1093/gji/ggx553

Röbke, B.R., Schüttrumpf, H., Vött, A., 2016. Effects of different boundary conditions and palaeotopographies on the onshore response of tsunamis in a numerical model - A case study from western Greece. Cont. Shelf Res. 124, 182–199. https://doi.org/10.1016/j.csr.2016.04.010

Röbke, B.R., Vött, A., Willershäuser, T., Fischer, P., Hadler, H., 2015. Considering coastal palaeogeographical changes in a numerical tsunami model - A progressive base to compare simulation results with field traces from three coastal settings in western Greece. Zeitschrift fur Geomorphol. 59, 157–188. https://doi.org/10.1127/zfg-suppl/2014/S-00210

Rodriguez, M., Chamot-Rooke, N., Hébert, H., Fournier, M., Huchon, P., 2013. Owen Ridge deep-water submarine landslides: Implications for tsunami hazard along the Oman coast. Nat. Hazards Earth Syst. Sci. 13, 417–424. https://doi.org/10.5194/nhess-13-417-2013

Rodriguez, M., Fournier, M., Chamot-Rooke, N., Huchon, P., Bourget, J., Sorbier, M., Zaragosi, S.,

Rabaute, A., 2011. Neotectonics of the Owen Fracture Zone (NW Indian Ocean): Structural evolution of an oceanic strike-slip plate boundary. Geochemistry, Geophys. Geosystems 12. https://doi.org/10.1029/2011GC003731

Rodriguez, M., Fournier, M., Chamot-Rooke, N., Huchon, P., Zaragosi, S., Rabaute, A., 2012. Mass wasting processes along the Owen Ridge (Northwest Indian Ocean). Mar. Geol. 326–328, 80–100. https://doi.org/10.1016/j.margeo.2012.08.008

Roshan, A.D., Basu, P.C., Jangid, R.S., 2016. Tsunami hazard assessment of Indian coast, Natural Hazards. https://doi.org/10.1007/s11069-016-2216-1

Saha, S., Srivastava, K., 2019. Tsunami simulation along the south west coast of India: Lakshadweep Islands acting as wave-barricade. Indian J. Geo-Marine Sci. 48, 1640–1647.

Salah, P., Sasaki, J., Soltanpour, M., 2021. Comprehensive Probabilistic Tsunami Hazard Assessment in the Makran Subduction Zone. Pure Appl. Geophys. 178, 5085–5107. https://doi.org/10.1007/s00024-021-02725-y

Salaree, A., Okal, E.A., 2015. Field survey and modelling of the Caspian Sea tsunami of 1990 June 20. Geophys. J. Int. 201, 621–639. https://doi.org/10.1093/gji/ggv044

Salmanidou, D.M., Heidarzadeh, M., Guillas, S., 2019. Probabilistic Landslide-Generated Tsunamis in the Indus Canyon, NW Indian Ocean, Using Statistical Emulation. Pure Appl. Geophys. 176, 3099–3114. https://doi.org/10.1007/s00024-019-02187-3

Sangode, S.J., Meshram, D.C., 2013. A comparative study on the style of paleotsunami deposits at two sites on the west coast of India. Nat. Hazards 66, 463–483. https://doi.org/10.1007/s11069-012-0542-5

Sanlaville, P., Besenval, R., Evin, J., Prieur, A., 1991. Evolution de la région littorale du Makran pakistanais à l'Holocène. Paléorient 17, 3–18. https://doi.org/10.3406/paleo.1991.4536

Sarker, M.A., 2019. Numerical modelling of tsunami in the Makran Subduction Zone–A case study on the 1945 event. J. Oper. Oceanogr. 12, S212–S229. https://doi.org/10.1080/1755876X.2018.1527883

Schneider, B., Hoffmann, G., Reicherter, K., 2016. Scenario-based tsunami risk assessment using a static flooding approach and high-resolution digital elevation data: An example from Muscat in Oman. Glob. Planet. Change 139, 183–194. https://doi.org/10.1016/j.gloplacha.2016.02.005

Shah-Hosseini, M., Morhange, C., Naderi Beni, A., Marriner, N., Lahijani, H., Hamzeh, M., Sabatier, F., 2011. Coastal boulders as evidence for high-energy waves on the Iranian coast of Makran. Mar. Geol. 290, 17–28. https://doi.org/10.1016/j.margeo.2011.10.003

Shah, S.T., Özacar, A.A., Gülerce, Z., 2021. Fault-based probabilistic seismic hazard assessment of the eastern Makran subduction and the Chaman transform fault, Pakistan: Emphasis on the source characterization of megathrust. J. Asian Earth Sci. 205. https://doi.org/10.1016/j.jseaes.2020.104604

Shi, S., Dawson, A.G., Smith, D.E., 1995. Coastal sedimentation associated with the December 12th, 1992 tsunami in Flores, Indonesia. Pure Appl. Geophys. PAGEOPH 144, 525–536. https://doi.org/10.1007/BF00874381

Sibuet, J.C., Rangin, C., Le Pichon, X., Singh, S., Cattaneo, A., Graindorge, D., Klingelhoefer, F., Lin, J.Y., Malod, J., Maury, T., Schneider, J.L., Sultan, N., Umber, M., Yamaguchi, H., 2007. 26th December 2004 great Sumatra-Andaman earthquake: Co-seismic and post-seismic motions in northern Sumatra. Earth Planet. Sci. Lett. 263, 88–103. https://doi.org/10.1016/j.epsl.2007.09.005

Silva, F.R.S. da, Borges, A.L. de O., Toldo Jr., E.E., Fick, C., Puhl, E., Oliveira, V.C.B., Cruz, F.E.G. da, 2023. Threshold of motion and orientation of bivalve shells under current flow. Brazilian J. Geol.

Smart, G.M., Crowley, K.H.M., Lane, E.M., 2016. Estimating tsunami run-up. Nat. Hazards 80, 1933–1947. https://doi.org/10.1007/s11069-015-2052-8

Smith, G.L., McNeill, L., Henstock, I.J., Bull, J., 2012. The structure and fault activity of the Makran accretionary prism. J. Geophys. Res. 117, 1–17. https://doi.org/10.1029/2012JB009312

Smith, G.L., McNeill, L.C., Wang, K.H., Jiangheng He., Henstock, T.J., 2013. Thermal structure and megathrust seismogenic potential of the Makran subduction zone. Geophys. Res. Lett. 40, 1528–1533. https://doi.org/10.1002/grl.50374

Snead, R.J., 2002. Uplifted marine terraces along the Makran coast of Pakistan and Iran, in: Himalaya to the Sea. Routledge, pp. 225–246.

Srinivasa Kumar, T., Manneela, S., 2021. A Review of the Progress, Challenges and Future Trends in Tsunami Early Warning Systems. J. Geol. Soc. India 97, 1533–1544. https://doi.org/10.1007/s12594-021-1910-0

Srivastava, K., Dimri, V.P., Swaroopa Rani, V., Krishna Kumar, R., Narain, L., 2011. Would makran Tsunami skip Mumbai, India? no it would reach 8 minutes later than Ratnagiri. Indian J. Geo-Marine Sci. 40, 620–623.

Steinritz, V., Pena-Castellnou, S., Marliyani, G.I., Reicherter, K., 2021a. GIS-based study of tsunami risk in the Special Region of Yogyakarta (Central GIS-based study of tsunami risk in the Special Region of Yogyakarta (Central Java , Indonesia), in: International Conference on Geological Engineering and Geosciences. https://doi.org/10.1088/1755-1315/851/1/012007

Steinritz, V., Pena-Castellnou, S., Marliyani, G.I., Reicherter, K., 2021b. GIS-based study of tsunami risk in the Special Region of Yogyakarta (Central Java, Indonesia), in: IOP Conference Series: Earth and Environmental Science. IOP Publishing, p. 12007. https://doi.org/10.1088/1755-1315/851/1/012007

Stoneley, R., 1974. Evolution of the Continental Margins Bounding a Former Southern Tethys. Geol. Cont. Margins 889–903. https://doi.org/10.1007/978-3-662-01141-6_65

Stuiver, M., Reimer, P.J., 1993. Extended 14C data base and revised Calib 3.0 14C age calibration program. Radiocarbon 35, 215–230.

Sujatmiko, K.A., Ichii, K., Murata, S., Mulia, I.E., 2023. Application of Stress Parameter from Liquefaction Analysis on the Landslide Induced Tsunami Simulation : A Case Study of the 2018 Palu Tsunami 18, 199–208. https://doi.org/10.20965/jdr.2023.p0199

Sultan, M., 2017. Statistical analysis of earthquakes and tsunami of Makran Subduction Zone (MSZ), and tsunami hazard assessment of Gwadar Coast. J. Astrophys. Aerosp. Technol. 08. https://doi.org/10.4172/2329-6542.1000408

Suppasri, A., Latcharotel, P., Pokavanich, T., Al-Salem, K., Al-Enezi, A., Toda, S., Imamura, F., 2016. Tsunami Hazard Assessment for the Arabian Gulf from Earthquakes and Surface Landslides. J. Japan Soc. Civ. Eng. Ser. B2 (Coastal Eng. 72, I_1675-I_1680. https://doi.org/10.2208/kaigan.72.i_1675

Swapna, M., Srivastava, K., 2014. Effect of Murray ridge on the tsunami propagation from Makran subduction zone. Geophys. J. Int. 199, 1430–1441. https://doi.org/10.1093/gji/ggu336

Tarbotton, C., Dall'Osso, F., Dominey-Howes, D., Goff, J., 2015. The use of empirical vulnerability functions to assess the response of buildings to tsunami impact: Comparative review and summary of best practice. Earth-Science Rev. 142, 120–134. https://doi.org/https://doi.org/10.1016/j.earscirev.2015.01.002

Tarbotton, C., Dominey-Howes, D., Goff, J.R., Papathoma-Kohle, M., Dall'osso, F., Turner, I.L., 2012. GIS-based techniques for assessing the vulnerability of buildings to tsunami: Current approaches and future steps. Geol. Soc. Spec. Publ. 361, 115–125. https://doi.org/10.1144/SP361.10

UNESCO/IOC, 2015. Remembering the 1945 Makran Tsunami interviews with survivors beside the Arabian Sea, IOC Brochu. ed, United Nations Educational, Scientific and Cultural Organization (UNESCO). Paris, France.

Van Ormondt, M., Nederhoff, K., Van Dongeren, A., 2020. Delft Dashboard: A quick set-up tool for hydrodynamic models. J. Hydroinformatics 22, 510–527. https://doi.org/10.2166/hydro.2020.092

Vaziri, S.H., Reinhart, E.G., Pilarczyk, J.E., 2016. Coastal foraminifera from the Iranian coast of Makran, Oman Sea (Chabahar Bay to Gawater Bay) as an indicator of tsunamis, in: Geological Society of America Annual Meeting. Denver, Colorado, pp. 43–63. https://doi.org/10.22059/geope.2018.255122.648378

Vernant, P., Nilforoushan, F., Hatzfeld, D., Abbassi, M.R., Vigny, C., Masson, F., Nankali, H., Martinod, J., Ashtiani, A., Bayer, R., Tavakoli, F., Chéry, J., 2004. Present-day crustal deformation and plate kinematics in the Middle East constrained by GPS measurements in Iran and northern Oman. Geophys. J. Int. 157, 381–398. https://doi.org/10.1111/j.1365-246X.2004.02222.x

Waseem, M., Khan, S., Asif Khan, M., 2020. Probabilistic Seismic Hazard Assessment of Pakistan Territory Using an Areal Source Model. Pure Appl. Geophys. 177, 3577–3597. https://doi.org/10.1007/s00024-020-02455-7

Watts, P., 1998. Wavemaker Curves for Tsunamis Generated by Underwater Landslides. J. Waterw. Port, Coastal, Ocean Eng. 124, 127–137. https://doi.org/10.1061/(asce)0733-950x(1998)124:3(127)

White, R.S., Louden, K.E., 1982. The Makran continental margin: structure of a thickly sedimented convergent plate boundary: convergent margins: field investigations of margin structure and stratigraphy.

Williams, S., Paulik, R., Weaving, R., Bosserelle, C., Chan Ting, J., Wall, K., Simi, T., Scheele, F., 2021. Multiscale Quantification of Tsunami Hazard Exposure in a Pacific Small Island Developing State: The Case of Samoa. GeoHazards 2, 63–79. https://doi.org/10.3390/geohazards2020004

Yanagisawa, H., Koshimura, S., Imamura, F., Watabe, H., Egashira, T., 2009. Tsunami hazard assessment along the coast of Pakistan based on the 1945 Makran tsunami. J. Japan Soc. Civ. Eng. Ser. B2 (Coastal Eng. B2-65, 306–310. https://doi.org/10.2208/kaigan.65.306

Yang, X., Qiu, Q., Feng, W., Lin, J., Zhang, J., Zhou, Z., Zhang, F., 2022. Mechanism of the 2017 Mw6.3 Pasni earthquake and its significance for future major earthquakes in the eastern Makran. Geophys. J. Int. 231, 1434–1445. https://doi.org/10.1093/gji/ggac257

Zaccagnino, D., Telesca, L., Doglioni, C., 2022. Scaling properties of seismicity and faulting. Earth Planet. Sci. Lett. 584, 117511. https://doi.org/10.1016/j.epsl.2022.117511

Zafarani, H., Etemadsaeed, L., Rahimi, M., Kheirdast, N., Rashidi, A., Ansari, A., Mokhtari, M., Eskandari-ghadi, M., 2022. Probabilistic tsunami hazard analysis for western Makran, Natural Hazards. Springer Netherlands. https://doi.org/10.1007/s11069-022-05595-2

Zuhair, M., Alam, S., 2017. Tsunami Impacts on Nuclear Power Plants along Western Coast of India Due to a Great Makran Earthquake: A Numerical Simulation Approach. Int. J. Geosci. 08, 1417–1426. https://doi.org/10.4236/ijg.2017.812083

Abbasi, M.A., 2020. Regional Connectivity and Pakistan-Iran Trade Corridors. J. Glob. Peace Secur. Stud. 1, 44–59.

Aguirre-Ayerbe, I., Martínez Sánchez, J., Aniel-Quiroga, I., González-Riancho, P., Al-Yahyai, S., González, M., Medina, R., 2018. From tsunami risk assessment to disaster risk reduction - The

case of Oman. Nat. Hazards Earth Syst. Sci. 18, 2241–2260. https://doi.org/10.5194/nhess-18-2241-2018

Ahmed, M., Lodi, S.H., Rafi, M.M., 2019. Probabilistic seismic hazard analysis based zoning map of Pakistan. J. Earthq. Eng. 1–36. https://doi.org/10.1080/13632469.2019.1684401

Akbarpour Jannat, M.R., 2021. Tsunami modeling in the Chabahar Bay-Iran from worst-case Makran seismic scenarios: new insights into spectral characterization, separation of the continental shelf, and topography effects. Arab. J. Geosci. 14. https://doi.org/10.1007/s12517-021-06449-0

Akbarpour Jannat, M.R., Noranian Esfahani, M., Chegini, V., Rezanejad, K., 2011. Hazards associated with tsunami waves in the gulf of Oman. J. Coast. Res. 865–869.

Al-Habsi, Z., Hereher, M., El-Hussain, I., Omira, R., Ana Baptista, M., Deif, A., Al-Awadhi, T., Al-Nasiri, N., 2022. Tsunami hazard and risk zoning for Qurayyat in northeast Oman coast: Worst-case credible scenarios along the Makran Subduction Zone, Western Asia. J. Asian Earth Sci. X 8, 100103. https://doi.org/10.1016/j.jaesx.2022.100103

Ali, B., Matsumaru, R., Janjuhah, H.T., 2023. A Source Model for Tsunami Hazards. A Case study from the Eastern Segment of the Makran Subduction Zone, Balochistan, Pakistan. J. Himal. Earth Sci. 56, 48–64.

Ali, K.F., De-Boer, D.H., 2008. Factors controlling specific sediment yield in the upper Indus River basin, northern Pakistan. Hydrol. Process. 2274, 2267–2274. https://doi.org/10.1002/hyp

Ambraseys, N.N., Melville, C., 1982. A history of Persian earthquakes. Cambridge University Press, Britain.

Aniel-Quiroga, Í., Álvarez-Gómez, J.A., González, M., Martínez Sánchez, J., Parro, L.M., Aguirre-Ayerbe, I., Fernández, F., Medina, R., Al-Yahyai, S., 2018. Tsunami Hazard assessment and Scenarios Database for the Tsunami Warning System for the coast of Oman. Nat. Hazards Earth Syst. Sci. 1–30. https://doi.org/10.5194/nhess-2018-221

Anshori, 2019. Tsunami-Inundation-Toolbox-ArcGIS-Desktop-10.x. https://github.com/anshori/Tsunami-Inundation-Toolbox-ArcGIS-Desktop-10.x (Last accessed: 01.02.2022).

Arjun, S., Kalarani, K., Dhanya, P., Praveen, S.S., Reshmi, A.K., Kurian, N.P., Murthy, M.V.R., Hameed, T.S.S., Prakash, T.N., 2011. Numerical simulation of the 1945 Makran tsunami on the southwest coast and Lakshadweep islands of India. Mar. Geod. 34, 68–76. https://doi.org/10.1080/01490419.2011.547801

ArRajehi, A., McClusky, S., Reilinger, R., Daoud, M., Alchalbi, A., Ergintav, S., Gomez, F., Sholan, J., Bou-Rabee, F., Ogubazghi, G., Haileab, B., Fisseha, S., Asfaw, L., Mahmoud, S., Rayan, A., Bendik, R., Kogan, L., 2010. Geodetic constraints on present-day motion of the Arabian Plate: Implications for Red Sea and Gulf of Aden rifting. Tectonics 29, 1–10. https://doi.org/10.1029/2009TC002482

Attenbrow, V., 1992. Shell Bed Or Shell Midden. Aust. Archaeol. 34, 3–21. https://doi.org/10.1080/03122417.1992.11681447

Baba, T., Cummins, P.R., Hori, T., Kaneda, Y., 2006. High precision slip distribution of the 1944

Tonankai earthquake inferred from tsunami waveforms: Possible slip on a splay fault. Tectonophysics 426, 119–134. https://doi.org/10.1016/j.tecto.2006.02.015

Banghar, A., Syke, L.R., 1981. Focal mechanism of an earthquake from the Southern Ocean. Tectonophysics 79, 37–41.

Baptista, M.A., Miranda, J.M., Omira, R., El-Hussain, I., 2020. Study of the 24 September 2013 Oman Sea tsunami using linear shallow water inversion. Arab. J. Geosci. 13. https://doi.org/10.1007/s12517-020-05632-z

Behrens, J., Løvholt, F., Jalayer, F., Lorito, S., Salgado-Gálvez, M.A., Sørensen, M., Abadie, S., Aguirre-Ayerbe, I., Aniel-Quiroga, I., Babeyko, A., Baiguera, M., Basili, R., Belliazzi, S., Grezio, A., Johnson, K., Murphy, S., Paris, R., Rafliana, I., De Risi, R., Rossetto, T., Selva, J., Taroni, M., Del Zoppo, M., Armigliato, A., Bureš, V., Cech, P., Cecioni, C., Christodoulides, P., Davies, G., Dias, F., Bayraktar, H.B., González, M., Gritsevich, M., Guillas, S., Harbitz, C.B., Kânoğlu, U., Macías, J., Papadopoulos, G.A., Polet, J., Romano, F., Salamon, A., Scala, A., Stepinac, M., Tappin, D.R., Thio, H.K., Tonini, R., Triantafyllou, I., Ulrich, T., Varini, E., Volpe, M., Vyhmeister, E., 2021. Probabilistic Tsunami Hazard and Risk Analysis: A Review of Research Gaps. Front. Earth Sci. 9, 1–28. https://doi.org/10.3389/feart.2021.628772

Bell, K.C., 2011. Lessons from the reconstruction of post-tsunami Aceh: Build back better through ensuring women are at the center of reconstruction of land and property. Washington, DC. © World Bank.

Bellanova, P., Frenken, M., Nishimura, Y., Schwarzbauer, J., Reicherter, K., 2021. Tracing woody-organic tsunami deposits of the 2011 Tohoku-oki event in Misawa (Japan). Sci. Rep. 11, 8947. https://doi.org/10.1038/s41598-021-88199-3

Berryman, K., 2005. Review of Tsunami Hazard and Risk in New Zealand. Inst. Geol. Nucl. Sci. 139.

Bhatt, N., Murari, M.K., Ukey, V., Prizomwala, S.P., Singhvi, A.K., 2016. Geological evidences of extreme waves along the Gujarat coast of western India. Nat. Hazards 84, 1685–1704. https://doi.org/10.1007/s11069-016-2507-6

Biagi, P., 2013. The shell middens of Las Bela coast and the Indus delta (Arabian Sea , Pakistan). https://doi.org/10.1111/aae.12013

Biagi, P., 2011. Changing the prehistory of Sindh and Las Bela coast: Twenty-five years of Italian contribution. World Archaeol. 43, 523–537. https://doi.org/10.1080/00438243.2011.624695

Biagi, P., Girod, A., Nisbet, R., 2013. Prehistoric shell middens, seascapes and landscapes at Lake Siranda (Las Bela, Balochistan) Preliminary results of the 2011 fieldwork season. J. Asian Civilizations 36, 1–25.

Biagi, P., Nisbet, R., Fantuzzi, T., 2018. Exploiting mangroves: Enviromental changes and human interference along the norhtern coast of the Arabian Sea (Pakistan) during the Holocene. Archaol. Mitteilungen aus Iran und Turan 1–34.

Bourget, J., Zaragosi, S., Ellouz-Zimmermann, S., Ducassou, E., Prins, M.A., Garlan, T., Lanfumey, V., Schneider, J.L., Rouillard, P., Giraudeau, J., 2010. Highstand vs. lowstand turbidite system growth in the Makran active margin: Imprints of high-frequency external controls on sediment

delivery mechanisms to deep water systems. Mar. Geol. 274, 187–208. https://doi.org/10.1016/j.margeo.2010.04.005

Brune, J.N., 1968. Seismic moment, seismicity, and rate of slip along Major fault zones. J. Geophys. Res. 73, 777–784.

Burbidge, D.R., Cummins, P.R., Mleczko, R., Latief, H., Mokhtari, M., Natawidjaja, D., Rajendran, C.P., Thomas, C., 2009. A probabilistic tsunami hazard assessment of the Indian Ocean Nations. Aust. Gov. Geosci. Aust. Prof. Opin.

Byrne, D.E., Sykes, L.R., Davis, D.M., 1992. Great thrust earthquakes and aseismic slip along the plate boundary of the Makran Subduction Zone. J. Geophys. Res. 97, 449–478.

Caron, V., 2011. Contrasted textural and taphonomic properties of high-energy wave deposits cemented in beachrocks (St. Bartholomew Island, French West Indies). Sediment. Geol. 237, 189–208. https://doi.org/10.1016/j.sedgeo.2011.03.002

Ceci, L., 1984. Shell midden deposits as coastal resources. World Archaeol. 16, 62–74. https://doi.org/10.1080/00438243.1984.9979916

Chacón-Barrantes, S., Narayanan, R., Mayerle, R., 2013. Several tsunami scenarios at the North Sea and their consequences at the German Bight.

Chen, Z., Lin, J., Qiu, Q., Zhou, Z., Zhang, F., 2024. Tsunami potential in the Makran subduction zone: Amplification effects from earthquake rupture directivity and speed. Terra Nov. 36, 201–209. https://doi.org/10.1111/ter.12698

Cheng, G., Bar, W.D., Small, D., 2024. Makran subduction zone and tsunami scenarios in the western Indian Ocean. Geophys. J. Int. 237, 288–301.

Choy, G.L., Kirby, S.H., 2004. Apparent stress, fault maturity and seismic hazard for normal-fault earthquakes at subduction zones. Geophys. J. Int. 159, 991–1012.

Clift, P.D., Giosan, L., 2014. Sediment fluxes and buffering in the post-glacial Indus Basin. Basin Res. 26, 369–386. https://doi.org/10.1111/bre.12038

Cornell, C.A., Vanmarcke, E.H., 1969. The major influences on seismic risk, in: Proceedings of the Fourth World Conference on Earthquake Engineering. pp. 69–83.

Coutts, P.J.F., 1966. Features of Prehistoric Campsites in Australia. Mankind 6, 338.

Cromie, C., Scarselli, N., Craig, J., Khan, M.R., Hussain, A., 2022. Tectonostratigraphic Evolution and Hydrocarbon Prospectivity South of Gwadar Bay, Makran Accretionary Wedge, Offshore Sw Pakistan. J. Pet. Geol. 45, 179–199. https://doi.org/10.1111/jpg.12812

Cummins, P.R., Kaneda, Y., 2000. Possible splay fault slip during the 1946 Nankai earthquake. Geophys. Res. Lett. 27, 2725–2728. https://doi.org/10.1029/1999GL011139

Davies, G., Griffin, J., Løvholt, F., Glimsdal, S., Harbitz, C., Thio, H.K., Lorito, S., Basili, R., Selva, J., Geist, E., Baptista, M.A., 2018. A global probabilistic tsunami hazard assessment from earthquake sources. Geol. Soc. Spec. Publ. 456, 219–244. https://doi.org/10.1144/SP456.5

De Martini, P.M., Bruins, H.J., Feist, L., Goodman-Tchernov, B.N., Hadler, H., Lario, J., Mastronuzzi, G., Obrocki, L., Pantosti, D., Paris, R., Reicherter, K., Smedile, A., Vött, A., 2021.

The Mediterranean Sea and the Gulf of Cadiz as a natural laboratory for paleotsunami research: Recent advancements. Earth-Science Rev. 216, 103578. https://doi.org/10.1016/j.earscirev.2021.103578

Decker, V., Gee, C.T., Schucht, P.J., Lindauer, S., Hoffmann, G., 2022. Life on the Edge : A Powerful Tsunami Overwhelmed Indian Ocean Mangroves Life on the Edge : A Powerful Tsunami Overwhelmed Indian Ocean Mangroves One Millennium Ago. https://doi.org/10.3390/f13060922

Delavar, M.R., Mohammadi, H., Sharifi, M.A., Pirooz, M.D., 2017. Tsunami risk assessment modelling in Chabahar port, Iran. Int. Arch. Photogramm. Remote Sens. Spat. Inf. Sci. - ISPRS Arch. 42, 461–467. https://doi.org/10.5194/isprs-archives-XLII-2-W7-461-2017

Deltares, 2023. Delft3d-Flow; simulation of multi-dimensional hydrodynamic flows and transport phenomena, including sediments. https://content.oss.deltares.nl/delft3d4/Delft3D-FLOW_User_Manual.pdf 1–725.

Deo, S.G., Ghate, S., Rajaguru, S.N., 2011. Holocene environmental changes and cultural patterns in coastal western India: A geoarchaeological perspective. Quat. Int. 229, 132–139. https://doi.org/10.1016/j.quaint.2010.05.001

Donato, S. V., Reinhardt, E.G., Boyce, J.I., Pilarczyk, J.E., Jupp, B.P., 2009. Particle-size distribution of inferred tsunami deposits in Sur Lagoon, Sultanate of Oman. Mar. Geol. 257, 54–64. https://doi.org/10.1016/j.margeo.2008.10.012

Donato, S. V., Reinhardt, E.G., Boyce, J.I., Rothaus, R., Vosmer, T., 2008. Identifying tsunami deposits using bivalve shell taphonomy. Geology 36, 199–202. https://doi.org/10.1130/G24554A.1

Dortch, C.E., 1991. Rottnest and Garden Island Prehistory and The Archaeological Potential of The Adjacent Continental Shelf, Western Australia. Aust. Archaeol. 33, 38–43. https://doi.org/10.1080/03122417.1991.11681430

Dutta, K., Bhushan, R., Somayajulu, B., 2001. ΔR Correction Values for the Northern Indian Ocean. Radiocarbon 43(2A). https://doi.org/10.1017/S0033822200038376

El-Hussain, I., Omira, R., Al-Bulushi, K., Deif, A., Al-Habsi, Z., Al-Rawas, G., Mohamad, A., Al-Jabri, K., Baptista, M.A., 2017. Tsunami hazard assessment along Diba-Oman and Diba-Al-Emirates coasts. MATEC Web Conf. 120, 1–11. https://doi.org/10.1051/matecconf/201712006007

El-Hussain, I., Omira, R., Al-Habsi, Z., Baptista, M.A., Deif, A., Mohamed, A.M.E., 2018. Probabilistic and deterministic estimates of near-field tsunami hazards in northeast Oman. Geosci. Lett. 5. https://doi.org/10.1186/s40562-018-0129-4

El-Hussain, I., Omira, R., Deif, A., Al-Habsi, Z., Al-Rawas, G., Mohamad, A., Al-Jabri, K., Baptista, M.A., 2016. Probabilistic tsunami hazard assessment along Oman coast from submarine earthquakes in the Makran subduction zone. Arab. J. Geosci. 9. https://doi.org/10.1007/s12517-016-2687-0

Ellouz-Zimmermann, N., Lallemant, S.J., Castilla, R., Mouchot, N., Leturmy, P., Battani, A., Buret, C., Cherel, L., Desaubliaux, G., Deville, E., Ferrand, J., Lügcke, A., Mahieux, G., Mascle, G.,

Mühr, P., Pierson-Wickmann, A.-C., Robion, P., Schmitz, J., Danish, M., Hasany, S., Shahzad, A., Tabreez, A., 2007. Offshore Frontal Part of the Makran Accretionary Prism: The Chamak Survey (Pakistan), Thrust Belts and Foreland Basins, Frontiers in Earth Sciences. https://doi.org/10.1007/978-3-540-69426-7_18

Fournier, M., Chamot-Rooke, N., Petit, C., Fabbri, O., Huchon, P., Maillot, B., Lepvrier, C., 2008. In situ evidence for dextral active motion at the Arabia-India plate boundary. Nat. Geosci. 1, 94–98. https://doi.org/10.1038/ngeo.2007.24

Fournier, M., Chamot-Rooke, N., Rodriguez, M., Huchon, P., Petit, C., Beslier, M.O., Zaragosi, S., 2011. Owen Fracture Zone: The Arabia-India plate boundary unveiled. Earth Planet. Sci. Lett. 302, 247–252. https://doi.org/10.1016/j.epsl.2010.12.027

Fournier, M., Patriat, P., Leroy, S., 2001. Reappraisal of the Arabia-India-Somalia triple junction kinematics. Earth Planet. Sci. Lett. 189, 103–114. https://doi.org/10.1016/S0012-821X(01)00371-5

Frank, N.L., Husain, S.A., 1971. The Deadliest Tropical Cyclone in History. Bull. Am. Meteorol. Soc. 52, 438–445. https://doi.org/10.1175/1520-0477(1971)052<0438:tdtcih>2.0.co;2

Frohling, E., Szeliga, W., 2016. GPS constraints on interplate locking within the Makran subduction zone. Geophys. J. Int. 205, 67–76. https://doi.org/10.1093/gji/ggw001

Gandhi, D., Chavare, K.A., Prizomwala, S.P., Bhatt, N., Bhatt, N.Y., Mohan, K., Rastogi, B.K., 2017. Testing the numerical models for boulder transport through high energy marine wave event: An example from southern Saurashtra, western India. Quat. Int. 444, 209–216. https://doi.org/10.1016/j.quaint.2016.05.021

Gardezi, S.A.H., Luan, X., Sun, Z., Haider, R., Zhang, Y., Qiu, Q., Raveendrasinghe, T.D., 2024. Geo-hazards in the North Arabian Sea with special emphasis on Makran Subduction Zone. Earth-Science Rev. 255, 104846. https://doi.org/https://doi.org/10.1016/j.earscirev.2024.104846

Gates, G.O., Page, W.D., Savage, W.U., Zuberi, S., 1977. The Makran Earthquake November 28, (Mag. 8.3)1975 Field appraisal of geology and cultural effects, in: The Sixth World Conference on Earthquake Engineering New Delhi, India.

Gelfenbaum, G., Vatvani, D., Jaffe, B., Dekker, F., 2007. Tsunami inundation and sediment transport in vicinity of coastal mangrove forest. Coast. Sediments '07 - Proc. 6th Int. Symp. Coast. Eng. Sci. Coast. Sediment Process. 1–12. https://doi.org/10.1061/40926(239)86

Giles, D., Gopinathan, D., Guillas, S., Dias, F., 2021. Faster Than Real Time Tsunami Warning with Associated Hazard Uncertainties. Front. Earth Sci. 8, 1–16. https://doi.org/10.3389/feart.2020.597865

Gill, E.D., 1954. Aboriginal Kitchen Middens and Marine Shell Beds. Mankind 4, 249.

Goff, J.R., Lane, E., Arnold, J., 2009. The tsunami geomorphology of coastal dunes. Nat. Hazards Earth Syst. Sci. 9, 847–854. https://doi.org/10.5194/nhess-9-847-2009

Gopinathan, D., Heidarzadeh, M., Guillas, S., 2021. Probabilistic quantification of tsunami current hazard using statistical emulation. Proc. R. Soc. A Math. Phys. Eng. Sci. 477. https://doi.org/10.1098/rspa.2021.0180

Gordon, R.G., Demets, C., 1989. Present-day motion along the Owen fracture zone and Dalrymple trough in the Arabian Sea. J. Geophys. Res. 94, 5560–5570. https://doi.org/10.1029/JB094iB05p05560

Grando, G., McClay, K., 2007. Morphotectonics domains and structural styles in the Makran accretionary prism, offshore Iran. Sediment. Geol. 196, 157–179. https://doi.org/10.1016/j.sedgeo.2006.05.030

Habib, R.A., Iqbal, M.T., Salam, M., Tahir, M., Iqbal, J., Iqbal, T., 2025. Probing the Complex Interaction of Makran Subduction Zone with Regional Tectonic Features: Insights from Gravity and Seismic Source Parameters. Pure Appl. Geophys. 182, 55–77. https://doi.org/10.1007/s00024-024-03631-9

Haider, R., Ali, S., Hoffmann, G., Reicherter, K., 2024. Tsunami inundation and vulnerability analysis on the Makran coast, Pakistan. Nat. Hazards Earth Syst. Sci. 24, 3279–3290. https://doi.org/10.5194/nhess-24-3279-2024

Haider, R., Ali, S., Hoffmann, G., Reicherter, K., 2023. A multi-proxy approach to assess tsunami hazard with a preliminary risk assessment: A case study of the Makran Coast, Pakistan. Mar. Geol. 107032. https://doi.org/https://doi.org/10.1016/j.margeo.2023.107032

Hammack, J.L., 1973. A note on tsunamis: Their generation and propagation in an ocean of uniform depth. J. Fluid Mech. 60, 769–799. https://doi.org/10.1017/S0022112073000479

Hanks, T.C., Kanamori, H., 1979. A moment magnitude scale. J. Geophys. Res. B Solid Earth 84, 2348–2350. https://doi.org/10.1029/JB084iB05p02348

Harbitz, C.B., Løvholt, F., Bungum, H., 2014. Submarine landslide tsunamis: How extreme and how likely? Nat. Hazards 72, 1341–1374. https://doi.org/10.1007/s11069-013-0681-3

Heck, N.H., 1947. List of seismic sea waves. Bull. Seismol. Soc. Am. 37, 269–286.

Heffernan, A.S., Moore, J.C., Bangs, N.L., Moore, G.F., Shipley, T.H., 2004. Initial deformation in a subduction thrust system: polygonal normal faulting in the incoming sedimentary sequence of the Nankai subduction zone, southwestern Japan. Geol. Soc. London, Mem. 29, 143–148.

Heidarzadeh, M., Ishibe, T., Harada, T., Natawidjaja, D.H., Pranantyo, I.R., Widyantoro, B.T., 2021. High potential for splay faulting in the molucca sea, indonesia: november 2019 mw 7.2 earthquake and tsunami. Seismol. Res. Lett. 92, 2915–2926. https://doi.org/10.1785/0220200442

Heidarzadeh, M., Kijko, A., 2011. A probabilistic tsunami hazard assessment for the Makran subduction zone at the northwestern Indian Ocean. Nat. Hazards 56, 577–593. https://doi.org/10.1007/s11069-010-9574-x

Heidarzadeh, M., Krastel, S., Yalciner, A.C., 2014. The state-of-the-art numerical tools for modeling landslide tsunamis: a short review, in: Submarine Mass Movements and Their Consequences: 6th International Symposium. Springer, pp. 483–495.

Heidarzadeh, M., Pirooz, M.D., Zaker, N.H., 2009a. Modeling the near-field effects of the worst-case tsunami in the Makran subduction zone. Ocean Eng. 36, 368–376. https://doi.org/10.1016/j.oceaneng.2009.01.004

Heidarzadeh, M., Pirooz, M.D., Zaker, N.H., Mokhtari, M., 2007. Modeling of tsunami propagation in the vicinity of the southern coasts of Iran. Int. J. Civ. Eng. 5, 223–234. https://doi.org/10.1115/OMAE2007-29082

Heidarzadeh, M., Pirooz, M.D., Zaker, N.H., Yalciner, A.C., 2009b. Preliminary estimation of the tsunami hazards associated with the Makran subduction zone at the northwestern Indian Ocean. Nat. Hazards 48, 229–243. https://doi.org/10.1007/s11069-008-9259-x

Heidarzadeh, M., Pirooz, M.D., Zaker, N.H., Yalciner, A.C., Mokhtari, M., Esmaeily, A., 2008. Historical tsunami in the Makran Subduction Zone off the southern coasts of Iran and Pakistan and results of numerical modeling. Ocean Eng. 35, 774–786. https://doi.org/10.1016/j.oceaneng.2008.01.017

Heidarzadeh, M., Rabinovich, A., Kusumoto, S., Rajendran, C.P., 2020. Field surveys and numerical modelling of the 2004 December 26 Indian Ocean tsunami in the area of Mumbai, west coast of India. Geophys. J. Int. 222, 1952–1964. https://doi.org/10.1093/gji/ggaa277

Heidarzadeh, M., Satake, K., 2017. A combined earthquake-landslide source model for the tsunami from the 27 november 1945 Mw 8.1 makran earthquake. Bull. Seismol. Soc. Am. 107, 1033–1040. https://doi.org/10.1785/0120160196

Heidarzadeh, M., Satake, K., 2014a. Possible sources of the tsunami observed in the northwestern Indian ocean following the 2013 September 24 Mw 7.7 Pakistan inland earthquake. Geophys. J. Int. 199, 752–766. https://doi.org/10.1093/gji/ggu297

Heidarzadeh, M., Satake, K., 2014b. New Insights into the Source of the Makran Tsunami of 27 November 1945 from Tsunami Waveforms and Coastal Deformation Data. Pure Appl. Geophys. 172, 621–640. https://doi.org/10.1007/s00024-014-0948-y

Hicks, S.P., Rietbrock, A., 2015. Seismic slip on an upper-plate normal fault during a large subduction megathrust rupture. Nat. Geosci. 8, 955–960.

Hoechner, A., Babeyko, A.Y., Zamora, N., 2016. Probabilistic tsunami hazard assessment for the Makran region with focus on maximum magnitude assumption. Nat. Hazards Earth Syst. Sci. 16, 1339–1350. https://doi.org/10.5194/nhess-16-1339-2016

Hoffmann, G., Al-Yahyai, S., Naeem, G., Kociok, M., Grützner, C., 2014. An Indian Ocean tsunami triggered remotely by an onshore earthquake in Balochistan, Pakistan. Geology 42, 883–886. https://doi.org/10.1130/G35756.1

Hoffmann, G., Grützner, C., Reicherter, K., Preusser, F., 2015. Geo-archaeological evidence for a Holocene extreme flooding event within the Arabian Sea (Ras al Hadd, Oman). Quat. Sci. Rev. 113, 123–133. https://doi.org/10.1016/j.quascirev.2014.09.033

Hoffmann, G., Grützner, C., Schneider, B., Preusser, F., Reicherter, K., 2020. Large Holocene tsunamis in the northern Arabian Sea. Mar. Geol. 419. https://doi.org/10.1016/j.margeo.2019.106068

Hoffmann, G., Reicherter, K., 2014. Reconstructing Anthropocene extreme flood events by using litter deposits. Glob. Planet. Change 122, 23–28. https://doi.org/10.1016/j.gloplacha.2014.07.012

Hoffmann, G., Reicherter, K., Wiatr, T., Grützner, C., 2011. Evidence For Holocene Tsunami-Impact

Along the Shoreline of Oman. 2nd INQUA-IGCP-567 Int. Work. Act. Tectonics, Earthq. Geol. Archaeol. Eng. 88–91.

Hoffmann, G., Reicherter, K., Wiatr, T., Grützner, C., Rausch, T., 2013a. Block and boulder accumulations along the coastline between Fins and Sur (Sultanate of Oman): Tsunamigenic remains? Nat. Hazards 65, 851–873. https://doi.org/10.1007/s11069-012-0399-7

Hoffmann, G., Rupprechter, M., Balushi, N. Al, Grützner, C., Reicherter, K., 2013b. The impact of the 1945 Makran tsunami along the coastlines of the Arabian Sea (Northern Indian Ocean) – a review. Zeitschrift für Geomorphol. Suppl. Issues 57, 257–277. https://doi.org/10.1127/0372-8854/2013/s-00134

Honarmand, M., Shanehsazzadeh, A., Zandi, S.M., 2020. 3D numerical simulation of tsunami generation and propagation, case study: Makran tsunami generation and penetrating in Chabahar Bay. Ocean Eng. 218, 108109. https://doi.org/10.1016/j.oceaneng.2020.108109

Hosseini Mehr, A., Maleki Asayesh, B., Mokhtari, M., 2018. Splay Faults in the Makran Subduction Zone and Changes of their Transferred Coulomb Stress. J. Earth Sp. Phys. 43, 1–10. https://doi.org/10.22059/jesphys.2017.61703

https://c14.arch.ox.ac.uk/calibration.html [WWW Document], n.d. URL https://c14.arch.ox.ac.uk/calibration.html

Hughes, P.J., Sullivan, M.E., 1974. The re-deposition of midden material by storm waves, in: Journal and Proceedings of the Royal Society of New South Wales. Australasian Medical Publishing Co., pp. 6–10.

Jackson, J., McKenzie, D., 1984. Active tectonics of the Alpine–Himalayan Belt between western Turkey and Pakistan. Geophys. J. R. Astron. Soc. 77, 185–264. https://doi.org/10.1111/j.1365-246X.1984.tb01931.x

Jacob, K.H., Quittmayer, R.C., 1979. The Makran Region of Pakistan and Iran: Trench–arc system with active plate subduction, in: Geodynamics of Pakistan. Geological Survey of Pakistan, Quetta, pp. 305–317.

Jade, S., Shrungeshwara, T.S., Kumar, K., Choudhury, P., Dumka, R.K., Bhu, H., 2017. India plate angular velocity and contemporary deformation rates from continuous GPS measurements from 1996 to 2015. Sci. Rep. 7, 1–16. https://doi.org/10.1038/s41598-017-11697-w

Jaiswal, R.K., Singh, A.P., Rastogi, B.K., 2009. Simulation of the Arabian Sea Tsunami propagation generated due to 1945 Makran Earthquake and its effect on western parts of Gujarat (India). Nat. Hazards 48, 245–258. https://doi.org/10.1007/s11069-008-9261-3

Juniansah, A., Tyas, B.I., Tama, G.C., Febriani, K.R., Farda, N.M., 2018. Spatial modelling for tsunami evacuation route in Parangtritis Village. IOP Conf. Ser. Earth Environ. Sci. 148. https://doi.org/10.1088/1755-1315/148/1/012003

Kakar, D.M., Naeem, G., Usman, A., Hasan, H., Lohdi, H.A., Srinivasalu, S., Andrade, V., Rajendran, C.P., Beni, A.N., Hamzeh, M.A., Hoffmann, G., 2014. Elders recall an earlier tsunami on Indian Ocean shores, Eos, Transactions American Geophysical Union. UNESCO.

Kalsi, S.R., Gupta, M., 2003. Success and failure of early warning systems: A case study of the Gujarat Cyclone of June, 1998, in: Zschau, J., Küppers, A. (Eds.), Early Warning Systems for

Natural Disaster Reduction. Springer Berlin Heidelberg, Berlin, Heidelberg, pp. 199–202. https://doi.org/10.1007/978-3-642-55903-7_26

Kame, N., Yamashita, T., 1999. Simulation of the spontaneous growth of a dynamic crack without constraints on the crack tip path. Geophys. J. Int. 139, 345–358.

Kerr, R., 1824. A general history and collection of voyages and travels, arranged in systematic order: forming a complete history of the origin and progress of navigation, discovery, and commerce, by sea and land, from the earliest ages to the present time. W. Blackwood.

Khaledzadeh, M., Ghods, A., 2022. Estimation of size of megathrust zone in the Makran subduction system by thermal modelling. Geophys. J. Int. 228, 1530–1540. https://doi.org/10.1093/gji/ggab417

Khan, M.A., Bendick, R., Bhat, M.I., Bilham, R., Kakar, D.M., Khan, S.F., Lodi, S.H., Qazi, M.S., Singh, B., Szeliga, W., Wahab, A., 2008. Preliminary geodetic constraints on plate boundary deformation on the western edge of the Indian plate from TriGGnet (Tri-University GPS Geodesy Network). J. Himal. Earth Sci. 41, 71–87.

Khan, M.J., Ali, M., Xu, M., Khan, M., 2020. Seismicity analysis of selected faults in Makran Southern Pakistan. Acta Geophys. 68, 965–978. https://doi.org/10.1007/s11600-020-00447-8

Khan, S.A., Shah, M.A., Qaisar, M., 2003a. Seismic risk analysis of coastal area of Pakistan. Acta Seismol. Sin. English Ed. 16, 382–394. https://doi.org/10.1007/s11589-003-0071-0

Khan, S.A., Shah, M.A., Qaisar, M., 2003b. Seismic risk analysis of coastal area of Pakistan. Acta Seismol. Sin. English Ed. 16, 382. https://doi.org/10.1007/s11589-003-0071-0

Khan, U., Khan, M., Wu, S., Jinwei, G., 2024. Middle Miocene renewed subduction of arabian-eurasian plates: Implications for convergent tectonic mechanisms, tectonically-induced fluid overpressures, and sediment recycling dynamics. Mar. Pet. Geol. 162, 106704. https://doi.org/https://doi.org/10.1016/j.marpetgeo.2024.106704

Klingelhoefer, F., Gutscher, M.A., Ladage, S., Dessa, J.X., Graindorge, D., Franke, D., André, C., Permana, H., Yudistira, T., Chauhan, A., 2010. Limits of the seismogenic zone in the epicentral region of the 26 December 2004 great Sumatra-Andaman earthquake: Results from seismic refraction and wide-angle reflection surveys and thermal modeling. J. Geophys. Res. Solid Earth 115, 1–23. https://doi.org/10.1029/2009JB006569

Knapp, K.R., Kruk, M.C., Levinson, D.H., Diamond, H.J., Neumann, C.J., 2010. The international best track archive for climate stewardship (IBTrACS). Bull. Am. Meteorol. Soc. 91, 363–376. https://doi.org/10.1175/2009BAMS2755.1

Kopp, C., Fruehn, J., Flueh, E.R., Reichert, C., Kukowski, N., Bialas, J., Klaeschen, D., 2000. Structure of the makran subduction zone from wide-angle and reflection seismic data. Tectonophysics 329, 171–191. https://doi.org/10.1016/S0040-1951(00)00195-5

Koshimura, S., Oie, T., Yanagisawa, H., Imamura, F., 2009. Developing fragility functions for tsunami damage estimation using numerical model and post-tsunami data from banda aceh, Indonesia. Coast. Eng. J. 51, 243–273. https://doi.org/10.1142/S0578563409002004

Koster, B., Hoffmann, G., Grützner, C., Reicherter, K., 2014. Ground penetrating radar facies of inferred tsunami deposits on the shores of the Arabian Sea (Northern Indian Ocean). Mar. Geol.

351, 13–24. https://doi.org/10.1016/j.margeo.2014.03.002

Kukowski, N., Schillhorn, T., Flueh, E.R., Huhn, K., 2000. Newly identified strike-slip plate boundary in the northeastern Arabian Sea. Geology 28, 355–358. https://doi.org/10.1130/0091-7613(2000)28<355:NISPBI>2.0.CO;2

Kukowski, N., Schillhorn, T., Huhn, K., Von Rad, U., Husen, S., Flueh, E.R., 2001. Morphotectonics and mechanics of the central Makran accretionary wedge off Pakistan. Mar. Geol. 173, 1–19. https://doi.org/10.1016/S0025-3227(00)00167-5

Kupriyanov, A. V, Makarevich, G.G., 2024. Chabahar Port: Between Geopolitics and Business, in: India's Economic Corridor Initiatives. Routledge, pp. 53–65.

Laane, J.L., Chen, W.-P., 1989. The Makran earthquake of 1983 April 18: A possible analogue to the Puget Sound earthquake of 1965. Geophys. J. Int. 98, 1–9.

Latcharote, P., Al-Salem, K., Suppasri, A., Pokavanich, T., Toda, S., Jayaramu, Y., Al-Enezi, A., Al-Ragum, A., Imamura, F., Anawat, K.A., 2018. Tsunami hazard evaluation for Kuwait and Arabian Gulf due to Makran Subduction Zone and Subaerial landslides. Nat. Hazards 93, 127–152. https://doi.org/10.1007/s11069-017-3097-7

Logan, W., 1887. Malabar Manual (2 volumes). Asia Educ. Serv. (1995 Repr. New Delhi.

Loveless, J.P., Allmendinger, R.W., Pritchard, M.E., González, G., 2010. Normal and reverse faulting driven by the subduction zone earthquake cycle in the northern Chilean fore arc. Tectonics 29.

Løvholt, F., 2017. Tsunami Hazard and Risk Assessment. United Nations Off. Disaster Risk Reduct. 1–9.

Løvholt, F., Glimsdal, S., Harbitz, C.B., Zamora, N., Nadim, F., Peduzzi, P., Dao, H., Smebye, H., 2012. Tsunami hazard and exposure on the global scale. Earth-Science Rev. 110, 58–73. https://doi.org/10.1016/j.earscirev.2011.10.002

Macintosh, A., 2013. Coastal climate hazards and urban planning : how planning responses can lead to maladaptation 1035–1055. https://doi.org/10.1007/s11027-012-9406-2

Mahmood, N., Khan, K., Rafi, Z., Lovholt, D.F., 2012. Mapping of Tsunami Hazard along Makran Coast of Pakistan 1–39.

Malgrange, M., Madariaga, R., 1983. Complex distribution of large thrust and normal fault earthquakes in the Chilean subduction zone. Geophys. J. Int. 73, 489–505.

Manaman, N.S., Shomali, H., Koyi, H., 2011. New constraints on upper-mantle S-velocity structure and crustal thickness of the Iranian plateau using partitioned waveform inversion. Geophys. J. Int. 184, 247–267. https://doi.org/10.1111/j.1365-246X.2010.04822.x

Marathe, A., Chandrashekhar, B.S., 2011. Application of Remote Sensing in Studying Holocene Sediments and Tectonic Episodes at Kelshi, Ratnagiri District, Maharashtra, India. J. Indian Soc. Remote Sens. 39, 241–247. https://doi.org/10.1007/s12524-011-0087-1

Masuda, M., Williams, C., Shahkarami, A., Rafique, F., Bryngelson, J., 2012. Tsunami Vulnerability Function Development Based on the 2011 Tohoku Earthquake in Japan. 15 World Conf. Earthq. Eng.

Matin, S., Praveen, S.S., 2021. Numerical simulation and comparison of tsunami inundation for different satellite-derived datasets for the Gujarat coast of India. Adv. Remote Sens. Nat. Resour. Monit. 431–443. https://doi.org/10.1002/9781119616016.ch21

McCann, W.R., Dewey, J.W., Murphy, A.J., Harding, S.T., 1982. A large normal-fault earthquake in the overriding wedge of the Lesser Antilles subduction zone: The earthquake of 8 October 1974. Bull. Seismol. Soc. Am. 72, 2267–2283.

Mehrdar, A., Motaghi, K., Ghods, A., Sobouti, F., Priestley, K., Pachhai, S., Shabanian, E., Zarunizadeh, Z., Zeynaddini-Meymand, R., El-Hussain, I., 2025. Crustal and uppermost mantle structure of the Iranian Makran subduction zone from ambient noise and earthquake surface wave tomography. Geophys. J. Int. 241, 70–85. https://doi.org/10.1093/gji/ggae419

Mikumo, T., Singh, S.K., Santoyo, M.A., 1999. A possible stress interaction between large thrust and normal faulting earthquakes in the Mexican subduction zone. Bull. Seismol. Soc. Am. 89, 1418–1427.

Milliman, J.D., Syvitski, J.P.M., 1992. Geomorphic/tectonic control of sediment discharge to the ocean: the importance of small mountainous rivers. J. Geol. 100, 525–544. https://doi.org/10.1086/629606

Miranda, J.M., Baptista, M.A., Omira, R., 2014. On the use of Green's summation for tsunami waveform estimation: A case study. Geophys. J. Int. 199, 459–464. https://doi.org/10.1093/gji/ggu266

Mokhtari, M., 2015. The role of splay faulting in increasing the devastation effect of tsunami hazard in Makran, Oman Sea. Arab. J. Geosci. 8, 4291–4298. https://doi.org/10.1007/s12517-014-1375-1

Mokhtari, M., Ala Amjadi, A., Mahshadnia, L., Rafizadeh, M., 2019. A review of the seismotectonics of the Makran Subduction Zone as a baseline for Tsunami Hazard Assessments. Geosci. Lett. 6, 13.

Momeni, P., and Goda, K., 2024. Probabilistic tsunami hazard assessment for the makran subduction zone using logic tree and stochastic rupture sources. Coast. Eng. J. 66, 332–360. https://doi.org/10.1080/21664250.2024.2324520

Momeni, P., Goda, K., Heidarzadeh, M., Qin, J., 2020. Stochastic analysis of tsunami hazard of the 1945 Makran subduction zone MW 8.1–8.3 earthquakes. Geosci. 10, 1–20. https://doi.org/10.3390/geosciences10110452

Momeni, P., Goda, K., Mokhtari, M., Heidarzadeh, M., 2022. A new tsunami hazard assessment for eastern Makran subduction zone by considering splay faults and applying stochastic modeling. Coast. Eng. J. https://doi.org/10.1080/21664250.2022.2117585

Moradi, M., 2021. Integration of Geographical Information System and Tsunami generation/propagation models in the Makran region (North of the Arabian Sea). Int. J. Coast. Offshore Eng. 5, 40–48. https://doi.org/10.52547/ijcoe.5.3.40

Mouchot, N., Loncke, L., Mahieux, G., Bourget, J., Lallemant, S., Ellouz-Zimmermann, N., Leturmy, P., 2010. Recent sedimentary processes along the Makran trench (Makran active margin, off Pakistan). Mar. Geol. 271, 17–31. https://doi.org/10.1016/j.margeo.2010.01.006

Mourato, S., Fernandez, P., Pereira, L., Moreira, M., 2017. Improving a DSM Obtained by Unmanned Aerial Vehicles for Flood Modelling. IOP Conf. Ser. Earth Environ. Sci. 95. https://doi.org/10.1088/1755-1315/95/2/022014

Mousavi, N., Ardestani, V.E., Moosavi, N., 2022. Slab extension and normal faulting in a low-angle subduction-related environment: An example of the Makran subduction zone (Iran-Pakistan). J. Asian Earth Sci. 233, 105244. https://doi.org/https://doi.org/10.1016/j.jseaes.2022.105244

Neetu, S., Suresh, I., Shankar, R., Nagarajan, B., Sharma, R., Shenoi, S.S.C., Unnikrishnan, A.S., Sundar, D., 2011. Trapped waves of the 27 November 1945 Makran tsunami: Observations and numerical modeling. Nat. Hazards 59, 1609–1618. https://doi.org/10.1007/s11069-011-9854-0

Nemati, M., 2019. Seismotectonic and seismicity of Makran, a bimodal subduction zone, SE Iran. J. Asian Earth Sci. 169, 139–161. https://doi.org/10.1016/j.jseaes.2018.08.009

Nouri, M., Namin, M.M., Rashidi, A., 2020. A first-order Landslide Tsunami Hazard Assessment in the Western Makran, in: 18th Iranian Hydraulic Conference. University of Tehran, Tehran, Iran.

Nouri, M., Rashidi, A., Montazeri Namin, M., Shugar, D.H., 2023. Submarine landslide tsunami hazard assessment for the western Makran based on a deterministic approach. Nat. Hazards 118, 1117–1136. https://doi.org/10.1007/s11069-023-06040-8

Okada, Y., 1985. Surface deformation due to shear and tensile faults in a half space. Bull. - Seismol. Soc. Am. 75, 1135–1154. https://doi.org/10.1785/bssa0820021018

Okal, E.A., Synolakis, C.E., 2008. Far-field tsunami hazard from mega-thrust earthquakes in the Indian Ocean. Geophys. J. Int. 172, 995–1015. https://doi.org/10.1111/j.1365-246X.2007.03674.x

Oskamp, J.A., Dababneh, A.J.A., Barton, D.J., 2015. Tsunami Hazard in the Arabian Gulf Due to Earthquakes in the Makran Subduction Zone.

Page, W.D., Alt, J.N., Cluff, L.S., Plafker, G., 1979. Evidence for the recurrence of large-magnitude earthquakes along the makran coast of Iran and Pakistan. Tectonophysics 52, 533–547. https://doi.org/10.1016/B978-0-444-41783-1.50081-7

Pagnoni, G.I., Armigliato, A., Tinti, S., 2021. Estimation of human damage and economic loss of buildings related to tsunami inundation in the city of augusta, italy. Geol. Soc. Spec. Publ. 501, 327–342. https://doi.org/10.1144/SP501-2019-134

Pajang, S., Cubas, N., Letouzey, J., Le Pourhiet, L., Seyedali, S., Fournier, M., Agard, P., Khatib, M.M., Heyhat, M., Mokhtari, M., 2021. Seismic hazard of the western Makran subduction zone: Insight from mechanical modelling and inferred frictional properties. Earth Planet. Sci. Lett. 562, 116789. https://doi.org/10.1016/j.epsl.2021.116789

Pajang, S., Khatib, M.M., Heyhat, M., Cubas, N., Bessiere, E., Letouzey, J., Mokhtari, M., Le Pourhiet, L., 2022. The distinct morphologic signature of underplating and seamounts in accretionary prisms, insights from thermomechanical modeling applied to Coastal Iranian Makran. Tectonophysics 845, 229617. https://doi.org/10.1016/j.tecto.2022.229617

Park, J.-O., Tsuru, T., Kodaira, S., Cummins, P.R., Kaneda, Y., 2002. Splay fault branching along the Nankai subduction zone. Science (80-.). 297, 1157–1160.

Park, S., van de Lindt, J.W., Cox, D., Gupta, R., 2013. Concept of Community Fragilities for Tsunami Coastal Inundation Studies. Nat. Hazards Rev. 14, 220–228. https://doi.org/10.1061/(asce)nh.1527-6996.0000092

Parvaiz, S., Ali, A., Javed, F., Shah, M.A., 2022. Deformational pattern and seismogenic potential of the eastern Makran subduction zone. J. Asian Earth Sci. 235, 105298. https://doi.org/10.1016/j.jseaes.2022.105298

Patel, V.M., Dholakia, M.B., Singh, A.P., 2016. Emergency preparedness in the case of Makran tsunami: a case study on tsunami risk visualization for the western parts of Gujarat, India. Geomatics, Nat. Hazards Risk 7, 826–842. https://doi.org/10.1080/19475705.2014.983188

Patel, V.M., Patel, H.S., Singh, A.P., 2011. Comparative study of earthquake and tsunami loading on Vertical Evacuation Structure at Dwarka. Int. J. Earth Sci. Eng. 4, 659–663.

Payande, A.R., Niksokhan, M.H., Naserian, H., 2014. Tsunami hazard assessment of Chabahar bay related to megathrust seismogenic potential of the Makran subduction zone. Nat. Hazards 76, 161–176. https://doi.org/10.1007/s11069-014-1476-x

Pendse, C.G., 1946. The Mekran Earthquake of the 28th November 1945. Sci. Notes X, 141–146.

Penney, C., Tavakoli, F., Saadat, A., Nankali, H.R., Sedighi, M., Khorrami, F., Sobouti, F., Rafi, Z., Copley, A., Jackson, J., Priestley, K., 2017. Megathrust and accretionary wedge properties and behaviour in the Makran subduction zone. Geophys. J. Int. 209, 1800–1830. https://doi.org/10.1093/gji/ggx126

Pilarczyk, J.E., Reinhardt, E.G., 2012. Testing foraminiferal taphonomy as a tsunami indicator in a shallow arid system lagoon: Sur, Sultanate of Oman. Mar. Geol. 295–298, 128–136. https://doi.org/10.1016/j.margeo.2011.12.002

Pilarczyk, J.E., Reinhardt, E.G., Boyce, J.I., Schwarcz, H.P., Donato, S. V., 2011. Assessing surficial foraminiferal distributions as an overwash indicator in Sur Lagoon, Sultanate of Oman. Mar. Micropaleontol. 80, 62–73. https://doi.org/10.1016/j.marmicro.2011.06.001

Plafker, G., 1972. Alaskan earthquake of 1964 and Chilean earthquake of 1960: Implications for arc tectonics. J. Geophys. Res. 77, 901–925.

Platt, J.P., Leggett, J.K., Alam, S., 1988. Slip vectors and fault mechanics in the Makran accretionary wedge, southwest Pakistan. J. Geophys. Res. 93, 7955–7973. https://doi.org/10.1029/jb093ib07p07955

Platt, J.P., Leggett, J.K., Young, J., Raza, H., Alam, S., 1985. Large-scale sediment underplating in the Makran accretionary prism, southwest Pakistan. Geology 13, 507–511. https://doi.org/10.1130/0091-7613(1985)13<507:LSUITM>2.0.CO;2

Prasojo, K., Afwani, M.Z., Lestari, I., Bramono, A.M.C.W., Bustomi, A.F., 2017. Berryman Tsunami Inundation Modelling on Temon: The Location of NYIA. Int. Conf. Environ. Resour. Manag. Glob. Reg. 1–8.

Prins, M.A., Postma, G., Cleveringa, J., Cramp, A., Kenyon, N.H., 2000. Controls on terrigenous sediment supply to the Arabian Sea during the late quaternary: The Indus fan. Mar. Geol. 169, 327–349. https://doi.org/10.1016/S0025-3227(00)00086-4

Prizomwala, S.P., Gandhi, D., Bhatt, N.N., Winkler, W., Kumar, M.R., Makwana, N., Bhatt, N.N., 2018. Geological evidence for AD 1008 tsunami along the Kachchh coast, Western India: Implications for hazard along the Makran Subduction Zone. Sci. Rep. 8, 1–8. https://doi.org/10.1038/s41598-018-35193-x

Prizomwala, S.P., Gandhi, D., Ukey, V.M., Bhatt, N., Rastogi, B.K., 2015. Coastal boulders as evidences of high-energy marine events from Diu Island, west coast of India: storm or palaeotsunami? Nat. Hazards 75, 1187–1203. https://doi.org/10.1007/s11069-014-1371-5

Prizomwala, S.P., Tandon, A., Joshi, N., Makwana, N., 2021. Reconstructing the catalogue for extreme wave events from the Gujarat coastline (Western India) and their implications to coastal settlers during the last 6000 years. Quat. Int. 599–600, 24–31. https://doi.org/10.1016/j.quaint.2021.03.004

Prizomwala, S.P., Vedpathak, C., Tandon, A., Das, A., Makwana, N., Joshi, N., 2022. Geological footprints of the 1945 Makran tsunami from the west coast of India. Mar. Geol. 446, 106773. https://doi.org/10.1016/j.margeo.2022.106773

Qiu, Q., Zhou, Z., Lin, J., Zhang, F., Chen, Z., Yang, X., 2022. Great earthquake and tsunami potential in the eastern Makran subduction zone: New insights from geodetic and structural constraints. Tectonophysics 837. https://doi.org/10.1016/j.tecto.2022.229462

Quittmeyer, R.C., Farah, A., Jacob H., K., 1979. The seismicity of Pakistan and its relation to surface faults, in: Farah, A., Dejong, K.A. (Eds.), Geodynamics of Pakistan. Geological Survey of Pakistan, Quetta, pp. 271–284.

Quittmeyer, R.C., Kafka, A.L., 1984. Constraints on plate motions in southern Pakistan and the northern Arabian Sea from the focal mechanisms of small earthquakes. J. Geophys. Res. 89, 2444–2458.

Rafi, Z., Mahmood, N., 2010. Numerical Modeling of Tsunami Inundation for Potential Earthquake at Makran Subduction Zone. Tech. Rep. No. PMD-45/2010.

Rahimi, M., Zafarani, H., Eskandari-Ghadi, M., Etemadsaeed, L., 2025. Dual risk-targeted seismic and tsunami hazard assessment for western Makran coasts, southeast Iran. Nat. Hazards. https://doi.org/10.1007/s11069-025-07184-5

Rajendran, C.P., Heidarzadeh, M., Sanwal, J., Karthikeyan, A., Rajendran, K., 2020. The Orphan Tsunami of 1524 on the Konkan Coast, Western India, and Its Implications. Pure Appl. Geophys. https://doi.org/10.1007/s00024-020-02575-0

Rajendran, C.P., Ramanamurthy, M. V., Reddy, N.T., Rajendran, K., 2008. Hazard implications of the late arrival of the 1945 Makran tsunami. Curr. Sci. 95, 1739–1743.

Rashid, A., Shirazi, S.A., 2023. Gwadar Port-Pakistan as an Axis for Regional Connectivity under CPEC: A Geographer's Perspective. J. Polit. Int. Stud. 9, 105–120.

Rashidi, A., Dutykh, D., Shomali, Z.H., 2020a. Horizontal displacement effect in tsunami wave generation in the western Makran region. J. Ocean Eng. Mar. Energy. https://doi.org/10.1007/s40722-020-00182-8

Rashidi, A., Shomali, Z.H., Dutykh, D., Keshavarz Faraj Khah, N., 2018a. Evaluation of tsunami wave energy generated by earthquakes in the Makran subduction zone. Ocean Eng. 165, 131–

139. https://doi.org/10.1016/j.oceaneng.2018.07.027

Rashidi, A., Shomali, Z.H., Dutykh, D., Keshavarz Farajkhah, N., 2020b. Tsunami hazard assessment in the Makran subduction zone. Nat. Hazards 100, 861–875. https://doi.org/10.1007/s11069-019-03848-1

Rashidi, A., Shomali, Z.H., Keshavarz Farajkhah, N., 2018b. Tsunami Simulations in the Western Makran Using Hypothetical Heterogeneous Source Models from World's Great Earthquakes. Pure Appl. Geophys. 175, 1325–1340. https://doi.org/10.1007/s00024-018-1842-9

Rastgoftar, E., Soltanpour, M., 2016. Study and numerical modeling of 1945 Makran tsunami due to a probable submarine landslide. Nat. Hazards 83, 929–945. https://doi.org/10.1007/s11069-016-2356-3

Regard, V., Hatzfeld, D., Molinaro, M., Aubourg, C., Bayer, R., Bellier, O., Yamini-Fard, F., Peyret, M., Abbassi, M., 2010. The transition between Makran subduction and the Zagros collision: recent advances in its structure and active deformation. Geol. Soc. London, Spec. Publ. 330, 43–64. https://doi.org/10.1144/SP330.4

Rehman, A., Zhang, H., 2024a. Seismicity and return period investigation of destructive earthquake in Makran subduction zone. Discov. Geosci. 2. https://doi.org/10.1007/s44288-024-00047-9

Rehman, A., Zhang, H., 2024b. Probabilistic forecast of next earthquake event in Makran subduction zone using Weibull distribution. Contrib. to Geophys. Geod. 54, 85–93. https://doi.org/10.31577/congeo.2024.54.1.5

Rehman, K., Cho, Y.S., 2016. Building damage assessment using scenario based tsunami numerical analysis and fragility curves. Water (Switzerland) 8. https://doi.org/10.3390/w8030109

Rehman, K., Jadoon, T., Hussain, M., Ahmad, Z., Ali, Aamir, Ali, Asghar, Ahmed, S., 2015. Tsunamigenic analysis in and around makran. J. Earthq. Eng. 19, 332–355. https://doi.org/10.1080/13632469.2014.982835

Reilinger, R., McClusky, S., Vernant, P., Lawrence, S., Ergintav, S., Cakmak, R., Ozener, H., Kadirov, F., Guliev, I., Stepanyan, R., Nadariya, M., Hahubia, G., Mahmoud, S., Sakr, K., ArRajehi, A., Paradissis, D., Al-Aydrus, A., Prilepin, M., Guseva, T., Evren, E., Dmitrotsa, A., Filikov, S. V., Gomez, F., Al-Ghazzi, R., Karam, G., 2006. GPS constraints on continental deformation in the Africa-Arabia-Eurasia continental collision zone and implications for the dynamics of plate interactions. J. Geophys. Res. Solid Earth 111, 1–26. https://doi.org/10.1029/2005JB004051

Röbke, B.R., Schüttrumpf, H., Vött, A., 2018. Hydro- and morphodynamic tsunami simulations for the ambrakian gulf (Greece) and comparison with geoscientific field traces. Geophys. J. Int. 213, 317–339. https://doi.org/10.1093/gji/ggx553

Röbke, B.R., Schüttrumpf, H., Vött, A., 2016. Effects of different boundary conditions and palaeotopographies on the onshore response of tsunamis in a numerical model - A case study from western Greece. Cont. Shelf Res. 124, 182–199. https://doi.org/10.1016/j.csr.2016.04.010

Röbke, B.R., Vött, A., Willershäuser, T., Fischer, P., Hadler, H., 2015. Considering coastal palaeogeographical changes in a numerical tsunami model - A progressive base to compare simulation results with field traces from three coastal settings in western Greece. Zeitschrift fur

Geomorphol. 59, 157–188. https://doi.org/10.1127/zfg-suppl/2014/S-00210

Rodriguez, M., Chamot-Rooke, N., Hébert, H., Fournier, M., Huchon, P., 2013. Owen Ridge deep-water submarine landslides: Implications for tsunami hazard along the Oman coast. Nat. Hazards Earth Syst. Sci. 13, 417–424. https://doi.org/10.5194/nhess-13-417-2013

Rodriguez, M., Fournier, M., Chamot-Rooke, N., Huchon, P., Bourget, J., Sorbier, M., Zaragosi, S., Rabaute, A., 2011. Neotectonics of the Owen Fracture Zone (NW Indian Ocean): Structural evolution of an oceanic strike-slip plate boundary. Geochemistry, Geophys. Geosystems 12. https://doi.org/10.1029/2011GC003731

Rodriguez, M., Fournier, M., Chamot-Rooke, N., Huchon, P., Zaragosi, S., Rabaute, A., 2012. Mass wasting processes along the Owen Ridge (Northwest Indian Ocean). Mar. Geol. 326–328, 80–100. https://doi.org/10.1016/j.margeo.2012.08.008

Roshan, A.D., Basu, P.C., Jangid, R.S., 2016. Tsunami hazard assessment of Indian coast, Natural Hazards. https://doi.org/10.1007/s11069-016-2216-1

Saha, S., Srivastava, K., 2019. Tsunami simulation along the south west coast of India: Lakshadweep Islands acting as wave-barricade. Indian J. Geo-Marine Sci. 48, 1640–1647.

Salah, P., Sasaki, J., Soltanpour, M., 2021. Comprehensive Probabilistic Tsunami Hazard Assessment in the Makran Subduction Zone. Pure Appl. Geophys. 178, 5085–5107. https://doi.org/10.1007/s00024-021-02725-y

Salaree, A., Okal, E.A., 2015. Field survey and modelling of the Caspian Sea tsunami of 1990 June 20. Geophys. J. Int. 201, 621–639. https://doi.org/10.1093/gji/ggv044

Salmanidou, D.M., Heidarzadeh, M., Guillas, S., 2019. Probabilistic Landslide-Generated Tsunamis in the Indus Canyon, NW Indian Ocean, Using Statistical Emulation. Pure Appl. Geophys. 176, 3099–3114. https://doi.org/10.1007/s00024-019-02187-3

Sangode, S.J., Meshram, D.C., 2013. A comparative study on the style of paleotsunami deposits at two sites on the west coast of India. Nat. Hazards 66, 463–483. https://doi.org/10.1007/s11069-012-0542-5

Sanlaville, P., Besenval, R., Evin, J., Prieur, A., 1991. Evolution de la région littorale du Makran pakistanais à l'Holocène. Paléorient 17, 3–18. https://doi.org/10.3406/paleo.1991.4536

Sarker, M.A., 2019. Numerical modelling of tsunami in the Makran Subduction Zone–A case study on the 1945 event. J. Oper. Oceanogr. 12, S212–S229. https://doi.org/10.1080/1755876X.2018.1527883

Schneider, B., Hoffmann, G., Reicherter, K., 2016. Scenario-based tsunami risk assessment using a static flooding approach and high-resolution digital elevation data: An example from Muscat in Oman. Glob. Planet. Change 139, 183–194. https://doi.org/10.1016/j.gloplacha.2016.02.005

Shah-Hosseini, M., Morhange, C., Naderi Beni, A., Marriner, N., Lahijani, H., Hamzeh, M., Sabatier, F., 2011. Coastal boulders as evidence for high-energy waves on the Iranian coast of Makran. Mar. Geol. 290, 17–28. https://doi.org/10.1016/j.margeo.2011.10.003

Shah, S.T., Özacar, A.A., Gülerce, Z., 2021. Fault-based probabilistic seismic hazard assessment of the eastern Makran subduction and the Chaman transform fault, Pakistan: Emphasis on the

source characterization of megathrust. J. Asian Earth Sci. 205. https://doi.org/10.1016/j.jseaes.2020.104604

Shi, S., Dawson, A.G., Smith, D.E., 1995. Coastal sedimentation associated with the December 12th, 1992 tsunami in Flores, Indonesia. Pure Appl. Geophys. PAGEOPH 144, 525–536. https://doi.org/10.1007/BF00874381

Sibuet, J.C., Rangin, C., Le Pichon, X., Singh, S., Cattaneo, A., Graindorge, D., Klingelhoefer, F., Lin, J.Y., Malod, J., Maury, T., Schneider, J.L., Sultan, N., Umber, M., Yamaguchi, H., 2007. 26th December 2004 great Sumatra-Andaman earthquake: Co-seismic and post-seismic motions in northern Sumatra. Earth Planet. Sci. Lett. 263, 88–103. https://doi.org/10.1016/j.epsl.2007.09.005

Silva, F.R.S. da, Borges, A.L. de O., Toldo Jr., E.E., Fick, C., Puhl, E., Oliveira, V.C.B., Cruz, F.E.G. da, 2023. Threshold of motion and orientation of bivalve shells under current flow. Brazilian J. Geol.

Smart, G.M., Crowley, K.H.M., Lane, E.M., 2016. Estimating tsunami run-up. Nat. Hazards 80, 1933–1947. https://doi.org/10.1007/s11069-015-2052-8

Smith, G.L., McNeill, L., Henstock, I.J., Bull, J., 2012. The structure and fault activity of the Makran accretionary prism. J. Geophys. Res. 117, 1–17. https://doi.org/10.1029/2012JB009312

Smith, G.L., McNeill, L.C., Wang, K.H., Jiangheng He., Henstock, T.J., 2013. Thermal structure and megathrust seismogenic potential of the Makran subduction zone. Geophys. Res. Lett. 40, 1528–1533. https://doi.org/10.1002/grl.50374

Snead, R.J., 2002. Uplifted marine terraces along the Makran coast of Pakistan and Iran, in: Himalaya to the Sea. Routledge, pp. 225–246.

Srinivasa Kumar, T., Manneela, S., 2021. A Review of the Progress, Challenges and Future Trends in Tsunami Early Warning Systems. J. Geol. Soc. India 97, 1533–1544. https://doi.org/10.1007/s12594-021-1910-0

Srivastava, K., Dimri, V.P., Swaroopa Rani, V., Krishna Kumar, R., Narain, L., 2011. Would makran Tsunami skip Mumbai, India? no it would reach 8 minutes later than Ratnagiri. Indian J. Geo-Marine Sci. 40, 620–623.

Steinritz, V., Pena-Castellnou, S., Marliyani, G.I., Reicherter, K., 2021a. GIS-based study of tsunami risk in the Special Region of Yogyakarta (Central GIS-based study of tsunami risk in the Special Region of Yogyakarta (Central Java , Indonesia), in: International Conference on Geological Engineering and Geosciences. https://doi.org/10.1088/1755-1315/851/1/012007

Steinritz, V., Pena-Castellnou, S., Marliyani, G.I., Reicherter, K., 2021b. GIS-based study of tsunami risk in the Special Region of Yogyakarta (Central Java, Indonesia), in: IOP Conference Series: Earth and Environmental Science. IOP Publishing, p. 12007. https://doi.org/10.1088/1755-1315/851/1/012007

Stoneley, R., 1974. Evolution of the Continental Margins Bounding a Former Southern Tethys. Geol. Cont. Margins 889–903. https://doi.org/10.1007/978-3-662-01141-6_65

Stuiver, M., Reimer, P.J., 1993. Extended 14C data base and revised Calib 3.0 14C age calibration program. Radiocarbon 35, 215–230.

Sujatmiko, K.A., Ichii, K., Murata, S., Mulia, I.E., 2023. Application of Stress Parameter from Liquefaction Analysis on the Landslide Induced Tsunami Simulation : A Case Study of the 2018 Palu Tsunami 18, 199–208. https://doi.org/10.20965/jdr.2023.p0199

Sultan, M., 2017. Statistical analysis of earthquakes and tsunami of Makran Subduction Zone (MSZ), and tsunami hazard assessment of Gwadar Coast. J. Astrophys. Aerosp. Technol. 08. https://doi.org/10.4172/2329-6542.1000408

Suppasri, A., Latcharotel, P., Pokavanich, T., Al-Salem, K., Al-Enezi, A., Toda, S., Imamura, F., 2016. Tsunami Hazard Assessment for the Arabian Gulf from Earthquakes and Surface Landslides. J. Japan Soc. Civ. Eng. Ser. B2 (Coastal Eng. 72, I_1675-I_1680. https://doi.org/10.2208/kaigan.72.i_1675

Swapna, M., Srivastava, K., 2014. Effect of Murray ridge on the tsunami propagation from Makran subduction zone. Geophys. J. Int. 199, 1430–1441. https://doi.org/10.1093/gji/ggu336

Tarbotton, C., Dall'Osso, F., Dominey-Howes, D., Goff, J., 2015. The use of empirical vulnerability functions to assess the response of buildings to tsunami impact: Comparative review and summary of best practice. Earth-Science Rev. 142, 120–134. https://doi.org/https://doi.org/10.1016/j.earscirev.2015.01.002

Tarbotton, C., Dominey-Howes, D., Goff, J.R., Papathoma-Kohle, M., Dall'osso, F., Turner, I.L., 2012. GIS-based techniques for assessing the vulnerability of buildings to tsunami: Current approaches and future steps. Geol. Soc. Spec. Publ. 361, 115–125. https://doi.org/10.1144/SP361.10

UNESCO/IOC, 2015. Remembering the 1945 Makran Tsunami interviews with survivors beside the Arabian Sea, IOC Brochu. ed, United Nations Educational, Scientific and Cultural Organization (UNESCO). Paris, France.

Van Ormondt, M., Nederhoff, K., Van Dongeren, A., 2020. Delft Dashboard: A quick set-up tool for hydrodynamic models. J. Hydroinformatics 22, 510–527. https://doi.org/10.2166/hydro.2020.092

Vaziri, S.H., Reinhart, E.G., Pilarczyk, J.E., 2016. Coastal foraminifera from the Iranian coast of Makran, Oman Sea (Chabahar Bay to Gawater Bay) as an indicator of tsunamis, in: Geological Society of America Annual Meeting. Denver, Colorado, pp. 43–63. https://doi.org/10.22059/geope.2018.255122.648378

Vernant, P., Nilforoushan, F., Hatzfeld, D., Abbassi, M.R., Vigny, C., Masson, F., Nankali, H., Martinod, J., Ashtiani, A., Bayer, R., Tavakoli, F., Chéry, J., 2004. Present-day crustal deformation and plate kinematics in the Middle East constrained by GPS measurements in Iran and northern Oman. Geophys. J. Int. 157, 381–398. https://doi.org/10.1111/j.1365-246X.2004.02222.x

Waseem, M., Khan, S., Asif Khan, M., 2020. Probabilistic Seismic Hazard Assessment of Pakistan Territory Using an Areal Source Model. Pure Appl. Geophys. 177, 3577–3597. https://doi.org/10.1007/s00024-020-02455-7

Watts, P., 1998. Wavemaker Curves for Tsunamis Generated by Underwater Landslides. J. Waterw. Port, Coastal, Ocean Eng. 124, 127–137. https://doi.org/10.1061/(asce)0733-950x(1998)124:3(127)

White, R.S., Louden, K.E., 1982. The Makran continental margin: structure of a thickly sedimented convergent plate boundary: convergent margins: field investigations of margin structure and stratigraphy.

Williams, S., Paulik, R., Weaving, R., Bosserelle, C., Chan Ting, J., Wall, K., Simi, T., Scheele, F., 2021. Multiscale Quantification of Tsunami Hazard Exposure in a Pacific Small Island Developing State: The Case of Samoa. GeoHazards 2, 63–79. https://doi.org/10.3390/geohazards2020004

Yanagisawa, H., Koshimura, S., Imamura, F., Watabe, H., Egashira, T., 2009. Tsunami hazard assessment along the coast of Pakistan based on the 1945 Makran tsunami. J. Japan Soc. Civ. Eng. Ser. B2 (Coastal Eng. B2-65, 306–310. https://doi.org/10.2208/kaigan.65.306

Yang, X., Qiu, Q., Feng, W., Lin, J., Zhang, J., Zhou, Z., Zhang, F., 2022. Mechanism of the 2017 Mw6.3 Pasni earthquake and its significance for future major earthquakes in the eastern Makran. Geophys. J. Int. 231, 1434–1445. https://doi.org/10.1093/gji/ggac257

Zaccagnino, D., Telesca, L., Doglioni, C., 2022. Scaling properties of seismicity and faulting. Earth Planet. Sci. Lett. 584, 117511. https://doi.org/10.1016/j.epsl.2022.117511

Zafarani, H., Etemadsaeed, L., Rahimi, M., Kheirdast, N., Rashidi, A., Ansari, A., Mokhtari, M., Eskandari-ghadi, M., 2022. Probabilistic tsunami hazard analysis for western Makran, Natural Hazards. Springer Netherlands. https://doi.org/10.1007/s11069-022-05595-2

Zuhair, M., Alam, S., 2017. Tsunami Impacts on Nuclear Power Plants along Western Coast of India Due to a Great Makran Earthquake: A Numerical Simulation Approach. Int. J. Geosci. 08, 1417–1426. https://doi.org/10.4236/ijg.2017.812083

Abbasi, M.A., 2020. Regional Connectivity and Pakistan-Iran Trade Corridors. J. Glob. Peace Secur. Stud. 1, 44–59.

Aguirre-Ayerbe, I., Martínez Sánchez, J., Aniel-Quiroga, I., González-Riancho, P., Al-Yahyai, S., González, M., Medina, R., 2018. From tsunami risk assessment to disaster risk reduction - The case of Oman. Nat. Hazards Earth Syst. Sci. 18, 2241–2260. https://doi.org/10.5194/nhess-18-2241-2018

Ahmed, M., Lodi, S.H., Rafi, M.M., 2019. Probabilistic seismic hazard analysis based zoning map of Pakistan. J. Earthq. Eng. 1–36. https://doi.org/10.1080/13632469.2019.1684401

Akbarpour Jannat, M.R., 2021. Tsunami modeling in the Chabahar Bay-Iran from worst-case Makran seismic scenarios: new insights into spectral characterization, separation of the continental shelf, and topography effects. Arab. J. Geosci. 14. https://doi.org/10.1007/s12517-021-06449-0

Akbarpour Jannat, M.R., Noranian Esfahani, M., Chegini, V., Rezanejad, K., 2011. Hazards associated with tsunami waves in the gulf of Oman. J. Coast. Res. 865–869.

Al-Habsi, Z., Hereher, M., El-Hussain, I., Omira, R., Ana Baptista, M., Deif, A., Al-Awadhi, T., Al-Nasiri, N., 2022. Tsunami hazard and risk zoning for Qurayyat in northeast Oman coast: Worst-case credible scenarios along the Makran Subduction Zone, Western Asia. J. Asian Earth Sci. X 8, 100103. https://doi.org/10.1016/j.jaesx.2022.100103

Ali, B., Matsumaru, R., Janjuhah, H.T., 2023. A Source Model for Tsunami Hazards. A Case study from the Eastern Segment of the Makran Subduction Zone, Balochistan, Pakistan. J. Himal. Earth Sci. 56, 48–64.

Ali, K.F., De-Boer, D.H., 2008. Factors controlling specific sediment yield in the upper Indus River basin, northern Pakistan. Hydrol. Process. 2274, 2267–2274. https://doi.org/10.1002/hyp

Ambraseys, N.N., Melville, C., 1982. A history of Persian earthquakes. Cambridge University Press, Britain.

Aniel-Quiroga, Í., Álvarez-Gómez, J.A., González, M., Martínez Sánchez, J., Parro, L.M., Aguirre-Ayerbe, I., Fernández, F., Medina, R., Al-Yahyai, S., 2018. Tsunami Hazard assessment and Scenarios Database for the Tsunami Warning System for the coast of Oman. Nat. Hazards Earth Syst. Sci. 1–30. https://doi.org/10.5194/nhess-2018-221

Anshori, 2019. Tsunami-Inundation-Toolbox-ArcGIS-Desktop-10.x. https://github.com/anshori/Tsunami-Inundation-Toolbox-ArcGIS-Desktop-10.x (Last accessed: 01.02.2022).

Arjun, S., Kalarani, K., Dhanya, P., Praveen, S.S., Reshmi, A.K., Kurian, N.P., Murthy, M.V.R., Hameed, T.S.S., Prakash, T.N., 2011. Numerical simulation of the 1945 Makran tsunami on the southwest coast and Lakshadweep islands of India. Mar. Geod. 34, 68–76. https://doi.org/10.1080/01490419.2011.547801

ArRajehi, A., McClusky, S., Reilinger, R., Daoud, M., Alchalbi, A., Ergintav, S., Gomez, F., Sholan, J., Bou-Rabee, F., Ogubazghi, G., Haileab, B., Fisseha, S., Asfaw, L., Mahmoud, S., Rayan, A., Bendik, R., Kogan, L., 2010. Geodetic constraints on present-day motion of the Arabian Plate: Implications for Red Sea and Gulf of Aden rifting. Tectonics 29, 1–10. https://doi.org/10.1029/2009TC002482

Attenbrow, V., 1992. Shell Bed Or Shell Midden. Aust. Archaeol. 34, 3–21. https://doi.org/10.1080/03122417.1992.11681447

Baba, T., Cummins, P.R., Hori, T., Kaneda, Y., 2006. High precision slip distribution of the 1944 Tonankai earthquake inferred from tsunami waveforms: Possible slip on a splay fault. Tectonophysics 426, 119–134. https://doi.org/10.1016/j.tecto.2006.02.015

Banghar, A., Syke, L.R., 1981. Focal mechanism of an earthquake from the Southern Ocean. Tectonophysics 79, 37–41.

Baptista, M.A., Miranda, J.M., Omira, R., El-Hussain, I., 2020. Study of the 24 September 2013 Oman Sea tsunami using linear shallow water inversion. Arab. J. Geosci. 13. https://doi.org/10.1007/s12517-020-05632-z

Behrens, J., Løvholt, F., Jalayer, F., Lorito, S., Salgado-Gálvez, M.A., Sørensen, M., Abadie, S., Aguirre-Ayerbe, I., Aniel-Quiroga, I., Babeyko, A., Baiguera, M., Basili, R., Belliazzi, S., Grezio, A., Johnson, K., Murphy, S., Paris, R., Rafliana, I., De Risi, R., Rossetto, T., Selva, J., Taroni, M., Del Zoppo, M., Armigliato, A., Bureš, V., Cech, P., Cecioni, C., Christodoulides, P., Davies, G., Dias, F., Bayraktar, H.B., González, M., Gritsevich, M., Guillas, S., Harbitz, C.B., Kânoğlu, U., Macías, J., Papadopoulos, G.A., Polet, J., Romano, F., Salamon, A., Scala, A., Stepinac, M., Tappin, D.R., Thio, H.K., Tonini, R., Triantafyllou, I., Ulrich, T., Varini, E., Volpe, M., Vyhmeister, E., 2021. Probabilistic Tsunami Hazard and Risk Analysis: A Review

of Research Gaps. Front. Earth Sci. 9, 1–28. https://doi.org/10.3389/feart.2021.628772

Bell, K.C., 2011. Lessons from the reconstruction of post-tsunami Aceh: Build back better through ensuring women are at the center of reconstruction of land and property. Washington, DC. © World Bank.

Bellanova, P., Frenken, M., Nishimura, Y., Schwarzbauer, J., Reicherter, K., 2021. Tracing woody-organic tsunami deposits of the 2011 Tohoku-oki event in Misawa (Japan). Sci. Rep. 11, 8947. https://doi.org/10.1038/s41598-021-88199-3

Berryman, K., 2005. Review of Tsunami Hazard and Risk in New Zealand. Inst. Geol. Nucl. Sci. 139.

Bhatt, N., Murari, M.K., Ukey, V., Prizomwala, S.P., Singhvi, A.K., 2016. Geological evidences of extreme waves along the Gujarat coast of western India. Nat. Hazards 84, 1685–1704. https://doi.org/10.1007/s11069-016-2507-6

Biagi, P., 2013. The shell middens of Las Bela coast and the Indus delta (Arabian Sea , Pakistan). https://doi.org/10.1111/aae.12013

Biagi, P., 2011. Changing the prehistory of Sindh and Las Bela coast: Twenty-five years of Italian contribution. World Archaeol. 43, 523–537. https://doi.org/10.1080/00438243.2011.624695

Biagi, P., Girod, A., Nisbet, R., 2013. Prehistoric shell middens, seascapes and landscapes at Lake Siranda (Las Bela, Balochistan) Preliminary results of the 2011 fieldwork season. J. Asian Civilizations 36, 1–25.

Biagi, P., Nisbet, R., Fantuzzi, T., 2018. Exploiting mangroves: Enviromental changes and human interference along the norhtern coast of the Arabian Sea (Pakistan) during the Holocene. Archaol. Mitteilungen aus Iran und Turan 1–34.

Bourget, J., Zaragosi, S., Ellouz-Zimmermann, S., Ducassou, E., Prins, M.A., Garlan, T., Lanfumey, V., Schneider, J.L., Rouillard, P., Giraudeau, J., 2010. Highstand vs. lowstand turbidite system growth in the Makran active margin: Imprints of high-frequency external controls on sediment delivery mechanisms to deep water systems. Mar. Geol. 274, 187–208. https://doi.org/10.1016/j.margeo.2010.04.005

Brune, J.N., 1968. Seismic moment, seismicity, and rate of slip along Major fault zones. J. Geophys. Res. 73, 777–784.

Burbidge, D.R., Cummins, P.R., Mleczko, R., Latief, H., Mokhtari, M., Natawidjaja, D., Rajendran, C.P., Thomas, C., 2009. A probabilistic tsunami hazard assessment of the Indian Ocean Nations. Aust. Gov. Geosci. Aust. Prof. Opin.

Byrne, D.E., Sykes, L.R., Davis, D.M., 1992. Great thrust earthquakes and aseismic slip along the plate boundary of the Makran Subduction Zone. J. Geophys. Res. 97, 449–478.

Caron, V., 2011. Contrasted textural and taphonomic properties of high-energy wave deposits cemented in beachrocks (St. Bartholomew Island, French West Indies). Sediment. Geol. 237, 189–208. https://doi.org/10.1016/j.sedgeo.2011.03.002

Ceci, L., 1984. Shell midden deposits as coastal resources. World Archaeol. 16, 62–74. https://doi.org/10.1080/00438243.1984.9979916

Chacón-Barrantes, S., Narayanan, R., Mayerle, R., 2013. Several tsunami scenarios at the North Sea and their consequences at the German Bight.

Chen, Z., Lin, J., Qiu, Q., Zhou, Z., Zhang, F., 2024. Tsunami potential in the Makran subduction zone: Amplification effects from earthquake rupture directivity and speed. Terra Nov. 36, 201–209. https://doi.org/10.1111/ter.12698

Cheng, G., Bar, W.D., Small, D., 2024. Makran subduction zone and tsunami scenarios in the western Indian Ocean. Geophys. J. Int. 237, 288–301.

Choy, G.L., Kirby, S.H., 2004. Apparent stress, fault maturity and seismic hazard for normal-fault earthquakes at subduction zones. Geophys. J. Int. 159, 991–1012.

Clift, P.D., Giosan, L., 2014. Sediment fluxes and buffering in the post-glacial Indus Basin. Basin Res. 26, 369–386. https://doi.org/10.1111/bre.12038

Cornell, C.A., Vanmarcke, E.H., 1969. The major influences on seismic risk, in: Proceedings of the Fourth World Conference on Earthquake Engineering. pp. 69–83.

Coutts, P.J.F., 1966. Features of Prehistoric Campsites in Australia. Mankind 6, 338.

Cromie, C., Scarselli, N., Craig, J., Khan, M.R., Hussain, A., 2022. Tectonostratigraphic Evolution and Hydrocarbon Prospectivity South of Gwadar Bay, Makran Accretionary Wedge, Offshore Sw Pakistan. J. Pet. Geol. 45, 179–199. https://doi.org/10.1111/jpg.12812

Cummins, P.R., Kaneda, Y., 2000. Possible splay fault slip during the 1946 Nankai earthquake. Geophys. Res. Lett. 27, 2725–2728. https://doi.org/10.1029/1999GL011139

Davies, G., Griffin, J., Løvholt, F., Glimsdal, S., Harbitz, C., Thio, H.K., Lorito, S., Basili, R., Selva, J., Geist, E., Baptista, M.A., 2018. A global probabilistic tsunami hazard assessment from earthquake sources. Geol. Soc. Spec. Publ. 456, 219–244. https://doi.org/10.1144/SP456.5

De Martini, P.M., Bruins, H.J., Feist, L., Goodman-Tchernov, B.N., Hadler, H., Lario, J., Mastronuzzi, G., Obrocki, L., Pantosti, D., Paris, R., Reicherter, K., Smedile, A., Vött, A., 2021. The Mediterranean Sea and the Gulf of Cadiz as a natural laboratory for paleotsunami research: Recent advancements. Earth-Science Rev. 216, 103578. https://doi.org/10.1016/j.earscirev.2021.103578

Decker, V., Gee, C.T., Schucht, P.J., Lindauer, S., Hoffmann, G., 2022. Life on the Edge : A Powerful Tsunami Overwhelmed Indian Ocean Mangroves Life on the Edge : A Powerful Tsunami Overwhelmed Indian Ocean Mangroves One Millennium Ago. https://doi.org/10.3390/f13060922

Delavar, M.R., Mohammadi, H., Sharifi, M.A., Pirooz, M.D., 2017. Tsunami risk assessment modelling in Chabahar port, Iran. Int. Arch. Photogramm. Remote Sens. Spat. Inf. Sci. - ISPRS Arch. 42, 461–467. https://doi.org/10.5194/isprs-archives-XLII-2-W7-461-2017

Deltares, 2023. Delft3d-Flow; simulation of multi-dimensional hydrodynamic flows and transport phenomena, including sediments. https://content.oss.deltares.nl/delft3d4/Delft3D-FLOW_User_Manual.pdf 1–725.

Deo, S.G., Ghate, S., Rajaguru, S.N., 2011. Holocene environmental changes and cultural patterns in coastal western India: A geoarchaeological perspective. Quat. Int. 229, 132–139.

https://doi.org/10.1016/j.quaint.2010.05.001

Donato, S. V., Reinhardt, E.G., Boyce, J.I., Pilarczyk, J.E., Jupp, B.P., 2009. Particle-size distribution of inferred tsunami deposits in Sur Lagoon, Sultanate of Oman. Mar. Geol. 257, 54–64. https://doi.org/10.1016/j.margeo.2008.10.012

Donato, S. V., Reinhardt, E.G., Boyce, J.I., Rothaus, R., Vosmer, T., 2008. Identifying tsunami deposits using bivalve shell taphonomy. Geology 36, 199–202. https://doi.org/10.1130/G24554A.1

Dortch, C.E., 1991. Rottnest and Garden Island Prehistory and The Archaeological Potential of The Adjacent Continental Shelf, Western Australia. Aust. Archaeol. 33, 38–43. https://doi.org/10.1080/03122417.1991.11681430

Dutta, K., Bhushan, R., Somayajulu, B., 2001. ΔR Correction Values for the Northern Indian Ocean. Radiocarbon 43(2A). https://doi.org/10.1017/S0033822200038376

El-Hussain, I., Omira, R., Al-Bulushi, K., Deif, A., Al-Habsi, Z., Al-Rawas, G., Mohamad, A., Al-Jabri, K., Baptista, M.A., 2017. Tsunami hazard assessment along Diba-Oman and Diba-Al-Emirates coasts. MATEC Web Conf. 120, 1–11. https://doi.org/10.1051/matecconf/201712006007

El-Hussain, I., Omira, R., Al-Habsi, Z., Baptista, M.A., Deif, A., Mohamed, A.M.E., 2018. Probabilistic and deterministic estimates of near-field tsunami hazards in northeast Oman. Geosci. Lett. 5. https://doi.org/10.1186/s40562-018-0129-4

El-Hussain, I., Omira, R., Deif, A., Al-Habsi, Z., Al-Rawas, G., Mohamad, A., Al-Jabri, K., Baptista, M.A., 2016. Probabilistic tsunami hazard assessment along Oman coast from submarine earthquakes in the Makran subduction zone. Arab. J. Geosci. 9. https://doi.org/10.1007/s12517-016-2687-0

Ellouz-Zimmermann, N., Lallemant, S.J., Castilla, R., Mouchot, N., Leturmy, P., Battani, A., Buret, C., Cherel, L., Desaubliaux, G., Deville, E., Ferrand, J., Lügcke, A., Mahieux, G., Mascle, G., Mühr, P., Pierson-Wickmann, A.-C., Robion, P., Schmitz, J., Danish, M., Hasany, S., Shahzad, A., Tabreez, A., 2007. Offshore Frontal Part of the Makran Accretionary Prism: The Chamak Survey (Pakistan), Thrust Belts and Foreland Basins, Frontiers in Earth Sciences. https://doi.org/10.1007/978-3-540-69426-7_18

Fournier, M., Chamot-Rooke, N., Petit, C., Fabbri, O., Huchon, P., Maillot, B., Lepvrier, C., 2008. In situ evidence for dextral active motion at the Arabia-India plate boundary. Nat. Geosci. 1, 94–98. https://doi.org/10.1038/ngeo.2007.24

Fournier, M., Chamot-Rooke, N., Rodriguez, M., Huchon, P., Petit, C., Beslier, M.O., Zaragosi, S., 2011. Owen Fracture Zone: The Arabia-India plate boundary unveiled. Earth Planet. Sci. Lett. 302, 247–252. https://doi.org/10.1016/j.epsl.2010.12.027

Fournier, M., Patriat, P., Leroy, S., 2001. Reappraisal of the Arabia-India-Somalia triple junction kinematics. Earth Planet. Sci. Lett. 189, 103–114. https://doi.org/10.1016/S0012-821X(01)00371-5

Frank, N.L., Husain, S.A., 1971. The Deadliest Tropical Cyclone in History. Bull. Am. Meteorol. Soc. 52, 438–445. https://doi.org/10.1175/1520-0477(1971)052<0438:tdtcih>2.0.co;2

Frohling, E., Szeliga, W., 2016. GPS constraints on interplate locking within the Makran subduction zone. Geophys. J. Int. 205, 67–76. https://doi.org/10.1093/gji/ggw001

Gandhi, D., Chavare, K.A., Prizomwala, S.P., Bhatt, N., Bhatt, N.Y., Mohan, K., Rastogi, B.K., 2017. Testing the numerical models for boulder transport through high energy marine wave event: An example from southern Saurashtra, western India. Quat. Int. 444, 209–216. https://doi.org/10.1016/j.quaint.2016.05.021

Gardezi, S.A.H., Luan, X., Sun, Z., Haider, R., Zhang, Y., Qiu, Q., Raveendrasinghe, T.D., 2024. Geo-hazards in the North Arabian Sea with special emphasis on Makran Subduction Zone. Earth-Science Rev. 255, 104846. https://doi.org/https://doi.org/10.1016/j.earscirev.2024.104846

Gates, G.O., Page, W.D., Savage, W.U., Zuberi, S., 1977. The Makran Earthquake November 28, (Mag. 8.3)1975 Field appraisal of geology and cultural effects, in: The Sixth World Conference on Earthquake Engineering New Delhi, India.

Gelfenbaum, G., Vatvani, D., Jaffe, B., Dekker, F., 2007. Tsunami inundation and sediment transport in vicinity of coastal mangrove forest. Coast. Sediments '07 - Proc. 6th Int. Symp. Coast. Eng. Sci. Coast. Sediment Process. 1–12. https://doi.org/10.1061/40926(239)86

Giles, D., Gopinathan, D., Guillas, S., Dias, F., 2021. Faster Than Real Time Tsunami Warning with Associated Hazard Uncertainties. Front. Earth Sci. 8, 1–16. https://doi.org/10.3389/feart.2020.597865

Gill, E.D., 1954. Aboriginal Kitchen Middens and Marine Shell Beds. Mankind 4, 249.

Goff, J.R., Lane, E., Arnold, J., 2009. The tsunami geomorphology of coastal dunes. Nat. Hazards Earth Syst. Sci. 9, 847–854. https://doi.org/10.5194/nhess-9-847-2009

Gopinathan, D., Heidarzadeh, M., Guillas, S., 2021. Probabilistic quantification of tsunami current hazard using statistical emulation. Proc. R. Soc. A Math. Phys. Eng. Sci. 477. https://doi.org/10.1098/rspa.2021.0180

Gordon, R.G., Demets, C., 1989. Present-day motion along the Owen fracture zone and Dalrymple trough in the Arabian Sea. J. Geophys. Res. 94, 5560–5570. https://doi.org/10.1029/JB094iB05p05560

Grando, G., McClay, K., 2007. Morphotectonics domains and structural styles in the Makran accretionary prism, offshore Iran. Sediment. Geol. 196, 157–179. https://doi.org/10.1016/j.sedgeo.2006.05.030

Habib, R.A., Iqbal, M.T., Salam, M., Tahir, M., Iqbal, J., Iqbal, T., 2025. Probing the Complex Interaction of Makran Subduction Zone with Regional Tectonic Features: Insights from Gravity and Seismic Source Parameters. Pure Appl. Geophys. 182, 55–77. https://doi.org/10.1007/s00024-024-03631-9

Haider, R., Ali, S., Hoffmann, G., Reicherter, K., 2024. Tsunami inundation and vulnerability analysis on the Makran coast, Pakistan. Nat. Hazards Earth Syst. Sci. 24, 3279–3290. https://doi.org/10.5194/nhess-24-3279-2024

Haider, R., Ali, S., Hoffmann, G., Reicherter, K., 2023. A multi-proxy approach to assess tsunami hazard with a preliminary risk assessment: A case study of the Makran Coast, Pakistan. Mar.

Geol. 107032. https://doi.org/https://doi.org/10.1016/j.margeo.2023.107032

Hammack, J.L., 1973. A note on tsunamis: Their generation and propagation in an ocean of uniform depth. J. Fluid Mech. 60, 769–799. https://doi.org/10.1017/S0022112073000479

Hanks, T.C., Kanamori, H., 1979. A moment magnitude scale. J. Geophys. Res. B Solid Earth 84, 2348–2350. https://doi.org/10.1029/JB084iB05p02348

Harbitz, C.B., Løvholt, F., Bungum, H., 2014. Submarine landslide tsunamis: How extreme and how likely? Nat. Hazards 72, 1341–1374. https://doi.org/10.1007/s11069-013-0681-3

Heck, N.H., 1947. List of seismic sea waves. Bull. Seismol. Soc. Am. 37, 269–286.

Heffernan, A.S., Moore, J.C., Bangs, N.L., Moore, G.F., Shipley, T.H., 2004. Initial deformation in a subduction thrust system: polygonal normal faulting in the incoming sedimentary sequence of the Nankai subduction zone, southwestern Japan. Geol. Soc. London, Mem. 29, 143–148.

Heidarzadeh, M., Ishibe, T., Harada, T., Natawidjaja, D.H., Pranantyo, I.R., Widyantoro, B.T., 2021. High potential for splay faulting in the molucca sea, indonesia: november 2019 mw 7.2 earthquake and tsunami. Seismol. Res. Lett. 92, 2915–2926. https://doi.org/10.1785/0220200442

Heidarzadeh, M., Kijko, A., 2011. A probabilistic tsunami hazard assessment for the Makran subduction zone at the northwestern Indian Ocean. Nat. Hazards 56, 577–593. https://doi.org/10.1007/s11069-010-9574-x

Heidarzadeh, M., Krastel, S., Yalciner, A.C., 2014. The state-of-the-art numerical tools for modeling landslide tsunamis: a short review, in: Submarine Mass Movements and Their Consequences: 6th International Symposium. Springer, pp. 483–495.

Heidarzadeh, M., Pirooz, M.D., Zaker, N.H., 2009a. Modeling the near-field effects of the worst-case tsunami in the Makran subduction zone. Ocean Eng. 36, 368–376. https://doi.org/10.1016/j.oceaneng.2009.01.004

Heidarzadeh, M., Pirooz, M.D., Zaker, N.H., Mokhtari, M., 2007. Modeling of tsunami propagation in the vicinity of the southern coasts of Iran. Int. J. Civ. Eng. 5, 223–234. https://doi.org/10.1115/OMAE2007-29082

Heidarzadeh, M., Pirooz, M.D., Zaker, N.H., Yalciner, A.C., 2009b. Preliminary estimation of the tsunami hazards associated with the Makran subduction zone at the northwestern Indian Ocean. Nat. Hazards 48, 229–243. https://doi.org/10.1007/s11069-008-9259-x

Heidarzadeh, M., Pirooz, M.D., Zaker, N.H., Yalciner, A.C., Mokhtari, M., Esmaeily, A., 2008. Historical tsunami in the Makran Subduction Zone off the southern coasts of Iran and Pakistan and results of numerical modeling. Ocean Eng. 35, 774–786. https://doi.org/10.1016/j.oceaneng.2008.01.017

Heidarzadeh, M., Rabinovich, A., Kusumoto, S., Rajendran, C.P., 2020. Field surveys and numerical modelling of the 2004 December 26 Indian Ocean tsunami in the area of Mumbai, west coast of India. Geophys. J. Int. 222, 1952–1964. https://doi.org/10.1093/gji/ggaa277

Heidarzadeh, M., Satake, K., 2017. A combined earthquake-landslide source model for the tsunami from the 27 november 1945 Mw 8.1 makran earthquake. Bull. Seismol. Soc. Am. 107, 1033–

1040. https://doi.org/10.1785/0120160196

Heidarzadeh, M., Satake, K., 2014a. Possible sources of the tsunami observed in the northwestern Indian ocean following the 2013 September 24 Mw 7.7 Pakistan inland earthquake. Geophys. J. Int. 199, 752–766. https://doi.org/10.1093/gji/ggu297

Heidarzadeh, M., Satake, K., 2014b. New Insights into the Source of the Makran Tsunami of 27 November 1945 from Tsunami Waveforms and Coastal Deformation Data. Pure Appl. Geophys. 172, 621–640. https://doi.org/10.1007/s00024-014-0948-y

Hicks, S.P., Rietbrock, A., 2015. Seismic slip on an upper-plate normal fault during a large subduction megathrust rupture. Nat. Geosci. 8, 955–960.

Hoechner, A., Babeyko, A.Y., Zamora, N., 2016. Probabilistic tsunami hazard assessment for the Makran region with focus on maximum magnitude assumption. Nat. Hazards Earth Syst. Sci. 16, 1339–1350. https://doi.org/10.5194/nhess-16-1339-2016

Hoffmann, G., Al-Yahyai, S., Naeem, G., Kociok, M., Grützner, C., 2014. An Indian Ocean tsunami triggered remotely by an onshore earthquake in Balochistan, Pakistan. Geology 42, 883–886. https://doi.org/10.1130/G35756.1

Hoffmann, G., Grützner, C., Reicherter, K., Preusser, F., 2015. Geo-archaeological evidence for a Holocene extreme flooding event within the Arabian Sea (Ras al Hadd, Oman). Quat. Sci. Rev. 113, 123–133. https://doi.org/10.1016/j.quascirev.2014.09.033

Hoffmann, G., Grützner, C., Schneider, B., Preusser, F., Reicherter, K., 2020. Large Holocene tsunamis in the northern Arabian Sea. Mar. Geol. 419. https://doi.org/10.1016/j.margeo.2019.106068

Hoffmann, G., Reicherter, K., 2014. Reconstructing Anthropocene extreme flood events by using litter deposits. Glob. Planet. Change 122, 23–28. https://doi.org/10.1016/j.gloplacha.2014.07.012

Hoffmann, G., Reicherter, K., Wiatr, T., Grützner, C., 2011. Evidence For Holocene Tsunami-Impact Along the Shoreline of Oman. 2nd INQUA-IGCP-567 Int. Work. Act. Tectonics, Earthq. Geol. Archaeol. Eng. 88–91.

Hoffmann, G., Reicherter, K., Wiatr, T., Grützner, C., Rausch, T., 2013a. Block and boulder accumulations along the coastline between Fins and Sur (Sultanate of Oman): Tsunamigenic remains? Nat. Hazards 65, 851–873. https://doi.org/10.1007/s11069-012-0399-7

Hoffmann, G., Rupprechter, M., Balushi, N. Al, Grützner, C., Reicherter, K., 2013b. The impact of the 1945 Makran tsunami along the coastlines of the Arabian Sea (Northern Indian Ocean) – a review. Zeitschrift für Geomorphol. Suppl. Issues 57, 257–277. https://doi.org/10.1127/0372-8854/2013/s-00134

Honarmand, M., Shanehsazzadeh, A., Zandi, S.M., 2020. 3D numerical simulation of tsunami generation and propagation, case study: Makran tsunami generation and penetrating in Chabahar Bay. Ocean Eng. 218, 108109. https://doi.org/10.1016/j.oceaneng.2020.108109

Hosseini Mehr, A., Maleki Asayesh, B., Mokhtari, M., 2018. Splay Faults in the Makran Subduction Zone and Changes of their Transferred Coulomb Stress. J. Earth Sp. Phys. 43, 1–10. https://doi.org/10.22059/jesphys.2017.61703

https://c14.arch.ox.ac.uk/calibration.html [WWW Document], n.d. URL https://c14.arch.ox.ac.uk/calibration.html

Hughes, P.J., Sullivan, M.E., 1974. The re-deposition of midden material by storm waves, in: Journal and Proceedings of the Royal Society of New South Wales. Australasian Medical Publishing Co., pp. 6–10.

Jackson, J., McKenzie, D., 1984. Active tectonics of the Alpine–Himalayan Belt between western Turkey and Pakistan. Geophys. J. R. Astron. Soc. 77, 185–264. https://doi.org/10.1111/j.1365-246X.1984.tb01931.x

Jacob, K.H., Quittmayer, R.C., 1979. The Makran Region of Pakistan and Iran: Trench–arc system with active plate subduction, in: Geodynamics of Pakistan. Geological Survey of Pakistan, Quetta, pp. 305–317.

Jade, S., Shrungeshwara, T.S., Kumar, K., Choudhury, P., Dumka, R.K., Bhu, H., 2017. India plate angular velocity and contemporary deformation rates from continuous GPS measurements from 1996 to 2015. Sci. Rep. 7, 1–16. https://doi.org/10.1038/s41598-017-11697-w

Jaiswal, R.K., Singh, A.P., Rastogi, B.K., 2009. Simulation of the Arabian Sea Tsunami propagation generated due to 1945 Makran Earthquake and its effect on western parts of Gujarat (India). Nat. Hazards 48, 245–258. https://doi.org/10.1007/s11069-008-9261-3

Juniansah, A., Tyas, B.I., Tama, G.C., Febriani, K.R., Farda, N.M., 2018. Spatial modelling for tsunami evacuation route in Parangtritis Village. IOP Conf. Ser. Earth Environ. Sci. 148. https://doi.org/10.1088/1755-1315/148/1/012003

Kakar, D.M., Naeem, G., Usman, A., Hasan, H., Lohdi, H.A., Srinivasalu, S., Andrade, V., Rajendran, C.P., Beni, A.N., Hamzeh, M.A., Hoffmann, G., 2014. Elders recall an earlier tsunami on Indian Ocean shores, Eos, Transactions American Geophysical Union. UNESCO.

Kalsi, S.R., Gupta, M., 2003. Success and failure of early warning systems: A case study of the Gujarat Cyclone of June, 1998, in: Zschau, J., Küppers, A. (Eds.), Early Warning Systems for Natural Disaster Reduction. Springer Berlin Heidelberg, Berlin, Heidelberg, pp. 199–202. https://doi.org/10.1007/978-3-642-55903-7_26

Kame, N., Yamashita, T., 1999. Simulation of the spontaneous growth of a dynamic crack without constraints on the crack tip path. Geophys. J. Int. 139, 345–358.

Kerr, R., 1824. A general history and collection of voyages and travels, arranged in systematic order: forming a complete history of the origin and progress of navigation, discovery, and commerce, by sea and land, from the earliest ages to the present time. W. Blackwood.

Khaledzadeh, M., Ghods, A., 2022. Estimation of size of megathrust zone in the Makran subduction system by thermal modelling. Geophys. J. Int. 228, 1530–1540. https://doi.org/10.1093/gji/ggab417

Khan, M.A., Bendick, R., Bhat, M.I., Bilham, R., Kakar, D.M., Khan, S.F., Lodi, S.H., Qazi, M.S., Singh, B., Szeliga, W., Wahab, A., 2008. Preliminary geodetic constraints on plate boundary deformation on the western edge of the Indian plate from TriGGnet (Tri-University GPS Geodesy Network). J. Himal. Earth Sci. 41, 71–87.

Khan, M.J., Ali, M., Xu, M., Khan, M., 2020. Seismicity analysis of selected faults in Makran

Southern Pakistan. Acta Geophys. 68, 965–978. https://doi.org/10.1007/s11600-020-00447-8

Khan, S.A., Shah, M.A., Qaisar, M., 2003a. Seismic risk analysis of coastal area of Pakistan. Acta Seismol. Sin. English Ed. 16, 382–394. https://doi.org/10.1007/s11589-003-0071-0

Khan, S.A., Shah, M.A., Qaisar, M., 2003b. Seismic risk analysis of coastal area of Pakistan. Acta Seismol. Sin. English Ed. 16, 382. https://doi.org/10.1007/s11589-003-0071-0

Khan, U., Khan, M., Wu, S., Jinwei, G., 2024. Middle Miocene renewed subduction of arabian-eurasian plates: Implications for convergent tectonic mechanisms, tectonically-induced fluid overpressures, and sediment recycling dynamics. Mar. Pet. Geol. 162, 106704. https://doi.org/https://doi.org/10.1016/j.marpetgeo.2024.106704

Klingelhoefer, F., Gutscher, M.A., Ladage, S., Dessa, J.X., Graindorge, D., Franke, D., André, C., Permana, H., Yudistira, T., Chauhan, A., 2010. Limits of the seismogenic zone in the epicentral region of the 26 December 2004 great Sumatra-Andaman earthquake: Results from seismic refraction and wide-angle reflection surveys and thermal modeling. J. Geophys. Res. Solid Earth 115, 1–23. https://doi.org/10.1029/2009JB006569

Knapp, K.R., Kruk, M.C., Levinson, D.H., Diamond, H.J., Neumann, C.J., 2010. The international best track archive for climate stewardship (IBTrACS). Bull. Am. Meteorol. Soc. 91, 363–376. https://doi.org/10.1175/2009BAMS2755.1

Kopp, C., Fruehn, J., Flueh, E.R., Reichert, C., Kukowski, N., Bialas, J., Klaeschen, D., 2000. Structure of the makran subduction zone from wide-angle and reflection seismic data. Tectonophysics 329, 171–191. https://doi.org/10.1016/S0040-1951(00)00195-5

Koshimura, S., Oie, T., Yanagisawa, H., Imamura, F., 2009. Developing fragility functions for tsunami damage estimation using numerical model and post-tsunami data from banda aceh, Indonesia. Coast. Eng. J. 51, 243–273. https://doi.org/10.1142/S0578563409002004

Koster, B., Hoffmann, G., Grützner, C., Reicherter, K., 2014. Ground penetrating radar facies of inferred tsunami deposits on the shores of the Arabian Sea (Northern Indian Ocean). Mar. Geol. 351, 13–24. https://doi.org/10.1016/j.margeo.2014.03.002

Kukowski, N., Schillhorn, T., Flueh, E.R., Huhn, K., 2000. Newly identified strike-slip plate boundary in the northeastern Arabian Sea. Geology 28, 355–358. https://doi.org/10.1130/0091-7613(2000)28<355:NISPBI>2.0.CO;2

Kukowski, N., Schillhorn, T., Huhn, K., Von Rad, U., Husen, S., Flueh, E.R., 2001. Morphotectonics and mechanics of the central Makran accretionary wedge off Pakistan. Mar. Geol. 173, 1–19. https://doi.org/10.1016/S0025-3227(00)00167-5

Kupriyanov, A. V, Makarevich, G.G., 2024. Chabahar Port: Between Geopolitics and Business, in: India's Economic Corridor Initiatives. Routledge, pp. 53–65.

Laane, J.L., Chen, W.-P., 1989. The Makran earthquake of 1983 April 18: A possible analogue to the Puget Sound earthquake of 1965. Geophys. J. Int. 98, 1–9.

Latcharote, P., Al-Salem, K., Suppasri, A., Pokavanich, T., Toda, S., Jayaramu, Y., Al-Enezi, A., Al-Ragum, A., Imamura, F., Anawat, K.A., 2018. Tsunami hazard evaluation for Kuwait and Arabian Gulf due to Makran Subduction Zone and Subaerial landslides. Nat. Hazards 93, 127–152. https://doi.org/10.1007/s11069-017-3097-7

Logan, W., 1887. Malabar Manual (2 volumes). Asia Educ. Serv. (1995 Repr. New Delhi.

Loveless, J.P., Allmendinger, R.W., Pritchard, M.E., González, G., 2010. Normal and reverse faulting driven by the subduction zone earthquake cycle in the northern Chilean fore arc. Tectonics 29.

Løvholt, F., 2017. Tsunami Hazard and Risk Assessment. United Nations Off. Disaster Risk Reduct. 1–9.

Løvholt, F., Glimsdal, S., Harbitz, C.B., Zamora, N., Nadim, F., Peduzzi, P., Dao, H., Smebye, H., 2012. Tsunami hazard and exposure on the global scale. Earth-Science Rev. 110, 58–73. https://doi.org/10.1016/j.earscirev.2011.10.002

Macintosh, A., 2013. Coastal climate hazards and urban planning : how planning responses can lead to maladaptation 1035–1055. https://doi.org/10.1007/s11027-012-9406-2

Mahmood, N., Khan, K., Rafi, Z., Lovholt, D.F., 2012. Mapping of Tsunami Hazard along Makran Coast of Pakistan 1–39.

Malgrange, M., Madariaga, R., 1983. Complex distribution of large thrust and normal fault earthquakes in the Chilean subduction zone. Geophys. J. Int. 73, 489–505.

Manaman, N.S., Shomali, H., Koyi, H., 2011. New constraints on upper-mantle S-velocity structure and crustal thickness of the Iranian plateau using partitioned waveform inversion. Geophys. J. Int. 184, 247–267. https://doi.org/10.1111/j.1365-246X.2010.04822.x

Marathe, A., Chandrashekhar, B.S., 2011. Application of Remote Sensing in Studying Holocene Sediments and Tectonic Episodes at Kelshi, Ratnagiri District, Maharashtra, India. J. Indian Soc. Remote Sens. 39, 241–247. https://doi.org/10.1007/s12524-011-0087-1

Masuda, M., Williams, C., Shahkarami, A., Rafique, F., Bryngelson, J., 2012. Tsunami Vulnerability Function Development Based on the 2011 Tohoku Earthquake in Japan. 15 World Conf. Earthq. Eng.

Matin, S., Praveen, S.S., 2021. Numerical simulation and comparison of tsunami inundation for different satellite-derived datasets for the Gujarat coast of India. Adv. Remote Sens. Nat. Resour. Monit. 431–443. https://doi.org/10.1002/9781119616016.ch21

McCann, W.R., Dewey, J.W., Murphy, A.J., Harding, S.T., 1982. A large normal-fault earthquake in the overriding wedge of the Lesser Antilles subduction zone: The earthquake of 8 October 1974. Bull. Seismol. Soc. Am. 72, 2267–2283.

Mehrdar, A., Motaghi, K., Ghods, A., Sobouti, F., Priestley, K., Pachhai, S., Shabanian, E., Zarunizadeh, Z., Zeynaddini-Meymand, R., El-Hussain, I., 2025. Crustal and uppermost mantle structure of the Iranian Makran subduction zone from ambient noise and earthquake surface wave tomography. Geophys. J. Int. 241, 70–85. https://doi.org/10.1093/gji/ggae419

Mikumo, T., Singh, S.K., Santoyo, M.A., 1999. A possible stress interaction between large thrust and normal faulting earthquakes in the Mexican subduction zone. Bull. Seismol. Soc. Am. 89, 1418–1427.

Milliman, J.D., Syvitski, J.P.M., 1992. Geomorphic/tectonic control of sediment discharge to the ocean: the importance of small mountainous rivers. J. Geol. 100, 525–544.

https://doi.org/10.1086/629606

Miranda, J.M., Baptista, M.A., Omira, R., 2014. On the use of Green's summation for tsunami waveform estimation: A case study. Geophys. J. Int. 199, 459–464. https://doi.org/10.1093/gji/ggu266

Mokhtari, M., 2015. The role of splay faulting in increasing the devastation effect of tsunami hazard in Makran, Oman Sea. Arab. J. Geosci. 8, 4291–4298. https://doi.org/10.1007/s12517-014-1375-1

Mokhtari, M., Ala Amjadi, A., Mahshadnia, L., Rafizadeh, M., 2019. A review of the seismotectonics of the Makran Subduction Zone as a baseline for Tsunami Hazard Assessments. Geosci. Lett. 6, 13.

Momeni, P., and Goda, K., 2024. Probabilistic tsunami hazard assessment for the makran subduction zone using logic tree and stochastic rupture sources. Coast. Eng. J. 66, 332–360. https://doi.org/10.1080/21664250.2024.2324520

Momeni, P., Goda, K., Heidarzadeh, M., Qin, J., 2020. Stochastic analysis of tsunami hazard of the 1945 Makran subduction zone MW 8.1–8.3 earthquakes. Geosci. 10, 1–20. https://doi.org/10.3390/geosciences10110452

Momeni, P., Goda, K., Mokhtari, M., Heidarzadeh, M., 2022. A new tsunami hazard assessment for eastern Makran subduction zone by considering splay faults and applying stochastic modeling. Coast. Eng. J. https://doi.org/10.1080/21664250.2022.2117585

Moradi, M., 2021. Integration of Geographical Information System and Tsunami generation/propagation models in the Makran region (North of the Arabian Sea). Int. J. Coast. Offshore Eng. 5, 40–48. https://doi.org/10.52547/ijcoe.5.3.40

Mouchot, N., Loncke, L., Mahieux, G., Bourget, J., Lallemant, S., Ellouz-Zimmermann, N., Leturmy, P., 2010. Recent sedimentary processes along the Makran trench (Makran active margin, off Pakistan). Mar. Geol. 271, 17–31. https://doi.org/10.1016/j.margeo.2010.01.006

Mourato, S., Fernandez, P., Pereira, L., Moreira, M., 2017. Improving a DSM Obtained by Unmanned Aerial Vehicles for Flood Modelling. IOP Conf. Ser. Earth Environ. Sci. 95. https://doi.org/10.1088/1755-1315/95/2/022014

Mousavi, N., Ardestani, V.E., Moosavi, N., 2022. Slab extension and normal faulting in a low-angle subduction-related environment: An example of the Makran subduction zone (Iran-Pakistan). J. Asian Earth Sci. 233, 105244. https://doi.org/https://doi.org/10.1016/j.jseaes.2022.105244

Neetu, S., Suresh, I., Shankar, R., Nagarajan, B., Sharma, R., Shenoi, S.S.C., Unnikrishnan, A.S., Sundar, D., 2011. Trapped waves of the 27 November 1945 Makran tsunami: Observations and numerical modeling. Nat. Hazards 59, 1609–1618. https://doi.org/10.1007/s11069-011-9854-0

Nemati, M., 2019. Seismotectonic and seismicity of Makran, a bimodal subduction zone, SE Iran. J. Asian Earth Sci. 169, 139–161. https://doi.org/10.1016/j.jseaes.2018.08.009

Nouri, M., Namin, M.M., Rashidi, A., 2020. A first-order Landslide Tsunami Hazard Assessment in the Western Makran, in: 18th Iranian Hydraulic Conference. University of Tehran, Tehran, Iran.

Nouri, M., Rashidi, A., Montazeri Namin, M., Shugar, D.H., 2023. Submarine landslide tsunami hazard assessment for the western Makran based on a deterministic approach. Nat. Hazards 118, 1117–1136. https://doi.org/10.1007/s11069-023-06040-8

Okada, Y., 1985. Surface deformation due to shear and tensile faults in a half space. Bull. - Seismol. Soc. Am. 75, 1135–1154. https://doi.org/10.1785/bssa0820021018

Okal, E.A., Synolakis, C.E., 2008. Far-field tsunami hazard from mega-thrust earthquakes in the Indian Ocean. Geophys. J. Int. 172, 995–1015. https://doi.org/10.1111/j.1365-246X.2007.03674.x

Oskamp, J.A., Dababneh, A.J.A., Barton, D.J., 2015. Tsunami Hazard in the Arabian Gulf Due to Earthquakes in the Makran Subduction Zone.

Page, W.D., Alt, J.N., Cluff, L.S., Plafker, G., 1979. Evidence for the recurrence of large-magnitude earthquakes along the makran coast of Iran and Pakistan. Tectonophysics 52, 533–547. https://doi.org/10.1016/B978-0-444-41783-1.50081-7

Pagnoni, G.I., Armigliato, A., Tinti, S., 2021. Estimation of human damage and economic loss of buildings related to tsunami inundation in the city of augusta, italy. Geol. Soc. Spec. Publ. 501, 327–342. https://doi.org/10.1144/SP501-2019-134

Pajang, S., Cubas, N., Letouzey, J., Le Pourhiet, L., Seyedali, S., Fournier, M., Agard, P., Khatib, M.M., Heyhat, M., Mokhtari, M., 2021. Seismic hazard of the western Makran subduction zone: Insight from mechanical modelling and inferred frictional properties. Earth Planet. Sci. Lett. 562, 116789. https://doi.org/10.1016/j.epsl.2021.116789

Pajang, S., Khatib, M.M., Heyhat, M., Cubas, N., Bessiere, E., Letouzey, J., Mokhtari, M., Le Pourhiet, L., 2022. The distinct morphologic signature of underplating and seamounts in accretionary prisms, insights from thermomechanical modeling applied to Coastal Iranian Makran. Tectonophysics 845, 229617. https://doi.org/10.1016/j.tecto.2022.229617

Park, J.-O., Tsuru, T., Kodaira, S., Cummins, P.R., Kaneda, Y., 2002. Splay fault branching along the Nankai subduction zone. Science (80-.). 297, 1157–1160.

Park, S., van de Lindt, J.W., Cox, D., Gupta, R., 2013. Concept of Community Fragilities for Tsunami Coastal Inundation Studies. Nat. Hazards Rev. 14, 220–228. https://doi.org/10.1061/(asce)nh.1527-6996.0000092

Parvaiz, S., Ali, A., Javed, F., Shah, M.A., 2022. Deformational pattern and seismogenic potential of the eastern Makran subduction zone. J. Asian Earth Sci. 235, 105298. https://doi.org/10.1016/j.jseaes.2022.105298

Patel, V.M., Dholakia, M.B., Singh, A.P., 2016. Emergency preparedness in the case of Makran tsunami: a case study on tsunami risk visualization for the western parts of Gujarat, India. Geomatics, Nat. Hazards Risk 7, 826–842. https://doi.org/10.1080/19475705.2014.983188

Patel, V.M., Patel, H.S., Singh, A.P., 2011. Comparative study of earthquake and tsunami loading on Vertical Evacuation Structure at Dwarka. Int. J. Earth Sci. Eng. 4, 659–663.

Payande, A.R., Niksokhan, M.H., Naserian, H., 2014. Tsunami hazard assessment of Chabahar bay related to megathrust seismogenic potential of the Makran subduction zone. Nat. Hazards 76, 161–176. https://doi.org/10.1007/s11069-014-1476-x

Pendse, C.G., 1946. The Mekran Earthquake of the 28th November 1945. Sci. Notes X, 141–146.

Penney, C., Tavakoli, F., Saadat, A., Nankali, H.R., Sedighi, M., Khorrami, F., Sobouti, F., Rafi, Z., Copley, A., Jackson, J., Priestley, K., 2017. Megathrust and accretionary wedge properties and behaviour in the Makran subduction zone. Geophys. J. Int. 209, 1800–1830. https://doi.org/10.1093/gji/ggx126

Pilarczyk, J.E., Reinhardt, E.G., 2012. Testing foraminiferal taphonomy as a tsunami indicator in a shallow arid system lagoon: Sur, Sultanate of Oman. Mar. Geol. 295–298, 128–136. https://doi.org/10.1016/j.margeo.2011.12.002

Pilarczyk, J.E., Reinhardt, E.G., Boyce, J.I., Schwarcz, H.P., Donato, S. V., 2011. Assessing surficial foraminiferal distributions as an overwash indicator in Sur Lagoon, Sultanate of Oman. Mar. Micropaleontol. 80, 62–73. https://doi.org/10.1016/j.marmicro.2011.06.001

Plafker, G., 1972. Alaskan earthquake of 1964 and Chilean earthquake of 1960: Implications for arc tectonics. J. Geophys. Res. 77, 901–925.

Platt, J.P., Leggett, J.K., Alam, S., 1988. Slip vectors and fault mechanics in the Makran accretionary wedge, southwest Pakistan. J. Geophys. Res. 93, 7955–7973. https://doi.org/10.1029/jb093ib07p07955

Platt, J.P., Leggett, J.K., Young, J., Raza, H., Alam, S., 1985. Large-scale sediment underplating in the Makran accretionary prism, southwest Pakistan. Geology 13, 507–511. https://doi.org/10.1130/0091-7613(1985)13<507:LSUITM>2.0.CO;2

Prasojo, K., Afwani, M.Z., Lestari, I., Bramono, A.M.C.W., Bustomi, A.F., 2017. Berryman Tsunami Inundation Modelling on Temon: The Location of NYIA. Int. Conf. Environ. Resour. Manag. Glob. Reg. 1–8.

Prins, M.A., Postma, G., Cleveringa, J., Cramp, A., Kenyon, N.H., 2000. Controls on terrigenous sediment supply to the Arabian Sea during the late quaternary: The Indus fan. Mar. Geol. 169, 327–349. https://doi.org/10.1016/S0025-3227(00)00086-4

Prizomwala, S.P., Gandhi, D., Bhatt, N.N., Winkler, W., Kumar, M.R., Makwana, N., Bhatt, N.N., 2018. Geological evidence for AD 1008 tsunami along the Kachchh coast, Western India: Implications for hazard along the Makran Subduction Zone. Sci. Rep. 8, 1–8. https://doi.org/10.1038/s41598-018-35193-x

Prizomwala, S.P., Gandhi, D., Ukey, V.M., Bhatt, N., Rastogi, B.K., 2015. Coastal boulders as evidences of high-energy marine events from Diu Island, west coast of India: storm or palaeotsunami? Nat. Hazards 75, 1187–1203. https://doi.org/10.1007/s11069-014-1371-5

Prizomwala, S.P., Tandon, A., Joshi, N., Makwana, N., 2021. Reconstructing the catalogue for extreme wave events from the Gujarat coastline (Western India) and their implications to coastal settlers during the last 6000 years. Quat. Int. 599–600, 24–31. https://doi.org/10.1016/j.quaint.2021.03.004

Prizomwala, S.P., Vedpathak, C., Tandon, A., Das, A., Makwana, N., Joshi, N., 2022. Geological footprints of the 1945 Makran tsunami from the west coast of India. Mar. Geol. 446, 106773. https://doi.org/10.1016/j.margeo.2022.106773

Qiu, Q., Zhou, Z., Lin, J., Zhang, F., Chen, Z., Yang, X., 2022. Great earthquake and tsunami

potential in the eastern Makran subduction zone: New insights from geodetic and structural constraints. Tectonophysics 837. https://doi.org/10.1016/j.tecto.2022.229462

Quittmeyer, R.C., Farah, A., Jacob H., K., 1979. The seismicity of Pakistan and its relation to surface faults, in: Farah, A., Dejong, K.A. (Eds.), Geodynamics of Pakistan. Geological Survey of Pakistan, Quetta, pp. 271–284.

Quittmeyer, R.C., Kafka, A.L., 1984. Constraints on plate motions in southern Pakistan and the northern Arabian Sea from the focal mechanisms of small earthquakes. J. Geophys. Res. 89, 2444–2458.

Rafi, Z., Mahmood, N., 2010. Numerical Modeling of Tsunami Inundation for Potential Earthquake at Makran Subduction Zone. Tech. Rep. No. PMD-45/2010.

Rahimi, M., Zafarani, H., Eskandari-Ghadi, M., Etemadsaeed, L., 2025. Dual risk-targeted seismic and tsunami hazard assessment for western Makran coasts, southeast Iran. Nat. Hazards. https://doi.org/10.1007/s11069-025-07184-5

Rajendran, C.P., Heidarzadeh, M., Sanwal, J., Karthikeyan, A., Rajendran, K., 2020. The Orphan Tsunami of 1524 on the Konkan Coast, Western India, and Its Implications. Pure Appl. Geophys. https://doi.org/10.1007/s00024-020-02575-0

Rajendran, C.P., Ramanamurthy, M. V., Reddy, N.T., Rajendran, K., 2008. Hazard implications of the late arrival of the 1945 Makran tsunami. Curr. Sci. 95, 1739–1743.

Rashid, A., Shirazi, S.A., 2023. Gwadar Port-Pakistan as an Axis for Regional Connectivity under CPEC: A Geographer's Perspective. J. Polit. Int. Stud. 9, 105–120.

Rashidi, A., Dutykh, D., Shomali, Z.H., 2020a. Horizontal displacement effect in tsunami wave generation in the western Makran region. J. Ocean Eng. Mar. Energy. https://doi.org/10.1007/s40722-020-00182-8

Rashidi, A., Shomali, Z.H., Dutykh, D., Keshavarz Faraj Khah, N., 2018a. Evaluation of tsunami wave energy generated by earthquakes in the Makran subduction zone. Ocean Eng. 165, 131–139. https://doi.org/10.1016/j.oceaneng.2018.07.027

Rashidi, A., Shomali, Z.H., Dutykh, D., Keshavarz Farajkhah, N., 2020b. Tsunami hazard assessment in the Makran subduction zone. Nat. Hazards 100, 861–875. https://doi.org/10.1007/s11069-019-03848-1

Rashidi, A., Shomali, Z.H., Keshavarz Farajkhah, N., 2018b. Tsunami Simulations in the Western Makran Using Hypothetical Heterogeneous Source Models from World's Great Earthquakes. Pure Appl. Geophys. 175, 1325–1340. https://doi.org/10.1007/s00024-018-1842-9

Rastgoftar, E., Soltanpour, M., 2016. Study and numerical modeling of 1945 Makran tsunami due to a probable submarine landslide. Nat. Hazards 83, 929–945. https://doi.org/10.1007/s11069-016-2356-3

Regard, V., Hatzfeld, D., Molinaro, M., Aubourg, C., Bayer, R., Bellier, O., Yamini-Fard, F., Peyret, M., Abbassi, M., 2010. The transition between Makran subduction and the Zagros collision: recent advances in its structure and active deformation. Geol. Soc. London, Spec. Publ. 330, 43–64. https://doi.org/10.1144/SP330.4

Rehman, A., Zhang, H., 2024a. Seismicity and return period investigation of destructive earthquake in Makran subduction zone. Discov. Geosci. 2. https://doi.org/10.1007/s44288-024-00047-9

Rehman, A., Zhang, H., 2024b. Probabilistic forecast of next earthquake event in Makran subduction zone using Weibull distribution. Contrib. to Geophys. Geod. 54, 85–93. https://doi.org/10.31577/congeo.2024.54.1.5

Rehman, K., Cho, Y.S., 2016. Building damage assessment using scenario based tsunami numerical analysis and fragility curves. Water (Switzerland) 8. https://doi.org/10.3390/w8030109

Rehman, K., Jadoon, T., Hussain, M., Ahmad, Z., Ali, Aamir, Ali, Asghar, Ahmed, S., 2015. Tsunamigenic analysis in and around makran. J. Earthq. Eng. 19, 332–355. https://doi.org/10.1080/13632469.2014.982835

Reilinger, R., McClusky, S., Vernant, P., Lawrence, S., Ergintav, S., Cakmak, R., Ozener, H., Kadirov, F., Guliev, I., Stepanyan, R., Nadariya, M., Hahubia, G., Mahmoud, S., Sakr, K., ArRajehi, A., Paradissis, D., Al-Aydrus, A., Prilepin, M., Guseva, T., Evren, E., Dmitrotsa, A., Filikov, S. V., Gomez, F., Al-Ghazzi, R., Karam, G., 2006. GPS constraints on continental deformation in the Africa-Arabia-Eurasia continental collision zone and implications for the dynamics of plate interactions. J. Geophys. Res. Solid Earth 111, 1–26. https://doi.org/10.1029/2005JB004051

Röbke, B.R., Schüttrumpf, H., Vött, A., 2018. Hydro- and morphodynamic tsunami simulations for the ambrakian gulf (Greece) and comparison with geoscientific field traces. Geophys. J. Int. 213, 317–339. https://doi.org/10.1093/gji/ggx553

Röbke, B.R., Schüttrumpf, H., Vött, A., 2016. Effects of different boundary conditions and palaeotopographies on the onshore response of tsunamis in a numerical model - A case study from western Greece. Cont. Shelf Res. 124, 182–199. https://doi.org/10.1016/j.csr.2016.04.010

Röbke, B.R., Vött, A., Willershäuser, T., Fischer, P., Hadler, H., 2015. Considering coastal palaeogeographical changes in a numerical tsunami model - A progressive base to compare simulation results with field traces from three coastal settings in western Greece. Zeitschrift fur Geomorphol. 59, 157–188. https://doi.org/10.1127/zfg-suppl/2014/S-00210

Rodriguez, M., Chamot-Rooke, N., Hébert, H., Fournier, M., Huchon, P., 2013. Owen Ridge deep-water submarine landslides: Implications for tsunami hazard along the Oman coast. Nat. Hazards Earth Syst. Sci. 13, 417–424. https://doi.org/10.5194/nhess-13-417-2013

Rodriguez, M., Fournier, M., Chamot-Rooke, N., Huchon, P., Bourget, J., Sorbier, M., Zaragosi, S., Rabaute, A., 2011. Neotectonics of the Owen Fracture Zone (NW Indian Ocean): Structural evolution of an oceanic strike-slip plate boundary. Geochemistry, Geophys. Geosystems 12. https://doi.org/10.1029/2011GC003731

Rodriguez, M., Fournier, M., Chamot-Rooke, N., Huchon, P., Zaragosi, S., Rabaute, A., 2012. Mass wasting processes along the Owen Ridge (Northwest Indian Ocean). Mar. Geol. 326–328, 80–100. https://doi.org/10.1016/j.margeo.2012.08.008

Roshan, A.D., Basu, P.C., Jangid, R.S., 2016. Tsunami hazard assessment of Indian coast, Natural Hazards. https://doi.org/10.1007/s11069-016-2216-1

Saha, S., Srivastava, K., 2019. Tsunami simulation along the south west coast of India: Lakshadweep

Islands acting as wave-barricade. Indian J. Geo-Marine Sci. 48, 1640–1647.

Salah, P., Sasaki, J., Soltanpour, M., 2021. Comprehensive Probabilistic Tsunami Hazard Assessment in the Makran Subduction Zone. Pure Appl. Geophys. 178, 5085–5107. https://doi.org/10.1007/s00024-021-02725-y

Salaree, A., Okal, E.A., 2015. Field survey and modelling of the Caspian Sea tsunami of 1990 June 20. Geophys. J. Int. 201, 621–639. https://doi.org/10.1093/gji/ggv044

Salmanidou, D.M., Heidarzadeh, M., Guillas, S., 2019. Probabilistic Landslide-Generated Tsunamis in the Indus Canyon, NW Indian Ocean, Using Statistical Emulation. Pure Appl. Geophys. 176, 3099–3114. https://doi.org/10.1007/s00024-019-02187-3

Sangode, S.J., Meshram, D.C., 2013. A comparative study on the style of paleotsunami deposits at two sites on the west coast of India. Nat. Hazards 66, 463–483. https://doi.org/10.1007/s11069-012-0542-5

Sanlaville, P., Besenval, R., Evin, J., Prieur, A., 1991. Evolution de la région littorale du Makran pakistanais à l'Holocène. Paléorient 17, 3–18. https://doi.org/10.3406/paleo.1991.4536

Sarker, M.A., 2019. Numerical modelling of tsunami in the Makran Subduction Zone–A case study on the 1945 event. J. Oper. Oceanogr. 12, S212–S229. https://doi.org/10.1080/1755876X.2018.1527883

Schneider, B., Hoffmann, G., Reicherter, K., 2016. Scenario-based tsunami risk assessment using a static flooding approach and high-resolution digital elevation data: An example from Muscat in Oman. Glob. Planet. Change 139, 183–194. https://doi.org/10.1016/j.gloplacha.2016.02.005

Shah-Hosseini, M., Morhange, C., Naderi Beni, A., Marriner, N., Lahijani, H., Hamzeh, M., Sabatier, F., 2011. Coastal boulders as evidence for high-energy waves on the Iranian coast of Makran. Mar. Geol. 290, 17–28. https://doi.org/10.1016/j.margeo.2011.10.003

Shah, S.T., Özacar, A.A., Gülerce, Z., 2021. Fault-based probabilistic seismic hazard assessment of the eastern Makran subduction and the Chaman transform fault, Pakistan: Emphasis on the source characterization of megathrust. J. Asian Earth Sci. 205. https://doi.org/10.1016/j.jseaes.2020.104604

Shi, S., Dawson, A.G., Smith, D.E., 1995. Coastal sedimentation associated with the December 12th, 1992 tsunami in Flores, Indonesia. Pure Appl. Geophys. PAGEOPH 144, 525–536. https://doi.org/10.1007/BF00874381

Sibuet, J.C., Rangin, C., Le Pichon, X., Singh, S., Cattaneo, A., Graindorge, D., Klingelhoefer, F., Lin, J.Y., Malod, J., Maury, T., Schneider, J.L., Sultan, N., Umber, M., Yamaguchi, H., 2007. 26th December 2004 great Sumatra-Andaman earthquake: Co-seismic and post-seismic motions in northern Sumatra. Earth Planet. Sci. Lett. 263, 88–103. https://doi.org/10.1016/j.epsl.2007.09.005

Silva, F.R.S. da, Borges, A.L. de O., Toldo Jr., E.E., Fick, C., Puhl, E., Oliveira, V.C.B., Cruz, F.E.G. da, 2023. Threshold of motion and orientation of bivalve shells under current flow. Brazilian J. Geol.

Smart, G.M., Crowley, K.H.M., Lane, E.M., 2016. Estimating tsunami run-up. Nat. Hazards 80, 1933–1947. https://doi.org/10.1007/s11069-015-2052-8

Smith, G.L., McNeill, L., Henstock, I.J., Bull, J., 2012. The structure and fault activity of the Makran accretionary prism. J. Geophys. Res. 117, 1–17. https://doi.org/10.1029/2012JB009312

Smith, G.L., McNeill, L.C., Wang, K.H., Jiangheng He., Henstock, T.J., 2013. Thermal structure and megathrust seismogenic potential of the Makran subduction zone. Geophys. Res. Lett. 40, 1528–1533. https://doi.org/10.1002/grl.50374

Snead, R.J., 2002. Uplifted marine terraces along the Makran coast of Pakistan and Iran, in: Himalaya to the Sea. Routledge, pp. 225–246.

Srinivasa Kumar, T., Manneela, S., 2021. A Review of the Progress, Challenges and Future Trends in Tsunami Early Warning Systems. J. Geol. Soc. India 97, 1533–1544. https://doi.org/10.1007/s12594-021-1910-0

Srivastava, K., Dimri, V.P., Swaroopa Rani, V., Krishna Kumar, R., Narain, L., 2011. Would makran Tsunami skip Mumbai, India? no it would reach 8 minutes later than Ratnagiri. Indian J. Geo-Marine Sci. 40, 620–623.

Steinritz, V., Pena-Castellnou, S., Marliyani, G.I., Reicherter, K., 2021a. GIS-based study of tsunami risk in the Special Region of Yogyakarta (Central GIS-based study of tsunami risk in the Special Region of Yogyakarta (Central Java , Indonesia), in: International Conference on Geological Engineering and Geosciences. https://doi.org/10.1088/1755-1315/851/1/012007

Steinritz, V., Pena-Castellnou, S., Marliyani, G.I., Reicherter, K., 2021b. GIS-based study of tsunami risk in the Special Region of Yogyakarta (Central Java, Indonesia), in: IOP Conference Series: Earth and Environmental Science. IOP Publishing, p. 12007. https://doi.org/10.1088/1755-1315/851/1/012007

Stoneley, R., 1974. Evolution of the Continental Margins Bounding a Former Southern Tethys. Geol. Cont. Margins 889–903. https://doi.org/10.1007/978-3-662-01141-6_65

Stuiver, M., Reimer, P.J., 1993. Extended 14C data base and revised Calib 3.0 14C age calibration program. Radiocarbon 35, 215–230.

Sujatmiko, K.A., Ichii, K., Murata, S., Mulia, I.E., 2023. Application of Stress Parameter from Liquefaction Analysis on the Landslide Induced Tsunami Simulation : A Case Study of the 2018 Palu Tsunami 18, 199–208. https://doi.org/10.20965/jdr.2023.p0199

Sultan, M., 2017. Statistical analysis of earthquakes and tsunami of Makran Subduction Zone (MSZ), and tsunami hazard assessment of Gwadar Coast. J. Astrophys. Aerosp. Technol. 08. https://doi.org/10.4172/2329-6542.1000408

Suppasri, A., Latcharotel, P., Pokavanich, T., Al-Salem, K., Al-Enezi, A., Toda, S., Imamura, F., 2016. Tsunami Hazard Assessment for the Arabian Gulf from Earthquakes and Surface Landslides. J. Japan Soc. Civ. Eng. Ser. B2 (Coastal Eng. 72, I_1675-I_1680. https://doi.org/10.2208/kaigan.72.i_1675

Swapna, M., Srivastava, K., 2014. Effect of Murray ridge on the tsunami propagation from Makran subduction zone. Geophys. J. Int. 199, 1430–1441. https://doi.org/10.1093/gji/ggu336

Tarbotton, C., Dall'Osso, F., Dominey-Howes, D., Goff, J., 2015. The use of empirical vulnerability functions to assess the response of buildings to tsunami impact: Comparative review and summary of best practice. Earth-Science Rev. 142, 120–134.

https://doi.org/https://doi.org/10.1016/j.earscirev.2015.01.002

Tarbotton, C., Dominey-Howes, D., Goff, J.R., Papathoma-Kohle, M., Dall'osso, F., Turner, I.L., 2012. GIS-based techniques for assessing the vulnerability of buildings to tsunami: Current approaches and future steps. Geol. Soc. Spec. Publ. 361, 115–125. https://doi.org/10.1144/SP361.10

UNESCO/IOC, 2015. Remembering the 1945 Makran Tsunami interviews with survivors beside the Arabian Sea, IOC Brochu. ed, United Nations Educational, Scientific and Cultural Organization (UNESCO). Paris, France.

Van Ormondt, M., Nederhoff, K., Van Dongeren, A., 2020. Delft Dashboard: A quick set-up tool for hydrodynamic models. J. Hydroinformatics 22, 510–527. https://doi.org/10.2166/hydro.2020.092

Vaziri, S.H., Reinhart, E.G., Pilarczyk, J.E., 2016. Coastal foraminifera from the Iranian coast of Makran, Oman Sea (Chabahar Bay to Gawater Bay) as an indicator of tsunamis, in: Geological Society of America Annual Meeting. Denver, Colorado, pp. 43–63. https://doi.org/10.22059/geope.2018.255122.648378

Vernant, P., Nilforoushan, F., Hatzfeld, D., Abbassi, M.R., Vigny, C., Masson, F., Nankali, H., Martinod, J., Ashtiani, A., Bayer, R., Tavakoli, F., Chéry, J., 2004. Present-day crustal deformation and plate kinematics in the Middle East constrained by GPS measurements in Iran and northern Oman. Geophys. J. Int. 157, 381–398. https://doi.org/10.1111/j.1365-246X.2004.02222.x

Waseem, M., Khan, S., Asif Khan, M., 2020. Probabilistic Seismic Hazard Assessment of Pakistan Territory Using an Areal Source Model. Pure Appl. Geophys. 177, 3577–3597. https://doi.org/10.1007/s00024-020-02455-7

Watts, P., 1998. Wavemaker Curves for Tsunamis Generated by Underwater Landslides. J. Waterw. Port, Coastal, Ocean Eng. 124, 127–137. https://doi.org/10.1061/(asce)0733-950x(1998)124:3(127)

White, R.S., Louden, K.E., 1982. The Makran continental margin: structure of a thickly sedimented convergent plate boundary: convergent margins: field investigations of margin structure and stratigraphy.

Williams, S., Paulik, R., Weaving, R., Bosserelle, C., Chan Ting, J., Wall, K., Simi, T., Scheele, F., 2021. Multiscale Quantification of Tsunami Hazard Exposure in a Pacific Small Island Developing State: The Case of Samoa. GeoHazards 2, 63–79. https://doi.org/10.3390/geohazards2020004

Yanagisawa, H., Koshimura, S., Imamura, F., Watabe, H., Egashira, T., 2009. Tsunami hazard assessment along the coast of Pakistan based on the 1945 Makran tsunami. J. Japan Soc. Civ. Eng. Ser. B2 (Coastal Eng. B2-65, 306–310. https://doi.org/10.2208/kaigan.65.306

Yang, X., Qiu, Q., Feng, W., Lin, J., Zhang, J., Zhou, Z., Zhang, F., 2022. Mechanism of the 2017 Mw6.3 Pasni earthquake and its significance for future major earthquakes in the eastern Makran. Geophys. J. Int. 231, 1434–1445. https://doi.org/10.1093/gji/ggac257

Zaccagnino, D., Telesca, L., Doglioni, C., 2022. Scaling properties of seismicity and faulting. Earth

Planet. Sci. Lett. 584, 117511. https://doi.org/10.1016/j.epsl.2022.117511

Zafarani, H., Etemadsaeed, L., Rahimi, M., Kheirdast, N., Rashidi, A., Ansari, A., Mokhtari, M., Eskandari-ghadi, M., 2022. Probabilistic tsunami hazard analysis for western Makran, Natural Hazards. Springer Netherlands. https://doi.org/10.1007/s11069-022-05595-2

Zuhair, M., Alam, S., 2017. Tsunami Impacts on Nuclear Power Plants along Western Coast of India Due to a Great Makran Earthquake: A Numerical Simulation Approach. Int. J. Geosci. 08, 1417–1426. https://doi.org/10.4236/ijg.2017.812083

List of Figures

Figure 2.1: Location map showing the regional plate tectonic setting (red) and the major cyclones tracks (gray) which hit the coasts in the Arabian Sea. The size of the grey circle on the cyclone's tracks corresponds to the Saffir-Simpson Hurricane Scale. Data sources: International Best Track Archive for Climate Stewardship-IBTrACS (Knapp et al., 2010). Earthquake data: International Seismological Centre (ISC-2020). The figure also includes the cyclone tracks and associated losses which is also a major hazard in the region. 7

Figure 2.2: Figure showing the tectonic setting and the geodetic motions of the study area. All the velocity vectors are in millimeters (mm). Black Arrows (thin): Speed vector, P: perpendicular vector, N: normal vector, grey arrows (thick): convergence vectors. Different numbers against the vectors show reporting by different researchers, as indicated by different colours in the legend. Makran Subduction Zone (MSZ), Chaman-Ornach Nal Fault Zone (CFZ), Owen Fracture Zone (OFZ), Sistan Fault Zone (SFZ), Sonne Fault (SF). 10

Figure 2.3: Seismo-tectonic map of the region Earthquake focal mechanisms are compiled from Quittmeyer and Kafka (1984); Gordon and Demets (1989); Byrne et al., (1992); Fournier et al., (2001). The simplified two-way travel time (TWT) map is from Smith et al., (2012) showing the nature of the horizon between the decollement and basement. The cross-sections are integrated from Byrne et al. (1992). ... 11

Figure 2.4: Flowchart showing sequential order of various processes used for hazard and risk assessment. 13

Figure 2.5: The left column shows probabilistic tsunami heights with different recurrence intervals by Hoechner et al. (2016). The right column shows the seismic hazard maps based on probabilistic peak ground acceleration (PGA) for different recurrence intervals by Ahmed et al. (2019). The probability of tsunami height is calculated from the instrumental and historical seismicity at the MSZ. 14

Figure 3.1: A) Location and regional tectonic setting of the study area. B) Map showing distribution of tsunamites along with inundation extents during the 1945 tsunami in the Pasni and surrounding area. 25

Figure 3.2: Results of radiocarbon dating at Pasni and Kelshi Tsunamites. The shaded area indicates the likely timing of the tsunami event (the shaded area is marked where at least three samples overlap within certainty). The red line in the shaded area marks the historical reporting of a 1524 AD tsunami event from the Gulf of Cambay, India (Kerr, 1824). All dates have been calibrated using the CALIB Radiocarbon Calibration (version 8.20) and the MARINE20 data set (Stuiver and Reimer, 1993). Two-sigma (r) ranges under 95.5% probability distribution curve. The Arabian Sea's marine correction factor DR = 163 ± 30 is after (Dutta et al., 2001). 28

Figure 3.3: A) Schematic x-sections showing the vertical and lateral distribution of tsunamites along with the hosting style. B) Simplified schematic model showing the depositional mechanism for Horizon-B. The flow magnitudes are computed from numerical modelling. The measured litho-stratigraphic logs and respective field photos are appended with. 29

Figure 3.4: Simulation results; inundation extent and water elevations are shown at the Pasni and surrounding areas overlayed on the satellite image (Supplements: Simulations). The line graphs show the flow depth and flow magnitude at each monitoring point shown with a number in a circle (M1 to M4). In the flow magnitude graph, the three wave-package can clearly be marked (detail in discussion section). The second wave, being a little lesser in wave height than the first one, shows the maximum flow depth. The first wave provides conducive conditions to the second and third wave to propagate and penetrate far inland. 31

Figure 3.5: Field photographs with spatial distribution of possible source material in the study area. The locations of the photos are tagged in the topmost image (satellite image on the shaded relief). The field photos with closeups show the thick deposit between Chur and Kohli villages at different locations comprising predominantly Meretrix shells. The western and middle parts (Photos F, G, H, I) lie on the valley floor along with shell mounds over the paleo-beach sand while on the eastern side the thin bivalve bed (Photos E) is embedded in the aeolian sand dunes at higher elevation. This embedded portion is interpreted to be a reworked deposit. 35

Figure 3.6: Examples of extreme wave deposits showing depositional style and architecture at Pasni and surrounding area. The location of the photos is tagged in Figure 3.5 (satellite image overlayed shaded relief). A) The 1945 tsunami deposits at Parhag. B) a curvilinear deposit of predominantly oysters in the lagoonal mud and sand. Such a curvilinear linear depositional style is exhibited by the tsunami waves losing their flow magnitude (quasi-stillstand) at maximum inundation limits (Bellanova et al., 2021). C) A modern-day example of an extreme wave deposit from cyclone-related inundation It is composed of shells and beach gravel in a coastal dune setting. The NE field of view shows (faded) cliffs responsible for unusual high tsunami wave height and multiple wave reflection at the Pasni shore. 36

Figure 3.7: Sedimentary log of the shallow trench at Pasni. trench location in Figure 3.1. 38

Figure 4.1 Location map of Makran region with major regional tectonic elements and cities along the Pakistan Coast. 40

Figure 4.2: A comparison of the DEM (left) and a satellite image (right) of a section of Karachi. The buildings in the oval circle show roof-top elevations as compared with the ground elevations in the surroundings. The arrows and squares point to the few ground elevation sites (roads, open lands) in between the densely populated areas used for the DTM interpolation. 42

Figure 4.3: Land use maps of four cities. The inset table shows the Manning's Surface Roughness used for each feature in the map. The lower most map is (colored) land use map of Pasni. 43

Figure 4.4: Inundation results for Karachi using bathtub model. 44

Figure 4.5: Inundation results for Karachi using standing wave model. 45

Figure 4.6: Inundation results for Pasni using bathtub model. 46

Figure 4.7: Inundation results for Pasni using standing wave model. 47

Figure 4.8: Inundation results for Gwadar using bathtub model. 48

Figure 4.9: Inundation results for Gwadar using standing wave model. 49

Figure 4.10: Inundation results for Ormara using bathtub model. 50

Figure 4.11: Inundation results for Ormara using standing wave model. 51

Figure 4.12: Comparative inundation curves for each model and scenario. The elevation-wise population spread (grey color) approximates the population under risk against each scenario. 51

Figure 4.13: Satellite image (Google Earth) and DEM (TanDEM-X 0.4 arcsec) of Karachi. At this resolution (12m) the densely pack buildings in oval shaped polygon acted as a solid cuboid, through which inundating water could not penetrate. The squares and arrows point to some of the bare land values in the DEM. 52

Figure 5.1: A Location and tectonic map of the study areas (Gwadar, Pasni). The circles with numbers show the reported palaeoextreme wave deposits; details are in Table 2.5: The compilation of tsunamites discovered at different coasts along the Arabian Sea (sorted age-wise). DART: Deep-ocean Assessment and Reporting of Tsunamis. 55

Figure 5.2: Hydrodynamic modeling results of each scenario with maximum inundation limits and depths at Pasni and surrounding areas. The graphs illustrate the flow depth and magnitude at monitoring points (M1 to M7). Simulation for each scenario are provided in the supplementary materials. 62

Figure 5.3: Hydrodynamic modeling results of each scenario with maximum inundation limits and depths at Gwadar and surrounding areas. The graphs illustrate the flow depth and magnitude at monitoring points (M1 to M5). Simulation for each scenario is provided in the supplementary materials. 63

Figure 5.4: A Probability structural damage plotted against the hydrodynamic force at each monitoring point. Top row: Pasni, Bottom row: Gwadar. The results plotted on fragility curves are developed by (Koshimura et al., 2009) 64

Figure 6.1 A) Location map of Makran with major regional tectonic elements. B) Schematic map showing location and type of faults on the bathymetric surface (GEBCO, 2023) used for modelling (numbered red along black circle). The thick shaded grey line under each fault shows an estimated ruptured part of the fault with parameters are given in Table 6.1. 69

Figure 6.2: Initial tsunami wave heights of four distinct scenarios. 75

Figure 6.3: Illustrates the inundation results of the three scenarios; spectral characteristics of flow depth at four Monitoring Points (MP). Notably, Scenario-2 exhibits the generation of a substantial wave package with delayed timing, attributed to the reflection-amplification phenomenon. This secondary wave package is absent in the other two scenarios. A) The map delineates the inundation limits of the 1945 Tsunami. The details of the numbers along the limit-line are given in Table 6.2 and Table 6.3. The satellite image overlays the inundation limit and Monitoring Points for enhanced visualization. 76

Figure 6.4: Temporal Evolution of Scenraio-4 Tsunami along the Pasni coast. A) Initial wave approaching the coast. It causes minimum inundation as can been seen in panel B. B) Generation of reflected waves. First reflection from the beach cliffs (norther one) and second reflected wave generated at the rim of the shelf (bathymetry in Figure 6.5). C) Interaction and amplification of both reflected waves forming a complex waveform. D) Inundation of integrated waveform at the Pasni beach. 76

Figure 6.5: Illustration of the two wave reflectors responsible for amplification and delayed wave arrivals. The first reflector is the beach-cliffs northeast of Pasni (indicated by black arrows). The second reflector, marked by a yellow line, is a bathymetric high forming a linear rim at the shelf break. The wave crossing over the shelf rim generates secondary waves, which subsequently interact with the reflected waves from the cliffs, resulting in wave amplification, east of the Pasni offshore area. 77

Figure 6.6: The line graphs above illustrate a comparison between the observed arrival times and the modeled ones at Karachi and Mumbai (Haider et al., 2024). The references to (Heidarzadeh et al. (2008, 2009), Jaiswal et al. (2009) are not explicitly mentioned in the text. The observed and modelled results align with the earthquake source and trigger timings and do not correspond to any time delay, as reported in the case of Pasni. This absence of delay reflects no secondary or delayed tsunami generation phenomenon. *78*

List of Tables

Table 2.1: Approaches, methodologies and data used. *13*

Table 2.2: A- The compilation of various tsunamis with fault source parameters in MSZ and adjoin tectonics. B- The compilation of various tsunamis for landslide source parameters in Arabian Sea. *15*

Table 2.3: Overview of Probabilistic Tsunami Hazard Assessment (PTHA) and Statistical Studies Undertaken in the MSZ, modified from (Zafarani et al., 2022). *17*

Table 2.4: Catalogue of the Makran historical and instrumental great earthquakes with Mw ≥ 6.5. updated after Heidarzadeh et al., (2008) *19*

Table 2.5: The compilation of tsunamites discovered at different coasts along the Arabian Sea (sorted age-wise) *20*

Table 3.1: Earthquake source parameters and initial wave height considered in the study. *30*

Table 3.2: Proxies and their comparative analysis distinguishing the depositional agent (shell middens, paleo-beach, and Tsunami-cyclones) at the Pasni and surrounding area. So far, no shell middens have been discovered at the Pasni Coast, therefore we compared our results with the shell midden found at the eastern part of the Makran Coast. *33*

Table 4.1: Summary of models and approaches with respective governing equations *41*

Table 5.1: Table showing the earthquake source parameters used to model each scenario with respective initial wave height. *57*

Table 5.2: Summarized methodology with flowchart showing sequential order of various processes used for hazard and vulnerability assessment. *58*

Table 5.3: Timeline for chain of events and issuance of warning alerts during three (03) tsunami cases in the Indian Ocean. *66*

Table 6.1: Earthquake source parameters used to model tsunami scenarios. *71*

Table 6.2: showing the compilation of inundation observations at Pasni with the interviews of 1945 survivors and the field observations (UNESCO/IOC, 2015). *73*

Table 6.3: Table showing compilation of technical reporting wave heights and times at Pasni, Karachi and Mumbai. *74*

Table 6.4: Table showing comparative analysis of tsunami scenarios based on the criteria. 74

List of Pre-Publications

Published (Peered-reviewed):

Haider, R., Ali, S., Hoffmann, G., Reicherter, K., 2023. A multi-proxy approach to assess tsunami hazard with a preliminary risk assessment: A case study of the Makran Coast, Pakistan. Mar. Geol. 107032.
https://doi.org/https://doi.org/10.1016/j.margeo.2023.107032.

Haider, R., Ali, S., Hoffmann, G., Reicherter, K., 2024. Tsunami inundation and vulnerability analysis on the Makran coast, Pakistan. Nat. Hazards Earth Syst. Sci. 24, 3279–3290.
https://doi.org/10.5194/nhess-24-3279-2024

Gardezi, S.A.H., Luan, X., Sun, Z., Haider, R., Zhang, Y., Qiu, Q., Raveendrasinghe, T.D., 2024. Geo-hazards in the North Arabian Sea with special emphasis on Makran Subduction Zone. Earth-Science Rev. 255, 104846.
https://doi.org/https://doi.org/10.1016/j.earscirev.2024.104846

Submitted (preprints under-revision):

…… No one to date……

Drafted:

Haider, R., Ali, S., Hoffmann, G., and Reicherter, K.: Tsunami hit the Pasni repeatedly; evidence for extreme wave events at the Pasni Coast, Pakistan.

Haider, R., Ali, S., Javed, H., Gardezi, S.A.H., Hoffmann, G., and Reicherter, K.; The case of 1945 Tsunami; wave height, number of waves and arrival time.